

https://dspace.org/

Characterization of DD-carboxypeptidase function in mycobacteria: genetic knockout and recombinant protein production

Ismail, Zaahida Sheik

2016-10-12
http://hdl.handle.net/10539/21179

Downloaded from a DSpace repository. https://dspace.org/

Characterization of DD-Carboxypeptidase function in mycobacteria: Genetic knockout and recombinant protein production

---

Zaahida Sheik Ismail (790012)



A dissertation submitted to the Faculty of Health Science, University of Witwatersrand, Johannesburg, in fulfilment of the requirements for the degree of Master of Science in Medicine.

2016

Declaration

I, Zaahida Sheik Ismail declare that this dissertation is my own work. It is being submitted for the degree of Master of Science at the University of the Witwatersrand, Johannesburg. It has not been submitted before for any degree or examination at this any other University.

_____ _____

(Zaahida Sheik Ismail) Date

Dedication

I dedicate this work to my late grandmother who always loved, cared and supported me until her very last breath.

Presentations arising from this dissertation

Conference:	4th Annual SA TB Conference
Presentation:	Poster
Title:	Characterization of DD-carboxypeptidase function in mycobacteria: Genetic knockout and recombinant protein production
Venue and year:	ICC Durban, 2014

Conference:	6th Biennial Research Day and Postgraduate Expo
Presentation:	Poster
Title:	Characterization of DD-carboxypeptidases in Mycobacteria
Venue and year:	University of Witwatersrand, 2014

Conference:	6th Cross Faculty Graduate Symposium
Presentation:	Poster
Title:	Characterization of DD-carboxypeptidases in Mycobacteria
Venue and year:	University of Witwatersrand, 2014

Achievement:	**1st prize in Faculty of Health Science**
Conference:	Molecular Biosciences Research Thrust (MBRT)
Presentation:	Poster
Title:	Characterization of DD-carboxypeptidases in Mycobacteria
Venue and year:	University of Witwatersrand, 2014
Conference:	PathRed Conference
Presentation:	Poster
Title:	Characterization of DD-carboxypeptidases in Mycobacteria
Venue and year:	Emperor's Palace, 2015
Achievement:	**1st prize in Infectious Diseases and Non-communicable Diseases Track**
Conference:	Molecular Biosciences Research Thrust (MBRT)
Presentation:	Poster

Title:	Characterization of DD-carboxypeptidases in Mycobacteria
Venue and year:	University of Witwatersrand, 2015
Conference:	7th Cross Faculty Graduate Symposium
Presentation:	Poster
Title:	Characterization of DD-carboxypeptidases in Mycobacteria
Venue and year:	University of Witwatersrand, 2016

Abstract

Tuberculosis (TB), a disease caused by the pathogenic bacterium *Mycobacterium tuberculosis* (Mtb), is responsible for killing over one million people each year with an alarming number categorized as multidrug resistant (MDR) or extensively drug resistant (XDR) infections. These high numbers, coupled with other factors such as the ability of Mtb to adapt to its host, its synergistic relationship with Human Immunodeficiency Virus (HIV) and the protracted treatment regimen required to treat TB has resulted in the urgent need for new TB drugs. In this regard, the peptidoglycan (PG) layer of the mycobacterial cell wall, which requires an array of enzymes for synthesis of this mesh-like polymer, have been of particular interest. The PG consists of sugars cross-linked by stem peptides and is synthesized, cross-linked and remodeled by carefully regulated enzymes such as penicillin binding proteins (PBPs) which perform the final cross-linking step in PG biosynthesis. This study focuses on a specific group of low molecular weight PBPs, namely the DD-carboxypeptidases (DD-CPases), which are responsible for regulating the amount of cross-links found in the PG by cleaving the terminal D-Alanine (D-Ala) from the stem peptide of nascent PG units. To date, these proteins have remained largely uncharacterized in mycobacteria. To investigate the functions of these proteins in *Mycobacterium smegmatis*, two double knockout mutants lacking different combinations of the DD-CPase-encoding genes (MSMEG_1661, MSMEG_2432 and/or MSMEG_2433) were created using two-step allelic exchange and assessed using a range of phenotypic analyses. In addition recombinant protein production of these DD-CPases as well as MSMEG_6113 was attempted. We were unable to create a double knockout mutant lacking both MSMEG_2432 and MSMEG_2433 from an existing single mutant strain, suggesting that the operonic structure of these two genes may require a different approach. We were able to generate two double knockout mutants,

ΔMSMEG_1661 ΔMSMEG_2432 and ΔMSMEG_2433 ΔMSMEG_1661, lacking two DD-CPases. Southern blot and gene expression analyses confirmed loss of the respective genes from *M. smegmatis*. The ΔMSMEG_1661 ΔMSMEG_2432 mutant and ΔMSMEG_2433 ΔMSMEG_1661 mutant displayed no alterations in colony morphology, biofilm formation, sliding motility and sodium dodecyl sulphate (SDS) sensitivity. However, loss of two DD-CPases resulted in increased sensitivity of *M. smegmatis* to vancomycin and a range of β-lactams antibiotics. Analysis of cellular morphology using transmission electron microscopy (TEM) demonstrated that the septum was fully formed in all strains but in some cases was not degraded during daughter cell separation. Scanning electron microscopy (SEM) and spatial localization of new PG units using BODIPY-labeled vancomycin revealed that late division processes were hampered in these double knockout mutants with new PG inserted across the cell as well as cells with multiple unresolved septa. To create recombinant derivatives of MSMEG_6113, MSMEG_1661, MSMEG_2432 and MSMEG_2433, proteins were His-tagged and purified using affinity chromatography. However, under all conditions tested soluble protein could not be acquired. Collectively, these data provide the first evidence that the DD-CPases of *M. smegmatis* may play a direct role in the late cell division process that lead to daughter cell separation in mycobacteria.

Acknowledgements

I would firstly like to thank the Almighty for allowing me this amazing opportunity to learn and grow as both a person and a scientist.

Secondly I would like to thank all my funders, the National Research Foundation (NRF), the DST/NRF Centre of Excellence for Biomedical TB Research (CBTBR) and the Howard Hughes Medical Institute, without whom this MSc would not have been possible.

My supervisor, Prof. Bavesh Kana – You are a true inspiration. Your endless support, guidance and understanding not only comes through in your mentorship but also as a kind, compassionate person who is always willing to listen regardless of how busy you are. Your scientific knowledge is unmeasurable and I will always appreciate the skills you have taught me.

To my colleagues at the CBTBR who became my family away from home. Thank you for you friendship, laughter and advice when it all seemed too much. A special thanks to Nikki, Sbu, Chris, Rukaya and Edith, who welcomed me and made me feel like I belonged. Dr. Gordhan, thank you for your inspiring insight on life and being a woman in science.

I would like to thank my parents for their unwavering support. Nothing I say or do will compensate for all that you have done for me. Your time, love and guidance have allowed me to always be successful in life's many endeavors.

And finally to my husband – Raees van der Schyff. Your positive attitude and loving smile reminds me each and every day that anything we wish to achieve is possible. I am grateful for all that you have done and sacrificed to help me achieve one of my many life's goals. I will continue to strive to be the best that I can be not only for myself but for our future.

Table of contents

Declaration i

Dedication ii

Presentations arising from this dissertation iii

Abstract vi

Acknowledgements viii

List of figures xiii

List of tables xvii

Nomenclature xviii

1. Introduction 1

1.1. Tuberculosis 1

1.2. Treatment and vaccines 1

1.3. Pathogenesis 4

1.4. Latent TB infection 4

1.5. Bacterial cell growth and division 6

1.6. The mycobacterial cell wall 10

1.6.1. Peptidoglycan 12

1.7. Antibiotics that target PG 14

1.7.1. β-lactam antibiotics 14

1.7.2. Vancomycin 15

1.7.3. D-cycloserine 15

1.8. PG remodeling enzymes 16

1.8.1. *N*-acetylmuramyl-L-alanine-amidases 18

1.8.2. Resuscitation Promoting Factors 20

1.8.3. *N*-acetyl-β-D-muramidases 20

1.8.4. *N*-acetyl-β-D-glucosaminidases 21

1.8.5. Penicillin binding proteins 21

1.9. Aims 28

2. Methods 30

2.1 Reagents 30

2.2 Bacterial strains and culture conditions 30
2.3 DNA extractions 33
2.3.1 Plasmid DNA extraction from *E. coli* 33
2.3.2 Chromosomal DNA extraction from mycobacteria 35
2.4 DNA quantification 36
2.5 DNA manipulation 36
2.5.1 Restriction digestion 36
2.5.2 Dephosphorylation of DNA 36
2.5.3 DNA ligation 36
2.6 DNA visualization and purification 37
2.6.1 Agarose gel electrophoresis 37
2.6.2 DNA fragment purification 37
2.6.3 DNA sequencing 37
2.7 DNA amplification 38
2.7.1 Roche Fast Start Taq PCR 38
2.7.2 Phusion High Fidelity DNA polymerase 39
2.8 Bacterial transformations 39
2.8.1 *E. coli* transformations 39
2.8.2 *M. smegmatis* electroporations 40
2.9 Generation of *M. smegmatis* knockout strains 40
2.9.1 Generation of ΔMSMEG_1661 ΔMSMEG_2432 double knockout mutant 42
2.9.2 Generation of double knockout mutants 42
2.10 Southern blot analysis 43
2.10.1 Electro-blotting 43
2.10.2 Probe labelling 43
2.10.3 Hybridization 44
2.10.4 Immunological detection 44
2.11 Generation of *M. smegmatis* complementation strains 45
2.12 Gene expression analysis 45
2.12.1 RNA extraction 45
2.12.3 Quantitative real-time PCR (qPCR) 47
2.13 Phenotypic analyses of *M. smegmatis* knockout strains 47

2.13.1 Growth rate determination in standard media 47
2.13.2 Growth rate analysis in Sauton's media 48
2.13.3 Colony forming ability 48
2.13.4 Biofilm formation 48
2.13.5 Sliding motility 48
2.13.6 Antibiotic sensitivity 49
2.13.7 SDS sensitivity 49
2.13.8 Microscopic analysis 50
2.14 Recombinant protein expression 51
2.14.1 Generation of inducible vectors for protein purification 52
2.14.2 Induction of protein expression 52
2.14.3 SDS-PAGE 54
2.14.4 Protein purification 53
2.14.5 Western blotting 55
3. Results 56
3.1 Generation of *M. smegmatis* double knockout DD-CPase mutants 56
3.1.1 Generation of ΔMSMEG_1661 ΔMSMEG_2432 56
3.1.2 Generation of ΔMSMEG_2433 ΔMSMEG_1661 62
3.1.3 Generation of a double knockout mutant lacking MSMEG_2432 and MSMEG_2433 67
3.2 Complementation of DD-CPase mutants with a single DD-CPase 71
3.3 Gene expression analysis of DD-CPases to confirm deletion and genetic complementation 74
3.4 The role of DD-CPases in cell growth 77
3.4.1 Regulation of *M. smegmatis* growth kinetics 77
3.4.2 Maintenance of *M. smegmatis* colony morphology 79
3.4.3 Maintenance of *M. smegmatis* biofilm formation 80
3.4.4. Maintenance of *M. smegmatis* sliding motility 82
3.5 DD-CPases play a role in antibiotic sensitivity 82
3.6 Effect of SDS on DD-CPase knockout mutants 86
3.7 DD-CPases play a role in cell shape and size 86
3.7.1 Role of DD-CPases on maintaining cell shape 86
3.7.2 The role of DD-CPases on maintaining cell size 90
3.8 DD-CPases play a role in cell division 91

3.8.1 Role of DD-CPases in septal formation/degradation 91
3.8.2 Role of DD-CPases in cell division 93
3.9 Recombinant expression of DD-CPases 95
3.9.1 Preparation of gene insert fragments for cloning 95
3.9.2 Preparation of protein expression vector pET29a 95
3.10 Transformation into expression host cell line 98
3.11 Protein induction of DD-CPases 99
3.12 Protein purification of DacB-His 102
3.13 Cloning of DacB domain variants 103
3.14 Induction of DacB variants 106
4. Discussion 108
5. Appendices 120
6. References 135

List of figures

Figure 1.1. Models of bacterial growth…….....7

Figure 1.2. Diagrammatic representation of the structure of the mycobacterial cell wall….....11

Figure 1.3. Diagrammatic representation of peptidoglycan biosynthesis pathway……..…….14

Figure 1.4. Diagrammatic representation of the structure of peptidoglycan illustrating peptidoglycan remodeling enzymes and cleavage sites……..……...17

Figure 1.5. Diagrammatic representation of high molecular weight penicillin binding proteins and DD-carboxypeptidase activity within the stem peptides of peptidoglycan...……..…25

Figure 2.1. Schematic of allelic exchange mutagenesis procedure using MSMEG_1661 as an example……..41

Figure 2.2. Schematic representation of cloning for recombinant protein production …..……..53

Figure 3.1. Construction of ΔMSMEG_1661 ΔMSMEG_2432 double mutants and its complemented derivative.……...……...56

Figure 3.2. PCR screening of ΔMSMEG_1661 ΔMSMEG_2432 knockout mutants……..57

Figure 3.3. Screening of ΔMSMEG_1661 ΔMSMEG_2432 possible double crossover mutants……...59

Figure 3.4. Genotypic confirmation of the ΔMSMEG_1661 ΔMSMEG_2432 strain...……..61

Figure 3.5. Construction of ΔMSMEG_2433 ΔMSMEG_1661 double mutant and its complemented derivative……...62

Figure 3.6. PCR screening of ΔMSMEG_1661 ΔMSMEG_2432 knockout mutants….……63

Figure 3.7. Screening of ΔMSMEG_2433 ΔMSMEG_1661 possible double crossover mutants…….…..65

Figure 3.8. Genotypic confirmation of the ΔMSMEG_2433 ΔMSMEG_1661 strain……..66

Figure 3.9. Analysis of possible ΔMSMEG_2432 ΔMSMEG_2433 double crossover mutants……...68

Figure 3.10. Screening of ΔMSMEG_2432 ΔMSMEG_2433 possible double crossover mutant……69

Figure 3.11. PCR screenings of possible ΔMSMEG_2433 ΔMSMEG_2432 double crossover mutants……...71

Figure 3.12. Schematic representation of integration of pMV1661 into the chromosome of *M. smegmatis*……72

Figure 3.13. PCR confirmation of site specific integration of pMV1661 into the double knockout mutants……...73

Figure 3.14. Expression analysis of cellular mRNA for MSMEG_2432 relative to *sig*A standard……..…….....74

Figure 3.15. Expression analysis of cellular mRNA for MSMEG_2433 relative to *sig*A standard…….....75

Figure 3.16. Expression analysis of cellular mRNA for MSMEG_1661 relative to *sig*A standard…….…….....76

Figure 3.17. Growth kinetics of strains lacking DD-CPases……..78

Figure 3.18. The effect of DD-CPase deletions on colony morphology……80

Figure 3.19. Biofilm formation in strains lacking DD-CPases……...81

Figure 3.20. Sliding motility of the wild type and DD-CPase knockout strains……82

Figure 3.21. Drug susceptibility of wild type and double DD-CPase knockout mutants……..85

Figure 3.22. SDS killing of wild type and double DD-CPase knockout mutants……..87

Figure 3.23. SEM images of phenotypes found in wild type and double knockout DD-CPase mutants……...88

Figure 3.24. Quantification of SEM phenotypes found in wild type and double knockout DD-CPase strains…….…...90

Figure 3.25. Quantification of SEM cell length…….....91

Figure 3.26. Septum formation in wild type and double knockout mutant strains……...92

Figure 3.27. Vancomycin staining of wild type and double DD-CPase knockout mutants……..94

Figure 3.28. Restriction mapping of pET29a_DacB……96

Figure 3.29. Restriction mapping of pET29a_1661……..97

Figure 3.30. Restriction mapping of pET29a_2432……..97

Figure 3.31. Restriction mapping of pET29a_2433…….…….98

Figure 3.32. PCR confirmation of DacB and MSMEG_1661 *E. coli* BL21 (DE3) pLysS transformants……...……..99

Figure 3.33. PCR confirmation of MSMEG_2432 and MSMEG_2433 *E. coli* BL21 (DE3) pLysS transformants…….……...……100

Figure 3.34. IPTG induction of DacB-His……..……101

Figure 3.35. IPTG induction of DacB-His at 30°C……..101

Figure 3.36. Purification of DacB-His at 37°C……..……..102

Figure 3.37. Restriction mapping of pET29a_DacB-domain……..104

Figure 3.38. Restriction mapping of pET29a_DacB-minus……104

Figure 3.39. Restriction mapping of pET29a_DacB-flank……..105

Figure 3.40. PCR confirmation of *E. coli* BL21 (DE3) pLysS DacB variants……106

Figure 3.41. IPTG induction of DacB variant proteins……107

Figure 4.1. Effect of DD-carboxypeptidase deletions of peptidoglycan cross-linking…..…..…..115

Figure 4.2. V-snapping division of mycobacteria……117

Figure D1. Restriction mapping of p2NIL_PAC_1661…….……..126

Figure D2. Restriction mapping of p2NIL_PAC_2432…….……..127

Figure D3. Restriction mapping of p2NIL_PAC_2433……...128

Figure D4. Generation of MSMEG_1661 probes for Southern blots……..129

Figure D5. Generation of MSMEG_2432 probes for Southern blots……..129

Figure D6. Generation of MSMEG_2433 probes for Southern blots……..129

Figure D7. Restriction mapping of pMV1661……130

Figure D8. Melt curves of amplicons from qPCR for MSMEG_1661……..……..131

Figure D9. SEM phenotypes observed in wild type, double knockout mutants and complemented strains……...132

Figure D10. Phusion PCR of gene fragments to be cloned into pET29a…..……...132

Figure D11. Restriction analysis of pET29a expression vector……..133

Figure D12. Digested fragments for cloning……...134

Figure D13. Phusion PCR of DacB variants to be cloned into pET29a……..134

Figure D14. Digested DacB variant fragments for cloning…….134

List of tables

Table 2.1. Strains and plasmids…….30

Table 2.2. Primer3 parameters used for primer design…….38

Table 3.1. MICs to various drugs with wild type, double knockout mutants and complemented strains……...…….83

Table A1. Culture media and supplements……..120

Table A2. Solutions used for plasmid extractions from *E. coli*……...120

Table A3. Solutions used for DNA extraction from *M. smegmatis*…….120

Table A4. Solutions used for precipitation of DNA……120

Table A5. Solutions used for electrophoresis of DNA……121

Table A6. Agarose gel recipes…….121

Table A7. Solutions used for *E. coli* competent cells preparation……...121

Table A8. Solutions used for Southern blotting……...121

Table A9. Solutions used for protein extractions…….122

Table A10. Solutions used for electrophoresis of proteins……..122

Table A11. SDS-PAGE gel recipes…….122

Table A12. Solutions used for purification of His-tagged proteins…….122

Table A13. Solutions used for Western blotting……..123

Table B1. Primers used for PCR confirmation of knockout mutants……..123

Table B2. Primers used for generation of Southern blot probes……..123

Table B3. Primers used to confirm site specific integration of complementing vector……..124

Table B4. Primers used for gene expression analysis by qPCR……..124

Table B5. Primers used for amplification of genes for protein expression…….124

Table B6. Primers used for sequencing of pET29a vectors…….124

Nomenclature

µ	Micro
AG	Arabinogalactan
Alr	Alanine racemase
Ami	Amidase
Amp	Ampicillin
ATP	Adenosine triphosphate
*att*B	$tRNA^{Gly}$ attachment site
BCG	Bacille Calmette-Guerin
BDQ	Bedaquiline
bp	base pairs
BSA	Bovine serum albumin
Camp	Chloroamphenicol
CFUs	Colony forming units
CFZ	Clofazamine
Cm	centimeter
CPS	Chemiluminescent peroxidase substrate
CSPD	Disodium 3-(4-methoxyspiro {1, 2-dioxetane-3, 2′-(5′-chloro) tricyclo [$3.3.1.1^{3,7}$] decan}-4-yl) phenyl phosphate
CTAB	Cetyltrimethylammonium bromide
D-Ala	D-Alanine
DD-CPases	DD-carboxypeptidases
Ddl	D-alanine ligase
D-Glu	D-Glutaminyl
DIG	Digoxygenin
DMSO	Dimethylsulphoxide
DNA	Deoxyribonucleic acid
dNTPs	Deoxynucleotide triphosphate
DOTS	Directly observed treatment, short course
DS	Drug sensitive
EDTA	Ethylenediaminetetraacetic acid
EMB	Ethambutol
FDA	Food and Drug Administration
g	grams
HCl	Hydrochloric acid
HIV	Human Immunodeficiency Virus
HMW	High molecular weight
Hyg	Hygromycin
INH	Isoniazid
IPTG	Isopropyl β-D-1-thiogalactopyranoside
Kan	Kanamycin
kbp	Kilo base pairs
LA	Luria-Bertani agar

lacZ	Gene encoding β-galactosidase
L-Ala	L-Alanine
LAM	Lipoarabinomannan
LB	Luria-Bertani broth
Ldts	LD-transpeptidases
LM	Low melting
LMW	Low molecular weight
LTBI	Latent tuberculosis infection
LTs	Lytic transglycosylases
m	Milli
M	Molar
MA	Mycolic acid
*m*DAP	Meso-diaminopimelic acid
MDR	Multidrug resistant
MIC	Minimum inhibitory concentration
min	Minutes
MRSA	Methicillin resistant *Staphylococcal aureus*
Mtb	*Mycobacterium tuberculosis*
NaCl	Sodium chloride
NAG	N-acetylglucosamine
NAM	N-acetylmuramic acid
NaOH	Sodium hydroxide
NEB	New England Biolabs
OD_{600nm}	Optical density at 600 nanometer wavelength
PAGE	Polyacrylamide gel electrophoresis
PBPs	Penicillin binding proteins
PBS	Phosphate buffered saline
PCR	Polymerase chain reaction
pDIM	Phtiocerol dimycocerosate
PG	Peptidoglycan
PZA	Pyrazinamide
RIF	Rifampicin
RipA	Resuscitation promoting factor interacting protein A
RNA	Ribonucleic acid
RPFs	Resuscitation promoting factors
rpm	Revolutions per minute
RT	Reverse transcriptase
SCO	Single crossover
sdH_20	Sterile distilled water
SDS	Sodium dodecyl sulphate
SEM	Scanning electron microscopy
TB	Tuberculosis
TBE	Tris borate EDTA
TDM	Trehalose-6, 6-dimycolate
TDR/XXDR	Totally drug resistant

TEM	Transmission electron microscopy
Tfb	Ruthidium chloride competent cell solution
TLRs	Toll-like receptors
Tm	Melting temperature
U	Units
UDP	Uridine diphosphate
UV	Ultraviolet
V	Volts
WHO	World health organization
XDR	Extensively drug resistant
X-gal	5-bromo-4-chloro-3-indolyl-D-thiogalactopyranoside
α	Alpha
β	Beta
Ω	Ohms

1. Introduction

1.1. Tuberculosis

Tuberculosis (TB), previously known as consumption, has been around for millennia, being recorded as early in history as the Egyptian and Greco-Roman civilizations (De Backer et al., 2006). In 2014, 9.6 million people fell ill with the TB disease, with 1.5 million succumbing (WHO, 2015). Additionally, approximately 480 000 people developed MDR TB with an estimated 190 000 cases resulting in death (WHO, 2015).

The human pathogen *Mycobacterium tuberculosis* (Mtb) is the causative agent of TB and is currently classified as being responsible for the largest number of deaths due to a single bacterium (Chao and Rubin, 2010). Mtb has the capacity to cause a spectrum of disease in the human host, which ranges from latent, asymptomatic infection to active granulomatous disease. Active TB disease is treated with a Food and Drug Administration (FDA) approved regimen consisting of six months of antimicrobial drug treatment (Zhang, 2005, CDC, 2015). However, the ability of Mtb to adopt a dormant like state, adapt to the host environment and readily evolve resistance to drugs has resulted in TB disease remaining of global health concern (Zhang, 2005, Hett and Rubin, 2008). In addition to this, high rates of co-infection with Human Immunodeficiency Virus (HIV) contribute to TB incidence rates, especially in high burden countries such as South Africa, with 1.2 million HIV-infected individuals developing TB in 2014 (WHO, 2015).

1.2. Treatment and vaccines

Bacille Calmette-Guerin (BCG) is currently the only TB vaccine available and was developed almost a century ago (Malmros, 1948). BCG is administered intradermally, providing effective protection for TB meningitis in children. However, in adults variable protection (0 - 80%), if any, is achieved for pulmonary TB and BCG does not protect against latent TB

infection (LTBI) (CDC, 2015). Considering this, an urgent preventative vaccine with long-lasting protective efficacy is urgently required to bolster prevention of TB transmission in the community setting.

Drug sensitive (DS) TB is treated with chemotherapeutics over a six-month period, known as directly observed treatment short course (DOTS) (CDC, 2015, WHO, 2015). The first two months of treatment involves administration of the first-line antimicrobial drugs isoniazid (INH), rifampicin (RIF), ethambutol (EMB) and pyrazinamide (PZA) (Ducati et al., 2006, CDC, 2015, WHO, 2015). This is followed by treatment with INH and RIF for the remaining four months. In cases of drug resistant TB, several alternate drug combinations are implemented (CDC, 2015, WHO, 2015). There are numerous problems with TB treatment including non-compliance where patients fail to complete treatment, negative drug interactions with medications such as anti-retroviral therapy, poor drug availability in some communities and prescription of inappropriate treatment. This has resulted in an increase in composite forms of drug resistance such as MDR, XDR and totally drug resistant (XXDR/TDR) TB (Gandhi et al., 2006, Migliori et al., 2007, Velayati et al., 2009, WHO, 2015). MDR Mtb strains are defined as those strains that are resistant to both the first line drugs, INH and RIF, whereas XDR strains are defined as being resistant to INH, RIF and two classes of the second line drugs: a fluroquinone and at least one of the injectable drugs (kanamycin, amikacin, and capreomycin) (Velayati et al., 2009, WHO, 2015). XXDR strains are resistant to all standard drugs, be it first line or second line chemotherapeutics (CDC, 2015).

There are ten FDA approved drugs for the treatment of TB (CDC, 2015). The first line drugs include INH, RIF, EMB, PZA, rifabutin and the recently added rifapentine (CDC, 2015). Second line drugs include but are not limited to cycloserine, ethiaonamide, streptomycin, amikacin, kanamycin and capreomycin (Cohen, 2013, CDC, 2015). These drugs can be

administered orally or can be injected. Second line drugs are quite expensive, toxic and are not as effective as first line medication.

The above-mentioned drugs have been in use for over fifty years, with new medications only being introduced recently. Bedaquiline (BDQ) represents a novel addition to the TB chemotherapeutic arsenal and was recently approved by the FDA for treatment of MDR-TB, making it the first new drug to be added to the TB regimen in over five decades (Cohen, 2013). BDQ is a diarylquinolone which inhibits adenosine triphosphate (ATP) synthase displaying a high specificity for the mycobacterial ATP synthase (Andries et al., 2005). When used in combination with PZA, BDQ has been shown to have increased activity (Diacon et al., 2012). Another drug clofazamine (CFZ), which has been used to treat leprosy for the past fifty years was repurposed for treating MDR-TB (Lechartier and Cole, 2015). CFZ is reduced by NADH dehydrogenase followed by reduction by oxygen which leads to the release of reactive oxygen species and eventually cell death (Yano et al., 2011). Adding CFZ to a regimen could possibly cure MDR TB in 9 – 12 months (Van Deun et al., 2010). However, use of CFX results in side effects such as skin discoloration which makes it undesirable for patient treatment.

Drug resistance can be acquired due to a number of reasons including lateral gene transfer, selective pressure under certain conditions and genetic mutations (Depardieu et al., 2007). Some microorganisms also have natural resistance to specific antibiotic classes. In mycobacteria, resistance to first line drugs is mainly due to mutations in the specific genes that encode drug targets. A number of genes are involved in EMB and INH resistance with the principle mutations occurring in the *embB* gene and the *katG* and *inhA* genes respectively (Banerjee et al., 1994, Ramaswamy et al., 2003). Mutations in the *pncA* gene confer resistance to PZA and those in the *rpoB* and *embB* genes confer resistance to RIF. (Telenti et al., 1993, Telenti, 1997, Ramaswamy et al., 2003, Zhang, 2005).

1.3. Pathogenesis

Infection with Mtb occurs when an individual inhales aerosol particles containing infectious tubercle bacteria (WHO, 2015). Bacteria then encounter the alveolar macrophages in the host lungs and are phagocytosed. In the case of an individual with a strong immune system, the bacteria are cleared and disease does not progress. Alternatively, TB infection occurs resulting in one of two outcomes. Where conditions are favorable for the bacteria to proliferate, development of active disease in less than 10% of cases occurs. In the remaining individuals, infection does not progress to disease leading to a clinically latent state in 90-95% of cases. However, it is estimated that these individuals carry a 10% lifetime risk of eventually progressing to active disease through a process termed reactivation disease (Bhatt and Salgame, 2007, Chao and Rubin, 2010). HIV infected or immune compromised individuals have an increased risk (~10% per year) of developing active disease when latently infected with TB (WHO, 2015).

Mtb interacts with toll-like receptors (TLRs) on the surface of macrophages and dendritic cells for phagocytosis. Activation of TLRs induces chemokine and cytokine secretion, which recruit other immune cells to the infection site and granuloma formation is initiated. Three types of granulomas have been identified including the classic caseous granulomas and non-necrotizing granulomas found in active disease, which arise due to an imbalance of pro- and anti- inflammatory responses (Scanga and Flynn, 2010). The third type, fibrotic granulomas, are well structured with activated macrophages able to control proliferation of bacteria resulting in LTBI (Scanga et al., 1999, Barry et al., 2009a, Scanga and Flynn, 2010).

1.4. Latent TB infection

Individuals that are infected with TB but do not display any of the symptoms of the disease are classified as latently infected. This form of TB affects approximately one third of the

world's population and since it is asymptotic, it generally goes undetected in most cases (WHO, 2015). Two hypotheses have been ascribed to bacterial physiology associated with LTBI, the first stating that LTBI is due to the transition from active growth to dormancy in the tubercle bacillus. The second hypothesis states that LTBI is due to a population of both growing and dying organisms that is maintained by an efficient immune system.

Dormancy is a term used to describe bacteria, usually grown in the laboratory, that are quiescent and metabolically inactive. Bacteria enter a low metabolic state when faced with stressful conditions and this state can be reversed with resumption of growth under favorable conditions (Scanga et al., 1999). Strains from the genus *Bacillus* adopt a form of dormancy during harsh conditions through spore formation. Mycobacteria lack the genes necessary for entry into spore-like state akin to that found in *Bacillus* and consequently, it is unlikely that they transition to a non-replicating state using a similar mechanism (Feucht et al., 2003, Higgins and Dworkin, 2011). *Mycobacterium smegmatis* has been shown to produce ovoid cells which are suggestive of dormant forms of the organism, as these cells have been shown to have low metabolic activity, increased resistance to heat and antibiotics as well as the inability to be cultured on solid media (Anuchin et al., 2009). Although Mtb has been shown to adopt a dormant state in vitro (Shleeva et al., 2010), a strong association between this and LTBI has not been demonstrated. In bacterial infections, the dormant state contributes to the difficulty in eradicating the disease since many of the current chemotherapeutics target those processes required for active growth and these targets lose their vulnerability to drugs under non-replicating conditions, resulting in a drug tolerant state.

Another phenomenon that is related to drug tolerance is bacterial persistence which is defined as a subpopulation of bacteria that persist and survive under harsh conditions (Kesavan et al., 2009). Persisters form a small population that are resistant to antibiotic killing through various mechanisms (Lewis, 2010). The tolerant state in persisters is not genetically

transmitted to daughter cells, which remain drug sensitive (Mc Dermott, 1958). Mtb has been shown to survive prolonged antibiotic treatment which has been attributed to these persisters cells (Gomez and McKinney, 2004, Lewis, 2010). There are a few theories that explain the presence of persisters in bacterial cultures including the presence of cells that rapidly adapt to antibiotic stress, cells that are in some protective stage of the cell cycle (Miller et al., 2004) and defective programmed cell death (Wang and Wood, 2011).

1.5. Bacterial cell growth and division

The proposed ability of mycobacteria to remain in non-replicating states within an individual for years before reactivation disease occurs, points to exceptionally controlled cell growth and cell division processes in the tubercle bacillus. Unlike the rod-shaped bacteria *Escherichia coli* and *Bacillus subtilis*, which grow by incorporating nascent cell wall material across the lateral axis of the cell with a right- or left- hand helical pattern respectively, Figure 1.1A. (Mendelson, 1976, Wang et al., 2012), mycobacteria grow by incorporating newly synthesized cell wall material at the sub-polar regions of the cell, Figure 1.1B and 1.1C (Brown et al., 2011). The proliferation process of bacterial cells can be divided into elongation and division of the parental cell. In most bacteria, cell division occurs at a similar rate producing two daughter cells of the same size (Trueba, 1982). In *E. coli* and *B. subtilis*, cell division and cell elongation occur separately and are controlled by the divisome and elongasome respectively, each containing a detailed set of proteins existing in complexes to perform these processes (Cabeen and Jacobs-Wagner, 2005).

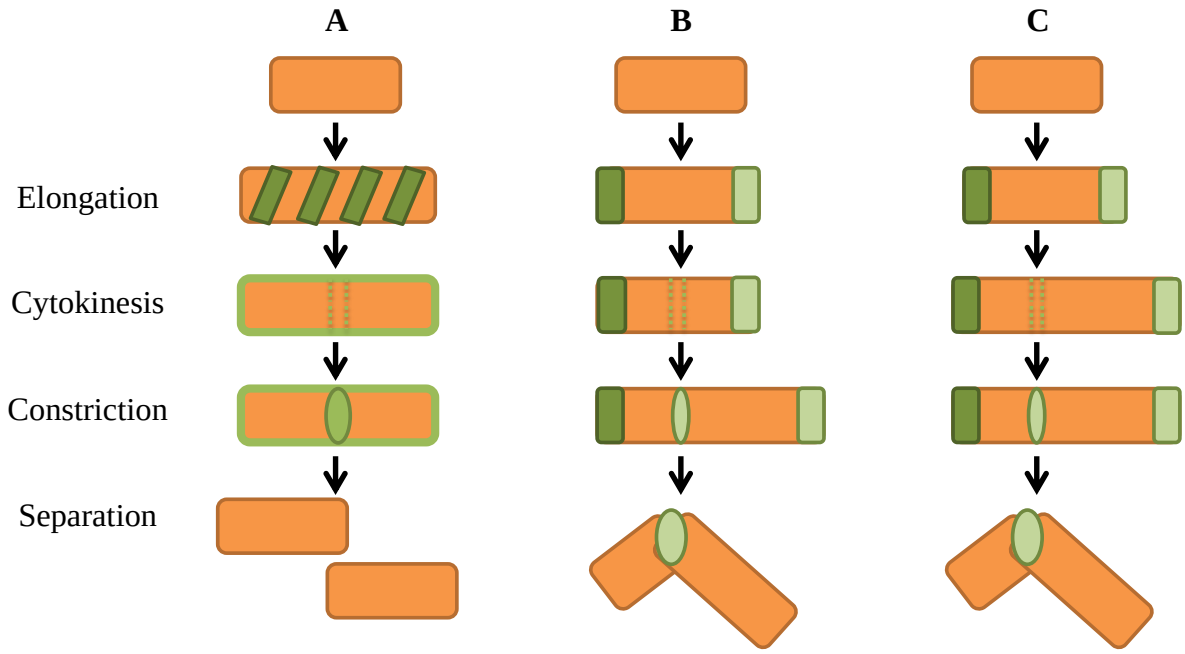

Figure 1.1. Models of bacterial growth. (A) Lateral cell wall incorporation in *E. coli* and *B. subtilis*. The green colour indicates the insertion of new cell wall. Elongation occurs with nascent peptidoglycan generated across the lateral axis of the cell. This is followed by formation of the septum at midcell and subsequent separation of the cytoplasm or cytokinesis. Constriction results in the separation of the parental cell into two identical daughter cells of the same size. (B) Model describing mycobacterial growth. Elongation of the bacteria occurs with the incorporation of nascent peptidoglycan at the poles, with the new pole and old pole shown in dark green and light green respectively. After cytokinesis, the septum is constricted resulting in the V-snapping or separation of the parental cell into two daughter cells of different lengths. (C) A second model of mycobacterial growth. Elongation begins and nascent peptidoglycan is incorporated at the poles with the old pole, shown in light green, growing faster than the new pole throughout the cycle until division occurs. V-snapping results in separation of the parental cell into two daughter cells of unequal sizes. (Santi et al, 2013)

Many rod-shaped bacteria such as *E. coli* use the actin-like MreB protein during the elongation process. MreB interacts with MreC, MreD and RodZ and is required for rod-shaped growth (Gitai et al., 2005, Young, 2010). Decreasing the expression of *mreB* results in increased diameter of cells that appear to have spherical morphology (Karczmarek et al., 2007). In *B. subtilis*, MreB and another protein, Mb1, are implicated in controlling the width and length of the lateral axis of the cell respectively (Jones et al., 2001). This mode of growth results in inert peptidoglycan (PG) at the poles.

The division process of *E. coli* and *B. subtilis* is regulated by the tubulin-like protein FtsZ which forms a ring-like structure at midcell called the Z-ring (Bi and Lutkenhaus, 1991,

Adams and Errington, 2009, Typas et al., 2011). The Z-ring initiates cell division and serves as a scaffold for recruiting many essential cell division proteins which together form the divisome (Typas et al., 2011). Both organisms control FtsZ assembly through the use of 'negative control systems' such as the Min system and nucleoid occlusion. In *E. coli*, the Min system comprises the MinCDE complex whereas in *B. subtilis* it comprises MinCD and DivIVA (Hett and Rubin, 2008). This system directs the assembly of the divisome away from the poles by preventing Z-ring formation and cell constriction at the poles. The nucleoid occlusion system comprises a protein called *SlmA* in *E. coli* and *Noc* in *B. subtilis* which inhibits FtsZ assembly near the nucleoid and prevents inadvertent guillotining of the chromosome by the cell division apparatus (Hett and Rubin, 2008). Both systems are triggered when the cell reaches the appropriate length, producing a division event resulting in identical daughter cells, each of which contains a nucleoid.

Mycobacterial elongation and division involves a number of proteins and complexes found in the cell wall, however, these organisms do not possess many of the cell division proteins used by *E. coli* and *B. subtilis*. The MreB proteins are not present in mycobacteria although it is possible that other actin-like proteins could perform similar functions. Due to the lack of MreB it is hypothesized that the FtsZ homologue in mycobacteria is responsible for both elongation and septation (Hett and Rubin, 2008). The FtsZ stabilizing proteins, FtsA and ZipA, are also not found in mycobacterial species although recently, SepF has been identified as an essential protein that interacts with FtsZ (Gola et al., 2015, Gupta et al., 2015). SepF has been identified as a key component of the cell division machinery (Gupta et al., 2015) with depletion of the protein resulting in elongated cells as well as a loss in growth and viability (Gola et al., 2015). FtsZ hydrolyses guanosine triphosphate (GTP) and forms the Z-ring structure at the midcell in mycobacteria which determines the future cell division site (Hett and Rubin, 2008). Once the Z-ring forms, several proteins are recruited to form multi-

protein complexes. The mycobacterial DivIVA homologue, Wag31, is essential for septal and polar PG synthesis and is recruited to the septum when division is nearly complete (Kang et al., 2008, Cava et al., 2013, Meniche et al., 2014).

Mycobacteria lack both FtsZ negative control systems found in *E. coli* and *B. subtilis* resulting in Z-ring formation not always being found at midcell (Singh et al., 2010). Cells grow and divide asymmetrically producing two daughter cells of unequal sizes. This unique growth pattern of mycobacteria produces a heterogeneous population of cells that vary in growth rate, size and composition of the cell wall (Aldridge et al., 2012, Joyce et al., 2012, Singh et al., 2013). Two modes of polar cell growth have been described for mycobacterial cells. Like all other rod-shaped bacteria, mycobacteria contain two poles termed the old and new pole (Aldridge et al., 2012). The old pole refers to the pole which is inherited from the parental cell and the new pole refers to the pole which is synthesized during division (Aldridge et al., 2012). The first model of growth uses cytokinesis to define cell division, Figure 1.1B (Santi et al., 2013, Kieser and Rubin, 2014). In this model it is proposed that the poles grow at equal rates until cytokinesis. After cytokinesis until the cells separate, growth is said to occur predominantly at the old pole. Once the cells separate both poles once again grow at the same rate until the next cytokinesis event. The second model of polar growth uses the initiation of constriction to define cell division, Figure 1.1C (Aldridge et al., 2012, Kieser and Rubin, 2014). In this model, it is proposed that the poles grow at different rates throughout the cell cycle, with the old pole always growing faster than the new pole with cell division being asymmetric. Both of these proposed models of polar growth result in the generation of daughter cells of unequal lengths. These models also show that the daughter cell that inherits the old pole elongates faster after separation and is larger than its sibling cell, rendering the longer daughter cell genetically identical but phenotypically different (different cell size, cell age and nature of cell poles) when compared to its smaller counterpart

(Kieser and Rubin, 2014). These phenotypic differences could possibly play a role in antibiotic resistance thus contributing to the success of the species.

The final step of mycobacterial cell division is referred to as snapping, which is identified by the V-shape form cells take on during the late stages of cell division, Figure 1.1B and 1.1C (Hett and Rubin, 2008).

1.6. The mycobacterial cell wall

The complex mycobacterial cell wall is a key contributor to the success of mycobacterial pathogens. Expansion of the cell wall is important for cell growth, virulence and resistance to antibiotics (Barry et al., 2007, Kaur et al., 2009, Bansal-Mutalik and Nikaido, 2014). Mycobacterial cell walls have been classified as gram variable since they differ from both gram positive and gram negative bacterial cell walls (Hett and Rubin, 2008). The structure of the mycobacterial cell wall is similar to that found in gram positives in that it contains a thick PG layer and no true outer membrane. However, mycobacteria do contain porins which are found in gram negative cell walls. The cell wall consists of three main components: a plasma membrane, cell wall core and a capsule (Alsteens et al., 2008). The cell wall core is made up of cross-linked PG which is covalently linked to arabinogalactan (AG), which in turn is linked to mycolic acids (MA) via a phosphodiester bond (Brennan, 2003), Figure 1.2. Together these components form an efficient barrier, protecting the bacterium from external stresses.

The mycobacterial capsule is the outermost layer and consists of lipids, polysaccharides and proteins (Daffe and Etienne, 1999, Lee et al., 2012).This outer layer of lipids and proteins intercalates into the MA acid layer which is composed of a variety of saturated short α-alkyl and long β-hydroxyl fatty acids containing between 20-26 and 60-90 carbons per chain

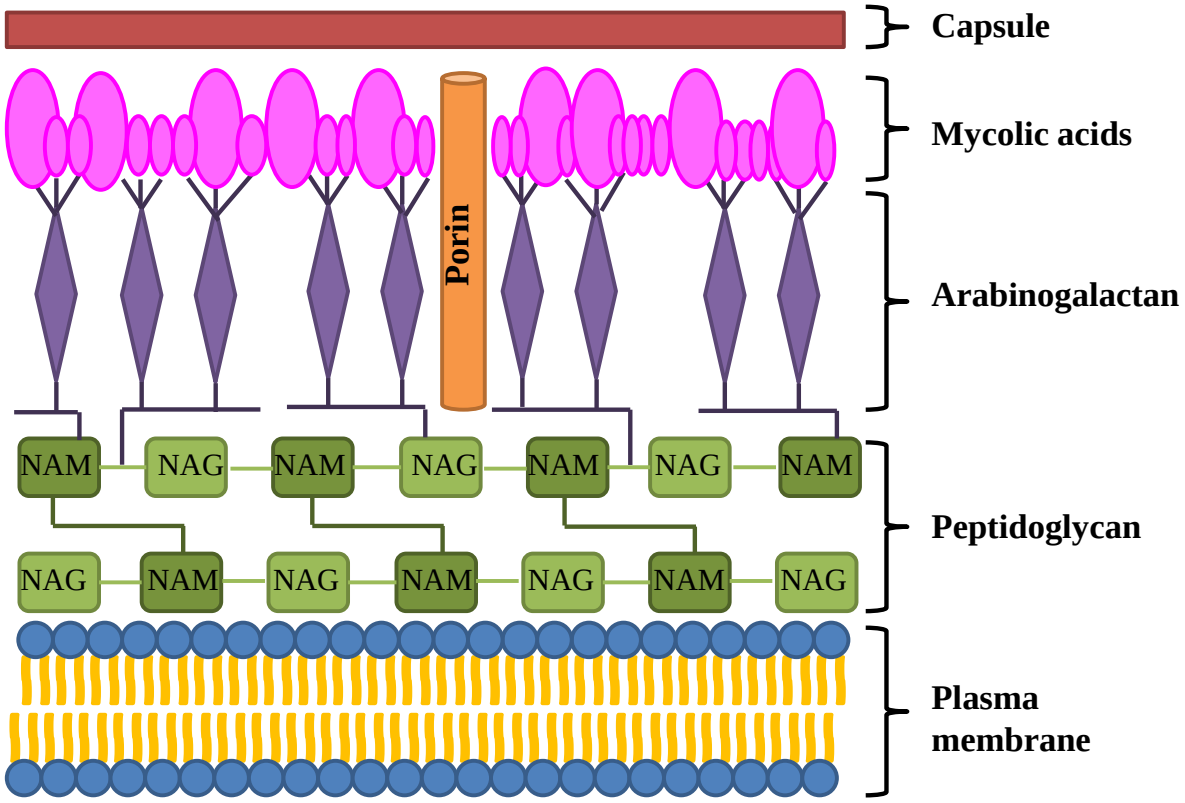

Figure1.2. Diagrammatic representation of the structure of the mycobacterial cell wall. The phospholipid bilayer is shown by the blue circles and yellow lines which indicate the hydrophilic and hydrophobic components of the plasma membrane. The green rectangles represent the peptidoglycan layer with the dark green lines representing the peptide cross-links between *N*-acetylmuramic acid residues. The purple diamonds represent the arabinogalactan layer; pink circles represent the mycolic acid layer with a porin shown in orange. The red rectangle represents the outer capsule-like layer. (Hett and Rubin, 2008)

respectively (Besra and Brennan, 1997, Crick et al., 2001). These lipid chains lie at a 90° angle to the cell surface and are generated by the FASI and FASII biosynthetic systems (Kieser and Rubin, 2014). They are processed and mature through the activity of a cascade of enzymes resulting in three meromycolate variants (alpha-, methoxy-, and keto- meromycolic acids) which are required for virulence during infection, stimulation of immune responses and various roles in pathogenicity (Takayama et al., 2005, Barry et al., 2007, Verschoor et al., 2012). The MA layer contributes to cell wall impermeability, antimicrobial resistance and virulence (Takayama et al., 2005, Barry et al., 2007, Hett and Rubin, 2008, Sani et al., 2010) with the long carbon chains responsible for the thick waxy lipid coat characteristic of mycobacteria (Hett and Rubin, 2008). Other molecules in the cell wall include the lipids such as lipoarabinomannan (LAM), phtiocerol dimycocerosate (DIM/pDIM), cord factor and

trehalose-6, 6-dimycolate (TDM), with the latter two being responsible for cord-like formations and clumping in mycobacteria (Brennan, 2003).

The majority of MAs are covalently linked to the AG by an ester link and are found as tetramycolyl-pentaarabinofuranosyl clusters on the AG (Besra and Brennan, 1997, Hett and Rubin, 2008). AG is a unique polymer consisting of branched arabinan chains attached to a galactan core with both sugars in the furanose configuration (Brennan, 2003). The galactan is linear and consists of ~30 residues arranged in alternating 1→5, 1→6 linkages with arabinan attached to the fifth carbon of the galactan (Daffe et al., 1990, Crick et al., 2001). This results in some galactan residues which do not have arabinan (Daffe et al., 1990, Crick et al., 2001). The AG layer plays an important role in cell wall integrity and anchors the MA layer to the PG layer (Hett and Rubin, 2008). AG is attached to the PG via a phosphoryl-*N*-acetylglucosaminosyl-rhamnosyl linkage known as a linker region (McNeil et al., 1990, Mikusova et al., 1996, Crick et al., 2001).

1.6.1. Peptidoglycan

PG is a linear polymer which surrounds the plasma membrane and is unique to bacteria, thus making it an excellent drug target as evidenced by decades of successful antibiotic therapy with penicillin. The PG layer is responsible for maintaining cell shape and size and consists of long glycan strands and peptides. The glycan strands form the sugar backbone of PG and consists of *N*-acetylglucosamine (NAG) and *N*-acetylmuramic acid (NAM), which are cross-linked by peptides that are attached to the NAM residue. These peptides vary across species with the mycobacterial stem peptide made up of L-alanyl (L-Ala), D-iso-glutaminyl (D-Glu), meso-diaminopimelic acid (*m*DAP) and a terminal D-Ala-D-Ala (Vollmer et al., 2008a). Mycobacterial PG has unique properties including the occurrence of *N*-glycosylated muramic acid, amidated L-glutamate and *m*DAP residues, extensively cross-linked PG and increased

resistance of the PG to lysozyme (Dhople, 1983, Mahapatra et al., 2005, Lavollay et al., 2008, Kumar et al., 2012). In mycobacteria 75% of the PG is cross-linked with the 80% of the cross-links in stationary phase consisting of 3→3 cross-linkages occurring between two *m*DAP residues of different stem peptides (Crick et al., 2001, Lavollay et al., 2008). These cross-linkages have been shown to be important for virulence and polar growth of mycobacteria. Another type of cross-link known as 3→4 cross-linkages forms between the *m*DAP residue on one stem peptide and the D-Ala residue of an adjacent stem peptide, which is the type of cross-link predominantly found in other bacterial species (Vollmer et al., 2008a).

1.6.1.1 Biosynthesis of PG

The PG precursor – Lipid II – is generated in the cytoplasm and is translocated to the periplasm where it is incorporated into existing, cross-linked PG by the penicillin binding proteins (PBPs) encoded by *ponA1* and *ponA2* and distinct glycosyl transferases (Hett and Rubin, 2008, Vollmer and Bertsche, 2008).

Synthesis of PG requires a number of enzymes and reactions that occur in both the cytoplasm and periplasm, Figure 1.3. The first step of synthesis begins when uridine diphosphate (UDP) is linked to a NAG residue forming UDP-NAG. Enol pyruvate is added to NAG which is then reduced to form NAM. A series of reactions then occur to attach the stem peptide beginning with L-Ala, then D-Glu, *m*DAP and then finally the addition of the two terminal D-Ala residues simultaneously to NAM. Lipid I is formed by the removal of UDP and UDP-NAG is linked to the NAM pentapeptide residue forming Lipid II which is then flipped across the plasma membrane into the periplasm. Lipid II is then incorporated into existing PG through a transglycosylase reaction and the PG is then further strengthened by cross-linking of the stem peptide through a transpeptidase reaction (Crick et al., 2001).

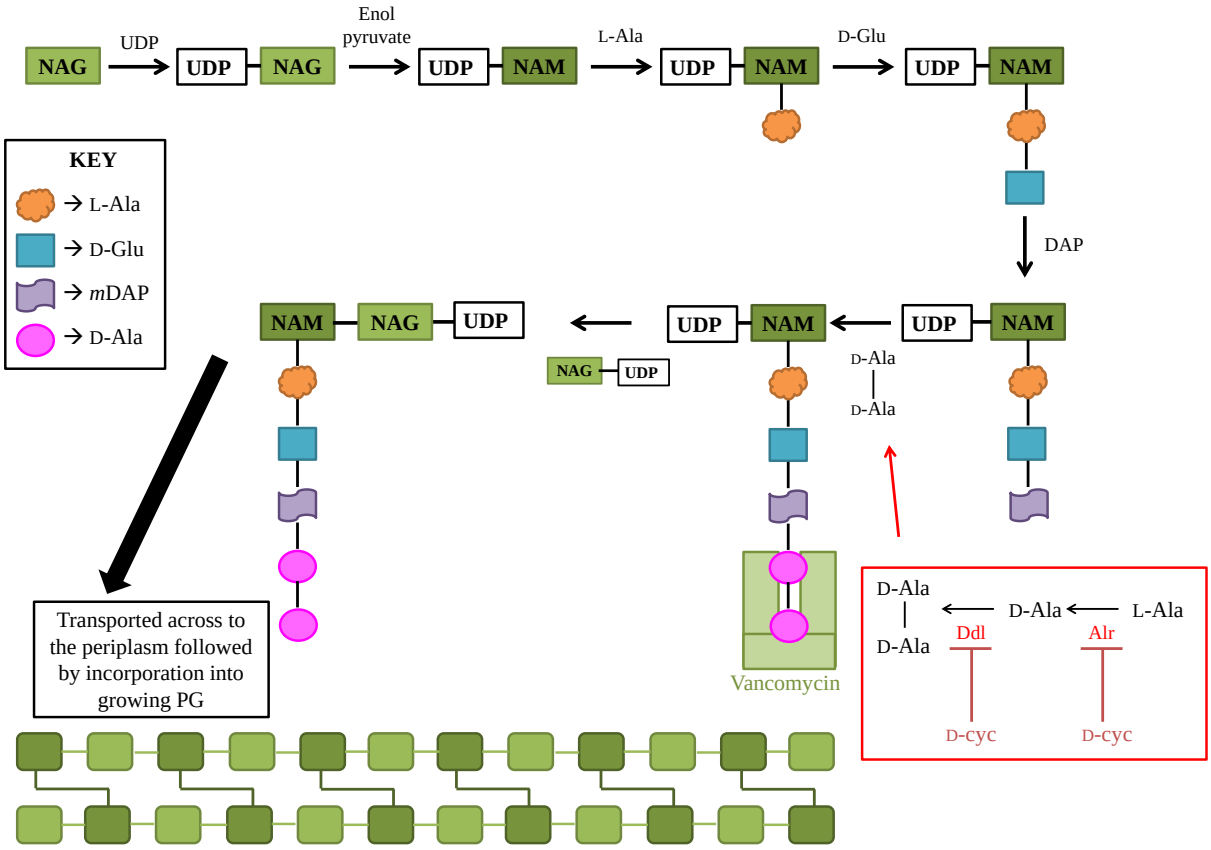

Figure 1.3. Diagrammatic representation of peptidoglycan biosynthesis pathway. The pathway begins with the linkage of uridine diphosphate to *N*-acetylglucosamine followed by the addition of enol pyruvate. Enol pyruvate is then reduced to form *N*-acetylmuramic acid and the stem peptide is then attached through a series of steps resulting in the formation of Lipid II which is flipped across into the periplasm where it is incorporated into the existing peptidoglycan. The red box indicates the racemization of L-Alanine and the condensation of two D-Alanine molecules by alanine racemase and D-alanine ligase respectively. The antibiotics vancomycin and D-cycloserine are also indicated. (Vollmer et al, 2008b)

1.7. Antibiotics that target PG

1.7.1. β-lactam antibiotics

β-lactam antibiotics are broad spectrum antibiotics that include penicillins, cephalosporins and carbapenems and are distinguished by a four-membered β-lactam active ring (Waxman and Strominger, 1983). They are substrate analogues of the PBPs that bear structural similarity to the D-Ala-D-Ala motif and inhibit PBPs by forming an irreversible intermediate within the active site of the enzyme (Waxman and Strominger, 1983). This leads to blockage of transpeptidation reactions resulting in weakened PG, inhibition of growth and in some

cases, cell lysis (Tipper and Strominger, 1965). β-lactams have been in use for decades, which has resulted in the emergence of a number of resistance mechanisms including the expression of low affinity PBPs, increased efflux of antibiotic, subtle changes in the PG to render it resistant, expression of LD-transpeptidases (Ldts) and degradation of β-lactams by β-lactamases (Nikolaidis et al., 2013). Expression of Ldts allows bypassing of the 3→4 cross-linking step and has resulted in a high prevalence of ampicillin resistance and a moderate increase in resistance to ceftriaxone. The expression of β-lactamases results in hydrolysis of the β-lactam ring which causes inactivation of the antibiotic before it reaches its target (Nikolaidis et al., 2013). PBPs involved in β-lactam resistance have mutations across the entire protein sequence, with the majority found around the active site (Nikolaidis et al., 2013).

1.7.2. Vancomycin

Vancomycin is a glycopeptide used to treat gram positive bacterial infections such as methicillin resistant *Staphylococcus aureus* (MRSA) (Weigel et al., 2003). The antibiotic binds to the D-Ala-D-Ala residues of the stem peptide preventing the cross-linking of stem peptides within the PG, Figure 1.3 (Barna and Williams, 1984). Vancomycin resistance in *S. aureus* has been attributed to the *vanG* gene which produces a D-Ala-D-Ala dimer (Weigel et al., 2003). This dimer is incorporated into the stem peptide during PG biosynthesis, thus decreasing the binding affinity of vancomycin by 1000-fold (Bugg et al., 1991).

1.7.3. D-cycloserine

D-cycloserine, known also as seromycin, is a broad spectrum antibiotic produced by some *Streptomyces* species (Barreteau et al., 2008). It is a cyclic structural analogue of D-Ala and is commonly used as a second line drug for the treatment of MDR and XDR TB (Caminero et al., 2010). The synthesis of D-Ala-D-Ala requires racemization of L-Ala and condensation of

two D-Ala molecules carried out by alanine racemase (Alr) and D-alanine ligase (Ddl) respectively, Figure 1.3 (Barreteau et al., 2008). D-cycloserine inhibits both Alr and Ddl but has been shown to preferentially interact with Ddl (Prosser and de Carvalho, 2013). In *M. smegmatis*, resistance to D-cycloserine is acquired through overexpression of the Alr encoding gene which occurs due to a mutation in the promoter region (Caceres et al., 1997).

1.8. PG remodeling enzymes

A number of enzymes are involved in remodeling the PG including synthases and hydrolases (Vollmer and Bertsche, 2008, Vollmer et al., 2008b). This constant remodeling of the PG is required for cell expansion, cell separation and signaling (Vollmer et al., 2008a). In order for remodeling to occur, existing PG needs to be degraded so that new subunits can be incorporated. Remodeling of the PG is carried out by hydrolases which break down a number of bonds, with a specific enzyme existing for each structurally distinct bond in the PG, Figure 1.4. Glycosidases hydrolyze glycosidic bonds (Vollmer et al., 2008a). Amidases and peptidases hydrolyze amide and peptide bonds respectively (Vollmer et al., 2008a). Hydrolases digest the PG into small fragments and if they are not carefully controlled, their activity could result in autolysis. Consequently, these enzymes have also been termed autolysins (Vollmer et al., 2008b).

Ldts are responsible for forming the 3→3 cross-links between stem peptides by cleaving between the D-Ala and *m*DAP of two separate peptides, followed by subsequent linkage between two *m*DAP residues of the stem peptides, Figure 1.4 (Mainardi et al., 2002). It has been demonstrated that the 3→3 cross-links are found in the stationary phase of mycobacterial growth however, recent evidence suggests that these cross-links predominate during all stages of mycobacterial growth (Wietzerbin et al., 1974, Lavollay et al., 2008, Kumar et al., 2012). Mtb encodes five Ldts – Ldt_{MT1}, Ldt_{MT2}, Ldt_{MT3}, Ldt_{MT4} and Ldt_{MT5}

(Gupta et al., 2010, Sanders et al., 2014). Deletion of Ldt_{MT1} only and Ldt_{MT1} combined with Ldt_{MT2}, resulted in decreased virulence, altered morphology, increased sensitivity to vancomycin, decreased growth in liquid culture, altered localization of some proteins and an increased sensitivity to amoxicillin-clavulanate with some of these phenotypes more pronounced in the double deletion mutants, indicating that these proteins may be functionally redundant (Gupta et al., 2010, Schoonmaker et al., 2014).

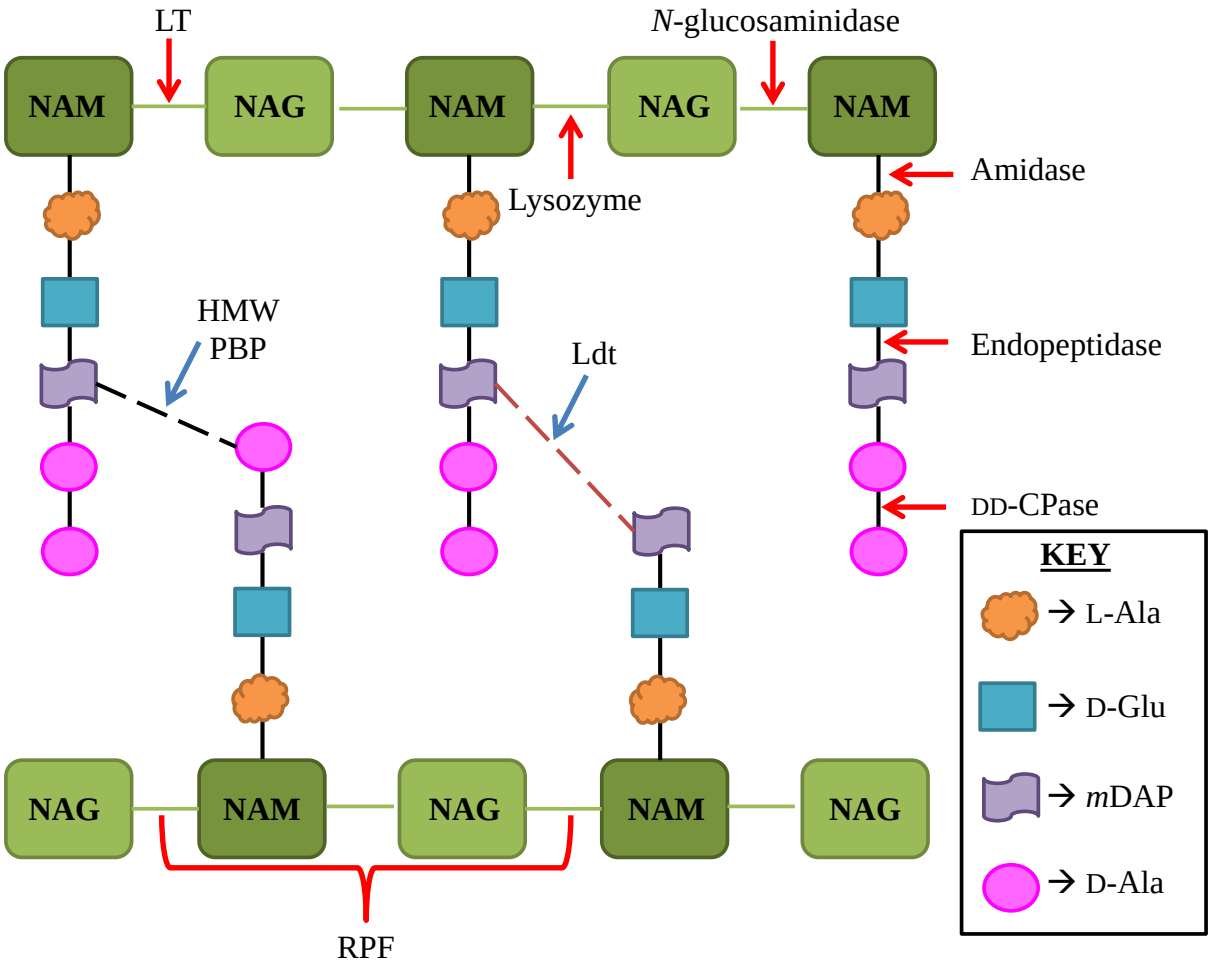

Figure 1.4. Diagrammatic representation of the structure of peptidoglycan illustrating peptidoglycan remodeling enzymes and cleavage sites. Amidases hydrolyze the bond connecting the stem peptide to the *N*-acetylmuramic acid residue; resuscitation promoting factors, lysozymes, lytic transglycosylases and *N*-glucosaminidases hydrolyze bonds in the glycan strand; endopeptidases and DD-carboxypeptidases hydrolyze bonds within the stem peptide, with the latter resulting in the release of the terminal D-Alanine. High molecular weight penicillin binding proteins remove the terminal D-Ala and form a 3→4 cross-link between stem peptides, shown by the black dashed line, whereas LD-transpeptidases form 3→3 cross-links, shown by the red dashed line. (Vollmer et al, 2008b)

1.8.1. *N*-acetylmuramyl-L-alanine-amidases

N-acetylmuramyl-L-alanine-amidases, henceforth referred to as amidases, are zinc metalloenzymes responsible for hydrolyzing the amide bond between NAM and the first L-Ala of the stem peptide, which results in separation of the peptide stem from the glycan strand, Figure 1.4 (McCall et al., 2000, Heidrich et al., 2001). Amidases carry a signal peptide at their N-terminus which allows for transport of the protein across the cytoplasmic membrane (Vollmer et al., 2008b). LytA is an amidase found in the cytoplasm of *Streptococcus pneumoniae*, which has been indicated as an essential disease causing factor and been shown to interact with the PG substrates (Hirst et al., 2008, Mellroth et al., 2013). *E. coli* has five amidases – AmiA, AmiB, AmiC, AmiD and AmpD – with AmiA, AmiB, AmiC and AmiD localizing in the periplasm and AmpD localizing in the cytoplasm (Heidrich et al., 2001, Korsak et al., 2005a). After removal of the signal peptide, AmiA - AmiC are soluble in the periplasm and AmiD is synthesized as a prelipoprotein (Heidrich et al., 2001, Korsak et al., 2005a). AmiA - AmiC only hydrolyzes PG in the cross-linked confirmation found in the cell wall whereas AmpD can only hydrolyze PG in the form of anhydromuropeptides. On the other hand, AmiD is able to hydrolyze PG irrespective of conformation (Heidrich et al., 2001, Korsak et al., 2005a). Mutational analysis in *E. coli* has identified a role for these enzymes in degradation of septal PG. This is evidenced by the demonstration that an *E. coli* triple mutant lacking AmiA, AmiB and AmiC produced miniature cells, which were part of long cell chains reflective of cells that were unable to complete cell separation (Heidrich et al., 2001). Additionally, this triple amidase mutant displayed increased sensitivity to certain antibiotics suggesting that the amidases play a role in cell growth and division as well as antibiotic resistance with chaining occurring due to a defect in septal cleavage (Heidrich et al., 2001). In order for the amidases to efficiently hydrolyze PG in *E. coli*, these proteins must be activated by LytM domain proteins (Peters et al., 2011). The known activators of *E. coli*

amidases are EnvC and NlpD with EnvC activating AmiA and AmiB and NlpD activating AmiC (Uehara et al., 2009, Uehara et al., 2010). The binding of the activators results in an open active site conformational change of the amidases and subsequent binding and hydrolysis of PG (Yang et al., 2012).

AmiD is bound to the plasma membrane and has been proposed to play a role in immune evasion due to its ability to hydrolyze PG in any conformation (Uehara and Park, 2007). AmpD is a cytoplasmic PG amidase and has been indicated in control of β-lactamase expression by hydrolyzing anhydromuropeptides, which serve as signaling molecules that activate β-lactamase expression (Jacobs et al., 1994, Heidrich et al., 2001).

Mtb encodes four amidase containing genes – *ami1, ami2, ami3* and *ami4* (Machowski et al., 2014) with *ami1* and *ami2* containing an amidase_3 domain and *ami3* and *ami4* containing an amidase_2 domain (Vollmer et al., 2008b, Machowski et al., 2014). A study conducted at the CBTBR (where this MSc was carried out) demonstrated that in *M. smegmatis*, Ami2 is essential and Ami1 plays a role in cell division (Senzani et al., unpublished). The Ami1 homologue encoded by Rv3717 in Mtb lacks a cell wall binding domain and is probably directed to PG by a partnering protein or other distinct mechanisms that have yet to be identified (Kumar et al., 2013). The enzymatic activity of Rv3717 was not required for growth in vitro, however its biochemical activity on PG suggests a possible role in recycling of the PG, which has not been established in mycobacterial species (Prigozhin et al., 2013). Another amidase in Mtb, Rv3915, is homologous to *E. coli* AmiC, with the ability to hydrolyze cell wall fragments and cross-linked PG (Prigozhin et al., 2013, Sharma et al., 2015).

1.8.2. Resuscitation Promoting Factors

Resuscitation promoting factors (RPFs) are a group of cell wall hydrolyzing enzymes that are found in the culture filtrate of growing cells and were first described in *M. luteus* (Mukamolova et al., 1998). These enzymes have been shown to play a role in the reactivation of dormant bacteria through an as yet unknown mechanism (Mukamolova et al., 1998, Mukamolova et al., 2002). Rpf-like homologues are found in GC-rich, gram positive bacteria including mycobacteria with Mtb encoding five homologues, RpfA – RpfE, which are collectively essential for resuscitation from a dormant state in vitro (Kana et al., 2008, Machowski et al., 2014). Various deletion studies conducted in Mtb have identified a level of functional specialization between Rpf homologues. Single deletion mutants lacking one of the five Rpfs were viable and grew similarly to wild type with each of the enzymes differentially expressed at various growth phases (Tufariello et al., 2004). The deletion of *rpfB* singularly and in combination with *rpfA* resulted in delayed reactivation of growth from dormancy and defects in colony morphology (Tufariello et al., 2006, Russell-Goldman et al., 2008), with two different triple mutants – Δ*rpfA* Δ*rpfC* Δ*rpfB* and Δ*rpfA* Δ*rpfC* Δ*rpfD* – showing poor resuscitation ability (Downing et al., 2005). A functional hierarchy between the Rpfs in Mtb has also been established with RpfB and RpfE ranking highest with respect to their ability to restore the colony forming defect in a quintuple Rpf-deletion mutant (Kana et al., 2008). These two Rpfs have also been shown to interact with the Rpf Interacting Protein A (RipA), with this interaction serving as the driving force for septal PG hydrolysis (Hett et al., 2007).

1.8.3. *N*-acetyl-β-D-muramidases

N-acetyl-β-D-muramidases (*N*-muramidases) cleave -1,4-glycosidic bonds between NAG and NAM residues and are subdivided into lysozymes and lytic transglycosylases (LTs) based on

cleavage products, Figure 1.4 (Vollmer et al., 2008b). Lysozymes are produced in a number of organisms including fungi, phages, bacteria, vertebrates and invertebrates. These are endolytic hydrolases that cleave within the glycan strands and are predicted to play a role in septation (Vollmer et al., 2008b). Modification of the NAM residue during catalysis results in the formation of a 1-6 anhydromuramyl ring produced by LTs (Vollmer et al., 2008b). LTs are exolytic hydrolases that produce the 1,6 anhydromuropeptide by cleaving the terminal NAM residue (Vollmer et al., 2008b).

1.8.4. *N*-acetyl-β-D-glucosaminidases

N-acetyl-β-D-glucosaminidases (*N*-glucosaminidases) hydrolyze the glycosidic bonds between the NAG and adjacent NAM residues, Figure 1.4 (Vollmer et al., 2008b). These enzymes are widely spread in bacteria and often have one or several PG binding domains (Vollmer et al., 2008b). No substantive research has been done on these enzymes although, they have been shown to play a role in cell wall turnover (Vollmer et al., 2008b).

1.8.5. Penicillin binding proteins

PBPs are a family of acyl-serine transferases that have been the primary target of β-lactam antibiotics for over fifty years and are ubiquitous in bacteria that have PG (Ghuysen, 1991, Sauvage et al., 2008). These enzymes are important for PG biosynthesis and remodeling as they perform the final steps of synthesis by polymerization and cross-linking of the PG (Sauvage et al., 2008, Vollmer et al., 2008a, Derouaux et al., 2013). PBPs are divided into high molecular weight (HMW) and low molecular weight (LMW) counterparts based on their mobility during SDS polyacrylamide gel electrophoresis (PAGE). HMW PBPs can be subdivided into class A and class B with the former comprising bifunctional enzymes possessing both transglycosylase and transpeptidase functions and class B enzymes possessing transpeptidase activity only (Sauvage et al., 2008). LMW or class C PBPs consist

of endopeptidases and carboxypeptidases (Sauvage et al., 2008). Most PBPs are anchored to the cytoplasmic membrane with the active site in the periplasm. All PBPs possess one of the following motifs – SXXK, SXN or KTG – which are responsible for enzymatic activity with 'X' being a variable amino acid (Sauvage et al., 2008). The serine residue of the SXXK motif is central to the catalytic core and mediates acylation and deacylation reactions during PG synthesis (Sauvage et al., 2008). In *B. subtilis*, these enzymes have been shown play a role in synthesis of PG during vegetative growth, cell division and sporulation (Sauvage et al., 2008).

1.8.5.1. HMW PBPs

HMW PBPs have been shown to be important for cell elongation, maintenance of cell morphology and septation. The bifunctional class A HMW PBPs possess an N-terminal glycosyltransferase domain and a C-terminal transpeptidase domain, which are responsible for catalyzing the polymerization of the glycan strand and cross-linking of the stem peptides between the glycan strands respectively, Figure 1.4 (Sauvage et al., 2008). Class B PBPs possess only a C-terminal transpeptidase domain and have been shown to be important for elongation in some organisms (Sauvage et al., 2008). Transglycosylation results in the extension of glycan strands, while transpeptidation results in linkage of the amino group of the *m*DAP of one stem peptides to the carbonyl group of D-Ala in an adjacent stem peptide, together with the release of the terminal D-Ala (Sauvage et al., 2008).

Most organisms contain a number of bifunctional PBPs with the exception of *Neisseria gonorrhea*, which possesses a single essential bifunctional PBP (PBP1), as well as one class B PBP, PBP2 (Sauvage et al., 2008). In *E. coli*, the class A PBPs - PBP1a and PBP1b – can be deleted individually but loss of both proteins is not tolerated (Denome et al., 1999). Similarly, the class B PBP2 and PBP3 have been shown to be essential for elongation and

division respectively (Sauvage et al., 2008). In *B. subtilis*, PBP1 is required for sporulation (Scheffers and Errington, 2004) and PBP2b is required for cell division (Daniel et al., 2000). *S. pneumonia* encodes three class A PBPs which are all dispensable for growth, indicating functional redundancy between the homologues (Paik et al., 1999). In addition, *S. pneumonia* has two essential class B PBPs, PBP2x and PBP2b, which play a role in septum formation and peripheral PG synthesis respectively (Kell et al., 1993, Sham et al., 2012). Mtb encodes two class A PBPs, PBP1 and PBP1a, encoded by *ponA1* and *ponA2* respectively and three class B PBPs, PBPa, PBP2 and PBP-lipoprotein, encoded by *pbpA*, *pbpB* and *Rv2864c* respectively (Sauvage et al., 2008, Machowski et al., 2014).

1.8.5.2. LMW PBPs

LMW PBPs consist of endopeptidases and carboxypeptidases (Sauvage et al., 2008, Vollmer et al., 2008b) and play a role in symmetrical cell division with their activity proposed to be linked to FtsZ as mutants defective for these enzymes have misshapen and branched cells (Frirdich and Gaynor, 2013). Endopeptidases cleave various non-terminal LD- and DD- bonds within the peptide stem, Figure 1.4, and can interact with teichoic acids (Vollmer et al., 2008b). *E. coli* encodes two LMW endopeptidases, these include PBP4 which displays DD-CPase activity and PBP7 plays a role in biofilm formation and septum cleavage (Ghosh et al., 2008, Sauvage et al., 2008, Vollmer et al., 2008b). The best characterized endopeptidase in Mtb is RipA, which is essential for growth in vitro and has been associated with reactivation from a dormant state due to its synergistic relationship with RpfB and RpfE (Hett et al., 2007). The RpfB-RipA interaction releases muropeptides which are able to resuscitate dormant cells (Nikitushkin et al., 2015).

The enzymatically redundant DD-CPases are proposed to be responsible for regulating the amount of cross-linking that occurs in the PG (Ghuysen, 1991). They act by cleaving the

terminal D-Ala from the pentapeptide side chain, Figure 1.4 (Ghosh et al., 2008, Sauvage et al., 2008, Vollmer et al., 2008b). This is achieved through a three step mechanism beginning with the formation of a reversible non-covalent complex between the enzyme and the PG stem pentapeptide, leading to the formation of an acyl-enzyme intermediate (Sauvage et al., 2008). In the case of a carboxypeptidation reaction, this is followed by deacylation, which occurs through hydrolysis resulting in the release of the terminal D-Ala, Figure 1.5B (Sauvage et al., 2008). A transpeptidation reaction differs in that the deacylation of the enzyme results in cross-linking of two stem peptides, Figure 1.5A (Sauvage et al., 2008). As the DD-CPases do not form cross-links per se, their activity is postulated to control the total amount of cross-linking as removal of the terminal D-Ala creates a tetrapeptide which cannot serve as a substrate for the formation of 3→4 cross-links (Hammes and Seidel, 1978).

E. coli contains four DD-CPases –PBP4, PBP5, PBP6 and PBP6b – encoded by *dacB, dacA dacC* and *dacD* genes respectively (Ghosh et al., 2008, Sauvage et al., 2008). These enzymes are non-essential for the growth of *E. coli* (Denome et al., 1999). PBP4 acts primarily as an endopeptidase in *E. coli* but has both endopeptidase and DD-CPase activity, with a single mutant showing no altered morphological or growth defects (Korat et al., 1991, Meberg et al., 2004, Ghosh et al., 2008). PBP5 of *E. coli* is the most abundant and best studied DD-CPase, playing an important role in maintaining the morphology, diameter and contour of *E. coli* cells (Sauvage et al., 2008). Deletion of PBP5 in an AmiC deletion background increased the chaining defect of the single amidase mutant (Priyadarshini et al., 2006), while overexpression of PBP5 is detrimental, resulting in the growth of spherical cells that eventually lyse (Ghosh et al., 2008). A PBP *E. coli* mutant, containing PBP5 but lacking PBP4, PBP6, PBP7, AmpC, AmpH and either PBP1 or PBP2 remained viable and displayed normal rod- shaped morphology (Denome et al., 1999). However, deletion of PBP5 in a mutant lacking the above-mentioned PBPs and other PBP mutant backgrounds resulted in

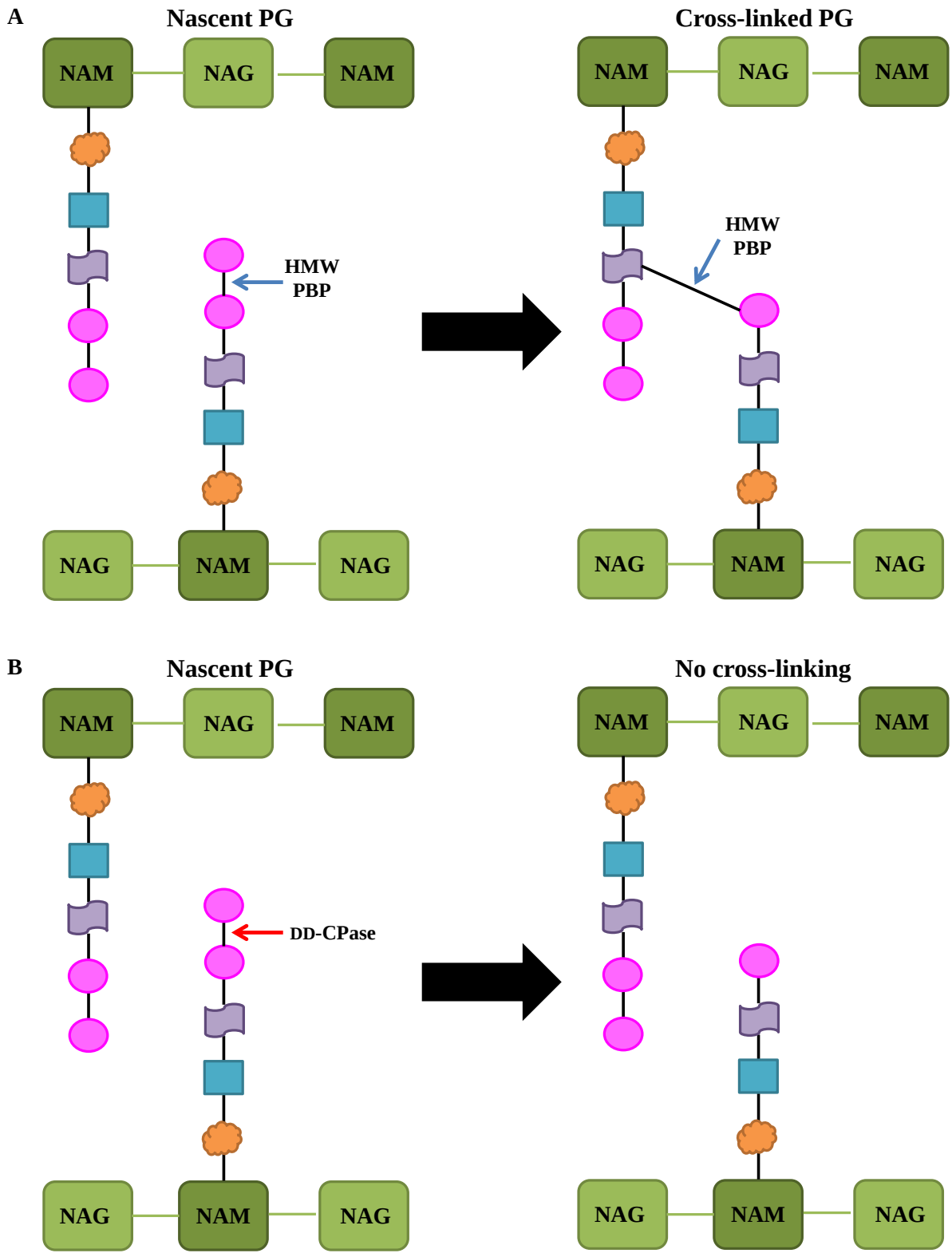

Figure 1.5. Diagrammatic representation of high molecular weight penicillin binding proteins and DD-carboxypeptidase activity within the stem peptides of peptidoglycan. (A) Activity of high molecular weight penicillin binding proteins. Nascent peptidoglycan is cross-linked by high molecular weight penicillin binding proteins which act by cleaving the terminal D-Alanine and through a transpeptidation reaction cross-links two stem peptides. (B) Activity of DD-carboxypeptidases. The terminal D-Alanine is cleaved by a DD-carboxypeptidases which is then removed by hydrolysis and does not result in crosslinking of the peptidoglycan. (Vollmer et al, 2008b)

increased cell lysis, enhanced antibiotic sensitivity, inhibition of biofilm formation and morphological defects (Denome et al., 1999). These phenotypes were restored when wild type PBP5 was expressed in the mutants, with restoration dependent on both the DD-CPase activity of PBP5 as well as the C-terminal domain (Ghosh et al., 2008). PBP6, which shares 65% identity with PBP5, is unable to compensate for loss of PBP5 and does not revert these phenotypic defects (Ghosh et al., 2008). PBP5 and PBP6 share the *bolA* transcriptional regulator with both enzymes being able to restore cell division in a PBP3 single deletion mutant (Ghosh et al., 2008). The deletion of PBP6 or PBP6b does not alter morphology with expression of these proteins increased during stationary and mid log phase respectively (Baquero et al., 1996, Santos et al., 2002). Although PBP5, PBP6 and PBP6b share similar primary structures, it is likely that they have distinct functions in vivo during the different stages of growth (Broome-Smith et al., 1988, Ghosh and Young, 2003, Ghosh et al., 2008).

B. subtilis encodes numerous PBPs including PBP4a, PBP5, PBP5* and DacF, with PBP5* being the best characterized DD-CPase (Sauvage et al., 2008). PBP4a is equivalent to PBP4 of *E. coli* and PBP5 has been found in vegetative growth, with no role in PG synthesis in *Bacillus* spores (Sauvage et al., 2008). A mutant lacking PBP5 has an increased ratio of pentapeptides to tripeptides in the PG (Atrih et al., 1999) confirming the role of DD-CPases in cleaving the terminal D-Ala. PBP5* and DacF are functionally redundant to some extent, with both proteins shown to regulate the amount of cross-linking in the PG of the spore (Popham et al., 1995, Popham et al., 1999).

Some bacterial species such as *Helicobacter pylori* and *Caulobacter crescentus* do not possess obvious DD-CPase homologues (Sauvage et al., 2008). Other bacterial species such as *S. aureus* contains only one LMW PBP (PBP4), which is equivalent to PBP5, and possesses secondary transpeptidase activity (Wyke et al., 1981). *Listeria monocytogenes* possesses one class C PBP (PBP5), with deletion resulting in altered shape and morphology

as well as a thicker cell wall (Korsak et al., 2005b, Guinane et al., 2006). *S. pneumonia* has a single class C PBP (PBP3), which plays a role in organization of growth and division processes with the deletion mutant displaying morphological and cell division defects (Morlot et al., 2004, Morlot et al., 2005). In *Vibrio cholerae* four LMW PBPs have been identified with two, DacA-1 and DacA-2, being DD-CPases (Moll et al., 2015). Deletion of the LMW PBPs with the exception of DacA-1 did not result in any changes (Moll et al., 2015). Deletion of DacA-1 has been shown to impair the growth and morphology of *V. cholerae* in standard laboratory media, an effect that is exacerbated in media with increased salt concentrations, suggesting that DacA-1 plays a role in adaptation to salt stress (Moll et al., 2015). These examples, in addition to sequence homology retained across species, indicate the importance of DD-CPases in cell wall homeostasis.

The role of LMW PBPs from mycobacterial species in bacterial growth and expansion of PG remains unknown. The mycobacterial species Mtb and *M. smegmatis* both harbor a number of LMW PBPs (Sauvage et al., 2008, Machowski et al., 2014). Mtb possesses three class C PBPs encoded by Rv3627c, *dacB1* and *dacB2* with homologues of these proteins identified in *M. smegmatis* as MSMEG_6113 (referred to as DacB) corresponding to Rv3627c, MSMEG_1661 corresponding to *dacB1*, and the duplicated MSMEG_2432 and MSMEG_2433 both corresponding to *dacB2* (Sauvage et al., 2008, Machowski et al., 2014). MSMEG_1990 has been found in the environmental strains as well as *M. abscessus* but is not present in other pathogenic mycobacterial species. A recent study showed that overproduction of Mtb *dacB2* in *M. smegmatis* resulted in altered colony morphology, reduced growth, defects in sliding motility and biofilm formation, while the deletion of *dacB2* lead to reduced growth in minimal media under acidic conditions and low oxygen availability (Bourai et al., 2011). Treatment with the β-lactam antibiotic meropenem directly

inhibited *dacB2*, leading to the accumulation of pentapeptides and lysis of cells (Kumar et al., 2012).

At the CBTBR, single knockout mutants lacking MSMEG_1661, MSMEG_2432 or MSMEG_2433 were created by Dr. C. Ealand and displayed no changes in growth rates, cell morphology, drug susceptibility or incorporation of new PG (Ealand et al., unpublished data). In addition, Dr. Ealand was unable to delete *dacB*, suggesting that this gene is essential. Additionally, these four proteins were also shown to play a role in cell size maintenance as heterologous expression of a single one of these DD-CPases resulted in cell length changes of an *E. coli* mutant lacking three PBPs (Ealand et al., unpublished).

1.9. Aims

Research in a diversity of organisms have highlighted functional redundancy in LMW PBPs, necessitating the deletion of more than a single DD-CPase to identify any notable phenotypic differences. Considering this, and the lack of any growth/cell division or morphological defects in single DD-CPase mutants of *M. smegmatis*, this MSc was aimed at generating and characterizing combinatorial mutants of *M. smegmatis* that are deficient for two DD-CPases in different combinations. We also attempted to create recombinant forms of these enzymes to test catalytic proficiency. The specific objectives were:

- To create knockout mutants of *M. smegmatis*, lacking two or three DD-CPases, using existing single deletion mutants. Mutants targeted for generation were: ΔMSMEG_2433 ΔMSMEG_2432, ΔMSMEG_2432 ΔMSMEG_1661 and ΔMSMEG_1661 ΔMSMEG_2433 and ΔMSMEG_2433 ΔMSMEG_2432 ΔMSMEG_1661.
- Characterizing phenotypic effects of these gene deletions on the growth and morphology of *M. smegmatis.*

- To create recombinant forms of the four DD-CPases (*dacB*, MSMEG_1661, MSMEG_2432 and MSMEG_2433) from *M. smegmatis*.

We hypothesize that deletion of multiple DD-CPases will result in abnormal colony morphology, defective growth rates, delayed biofilm formation, altered sliding motility and increased antibiotic sensitivity. We also hypothesize that deletion of the DD-CPases will affect cell growth and division *M. smegmatis*.

2. Methods

2.1 Reagents

A detailed list of reagents used in this study can be found in Appendix A.

2.2 Bacterial strains and culture conditions

For *E. coli* strains, cultures were grown in Luria-Bertani broth (LB) or agar (LA) supplemented with the appropriate antibiotics at the following concentrations: Kanamycin (Kan) 50 µg/ml, Hygromycin (Hyg) 200 µg/ml, Ampicillin (Amp) 100 µg/ml and Chloramphenicol (Camp) 34 µg/ml. Cultures were incubated at 37 °C for strains containing plasmids smaller than 8 kbp, whereas cultures with strains containing plasmids larger than 8 kbp were incubated at 30 °C. Liquid cultures grown in LB were done so with shaking at 250 rpm.

For *M. smegmatis* strains, cultures were grown in Middlebrook 7H9 broth (Difco) supplemented with 0.5% glycerol, 0.2% glucose, 0.085% NaCl and 0.05% Tween 80 with shaking or on Middlebrook 7H10 agar (Difco) supplemented with 0.5% glycerol, 0.2% glucose and 0.085% NaCl. Media was supplemented with the appropriate antibiotic at the following conditions: Kan 25 µg/ml, Hyg 50 µg/ml.

All strains and plasmids used/generated in this study are listed in Table 2.1.

Table 2.1. Strains and plasmids

	Description	**Source/ Reference**
Strains		
E. coli		
DH5α	Cloning strain with high transformation efficiency	Promega

BL21 (DE3) pLysS	Protein expression strain with IPTG-inducible gene for T7 RNA polymerase. Camp^r	Promega
M. smegmatis		
mc^{2}155	efficient plasmid transformation mutant of mc26	(Snapper et al., 1990)
ΔMSMEG_1661	Derivative of mc^{2}155 carrying an unmarked, in-frame deletion in *M. smegmatis* MSMEG_1661 (1158 bp internal region excised)	(Ealand et al., unpublished)
ΔMSMEG_2432	Derivative of mc^{2}155 carrying an unmarked, out-of-frame deletion in *M. smegmatis* MSMEG_2432 (786 bp internal region excised)	(Ealand et al., unpublished)
ΔMSMEG_2433	Derivative of mc^{2}155 carrying an unmarked, out-of-frame deletion in *M. smegmatis* MSMEG_2433 (870 bp internal region excised)	(Ealand et al., unpublished)
ΔMSMEG_1661 ΔMSMEG_2432	Derivative of ΔMSMEG_1661 carrying an unmarked , out-of-frame deletion in *M. smegmatis* MSMEG_2432 (786 bp internal region excised)	This study
ΔMSMEG_2433 ΔMSMEG_1661	Derivative of ΔMSMEG_2433 carrying an unmarked , in-frame deletion in *M. smegmatis* MSMEG_1661 (1158 bp internal region excised)	This study
ΔMSMEG_1661 ΔMSMEG_2432:: MSMEG_1661	Derivative of ΔMSMEG_1661 ΔMSMEG_2432 carrying a full length copy of MSMEG_1661 (1194 bp) at the *attB* site. Constructed by electroporation with the pMV1661 vector; Hyg^r	This study
ΔMSMEG_2433 ΔMSMEG_1661:: MSMEG 1661	Derivative of ΔMSMEG_2433 ΔMSMEG_1661 carrying a full length copy of MSMEG_1661 (1194 bp) at the *attB* site.	This study

	Constructed by electroporation with pMV1661 vector; Hyg^r	
Plasmids		
p2NIL	*E. coli* cloning vector, Kan^r	(Parish and Stoker, 2000)
pGOAL19	Plasmid carrying *lacZ-sacB-Hyg*^{r} markers as a *PacI* cassette; Hyg^r	(Parish and Stoker, 2000)
p2NIL_PAC_1661	Knockout vector for creating ΔMSMEG_1661 mutant. The 1.2 kbp upstream region including 18 bp of the 5' sequence of MSMEG_2433 was PCR-amplified to incorporate *Hin*DIII and *Nde*I restriction sites. The 1.2 kbp downstream was similarly obtained but incorporated at *Nde*I and *Acc*65I restriction sites. The fragments were cloned into p2NIL and the *PacI* cassette from pGOAL19 was inserted; Kan^r Hyg^r.	(Ealand et al., unpublished)
p2NIL_PAC_2432	Knockout vector for creating ΔMSMEG_2432 mutant. The 1.2 kbp upstream region including 18 bp of the 5' sequence of MSMEG_2432 was PCR-amplified to incorporate *Hin*DIII and *Nde*I restriction sites. The 1.2 kbp downstream was similarly obtained but incorporated at *Nde*I and *Acc*65I restriction sites. The fragments were cloned into p2NIL and the *PacI* cassette from pGOAL19 was inserted; Kan^{r}Hyg^r.	(Ealand et al., unpublished)
p2NIL_PAC_2433	Knockout vector for creating ΔMSMEG_2433 mutant. The 1.2 kbp upstream region including 18 bp of the 5' sequence of MSMEG_2433 was PCR-amplified to incorporate *Hin*DIII and *Nde*I restriction sites. The 1.2 kbp downstream was similarly	(Ealand et al., unpublished)

	obtained but incorporated at *Nde*I and *Acc*65I restriction sites. The fragments were cloned into p2NIL and the *PacI* cassette from pGOAL19 was inserted; Kan^rHyg^r.	
pMV306H	*E. coli-Mycobacterium* integrating shuttle vector. Integrates at the L5 *attB* site in mycobacteria. Hyg^r	H. Boshoff
pMV1661	Derivative of pMV306H carrying a full length copy of MSMEG_1661 (1194 bp) plus 150 bp upstream of start codon representative of native promoter sequence; Hyg^r	(Ealand et al., unpublished)
pET29a	*E. coli* protein expression vector carrying a C-terminal His-tag. Kan^r	Novagen
pET29a_dacB	Derivative of pET29a carrying a full length copy of *dacB*	This study
pET29a_1661	Derivative of pET29a carrying a full length copy of MSMEG_1661	This study
pET29a_2432	Derivative of pET29a carrying a full length copy of MSMEG_2432	This study
pET29a_2433	Derivative of pET29a carrying a full length copy of MSMEG_2433	This study

2.3 DNA extractions

2.3.1 Plasmid DNA extraction from *E. coli*

2.3.1.1 Mini-prep using alkaline lysis method

Plasmids of interest were grown using a single colony for inoculation into 2 ml LB overnight with appropriate antibiotics, from which 1 ml was used for the extraction of DNA. Cultures were centrifuged at 10 392 × g and the pellet was resuspended in 100 µl of cold Solution I (50 mM Glucose, 25 mM Tris-HCl (pH 8), 10 mM EDTA). Thereafter 200 µl of Solution II (1% SDS, 0.2 M NaOH) was added, mixed by inversion and incubated at room temperature

for 5 min. Following incubation, 150 µl of Solution III (3 M Potassium acetate, 11.5% Acetic acid) was added and the sample was incubated on ice for 5 min. Samples were then centrifuged at room temperature for 10 min and the supernatant was transferred to a clean Eppendorf tube. A 1 µl aliquot of RNaseA (10 mg/ml) was added to the supernatant and incubated at 42 °C for 15 min. Plasmid DNA was precipitated by the addition of 600 µl of Isopropanol, washed with 70% ethanol and resuspended in sterile distilled water (sdH_2O). DNA was then subjected to ethanol precipitation by adding 1/10 volume of 3 M sodium acetate (pH 5.3) and 3× volume of 100% cold ethanol. DNA was collected by centrifugation at 10 392 × g for 20 min at 4 °C. The pellet was then washed with 70% ethanol, dried using an Eppendorf Concentrator 5301, resuspended in sdH_2O and quantified using the Nanodrop.

2.3.1.2 Maxi-prep using Nucleobond kit

Bulk DNA extractions from *E. coli* were done by either up-scaling the mini-prep method described above or by using the Machery-Nagel Nucleobond plasmid extraction kit. DNA extractions using the kit were done as per manufacturer's instructions. Briefly, cells were harvested by centrifugation at 3082 × g for 15 min. The pellet was resuspended thoroughly in Buffer S1 containing RNaseA followed by the addition Buffer S2, mixed by gently inverting and incubated at room temperature for 3 min. Following incubation, Buffer S3 was added to lyse the sample, mixed gently by inversion and incubated on ice for 5 min. The lysate was then cleared by centrifugation at 3082 × g for 30 min. While the sample was in the centrifuge, a Nucleobond AX100 column was equilibrated by allowing Buffer N2 to flow through the column. After centrifugation, the lysate was loaded on the column and allowed to flow through. The column was washed with Buffer N3 and the flow through was discarded. Plasmid DNA was eluted from the column using Buffer N5 and collected in a sterile tube. DNA was precipitated by adding 3.5 ml isopropanol followed by centrifugation at max speed for 30 min. The pellet was washed in 70% ethanol, followed by ethanol precipitation and then

dried using an Eppendorf Concentrator 5301. The dried pellet was resuspended in sdH_2O and quantified using the Nanodrop.

2.3.2 Chromosomal DNA extraction from mycobacteria

2.3.2.1 Small scale DNA extraction

Half of a single colony was resuspended in 100 µl sdH_2O and incubated at 65 °C for 15 min. Thereafter, 100 µl of chloroform was added to the suspension and mixed by inversion. The sample was centrifuged at max speed for 5 min and the aqueous layer was placed into a new Eppendorf, from which 5 µl was used for PCR.

2.3.2.2 CTAB DNA extraction

This method was used for the extraction of large amounts of chromosomal DNA from *M. smegmatis*. Cells were grown to confluence on 7H10 agar plates for 3-4 days with appropriate antibiotic if necessary. Four loopfuls of cell were resuspended in 500 µl of TE buffer and incubated at 65 °C for 35 min to heat-kill the cells. Thereafter, 50 µl of lysozyme (10 mg/ml) was added to the sample and incubated at 37 °C for 1 hour. This was followed by the addition of 70 µl of 10% SDS and 6 µl of Proteinase K (10 mg/ml) to the sample and incubation at 65 °C for 2 hours. Following incubation, 100 µl of 5M NaCl and 80 µl of pre-warmed CTAB/NaCl were added to the sample. This resuspension was incubated at 65 °C for 10 min. An equal volume of chloroform: isoamyl (24:1 v/v) was added, mixed vigorously and centrifuged for 5 min at room temperature. The top aqueous layer was transferred to a new Eppendorf to which 600 µl of isopropanol was added and DNA was precipitated by centrifugation at 10 392 × g for 20 min. The pellet was washed in 70% ethanol, followed by ethanol precipitation as described in section 2.3.1.1 and then dried using an Eppendorf Concentrator 5301. The dried pellet was resuspended in sdH_2O and quantified using the Nanodrop as described in section 2.4.

2.4 DNA quantification

All DNA and RNA was quantified using the Nanodrop ND-100 Spectrophotometer (NanoDrop Technologies) and measuring absorbance of the sample at a wavelength of 260 nm.

2.5 DNA manipulation

2.5.1 Restriction digestion

Restriction enzymes were purchased either from Fermentas, New England Biolabs (NEB) or Roche Applied Science (Roche). Restriction digestions were carried out as per manufacturer's instructions with the appropriate buffers and addition of bovine serum albumin (BSA) to a final concentration of 10 µg/ml, when necessary. Briefly, 1 µg DNA was digested with 1 U enzyme and 1× appropriate buffer with the addition of sdH_2O to a final volume of 20 µl and incubated at 37 °C for 1 hour. The reaction was heat inactivated at 65 °C for 15 min unless prescribed otherwise by supplier.

2.5.2 Dephosphorylation of DNA

To prevent self-ligation of vectors during cloning, removal of phosphate groups from the termini of linearized vector was carried out. Dephosphorylation of plasmid DNA was carried out using Antarctic Alkaline Phosphotase (Roche) in 20 µl reactions containing 1 µg digested DNA, 1 U enzyme, 1× supplied buffer and sdH_2O. The reaction was incubated at 37 °C for 1 hour and then heat inactivated at 65 °C for 20 min.

2.5.3 DNA ligation

Ligations were carried out using T4 DNA Ligase enzyme (Epicentre Biotechnologies Fast-Link DNA Ligation Kit). A constant amount of vector DNA, 50 ng, was used in all ligations and the amount of insert DNA required for a 1:1 molar ratio of vector: insert was calculated using the following equation:

$$\text{Amount of insert DNA (ng)} = \frac{50\ \eta g\ x\ size\ of\ insert\ (bp)}{size\ of\ vector\ (bp)}$$

Ligation reactions contained the calculated volume of DNA, 5 U of enzyme, 0.75 µl of ATP, 1 µl of the supplied buffer and sdH_2O to a final volume of 15 µl. The reactions were incubated at room temperature for 20 min and heat inactivated at 65 °C for 10 min prior to transformation and visualization on a gel.

2.6 DNA visualization and purification

2.6.1 Agarose gel electrophoresis

Agarose gels (0.8% – 2%), Table A6, were prepared in TAE buffer with the addition of 0.5 µg/ml ethidium bromide. Electrophoresis was conducted at 80 – 100 V in electrophoresis tanks (Bio-Rad laboratories) containing TAE buffer. In all cases molecular weight markers were included on the gels to allow for size determination. Gels were visualized using a G-Box SYNGENE system with GeneSnap image acquisition software (Syngene).

2.6.2 DNA fragment purification

Fragment purification was done using the NucleoSpin Extract II Kit (Machery-Nagel). This kit allowed for the purification of PCR products as well as fragments excised from agarose gels. The protocol was carried out as per the manufacturer's instructions. Gel fragments were melted in binding buffer at 65 °C before being loaded onto the column, whereas PCR products were mixed with binding buffer and loaded directly onto the column. The column was washed with wash buffer and thereafter, DNA was eluted using 30 – 50 µl sterile distilled water.

2.6.3 DNA sequencing

Sequencing was performed by the DNA Sequencing Facility of Stellenbosch University and was carried out on all constructs generated in this study to ensure that no mutations had been

introduced into the gene of interest. Finch TV version 1.4 and the EditSeq module of the Lasergene suite software were used to analyze the sequencing data.

2.7 DNA amplification

Primers were designed using the online tool Primer3 (http://primer3.ut.ee/) using the following parameters:

Table 2.2. Primer3 parameters used for primer design

	Size (bp)	Tm (°C)	% GC
Minimum	18	55	55
Maximum	22	65	65
Optimum	20	60	62

2.7.1 Roche Fast Start Taq PCR

PCR screens for clones or mutants were carried out with the non-proof reading DNA polymerase enzyme, Fast Start Taq (Roche), following the manufacturers' instructions. PCR reactions were set up with the following components: dNTPs to a final concentration of 0.2 mM each, DNA template between 10-100 ng/µl, forward and reverse primers to a final concentration of 1 µM each, 1× GC Rich, 1× recommended buffer and 2 U Taq polymerase, made up with nuclease free water to 25 µl. These reactions were incubated in a thermo cycler using the following cycling conditions: one cycle of an initial denaturation at 94 °C for 4 min; 30-35 cycles of 30 sec denaturation at 94 °C, 30 sec annealing at temperature specific for primer set and 30-90 sec elongation at 72 °C, which was followed by a final elongation step at 72 °C for 5-7 min.

2.7.2 Phusion High Fidelity DNA polymerase

PCR products to be used for cloning were amplified with the high-fidelity, proof reading enzyme Phusion polymerase (Finnzymes) which ensures no second site mutations are introduced into the PCR product. PCR reactions were set up with the following components: dNTPs to a final concentration of 0.2 mM each, DNA template between 10-100 ng, forward and reverse primers to a final concentration of 1 µM each, 3% dimethyl sulfoxide (DMSO), 1× recommended buffer and 1 U Phusion polymerase. The final reaction was made up with nuclease free water to 25 µl. These reactions were incubated in a thermo cycler using the following cycling conditions: one cycle of an initial denaturation at 98 °C for 4 min; 30-35 cycles of 30 sec denaturation at 98 °C, 30 sec annealing at temperature specific for primer set and 30-90 sec elongation at 72 °C which was followed by a final elongation step at 72 °C for 5-7 min.

2.8 Bacterial transformations

2.8.1 *E. coli* transformations

Chemically competent cells were prepared and transformed using rubidium chloride. Briefly, *E. coli* cells were grown to mid–log phase (OD_{600nm} 0.4-0.6) in 100 ml LB. Cells were cooled on ice for 15 min and harvested by centrifugation at 4 °C and 3900 × g for 5 min (Beckman Coulter Allegra™ X-22R Centrifuge). The cell pellet was then resuspended in 20 ml TfbI solution (30 mM potassium acetate, 100 mM rubidium chloride, 10 mM calcium chloride, 50 mM manganese chloride, and 15 % v/v glycerol - pH 5.8), and cooled on ice for 15 min. Cells were harvested as before and the pellet resuspended in TfbII (10 mM MOPS, 75 mM calcium chloride, 10 mM rubidium chloride, 15 % v/v glycerol – pH 6.5) followed by cooling on ice for 15 min and 500 µl aliquots of the cell suspension were prepared and either used immediately or quick-frozen in ethanol prior to storage at - 80˚ C.

For transformations, plasmid DNA was added to 100 µl of chemically competent cells and incubated on ice for 10 min. This was followed by heat shock at 42 °C for 2 min, incubation on ice for 2 min, addition of 400 µl 2× TY and incubation at 37 °C for 1 hour. Cells were then plated on LA containing the appropriate antibiotic to allow for selection of positive transformants.

2.8.2 *M. smegmatis* electroporations

Cells were grown to mid-log phase (OD_{600nm} 0.5-0.8) in 50-100 ml of media and harvested at 2360 × g at 4 °C for 10 min. The bacterial cell pellet was resuspended in 10% glycerol and harvested as before - this wash step was done three times in total. After the final wash step, the pellet was resuspended in 2 ml ice cold 10% glycerol and these competent cells were used immediately.

Between 1 – 5 µg of DNA was added to 0.2 cm electroporation cuvettes into which 400 µl of electro-competent *M. smegmatis* cells were added and gently mixed. The BIO-RAD Gene PulserXCell™ system was used to perform electroporations with the following parameters: 2500 V, 25 µF, 1 000 Ω, 0.2 cm. Immediately after the pulse, cells were rescued by the addition of 1 ml 2X TY and incubation at 37 °C for 3 -16 hours. Transformed cells were selected on 7H10 containing the appropriate antibiotics and/or supplements for 3 – 7 days.

2.9 Generation of *M. smegmatis* knockout strains

M. smegmatis knockout mutants were generated using two-step allelic exchange by homologous recombination (Gordhan and Parish, 2001). A schematic representation of this procedure, using the MSMEG_1661 locus as an example, can be found in Figure 2.1. This method involves the incorporation of a suicide vector which carries a mutated copy of the gene of interest by fusing together homologous upstream and downstream regions. A single recombination event occurs when the suicide vector is integrated into the chromosome of *M.*

smegmatis at one of the regions of homology resulting in a single cross-over (SCO) strain. Positive SCO homologous recombinants can be identified as blue colonies growing on 7H10 agar supplemented with Kan, Hyg and X-gal since the suicide vector carries the selectable markers *aph*, *hyg* and *lacZ*. The suicide vector also contains a *sacB* gene which encodes the secreted enzyme, levansucrase. When grown in the presence of sucrose, the enzyme hydrolyses sucrose to levans which is toxic to the bacteria and results in cell death. Therefore, the *sacB* gene facilitates counter selection for the second recombination event resulting in the expulsion of the suicide vector from the chromosome, yielding either a knockout mutant or reversion to wild type. Cells which have successfully undergone the second recombination event can be identified as white colonies with the ability to grow on 7H10 agar in the presence of X-gal and sucrose. Since these cells can either be knockout mutants or wild type,

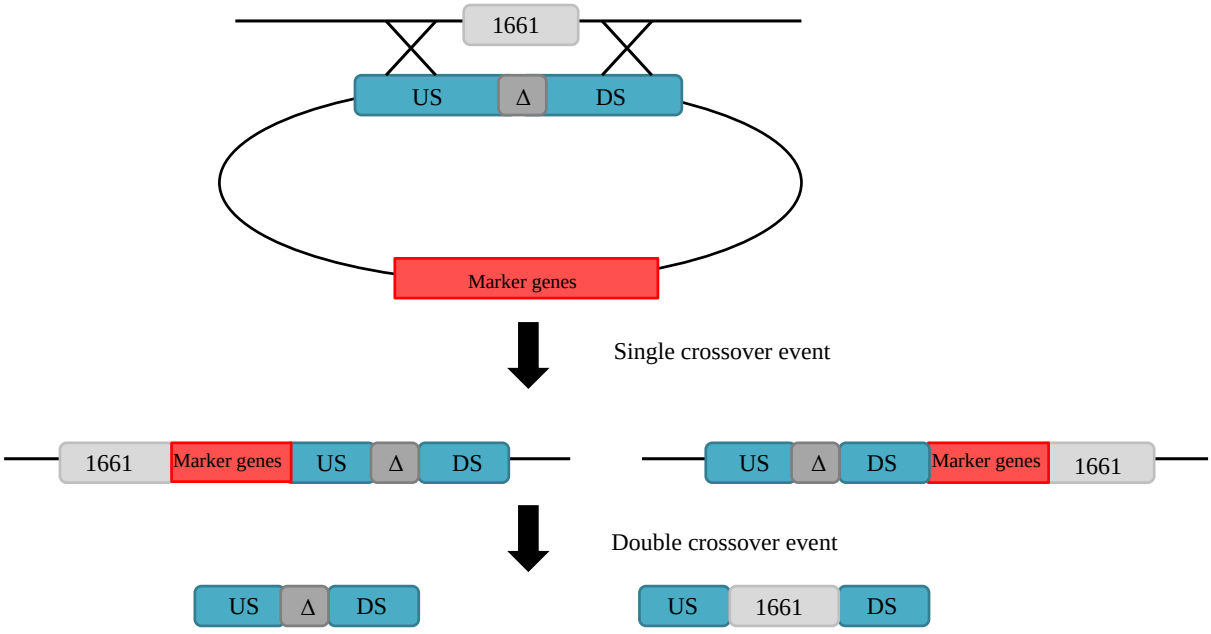

Figure 2.1. Schematic of allelic exchange mutagenesis procedure using MSMEG_1661 as an example. The suicide vector p2NIL_PAC_1661, carrying the *aph*, *hyg* and l*acZ* marker genes, is electroporated into an existing single knockout strain generating a SCO strain with the vector either upstream or downstream from the wild type gene. Selection for a double crossover event is carried out in the presence of sucrose which results in either a successful knockout mutant or reversion to wild type. Δ indicates a mutant gene, US and DS represents the upstream and downstream regions of the gene.

PCR screens were performed to determine the genotype. Suicide vectors, previously created by Dr. Christopher Ealand at the CBTBR, to generate the single knockout mutants

ΔMSMEG_1661, ΔMSMEG_2432 and ΔMSMEG_2433 were used to create double deletion mutants in this study. Consequently, double deletion mutants were created from pre-existing single deletion mutants (Table 2.1).

2.9.1 Generation of ΔMSMEG_1661 ΔMSMEG_2432 double knockout mutant

To generate the ΔMSMEG_1661 ΔMSMEG_2432 double knockout mutant, the suicide vector P2NIL_PAC_2432 (Table 2.1) was electroporated into the single deletion ΔMSMEG_1661 parental strain. A SCO was selected by incubation on 7H10 agar supplemented with Kan, Hyg and X-gal for 5 days at 30 °C to obtain blue colonies. A blue colony was selected and grown in 7H9 broth with Kan and X-gal overnight at 37 °C, followed by inoculation into fresh 7H9 broth without antibiotics to allow for the second recombination event to occur. Cells were harvested at 4000 rpm for 10 min and the pellet was resuspended in 400 µl of 7H9. A dilution series from 10^0 – 10^7 was prepared, using 100 µl of the cell suspension, from which 100 µl was used for plating on 7H10 agar containing X-gal and 7H10 agar containing X-gal and 5% sucrose. Plates were incubated at 37 °C for 5 days. White colonies were picked from the plates containing sucrose and spotted onto 7H10 agar containing X-gal with or without Kan to ensure that the suicide vector was removed. White colonies, sensitive to Kan, were picked and screened by PCR to confirm the genotype.

2.9.2 Generation of double knockout mutants

To generate a ΔMSMEG_2433 ΔMSMEG_1661 double knockout mutant, the suicide vector P2NIL_PAC_1661 (Table 2.1) was electroporated into a single deletion ΔMSMEG_2433 parental strain. To generate a ΔMSMEG_2432 ΔMSMEG_2433 double knockout mutant, the suicide vector P2NIL_PAC_2433 (Table 2.1) was electroporated into a single deletion ΔMSMEG_2432 parental strain and to generate a ΔMSMEG_2433 ΔMSMEG_2432 double knockout mutant, the suicide vector P2NIL_PAC_2432 (Table 2.1) was electroporated into a

single deletion ΔMSMEG_2433 parental strain. Selection for single and double recombination events were carried out as described in 2.9.1.

2.10 Southern blot analysis

Southern blots were used for genotypic confirmation of mutants generated in this study. Recipes for solutions can be found in Table A8.

2.10.1 Electro-blotting

Restriction digests were performed overnight using 2 µg chromosomal DNA and 5 U of selected enzyme. The digested DNA was separated on a 0.8% agarose gel for 2 – 3 hours at 80 V and imaged alongside a ruler using the G-Box SYNGENE system. The gel was then incubated in depurination solution (0.2 M HCl) for 15 min at room temperature with shaking. The depurination solution was decanted, followed by incubation in a denaturation solution (0.5 M NaOH, 1.5 M NaCl) for 30 min at room temperature with shaking. The gel was then equilibrated in 1X TBE. A transfer cassette, which contained the following: a nylon membrane packed against the agarose gel and sandwiched between two layers of Whatman filter paper and sponges was prepared. The DNA was then transferred to the membrane at 600 mA for 2 hours. The membrane was then exposed to UV radiation twice, at 2500 mJ/cm^3 in order to cross-link the DNA to the membrane.

2.10.2 Probe labelling

For Southern blots, the probes were generated using the commercially available kit PCR DIG Probe Synthesis Kit (Roche) which allows for specific labelling of probes with alkali-labile digoxygenin (DIG) dUTP. Primers used to generate probes are listed in Table B2. Incorporation of DIG dUTP into the fragment was confirmed on agarose gels by comparing labelled and unlabeled reactions. The DIG-labelled fragment is expected to run slower than

the unlabeled fragment. Once synthesized, probes were either used immediately or stored at -20 °C until required.

2.10.3 Hybridization

Hybridization of probes was carried out in roller bottles (Hybaid HB-OV-BM) in a hybridization oven (Hybaid Micro-4). Membranes were incubated in 12 ml DIG Easy Hyb solution (Roche) at 54 °C for 30 min. Probes were denatured by boiling at 95 °C for 5 min followed by immediate cooling on ice. Probes were then added to the hybridization solution using a volume of 2 µl per ml of hybridization buffer and hybridization performed at 54 °C overnight. Following hybridization, the membrane was washed in Solution I (2X SSC, 0.1% SDS) with shaking for 5 min at room temperature. This was followed by two washes in Solution II (0.5X SSC, 0.1% SDS) for 15 min each at 68 °C.

2.10.4 Immunological detection

Unless stated differently, all wash steps and incubations were performed at room temperature with shaking. The membrane was rinsed in wash buffer (0.1 M Maleic Acid Buffer, 0.3% Tween 20) for 5 min followed by incubation in 1x blocking solution for 30 min. This was followed by incubation in antibody (Anti-Digoxygenin-AP) solution for 30 min. The membrane was then washed twice with wash buffer for 15 min each followed by equilibration in detection buffer for 5 min. The membrane was transferred to a hybridization bag with the DNA side facing up and 1 ml CSPD substrate was spread evenly across the membrane. All air bubbles were removed and the membrane was incubated for 5 min. All excess substrate was removed and the membrane was incubated at 37 °C for 10 min followed by exposure to X-ray film for 30 – 60 min. The X-ray films were developed using the Axim automated developer.

2.11 Generation of *M. smegmatis* complementation strains

In order to confirm whether phenotypic variation seen in mutant strains are the result of the loss of a specific gene and not polar effects, genetic complementation is necessary. In this study, genetic complementation was achieved using an integrating vector carrying the full length gene of interest, for example MSMEG_1661, plus 150 bp upstream of the start codon to include the native promoter region. This approach allows for integration of a functional gene into the *att*B phage attachment for regulation and expression by the appropriate mechanisms in mycobacteria. The appropriate integrating vectors were electroporated into both double knockout mutant strains using 1, 3 and 5 µg of DNA. The transformants were plated on 7H10 agar containing Hyg and incubated at 37 °C for 4 days. Clones were picked and the DNA extracted using the colony boil method as described in section 2.3.2.1. Site specific integration of the plasmid was confirmed by PCR using the primers listed in Table C3.

2.12 Gene expression analysis

2.12.1 RNA extraction

RNA was extracted using the Nucleospin RNA II kit (Machery Nagel) as per manufacturer's instructions. Cells were grown to overnight at 37 °C to an OD_{600nm} of 0.3 in 10 ml 7H9 broth. Cells were then harvested at 3082 × g for 10 min at 4 °C followed by resuspension in 500 µl TE (10 mM Tris-HCl and 1 mM EDTA, pH 8), 350 µl lysis buffer and 3.5 µl β-mercaptoethanol. The suspension was transferred to MagNA Lyser Green Beads (Roche) lysing matrix and ribolyzed three times using the MagNA Lyser (Roche) for 35 secs (speed 6000) with cooling on ice for 2 min between each ribolysis. Lysates were transferred to Nucleospin Filters and centrifuged for 1 min at 11000 × g. RNA binding conditions were adjusted by mixing 350 µl 70% ethanol with the flowthrough which was then transferred to a Nucleospin RNA Column and centrifuged for 30 sec at 11000 × g. The flowthrough was

discarded, 350 µl Membrane Desalting Buffer (MDB) was added to the column followed by centrifugation for 1 min at 11 000 × g to dry the membrane. DNA was digested on the column by the addition of 100 µl DNase reaction mixture which contains 10 µl reconstituted rDNase and 90 µl reaction buffer for rDNase to the column and incubated at room temperature for 15 min. Following incubation, the column was washed with 200 µl of Buffer RAW2 and centrifuged for 30 secs at 11000 × g. This was followed by two washes with 600 µl Buffer RA3 and 250 µl Buffer RA3. Washes were carried out by centrifugation for 30 secs or 2 min at 11000 × g respectively. Following the washes, the column was placed into a nuclease-free Eppendorf tube and RNA was eluted with 50 µl RNase-free water by centrifugation for 1 min at 11000 × g. RNA was quantified using the Nanodrop – as described above for DNA.

2.12.2 Reverse Transcriptase PCR (RT-PCR)

Prior to RT-PCR, 1 µg of RNA was treated with 1 µl TURBO DNaseI (Life Technologies) for 30 min at 37°C to remove residual genomic DNA. DNaseI was inactivated by the addition of 7 µl DNaseI removal resin followed by centrifugation for 5 min at 10 392 × g. A 23 µl aliquot was used for RT-PCR. A 2.5 µM reverse primer mix containing MSMEG_1661, MSMEG_2432, MSMEG_2433 and *sigA* reverse primers was prepared and 2 µl of this mixture was added to TURBO DNase treated RNA. The housekeeping *sigA* gene allows for normalization because the gene is expressed at a consistent level throughout all growth phases. PCR reactions were performed using the following parameters: 94 °C for 90 secs, 65 °C for 3 min and 57 °C for 3 min followed by incubation on ice. RT reactions were carried out using SuperScript III reverse transcriptase (Invitrogen) as per manufacturer's instructions. Briefly, a 25 µl RT+ reaction was set up using 12.5 µl of the annealed product, 4 µl 25 mM $MgCl_2$, 5 µl 5× First Strand Buffer, 2 µl 0.1 M DTT, 1 µl 10 mM dNTPs and 0.8 µl SuperScript III. The RT- reaction was set up with nuclease-free water replacing SuperScript

III in the reaction. cDNA synthesis was carried out using the following parameters: 50 °C for 50 min and 85 °C for 5 min. The resulting cDNA was used for quantitative PCR.

2.12.3 Quantitative real-time PCR (qPCR)

qPCR was performed using Sso Fast Evagreen Supermix (Biorad) as per manufacturer's instructions. Briefly, 20 µl reactions were set up, each containing 10 µl Evagreen Supermix, 0.75 µl forward primer (10 µM), 0.75 µl reverse primer (10 µM), 2 µl cDNA and nuclease-free water. Primers used for gene expression analysis are listed in Table B4. All reactions were incubated in the CFX96 Real-Time PCR detection system (Biorad) using the following parameters: 98 °C for 2 min followed by 39 cycles consisting of three steps – 98 °C for 5 sec, 60 °C for 5 sec and 72 °C for 5 sec with SYBR Green quantification at the end of each cycle. Melt curve analysis was conducted from 65 °C with a gradual increase in 0.5 °C increments every 0.05 sec to 95 °C with SYBR Green quantification conducted continuously throughout this stage. The raw data was analyzed using the Biorad CFX Manager 3.0 Software (Biorad).

2.13 Phenotypic analyses of *M. smegmatis* knockout strains

2.13.1 Growth rate determination in standard media

To assess the growth rates of wild type and mutant strains, growth curve experiments were performed. A pre-culture was started using either a single colony or 1 ml of frozen culture in 10 ml media containing appropriate antibiotics and incubated at 37 °C and 100 rpm shaking overnight. The pre-culture was diluted to an OD_{600nm} of 0.01 in 50 ml media containing appropriate antibiotics and incubated at 37 °C with shaking at 100 rpm. Growth rates were determined by recording the OD_{600nm} reading at three hour intervals and data was used to generate a scatter plot.

2.13.2 Growth rate analysis in Sauton's media

To assess the effect of acid stress in minimal media on the growth rate of wild type and mutant strains, growth curve experiments in Sauton's media at different pH (5.5 and 7.3) were performed. Growth rates were determined as above in standard media.

2.13.3 Colony forming ability

Bacterial spotting assays were performed to assess the morphology of wild type and mutant strains on solid agar. Cells were grown to log phase in 7H9 broth. A 10-fold serial dilution ranging between $10^0 – 10^7$ was prepared and 10 µl from each dilution was spotted onto 7H10 agar plates with appropriate antibiotic where necessary. Plates were incubated at 37 °C for 3-5 days before images were captured using the Zeiss Stereo Microscope (1.3× magnification).

2.13.4 Biofilm formation

Cells were grown overnight in 7H9 media to an OD_{600nm}> 2. Cells were harvested by centrifugation at 3500 rpm and washed twice in Sauton's media. The pellets were resuspended in Sauton's media and the OD_{600nm} was adjusted to 2. A 10-fold serial dilution ranging from 10^0 -10^5 was prepared and 100 µl of each dilution was added to a 6-well plate containing 10 ml Sauton's media (1:100). Plates were incubated at 37 °C for 7-10 days before images were captured using the Zeiss Stereo Microscope (1.3× magnification).

2.13.5 Sliding motility

Wild type and mutant strains were streaked to single colonies on 7H10 agar plates and incubated at 37 °C for 3 days. A single colony was picked and placed onto the center of 7H9 agar plates containing 0.3% agar. Plates were incubated at 37 °C for 4-5 days before being photographed using the G-Box SYNGENE system.

2.13.6 Antibiotic sensitivity

2.13.6.1 Minimum Inhibitory Concentration (MIC) determination

To determine MIC concentrations, wild type and mutant strains were grown overnight at 37 °C to an OD_{600nm} of 0.3. An initial 1:10 dilution of the overnight cultures was carried out followed by a 1:50 dilution. The broth microdilution method (Domenech et al., 2005) was used to set up 96 well plates. The following antibiotics were tested: Ampicillin, Erythromycin, Vancomycin, Rifampicin, Cefoxitin, Cefotaxime, Cefamandole, Cefapirin and Cefatriaxone. Plates were incubated for 5 days at 37 °C and assessed visually with the MIC being determined as the lowest drug concentration that inhibited growth.

2.13.6.2 Antibiotic sensitivity Spotting Assay

Wild type and mutant strains were grown overnight at 37 °C to an OD_{600nm} of 0.3. A ten-fold dilution series ranging between 10^0 -10^7 was carried out and 10 µl of each dilution was spotted on 7H10 agar plates (145 x 20 mm) containing the appropriate antibiotic at the predetermined MIC concentration. A control plate containing no antibiotic was included. Plates were incubated for 5 days at 37 °C before being photographed using the G-Box SYNGENE system (upper white setting).

2.13.7 SDS sensitivity

2.13.7.1 SDS killing curves

Cells were grown overnight in 7H9 broth to an OD_{600nm} of 0.3. From the overnight culture, 1 ml was removed - 100 µl of this was used to prepare serial dilutions for CFUs and the remainder was used for visualization on the microscope. To the remaining culture, 0.2% SDS was added and the culture was incubated at 37 °C. After 3 and 6 hours, 1 ml of culture was removed and used for CFUs.

2.13.7.2 SDS spotting assay

Cells were grown overnight in 7H9 broth at 37 °C to an OD_{600nm} of 0.3. A ten-fold dilution series ranging between 10^0 -10^7 was carried out and 10 µl of each dilution was spotted on 7H10 agar plates (145 x 20 mm) containing either 0.01%, 0.005% 0.0025% or 0.001% SDS. A control plate containing no SDS was included. Plates were incubated for 5 days at 37 °C before being photographed using the G-Box SYNGENE system (upper white setting).

2.13.8 Microscopic analysis

2.13.8.1 Scanning Electron Microscopy

Cells were grown in 50 ml 7H9 broth overnight at 37 °C to an OD_{600nm} of 0.6. Cells were harvested by centrifugation at 4000 rpm for 10 min, followed by two washes with PBS and then resuspended in 2.5% gluteraldehyde in PBS overnight at 4 °C. Cells were washed twice with PBS and resuspended in 100 µl osmium tetraoxide in PBS and incubated for 1 hour at room temperature. Following incubation, cells were washed twice with PBS and then dehydrated with a series of ethanol concentrations: 30%, 50%, 70% and twice at 100%, for 2 min each. Cells were stored in 100% ethanol until they could be viewed. Before visualization, cells were spotted on a filter, carbon coated twice and then viewed using the FEI Nova NanoSEM 230.

2.13.8.2 Transmission Electron Microscopy

Cells were grown in 50 ml 7H9 broth overnight at 37 °C to an OD_{600nm} of 0.6. Cells were harvested by centrifugation at 3082 × g for 10 min, washed twice with PBS and resuspended in fixing solution containing 2% (v/v) formaldehyde, 2.5% (v/v) gluteraldehyde, 0.1 mM HEPES and 0.05% (v/v) ruthedium red, followed by incubation for 1 hour at room temperature. After incubation, cells were washed twice with PBS and then dehydrated with a series of ethanol concentrations: 30%, 50%, 70% and twice at 100%, for 2 min each. After

dehydration, samples were washed in propylene oxide and 50% resin mixture (15 g DDSA, 7.75 g epon 812 and 5.62 g araldite). The propylene oxide resin mixture was removed and cells were resuspended in 100% resin and incubated overnight at room temperature. Following overnight incubation, cells were pelleted, the resin was removed and fresh resin containing DMP at a ratio of 40: 1 (g: g) was added to the cells and incubated for 48 hours at 60 °C. The solidified resin was sectioned using a Relchert Ultracut Ultramicrotome (Circa) and viewed using a Tecnai F20 TEM.

2.13.8.3 Fluorescence Microscopy

Cells were grown in 10 ml of 7H9 broth overnight at 37 °C to an OD_{600nm} of 0.6. Cells were harvested by centrifugation at 3082 × g for 10 min, washed twice in PBS and resuspended in 1 ml 7H9 broth. Thereafter, 1 µl of 1 mg/ml BODIPY- fluorescent vancomycin (Invitrogen) and 0.2 µl of 5 mg/ml vancomycin was added to the suspension followed by incubation for 1.5 hours at 37 °C with shaking. Following incubation, cells were washed twice with 7H9, resuspended in 100 µl 7H9 and 5 µl was spread onto a 2% agarose pad on a slide. A drop of fluoramount (Sigma) was used to mount the coverslip onto the slide. The slides were viewed on the Zeiss Axio Observer z1 base and images were processed using the ZEN black version software (Zeiss).

2.14 Recombinant protein expression

For expression analysis, the pET29a-c, T7 expression vector was used. T7 promoters found on the vector only recognize the T7 RNA polymerase and not RNA polymerase generated by *E. coli*. However, the gene for T7 RNA polymerase is engineered into commercially available *E. coli* (DE3) strains. Additionally, the gene for T7 lysozyme, which prevents background expression of T7 RNA polymerase from expressing protein prior to induction, is engineered into commercially available *E. coli* pLysS strains. Isopropyl β-D-1- thiogalactopyranoside

(IPTG) is structurally similar to lactose and can bind to the Lac repressor encoded by the *lacI* gene, which leads to a conformational change and release of the repressor from the *lac* operator. This allows native *E. coli* RNA polymerase to bind and the *lac* operator then transcribes high numbers of T7 RNA polymerase. The T7 DNA polymerase can then bind to the T7 promoter sequence on the vector which is located upstream of the gene of interest, thus promoting transcription of the target gene.

2.14.1 Generation of inducible vectors for protein purification

Genes of interest (*dacB*, MSMEG_1661, MSMEG_2432 and MSMEG_2433) were amplified using Phusion PCR as described in 2.7.2 and cloned into the inducible promoter pET29a-c (Novagen), referred to as pET29a from this point forward, which carries a C-terminal His-tag sequence. Different variants of *dacB* were amplified using Phusion, with the primers listed in Table B5, and cloned into pET29a. These variants included the DacB catalytic domain only, the DacB domain lacking 50 amino acids and the DacB domain plus an additional flanking sequence. These plasmids were then transformed into *E. coli* DH5α and confirmed by restriction mapping as well as sequencing using primers listed in Table B6, as well as T7 promoter and T7 terminator primers. Once strains were confirmed, plasmids were transformed into the expression *E. coli* BL21 (DE3) pLysS host and successful transformants were confirmed by PCR. A schematic representation of this procedure using MSMEG_2432 as an example can be found in Figure 2.2.

2.14.2 Induction of protein expression

Cultures carrying the inducible plasmid were grown to an OD_{600nm} between 0.3-0.6 at which point IPTG was added to the culture at a final concentration of 1 mM or 0.3 mM. The cultures were grown for three hours followed by protein extraction with a sample being collected every hour to determine optimal induction time.

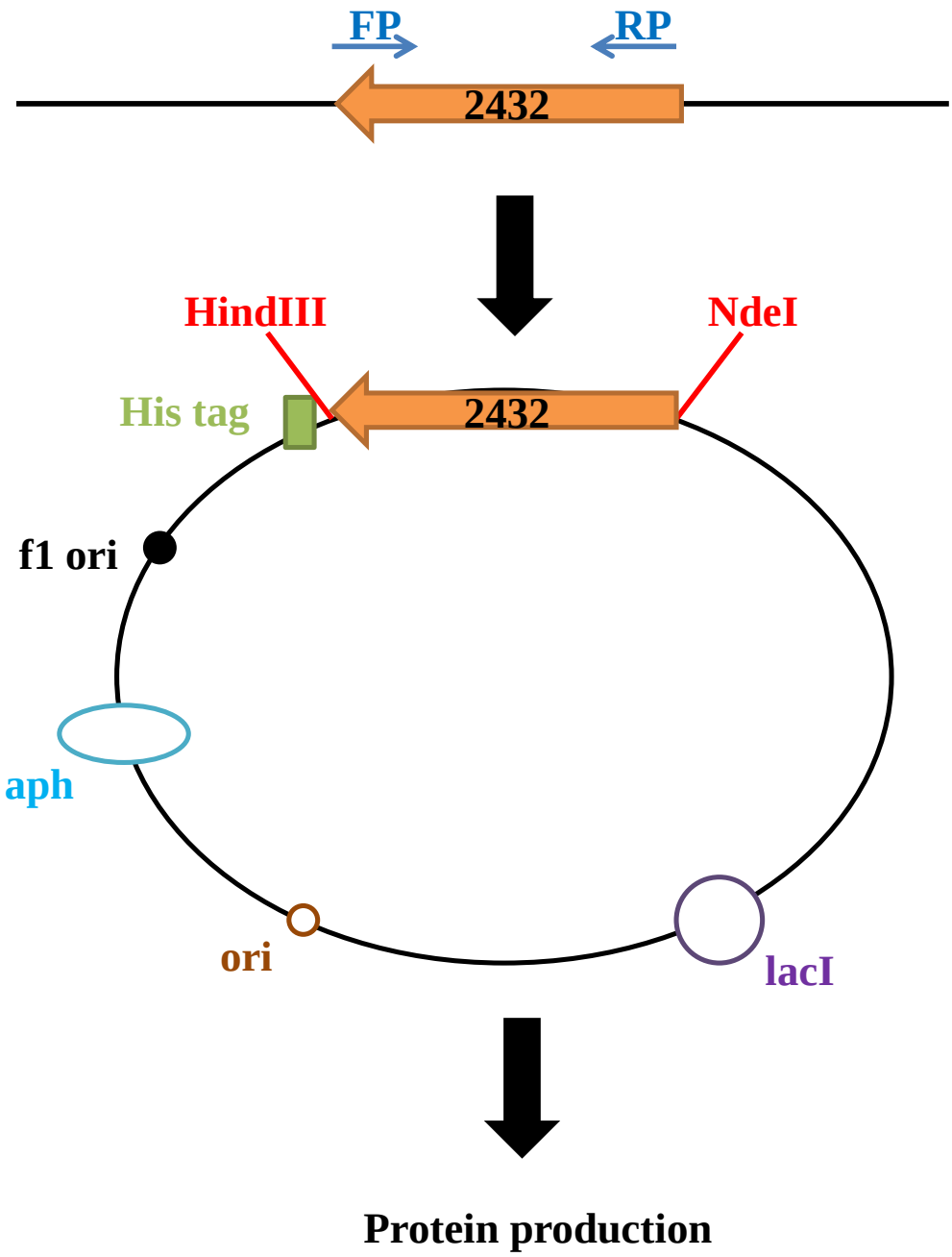

Figure 2.2. Schematic representation of cloning for recombinant protein production using MSMEG_2432 as an example. The gene of interest is cloned into pET29a which incorporates a His tag at the C-terminal end of the protein. The vector containing the gene is then induced using IPTG.

Cells were grown in 10 - 20 ml cultures with appropriate antibiotics and harvested by centrifugation at 3082 × g for 10 min. Pellets were then resuspended in 250 – 500 µl B-PER (Fischer Scientific) cocktail solution and incubated with shaking at room temperature for 10 min. The B-PER lysis solution allows for lysing of bacterial cells without the need for

mechanical methods. Soluble (supernatant) and insoluble fractions were separated by centrifugation at 10 392 × g for 15 min. An equal volume of 5× SDS Buffer was added to all samples.

2.14.3 SDS-PAGE

SDS-PAGE is a common method used to separate proteins based on their size. Acrylamide gels were prepared as outline in Table A11. Prior to loading gels, equal amounts of different protein samples in loading buffer were denatured at 95 °C for 5 min. Proteins were separated at 100 V in running buffer (Table A10) for 2 – 3 hours. Gels were stained overnight with Coomassie blue at room temperature with shaking followed by destaining at room temperature until bands could be visualized.

2.14.4 Protein purification

After separation of soluble and insoluble fractions, 250 µl of Ni-NTA resin (Qiagen) was added to a clean Eppendorf tube and centrifuged at 3082 × g for 30 secs. The top layer was removed and resin was equilibrated by the addition of 500 µl Buffer A (50 mM Tris, 500 mM NaCl, 20% glycerol and 10 mM imidazole) followed by centrifugation at 3082 × g for 30 sec. The top layer was discarded and the equilibration step was repeated. DNase I was added to the BPER II lysed soluble fraction from induced cells and then centrifuged for 10 min at 10 392 × g. The supernatant was transferred to a clean tube and the pellet was resuspended in 250 µl of Buffer A. From the supernatant, 250 µl was added to the resin and incubated for 10 min on ice. Following incubation, the resin was washed thrice using 1 ml Buffer A and centrifugation for 10 secs at 2360 × g. After each centrifugation the ‘flowthrough’ was collected. Following the final wash, the protein was eluted using 100 µl of Buffer B (50 mM Tris, 500 mM NaCl, 20% glycerol and 250 mM imidazole) and centrifuged for 10 sec at 3500 rpm. The top layer was containing the eluted protein and a sample of the resin was collected.

2.14.5 Western blotting

2.14.5.1 Electro-blotting

Following SDS-PAGE separation, proteins were transferred to a nitrocellulose blotting membrane (Pall Life Sciences) by preparing a cassette containing the following: a nitrocellulose membrane packed against the SDS-PAGE gel and sandwiched between two layers of Whatman filter paper and sponges. The proteins were transferred to the membrane at 100 V for 70 min at 4 °C.

2.14.5.2 Immunological detection

Unless stated differently, all wash steps and incubations were performed at room temperature with shaking. To prevent non-specific binding of the primary antibody, the membrane was incubated at 4 °C overnight in blocking solution (Table A14). Following incubation, the membrane was washed three times with Tris buffered saline with Tween 20 (TBST) for 5 min each. The membrane was incubated for 1 hour in blocking solution containing the primary antibody, in this case a monoclonal Anti-polyHistidine (Sigma) at a final concentration of 10 µg/ml. This was followed by three TBST washes for 5 min each. The membrane was then incubated in blocking solution for 1 hour with the secondary antibody, Rabbit Anti-Mouse IgG (Sigma) at a dilution of 1: 25000. This was followed by three TBST washes for 5 min each. The membrane was transferred to a hybridization bag, treated with a Chemiluminescent Peroxidase Substrate (CPS) and incubated at room temperature for 5 – 10 min. All excess substrate was removed and the membrane was exposed to X-ray film for 30–60 secs. The X-ray films were developed manually using the Axim automated developer.

3. Results

3.1 Generation of *M. smegmatis* double knockout DD-CPase mutants

Prior to all electroporations, all suicide vectors were extensively mapped using restriction enzymes to ensure the correct vector was being used. The results of these restriction analyses are given in Figure D1- D3 (pages 126 - 128), in all cases, the genetic integrity of the vector was confirmed.

3.1.1 Generation of ΔMSMEG_1661 ΔMSMEG_2432

The strategy for constructing combinatorial mutants is shown in Figure 3.1 with the single deletion mutant created by electroporation of P2NIL_PAC_1661 (Table 2.1) into wild type *M. smegmatis*. Using the P2NIL_PAC_2432 vector created by Dr. C. Ealand, a double knockout mutant was created as described in section 2.9.1. A single colony, representative of a SCO was obtained from the electroporation reaction with P2NIL_PAC_2432 (Table 2.1) into ΔMSMEG_1661 single knockout mutant. This SCO colony was taken forward and grown in the absence of antibiotics, followed by selection in the presence of sucrose. White colonies were picked and spotted onto 7H10 agar supplemented with X-gal and sucrose. Eleven of the colonies that remained white were screened using a PCR strategy.

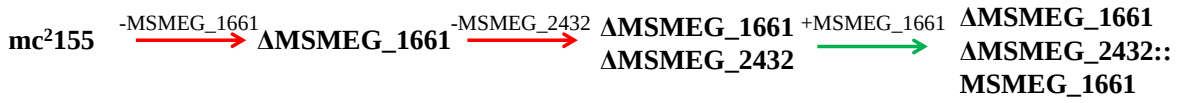

Figure 3.1. Construction of ΔMSMEG_1661 ΔMSMEG_2432 and its complemented derivative. A single knockout mutant was previously created by deleting MSMEG_1661 from the mc^2155 wild type strain. This was followed by deletion of MSMEG_2432 and subsequent complementation with pMV1661. Red arrows indicate deletion and green arrow indicates genetic complementation.

The PCR strategy used to screen knockouts contains three primers in a single reaction – two primers flank the gene (Primer 1 and 3) and the other is situated within the deleted region of the gene (Primer 2). A schematic of the expected amplicon sizes can be found in Figure 3.2.

In wild type and SCO DNA, all three primers have the ability to anneal to the template. The product amplified by Primers 1 and 3, which flank the gene, is 1028 bp and Primers 1 and 2 generate a 500 bp product, both of which represented the wild type gene, Figure 3.2A. However, in all cases the smaller band created by Primer 1 and 2 is preferentially amplified due to competition for PCR reagents such as dNTPs. For deletion of MSMEG_2432, the region for Primer 2 binding should be absent in the mutant and only Primers 1 and 3 will bind. This would result in the generation of a smaller product, 236 bp band, indicating the presence of the mutant allele. Of the eleven colonies screened, five appeared to be mutants, as confirmed by the 236 bp band observed in lanes 5, 7-9 and 15 of Figure 3.2B. The remaining six colonies appeared to be wild type revertants as confirmed by the 500 bp band found in lanes 6 and 10-14. Colonies corresponding to lanes 5 and 7-9 were picked and the genotype was further confirmed by Southern blot analysis.

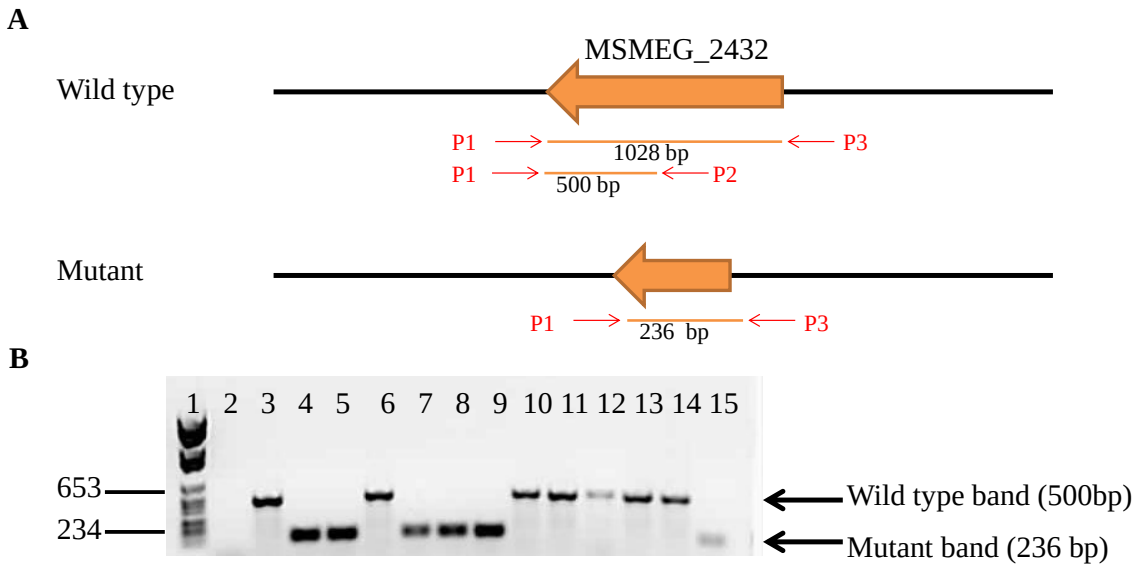

Figure 3.2. PCR screening of ΔMSMEG_1661 ΔMSMEG_2432 knockout mutants. (A) Schematic representation of genomic maps of wild type and mutant MSMEG_2432 region. Primer positions (red arrows) and expected amplicon sizes are shown. P1 = Primer 1, P2= Primer 2, P3 = Primer 3. (B) PCR screen for MSMEG_2432 deletion. Lane 1: Marker VI, Lane 2: No DNA, Lane 3: wild type, Lane 4: suicide vector, Lane 5 to 15: Clones 1 to 11. The 1028 bp band is not seen in any of the wild type strains due to competition of reagents resulting in preferential amplification of the 500 bp band.

All probes were synthesized for southern blots with DIG dUTP from the appropriate vector. Agarose gels for probes are given in Figures D4 – D6 (page 129). As expected the DIG labeled probe migrates higher than the corresponding unlabeled fragment.

Genomic DNA was extracted from wild type and the putative mutants using the CTAB DNA extraction method described in section 2.3.2.2. The enzymes chosen to perform Southern blot analysis on the MSMEG_1661 upstream and MSMEG_2432 upstream regions were *Mlu*I and *Pvu*II respectively, as these allowed for accurate differentiation between wild type and mutant strains. Restriction digestions were set up using the above mentioned enzymes and 2 µg CTAB DNA for each reaction. Southern blot analysis was carried out as described in section 2.10. In this study, double mutants defective for two DD-CPases encoding genes were generated and characterized. For this single deletion mutants were used and during genotypic analysis, the integrity of the pre-existing deletion in the parental strain was also confirmed to ensure that no chromosomal rearrangements took place during allelic exchange. To determine that the parental strain was correct, the probe created from the suicide vector P2NIL_PAC_1661 (Table 2.1) which corresponds to the region upstream of MSMEG_1661, was used, Figure 3.3A. To identify possible double knockout mutants, deficient in MSMEG_2432, in the background of the ΔMSMEG_1661 mutant, the probe created from the P2NIL_PAC_2432 suicide vector (Table 2.1) which corresponds to the region upstream of MSMEG_2432 was used, Figure 3.3C. The results of the Southern blots for the MSMEG_1661 and MSMEG_2432 upstream probes are shown in Figure 3.3B and 3.3D respectively with the expected sizes shown in Figure 3.3A and 3.3C respectively. From the Southern blot of the parental strain, Figure 3.3A and 3.3B, it can be seen that there is a size difference between the wild type and mutant strains in the region probed. The *Mlu*I digests produced a smaller band in the mutant strain (3.79 kbp vs 4.95 kbp in the mutant vs wild type respectively) due to the decrease in size of the MSMEG_1661 gene. This confirms that the

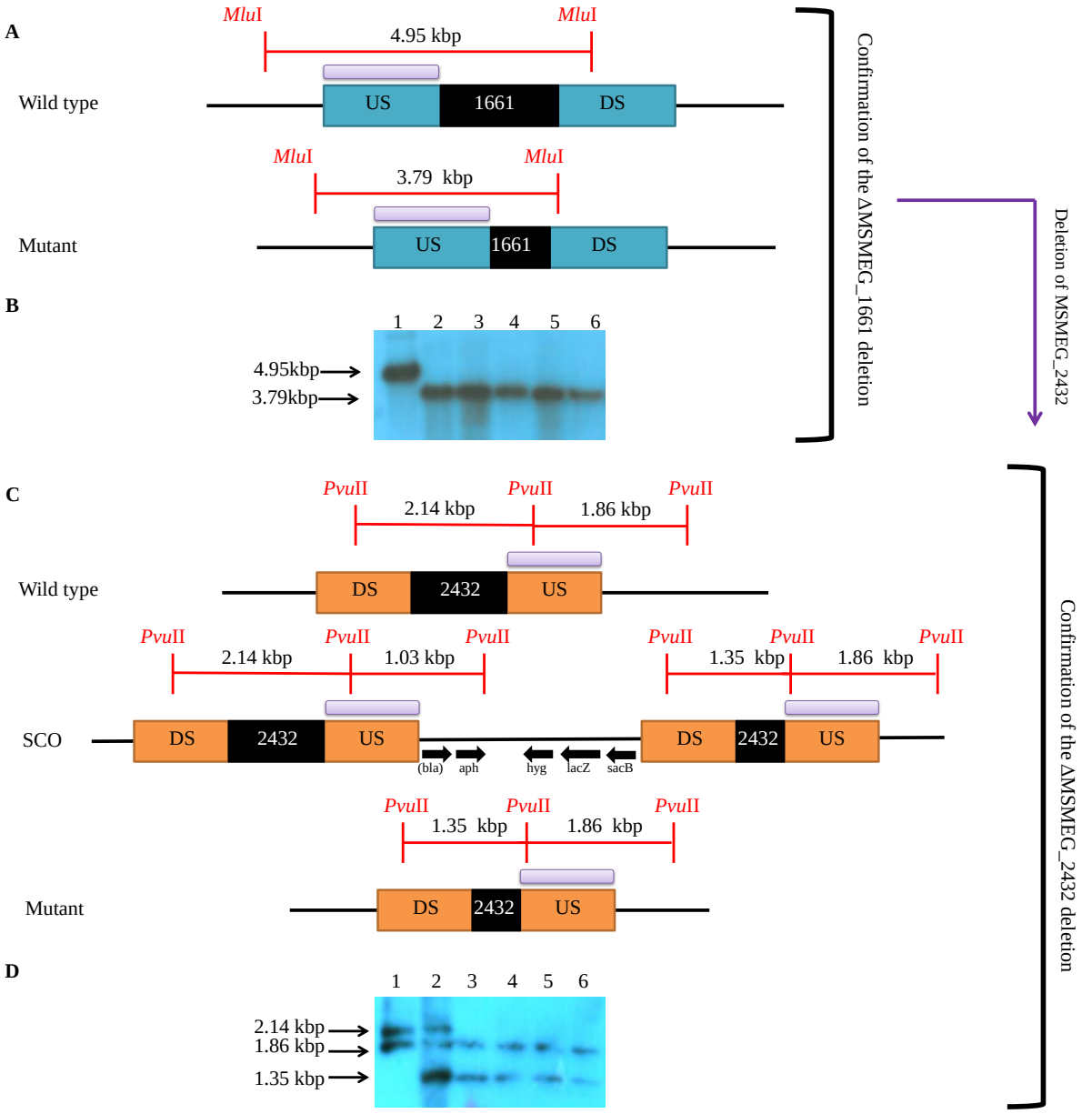

Figure 3.3. Screening of ΔMSMEG_1661 ΔMSMEG_2432 possible double crossover mutants. (A) Schematic representation of genomic maps of wild type and mutant MSMEG_1661 regions. Probes, restriction enzymes and expected fragment sizes are shown. (B) Southern blot with MSMEG_1661 upstream probe. Lane 1: *Mlu*I digested wild type DNA, Lane 2 to 6: *Mlu*I digested ΔMSMEG_1661 ΔMSMEG_2432 DNA. (C) Schematic representation of genomic maps of wild type, single crossover and mutant MSMEG_2432 regions. Probes, restriction enzymes and expected fragment sizes are shown. (D) Southern blot with MSMEG_2432 upstream probe. Lane 1: *Pvu*II digested wild type DNA, Lane 2: *Pvu*II digested single crossover DNA, Lane 3 to 6: *Pvu*II digested ΔMSMEG_1661 ΔMSMEG_2432 DNA.

parental strain is in fact a MSMEG_1661 knockout mutant. Confirmation of the loss of MSMEG_2432 in this background can be seen by the reduction in size of the band observed for the *Pvu*II digest (1.35 kbp vs 2.14 kbp in the mutant vs wild type respectively) in the mutant strain, Figure 3.3C and 3.3D. This decrease in size is due to the decrease in size of

the MSMEG_2432 gene confirming that this strain is also a MSMEG_2432 knockout mutant. The SCO for this strain displays all expected band sizes confirming that no mutations occurred during recombination. Since this is a double knockout strain, both the upstream and downstream regions of both the genes deleted need to be confirmed. One colony was chosen and further analyzed by Southern blot analysis using the restriction enzyme *Bam*HI which allows accurate differentiation between the wild type and mutant strains.

Genomic DNA was extracted from wild type, the single knockout mutants ΔMSMEG_1661 and ΔMSMEG_2432 as well as the double knockout clone that was selected. The parental strain was confirmed by using the probes shown in Figure 3.4A which correspond to the upstream and downstream regions used to generate the suicide vector P2NIL_PAC_1661 (Table 2.1). The Southern blot results for MSMEG_1661 upstream and downstream probes are shown in Figure 3.4B and 3.4C respectively. An increase in the band observed for the *Bam*HI digests in the mutant strains is due to loss of a restriction site present in the wild type gene. This can be seen with the upstream (5.08 kbp vs 2.82 kbp in the mutant vs wild type respectively) and the downstream (5.08 kbp vs 3.42 kbp in the mutant vs wild type respectively) probes confirming that MSMEG_1661 is deleted in the ΔMSMEG_1661 single knockout and the double knockout mutant strains. To confirm deletion of the second DD-CPase gene in the ΔMSMEG_1661 background, probes shown in Figure 3.4D which corresponds to the upstream and downstream regions used to generate the suicide vector P2NIL_PAC_2432 (Table 2.1) were used. A decrease in the band observed for the *Bam*HI digests in the mutant strains is due to the decrease in size of the MSMEG_2432 gene. This can be seen with both the upstream (1.08 kbp vs 1.87 kbp in the mutant vs wild type respectively) and the downstream (1.08 kbp vs 1.87 kbp in the mutant vs wild type respectively) probes. Together these data provide definitive evidence that both

MSMEG_1661 and MSMEG_2432 are deleted in this strain, now designated as ΔMSMEG_1661 ΔMSMEG_2432 (Δ1661 Δ2432 in images).

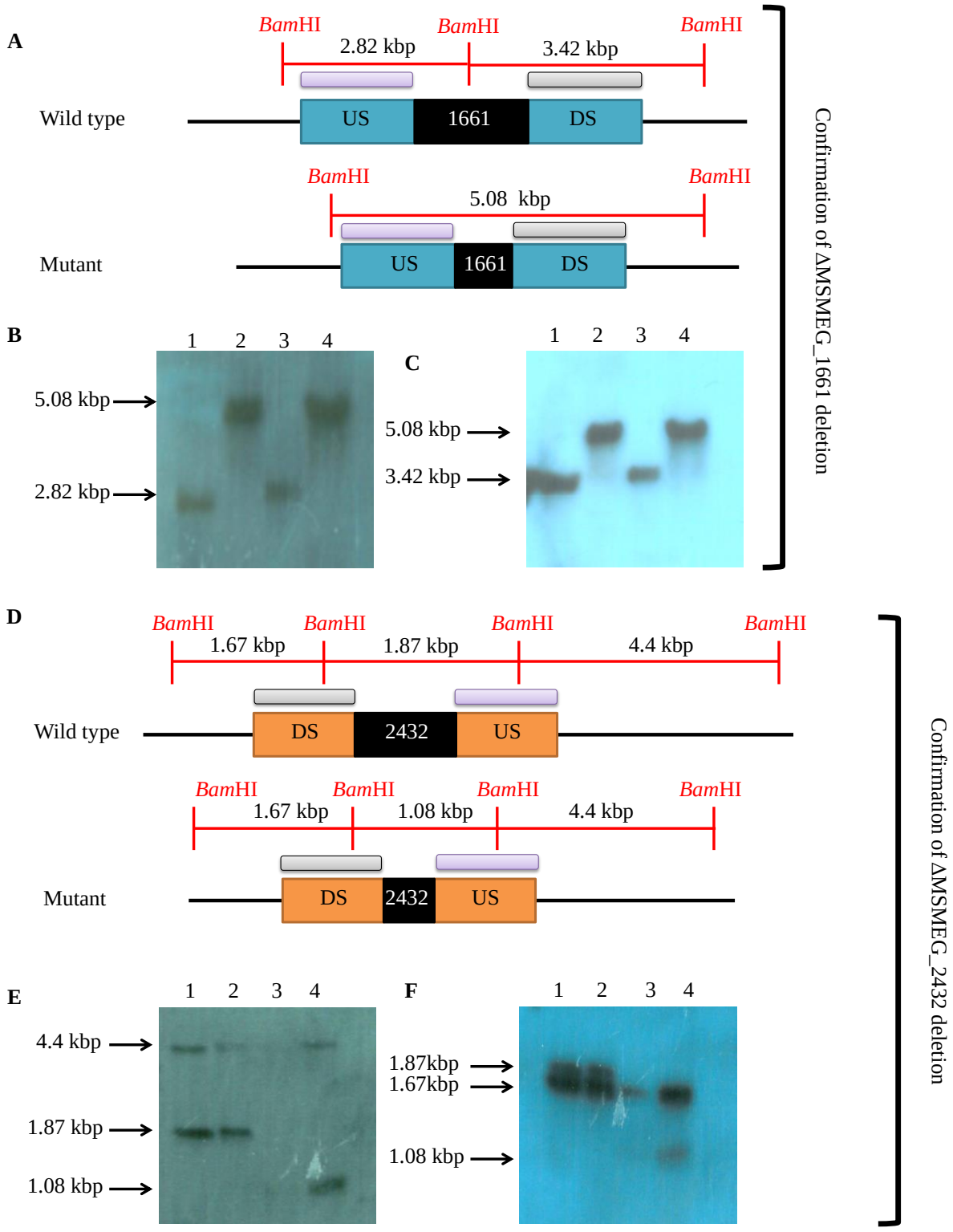

Figure 3.4. Genotypic confirmation of the ΔMSMEG_1661 ΔMSMEG_2432 strain. (A) Schematic representation of genomic maps of wild type and mutant MSMEG_1661 regions. Upstream and downstream probes are shown in purple and grey respectively. Restriction enzyme sites and expected fragment sizes are also

shown. (B) Southern blot with MSMEG_1661 upstream probe. (C) Southern blot with MSMEG_1661 downstream probe. (D) Schematic representation of genomic maps of wild type and mutant MSMEG_2432 regions. Upstream and downstream probes are shown in purple and grey respectively. Restriction enzyme sites and expected fragment sizes are also shown. (E) Southern blot with MSMEG_2432 upstream probe. (F) Southern blot with MSMEG_2432 downstream probe. Lane 1: *Bam*HI restricted wild type DNA, Lane 2: *Bam*HI restricted ΔMSMEG_1661 DNA, Lane 3: *Bam*HI restricted ΔMSMEG_2432 DNA, Lane 4: *Bam*HI restricted ΔMSMEG_1661 ΔMSMEG_2432 DNA.

3.1.2 Generation of ΔMSMEG_2433 ΔMSMEG_1661

Using the P2NIL_PAC_1661 (Table 2.1) vector created by Dr. C. Ealand, a double knockout mutant was created as described in section 2.9.1. A single colony representative of a SCO was obtained from the electroporation reaction with P2NIL_PAC_1661 (Table 2.1) into ΔMSMEG_2433 single knockout mutants, Figure 3.5. This SCO colony was taken forward and grown in the absence of antibiotics, followed by selection in the presence of sucrose. White colonies were picked and spotted onto 7H10 agar supplemented with X-gal and sucrose. Seven of the colonies that remained white were screened using a PCR strategy, that was similar to one mentioned above.

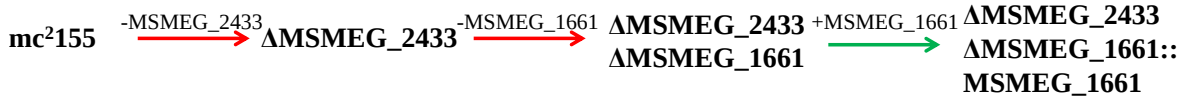

Figure 3.5. Construction of ΔMSMEG_2433 ΔMSMEG_1661 and its complemented derivative. A single knockout mutant was previously creating by removing MSMEG_2433 from the mc^{2}155 wild type strain. This was followed by deletion of MSMEG_1661 in the single knockout background and subsequent complementation with pMV1661. Red arrows indicate deletion and green arrow indicates complementation.

In this case, the product amplified by Primers 1 and 3, which flank the gene, is 1394 bp and the Primers 1 and 2 generate a 701 bp product, both of which represent the wild type gene. A schematic of the expected amplicon sizes can be found in Figure 3.6A. In the knockout mutant, the MSMEG_1661 gene should be absent, resulting in the generation of a smaller 236 bp band product, indicating the presence of the mutant allele. Of the seven colonies, five appeared to be mutants, as confirmed by the 236 bp band observed in lanes 9-13 of Figure

3.6B. Of the remaining colonies, one appeared to be a wild type revertant as confirmed by the 701 bp band found in lane 14 and the other appeared to be a SCO as confirmed by the presence of both the wild type and mutant bands in lane 15. Colonies corresponding to lanes 9-13 were picked and the genotype was further confirmed by Southern blot analysis.

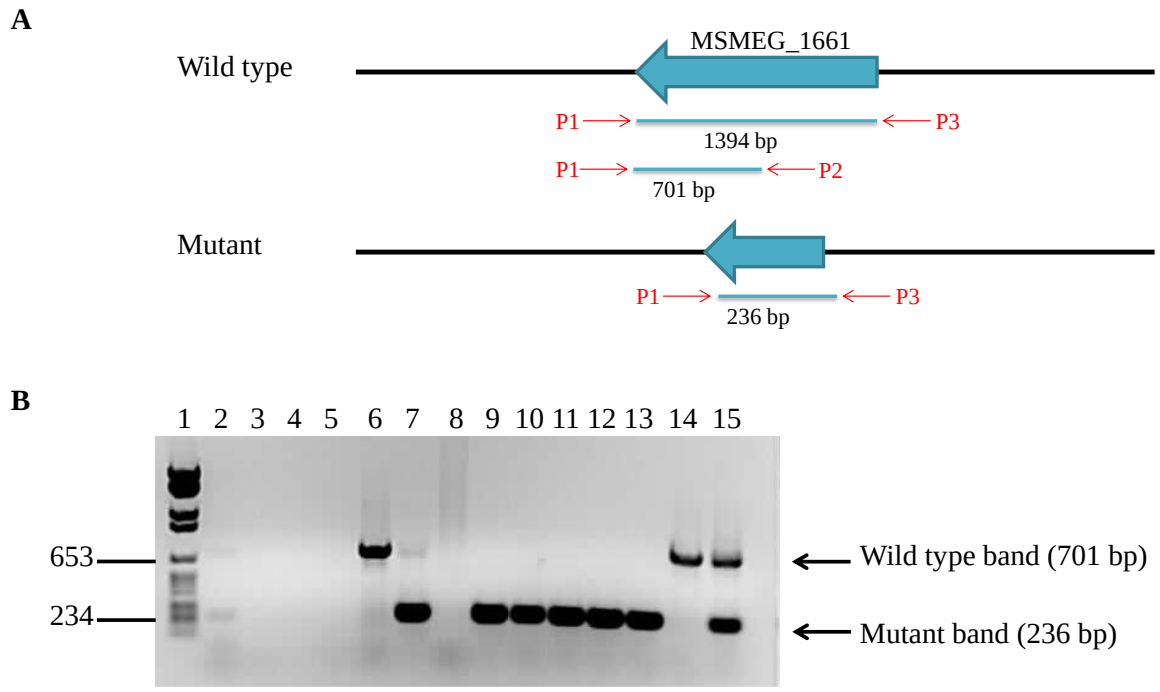

Figure 3.6. PCR screening for ΔMSMEG_1661 ΔMSMEG_2432 knockout mutants. (A) Schematic representation of genomic maps of wild type and mutant MSMEG_1661 region. Primer positions (red arrows) and expected amplicon sizes are shown. P1 = Primer 1, P2= Primer 2, P3 = Primer 3. (B) PCR screen for MSMEG_1661 deletion. Lane 1: Marker VI, Lane 2: No DNA, Lane 3 to 5: primer controls, Lane 6: wild type, Lane 7: SCO, Lane 9 to 15: Clones 1 to 7. Once again, the bigger band (1394 bp) is not seen in any of the wild type strains due to competition of reagents resulting in preferential amplification of the 701 bp band.

Genomic DNA was extracted from wild type, SCO and the selected colonies using the CTAB DNA extraction method described in section 2.3.2.2. The enzyme chosen to perform Southern blot analysis on the MSMEG_2433 upstream and MSMEG_1661 upstream regions was *Nco*I with digestions set up as mentioned previously, followed by Southern blot analysis. Once again, the integrity of the pre-existing deletion in the parental strain was confirmed to ensure that no chromosomal rearrangements took place during allelic exchange. To determine if the parental strain was correct, the probe used to create the suicide vector

P2NIL_PAC_2433 (Table 2.1), which corresponds to the region upstream of MSMEG_2433 was used, Figure 3.7A. To identify possible double knockout mutants, the probe created from the P2NIL_PAC_1661 (Figure 2.1) suicide vector which corresponds to the region upstream of MSMEG_1661 was used, Figure 3.7C. The results of the Southern blots for the MSMEG_2433 and MSMEG_1661 upstream probes are shown in Figure 3.7B and 3.7D respectively, with the expected sizes shown in Figure 3.7A and 3.7C respectively. From the Southern blot of the parental strain, Figure 3.7A and 3.7B, it can be seen that there is a size difference between the wild type and mutant strains in the region probed. The *Nco*I digests produced a smaller band in the mutant strain (0.82 kbp vs 1.67 kbp in the mutant vs wild type respectively) due to the decrease in size of the MSMEG_2433 gene. This confirms that the parental strain is indeed a MSMEG_2433 knockout mutant. Confirmation of the loss of MSMEG_1661 in this background can be seen by the reduction in size of the band observed for the *Nco*I digest (1.35 kbp vs 2.5 kbp in the mutant vs wild type respectively) in the mutant strain, Figure 3.7C and 3.7D. This decrease in size is due to the decrease in size of the MSMEG_1661 gene, confirming that this strain is also a MSMEG_1661 knockout mutant. The SCO for this strain displays all expected band sizes confirming that no mutations occurred during recombination. These data confirmed the deletion of MSMEG_1661 from ΔMSMEG_2433 background. However, the integrity of both the upstream and downstream regions, of both the genes, required confirmation. One clone was selected and further analyzed by Southern blot analysis using the restriction enzyme *Mlu*I. Genomic DNA was extracted from wild type, the single knockout mutants ΔMSMEG_1661 and ΔMSMEG_2433 as well as the selected double knockout mutant. The parental strain was confirmed by using the probes shown in Figure 3.8A which correspond to the upstream and downstream regions used to generate the suicide vector P2NIL_PAC_2433 (Table 1). The Southern blot results

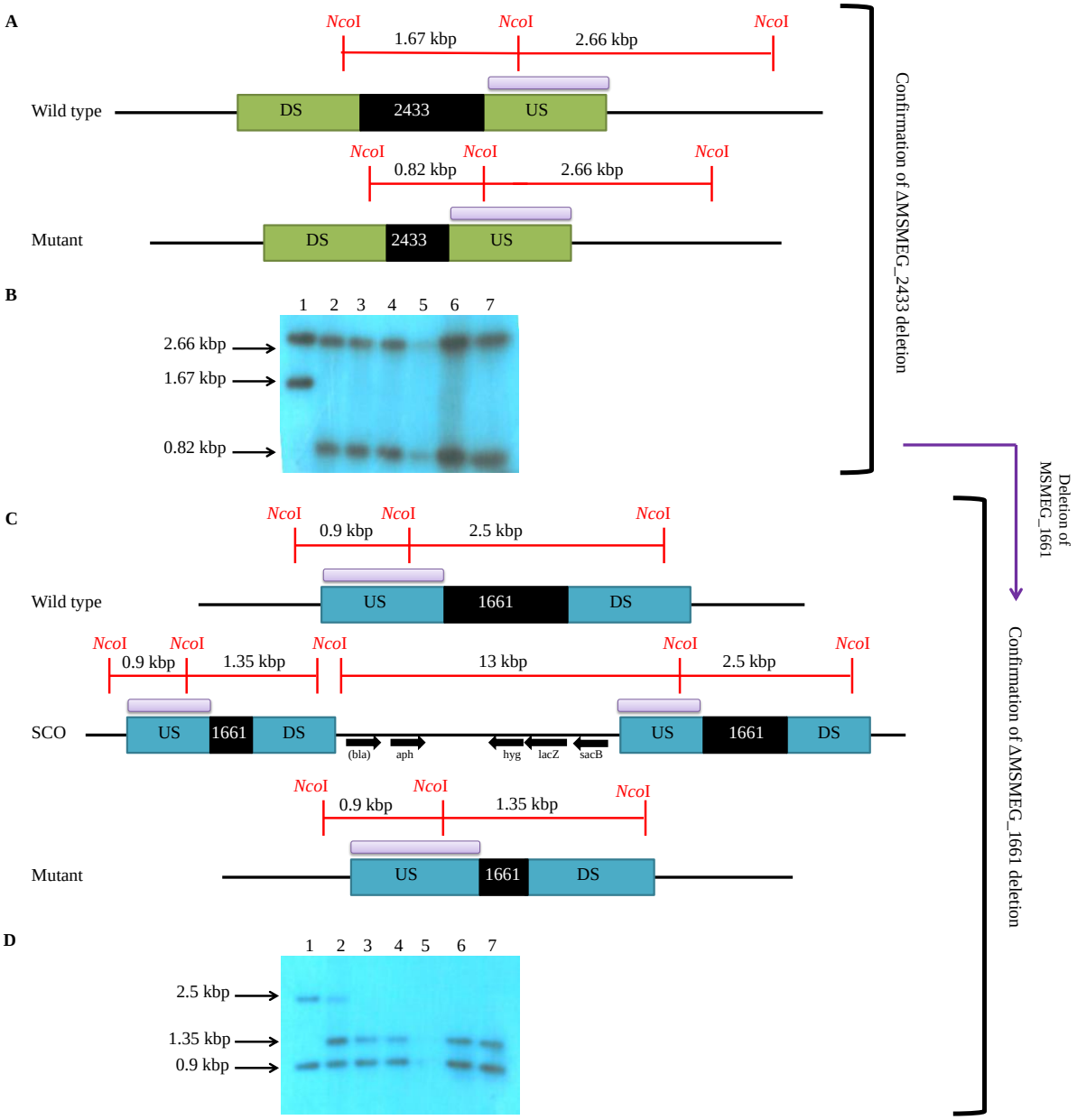

Figure 3.7. Screening of ΔMSMEG_2433 ΔMSMEG_1661 possible double crossover mutants. (A) Schematic representation of genomic maps of wild type and mutant MSMEG_2433 regions. Probes, restriction enzymes and expected fragment sizes are shown. (B) Southern blot with MSMEG_2433 upstream probe. Lane 1: *NcoI* digested wild type DNA, Lane 2 to 7: *Nco*I digested Δ2433Δ1661 DNA. (C) Schematic representation of genomic maps of wild type, SCO and mutant MSMEG_1661 regions. Probes, restriction enzymes and expected fragment sizes are shown. (D) Southern blot with 1661 upstream probe. Lane 1: *Nco*I digested wild type DNA, Lane 2: *Nco*I digested SCO DNA, Lane 3 to 7: *Nco*I digested ΔMSMEG_2433 ΔMSMEG_1661 DNA. The 13 kbp band did not appear.

for MSMEG_2433 upstream and downstream probes are shown in Figure 3.8B and 3.8C respectively. A decrease in the band observed for the *Mlu*I digests is due to the decrease in size of the MSMEG_2433 gene. This can be seen with the upstream (0.82 kbp vs 1.67 kbp in the mutant vs wild type respectively) and the downstream (0.82 kbp vs 1.67 kbp in the mutant

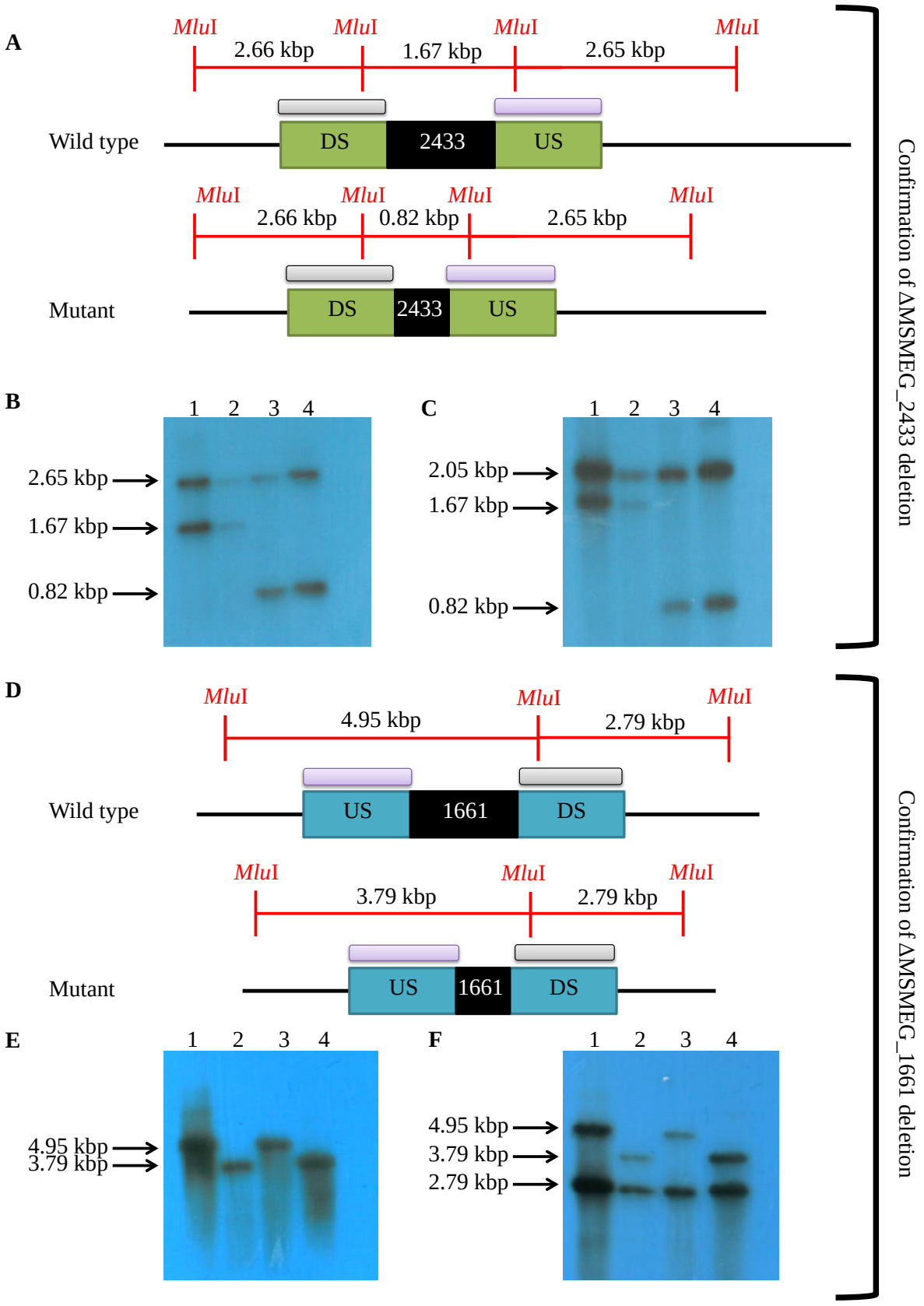

Figure 3.8. Genotypic confirmation of the ΔMSMEG_2433 ΔMSMEG_1661 strain. (A) Schematic representation of genomic maps of wild type and mutant MSMEG_2433 regions. Upstream and downstream probes are shown in purple and grey respectively. Restriction enzyme sites and expected fragment sizes are also shown. (B) Southern blot with MSMEG_2433 upstream probe. (C) Southern blot with MSMEG_2433

downstream probe. (D) Schematic representation of genomic maps of wild type and mutant MSMEG_1661 regions. Upstream and downstream probes are shown in purple and grey respectively. Restriction enzyme sites and expected fragment sizes are also shown. (E) Sothern blot with MSMEG_1661 upstream probe. (F) Southern blot with MSMEG_1661 downstream probe. (C to F) Lane 1: *Mlu*I restricted wild type DNA, Lane 2: *Mlu*I restricted ΔMSMEG_1661 DNA, Lane 3: *Mlu*I restricted ΔMSMEG_2433 DNA, Lane 4: *Mlu*I restricted ΔMSMEG_2433 ΔMSMEG_1661 DNA

vs wild type respectively) probes confirming that MSMEG_2433 is deleted in the ΔMSMEG_2433 single knockout and the double knockout mutant strains. To confirm deletion of MSMEG_1661, probes shown in Figure 3.8D which corresponds to the upstream and downstream regions used to generate the suicide vector P2NIL_PAC_1661 (Table 1) were used. A decrease in the band observed for the *Mlu*I digests in the mutant strains is due to the decrease in size of the MSMEG_1661 gene. This can be seen with both the upstream (3.79 kbp vs 4.95 kbp for the mutant vs the wild type respectively), Figure 3.8E, and the downstream (3.79 kbp vs 4.95 kbp for the mutant vs the wild type respectively) probes, Figure 3.8F. Together these data prove that both MSMEG_2433 and MSMEG_1661 are deleted in this strain, now designated as ΔMSMEG_2433 ΔMSMEG_1661 (Δ2433 Δ1661 in images).

3.1.3 Generation of a double knockout mutant lacking MSMEG_2432 and MSMEG_2433

Using the P2NIL_PAC_2433 (Table 2.1) vector created by Dr. C. Ealand, a double knockout mutant was created as described in section 2.9.1. A single colony representative of a SCO was obtained from the electroporation reaction with P2NIL_PAC_2433 (Table 2.1) into ΔMSMEG_2432 single knockout mutants. This SCO colony was taken forward and grown in the absence of antibiotics, followed by selection in the presence of sucrose. White colonies were picked and spotted onto 7H10 agar supplemented with X-gal and sucrose. Colonies that remained white were screened using a PCR strategy.

The product amplified by Primer 1 and 3, which flank the gene, is 1091 bp and Primers 1 and 2 generate a 500 bp probe both of which represent the wild type gene, Figure 3.9A. In the knockout mutant, the MSMEG_2433 gene should be absent in the mutant therefore resulting in the primer situated within the gene will be unable to anneal to the template. This would result in the generation of a smaller 236 bp band product from Primers 1 and 3, indicating the presence of the mutant band. A schematic of the expected amplicon sizes can be found in Figure 3.9A. Of the eight colonies, one appeared to be a mutant, as confirmed by the 236 bp band observed in lane 9 of Figure 3.9B. The remaining six colonies appeared to be wild type revertants as confirmed by the 500 bp band found in lanes 5-6, 8 and 10-12. The colony corresponding to lane 9 was picked and the genotype was further confirmed by Southern blot analysis.

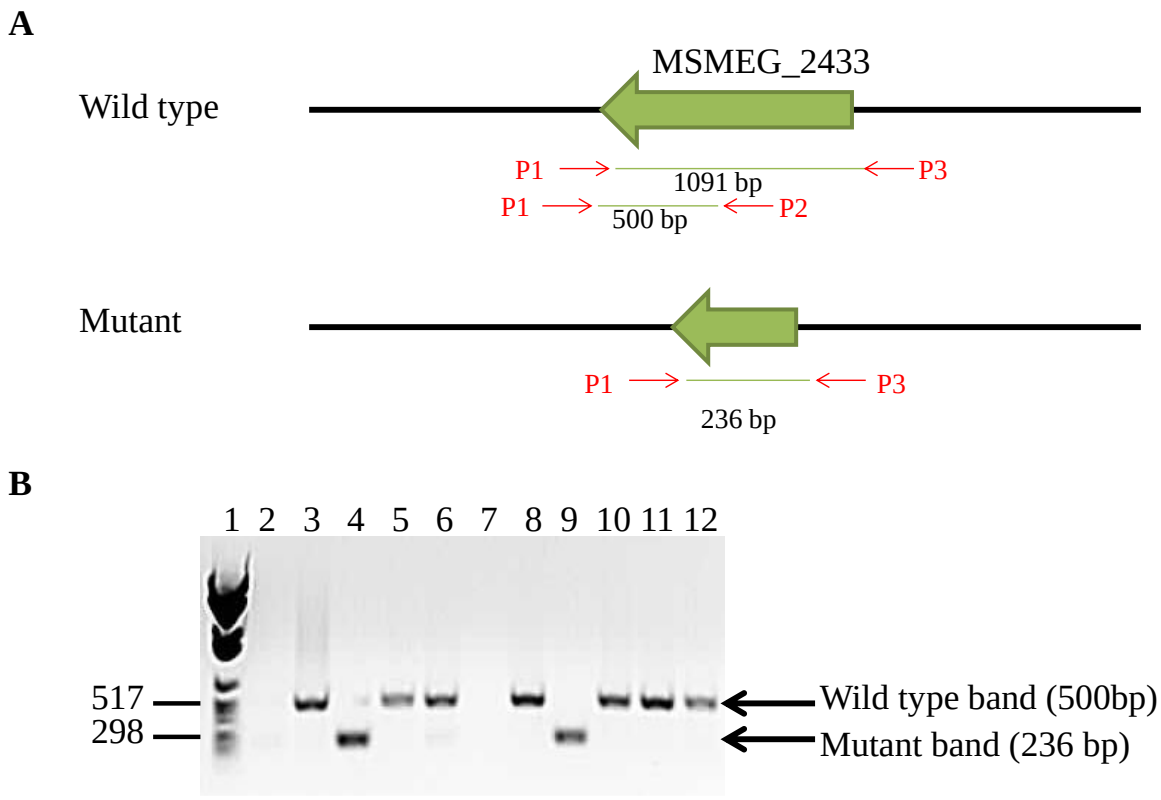

Figure 3.9. Analysis of possible ΔMSMEG_2432 ΔMSMEG_2433 double crossover mutants. (A) Schematic representation of genomic maps of wild type and mutant MSMEG_2433 region. Primer positions (red arrows) and expected amplicon sizes are shown. P1 = Primer 1, P2= Primer 2, P3 = Primer 3. (B) PCR screening of possible ΔMSMEG_2432 ΔMSMEG_2433 DCO mutants. Lane 1: marker VI, Lane 2: no DNA,

Lane 3: wild type, Lane 4: suicide vector, Lane 5-12: possible mutants. The 1091 bp band is not seen in any of the wild type strains due to competition of reagents resulting in preferential amplification of the 500 bp band.

The enzyme chosen to perform Southern blot analysis on the MSMEG_2433 upstream region was *Mlu*I, as it allows for differentiation between wild type and mutant strains. Restriction digestions and Southern blot analysis was carried out as described above. To identify possible double knockout mutants, the probe created from the P2NIL_PAC_2433 (Table 1) suicide vector, Figure 3.10A, which corresponds to the region upstream of MSMEG_2433 was used. The result of the Southern blot for the MSMEG_2433 upstream probe is shown in Figure 3.10B. The *Mlu*I digests for the wild type strain generated the bands expected – 2.65 kbp and 1.67 kbp. However, both the mutant and SCO *Mlu*I digests displayed an extra band (~2.9 kb), indicated by the blue arrow. The extra band in the SCO strain is a possible indication of

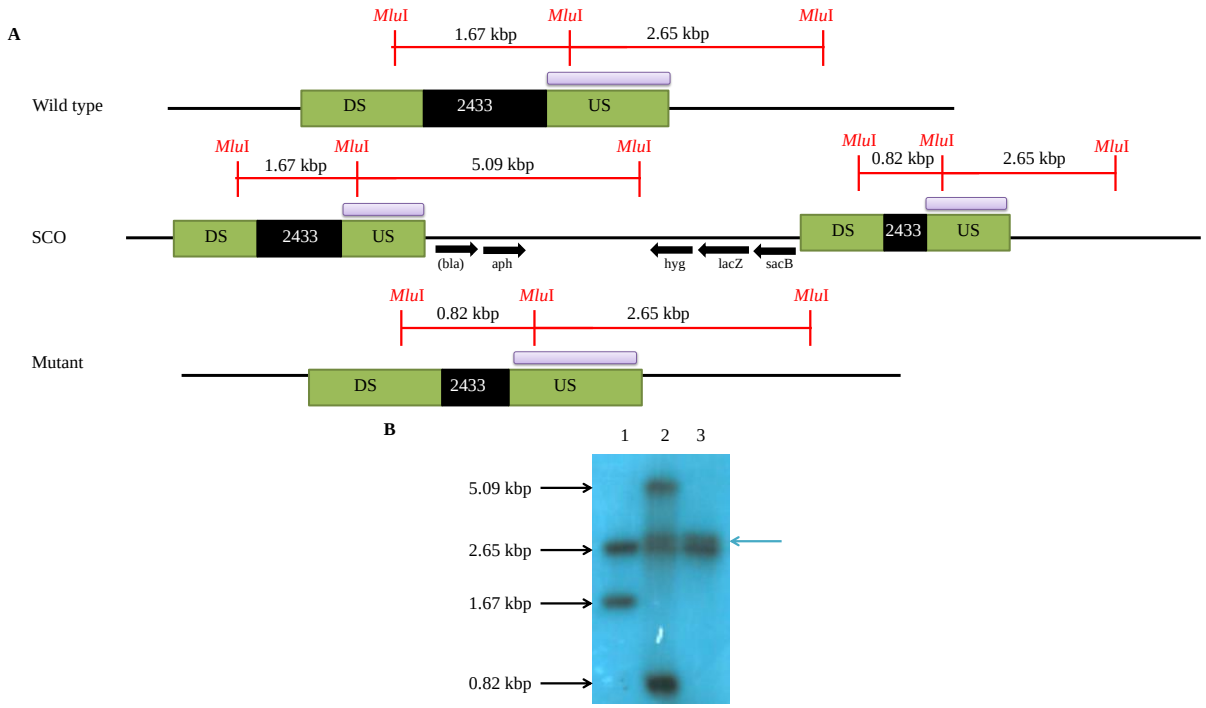

Figure 3.10. Screening of ΔMSMEG_2432 ΔMSMEG_2433 possible double crossover mutant. (A) Schematic representation of genomic maps of wild type, single crossover and mutant MSMEG_2433 regions. Probes, restriction enzyme sites and expected fragment sizes are also shown. (B) Southern blot of ΔMSMEG_2432 ΔMSMEG_2433 with MSMEG_2433 upstream probe. Blue arrow indicates additional band in single crossover and mutant strains.

mutation or rearrangement that occurred during recombination. In order to resolve this, various SCO strains were used to generate possible DCO mutants. However, of all the colonies screened none appeared to be mutants (data not shown), but the products of illegitimate recombination or wild type.

To circumvent this, another strategy was attempted which involved the electroporation of P2NIL_PAC_2432 (Table 2.1) into ΔMSMEG_2433 single knockout mutant. A SCO colony generated from this electroporation reaction was taken forward and grown in the absence of antibiotics, followed by selection in the presence of sucrose. White colonies were picked and spotted onto 7H10 agar supplemented with X-gal and sucrose. Colonies that remained white were screened using a PCR strategy.

As discussed previously, the product amplified by Primers 1 and 3 which flank the gene, is 1028 bp and Primers 1 and 2 generate a 500 bp product, both of which represent the wild type gene, Figure 3.2A. In the knockout mutant, the MSMEG_2432 gene should be absent therefore resulting in the generation of a smaller 236 bp band product indicating the presence of the mutant band. A schematic of the expected amplicon sizes can be found in Figure 3.2A. Of all the colonies screened none appeared to be mutants. All, except one which represented a SCO demonstrated in Lane 12 (top gel) of Figure 3.11, appeared to be wild type revertants as evidenced by the presence of a 500 bp band. Together, these data suggest that deletion of MSMEG_2432 in a ΔMSMEG_2433 background strain or deletion of MSMEG_2433 in a ΔMSMEG_2432 background strain proved to be problematic using the above-mentioned approaches. This could be due to the operonic nature of these genes. Consequently, no further attempt were made to construct a mutant lacking both MSMEG_2432 and MSMEG_2433.

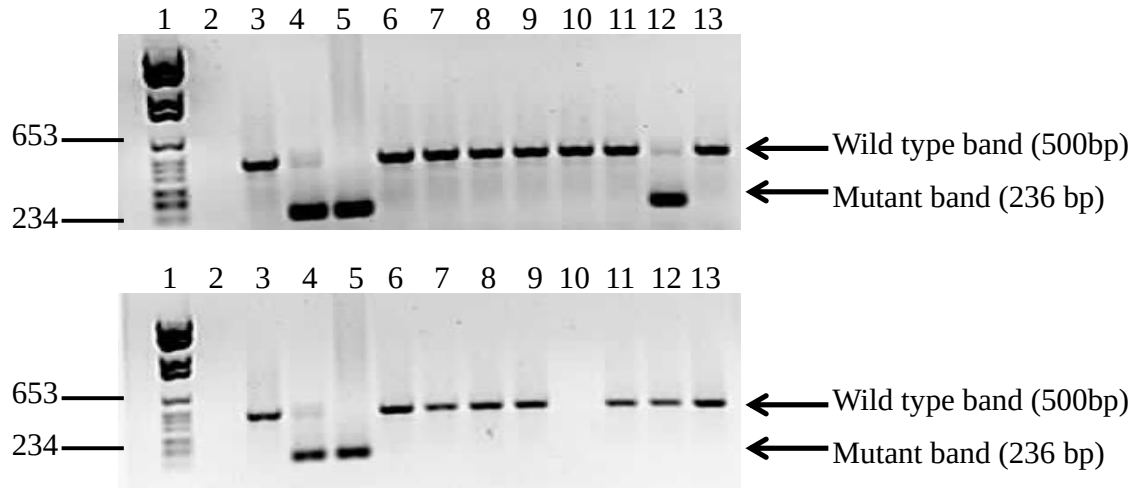

Figure 3.11. PCR screenings of possible ΔMSMEG_2433 ΔMSMEG_2432 double crossover mutants. Lane 1: Marker VI, Lane 2: no DNA, Lane 3: wild type, Lane 4: SCO, Lane 5: suicide vector, Lane 6-13: possible mutants. A schematic of the primer binding sites can be found in Figure 3.2A. Once again the 1028 bp product is not observed due to competition for PCR reagents.

3.2 Complementation of DD-CPase mutants with a single DD-CPase

Prior to electroporations, pMV1661 was extensively mapped using restriction enzymes, Figure D7 (page 130), to ensure that the correct vector was used.

Genetic complementation of both double knockout mutants was achieved by electroporation of the integrating vector pMV1661 (Table 2.1) into both ΔMSMEG_1661 ΔMSMEG_2432 and ΔMSMEG_2433 ΔMSMEG_1661 resulting in the re-introduction of the wild type allele into the genome as described in section 2.11. The pMV1661 vector is a derivative of the *E.coli*-Mycobacterium shuttle vector carrying a full length copy of MSMEG_1661 which integrates at the L5 *att*B site. A schematic of the integration process and the expected amplicon sizes can be found in Figure 3.12.

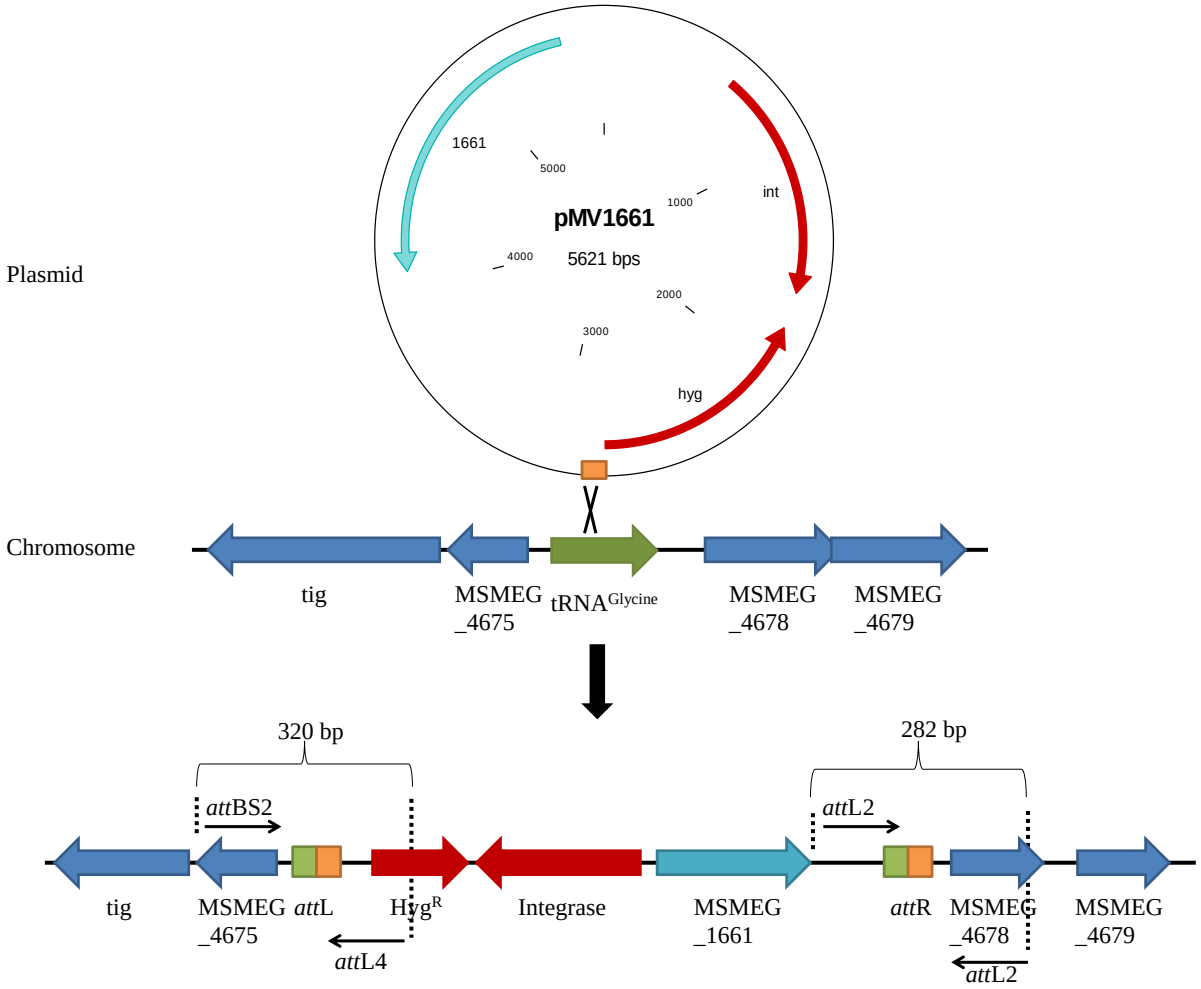

Figure 3.12. Schematic representation of integration of pMV1661 into the chromosome of *M. smegmatis*. The pMV1661 vector uses an L5 based integration system. The attachment site (orange block) integrates at the $tRNA^{Gly}$ locus on the chromosome (green arrow), which results in the incorporation of the $tRNA^{Gly}$ locus on either the left or right side of the plasmid, *att*L and *att*R. Primers used to confirm the site specific integration of pMV1661 and expected amplicon sizes are shown.

Six colonies were selected and screened by PCR to confirm site-specific integration of the complementation vector. Site specific integration of pMV1661 was confirmed using the upstream region of the integration site which is represented by the presence of a 320 bp amplicon as visualized in Figure 3.13A and 3.13C. Figure 3.13B and 3.13D confirms integration using the downstream region as evidenced by the 282 bp amplicon. This data confirmed that the ΔMSMEG_1661 ΔMSMEG_2432 and ΔMSMEG_2433 ΔMSMEG_1661 strains were successfully complemented with pMV1661 and will now be referred to as

ΔMSMEG_1661 ΔMSMEG_2432::MSMEG_1661 (Δ1661 Δ2432C in images) and ΔMSMEG_2433 ΔMSMEG_1661::MSMEG_1661 (Δ2433 Δ1661C in images) respectively.

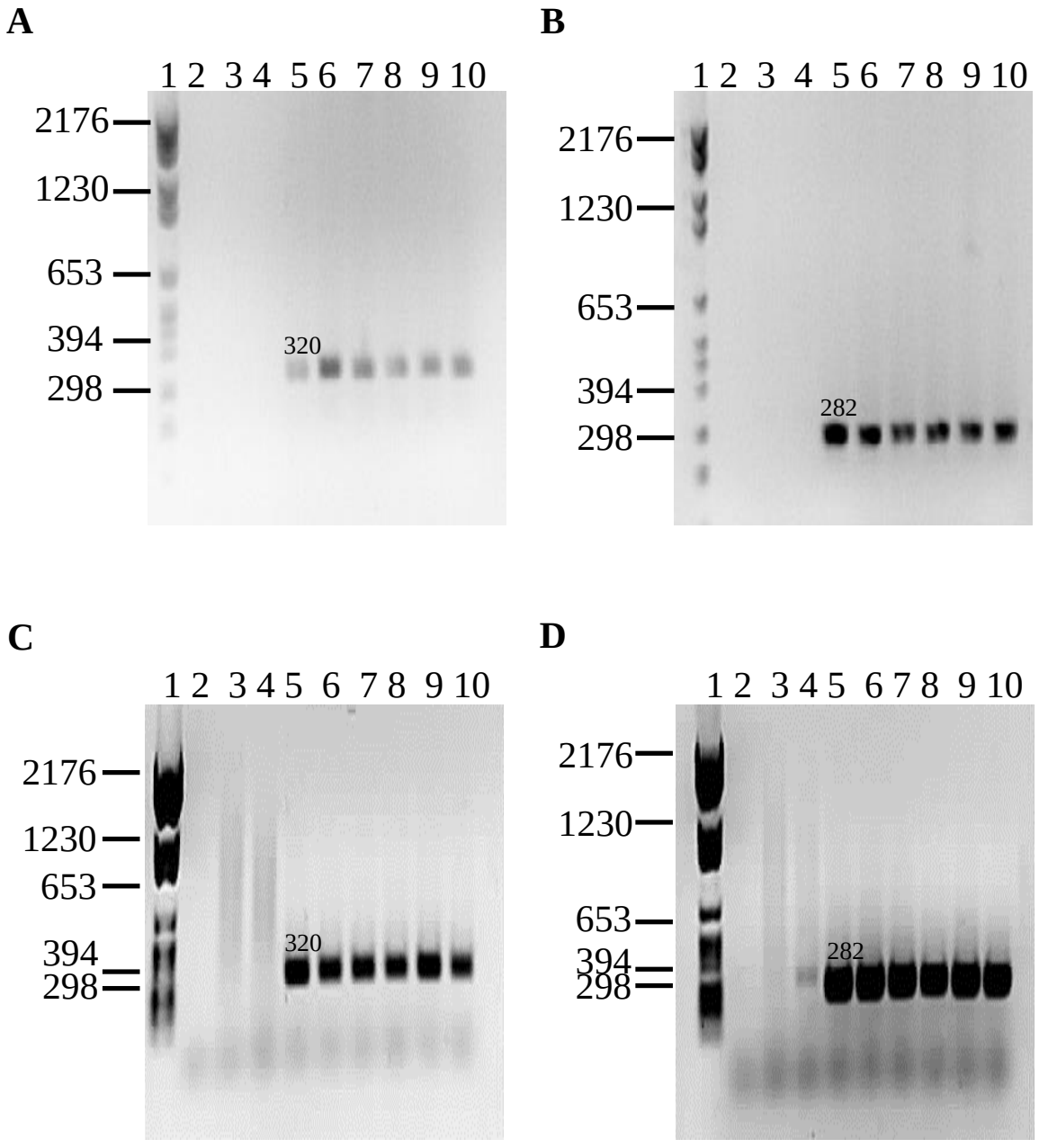

Figure 3.13. PCR confirmation of site specific integration of pMV1661 into the double knockout mutants. (A) ΔMSMEG_1661 ΔMSMEG_2432 amplicons for primer set attBS2 + attL4, (B) ΔMSMEG_1661 ΔMSMEG2432 amplicons for primer set attBS1 + attL2, (C) ΔMSMEG_2433 ΔMSMEG_1661 amplicons for primer set attBS2 + attL4, (D) ΔMSMEG_2433 ΔMSMEG_1661 amplicons for primer set attBS1 + attL2. Lane 1: Marker VI, Lane 2: No DNA, Lane 3: wild type, Lane 4: ΔMSMEG_1661 ΔMSMEG_2432 or ΔMSMEG_2433 ΔMSMEG_1661, Lane 5-10: possible clones carrying the complementation vector. See Figure 3.12 for primer binding regions.

3.3 Gene expression analysis of DD-CPases to confirm deletion and genetic complementation

Gene expression analysis was performed as described in section 2.12 in order to confirm deletion of genes as well as to assess whether these deletion results in compensatory gene expression changes in the remaining DD-CPases.

The expression profile for MSMEG_2432 can be found in Figure 3.14. The data revealed that all strains deficient of this gene (ΔMSMEG_2432, ΔMSMEG_1661 ΔMSMEG_2432 and ΔMSMEG_1661 ΔMSMEG_2432::MSMEG_1661) displayed no detectable levels of MSMEG_2432 mRNA, as expected. Strains in which MSMEG_2432 was present such as the wild type, ΔMSMEG_1661, ΔMSMEG_2433, ΔMSMEG_2433 ΔMSMEG_1661 and ΔMSMEG_2433 ΔMSMEG_1661::MSMEG_1661 all contained MSMEG_2432 mRNA

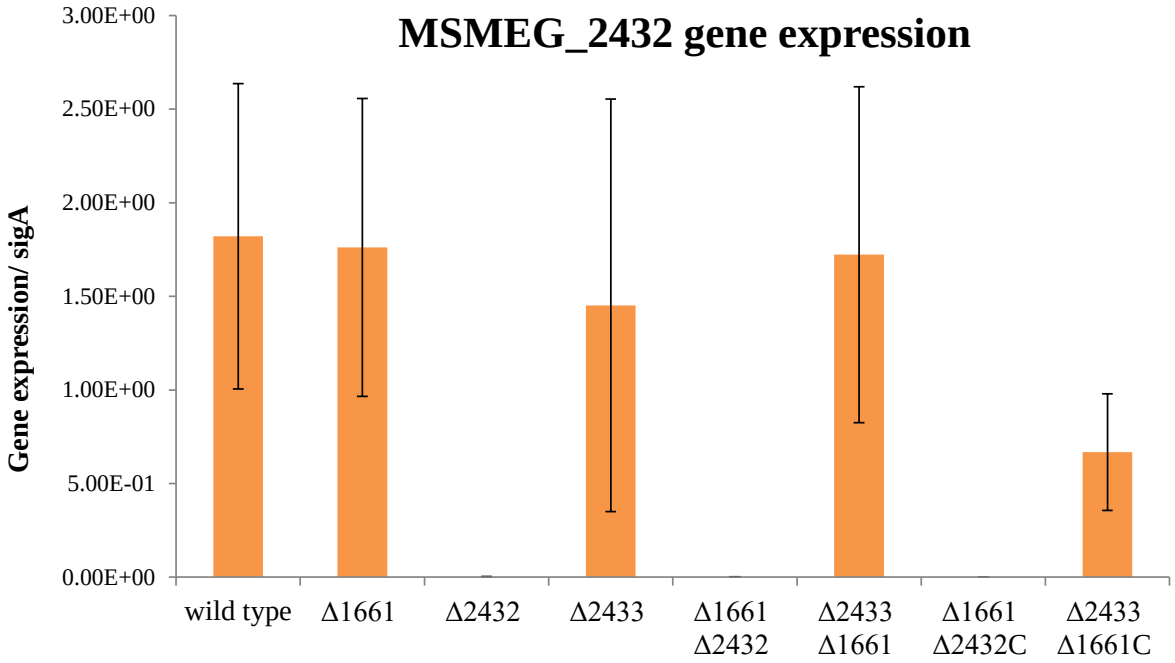

Figure 3.14. Expression analysis of cellular mRNA for MSMEG_2432 relative to *sig*A standard. Analysis was done on three different sets of RNA with the data indicating an average of these three experiments. Error bars indicate standard error.

expressed at an equivalent level. The levels of MSMEG_2432 mRNA detected in these strains were roughly similar to wild type except in the case of ΔMSMEG_2433 ΔMSMEG_1661::MSMEG_1661 where levels of transcript were decreased but this difference was not statistically significant. These data indicated that the MSMEG_2432 gene was successfully deleted in the ΔMSMEG_2432, ΔMSMEG_1661 ΔMSMEG_2432 and ΔMSMEG_1661 ΔMSMEG_2432::MSMEG_1661 strains. The data also shows that there is no compensatory increase in expression of MSMEG_2432 when other DD-CPases are deleted.

The expression profile for MSMEG_2433 can be found in Figure 3.15. The data for MSMEG_2433 was similar to that of MSMEG_2432 in that strains deficient for MSMEG_2433 (ΔMSMEG_2433, ΔMSMEG_2433 ΔMSMEG_1661 and ΔMSMEG_2433 ΔMSMEG_1661::MSMEG_1661) all displayed no detectable levels of the MSMEG_2433 mRNA transcript. Expression levels of the transcript were increased in the ΔMSMEG_2432

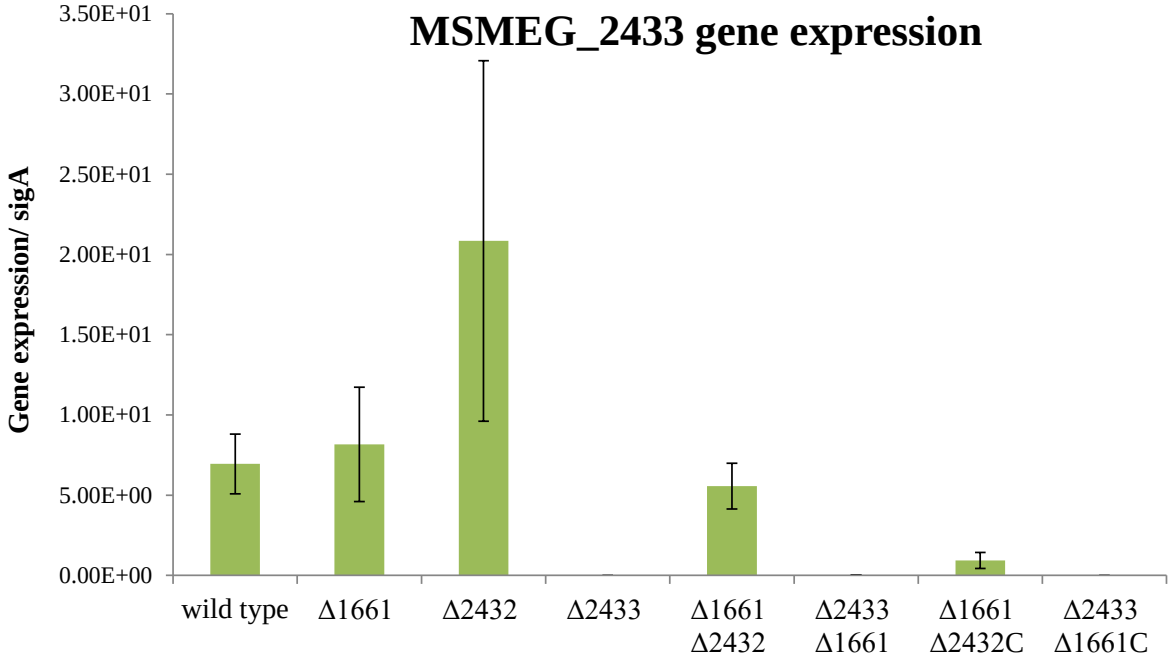

Figure 3.15. Expression analysis of cellular mRNA for MSMEG_2433 relative to *sig*A standard. Analysis was done on three different sets of RNA with the data indicating an average of these three experiments. Error bars indicate standard error.

single knockout mutant when compared to the wild type and decreased in the ΔMSMEG_1661 ΔMSMEG_2432::MSMEG_1661 strain with the latter being statistically significant ($p < 0.05$). These data indicated that MSMEG_2433 was successfully deleted in the ΔMSMEG_2433, ΔMSMEG_2433 ΔMSMEG_1661 and ΔMSMEG_2433 ΔMSMEG_1661::MSMEG_1661 strains. The data also demonstrates that when MSMEG_2432 is deleted, a higher level of MSMEG_2433 mRNA is observed, although this difference was not statistically significant.

The expression profile for MSMEG_1661 can be found in Figure 3.16. The data for MSMEG_1661 mRNA expression revealed that all strains deficient for the MSMEG_1661 gene yielded a basal level of expression. SYBR green is a fluorescent dye that binds all double stranded molecules. Since the data collected for the MSMEG_1661 gene in corresponding mutant strains were not as expected, the melt curve data was analyzed shown in Figure D8 (page 131). The data revealed that the signal produced in the mutant strains was

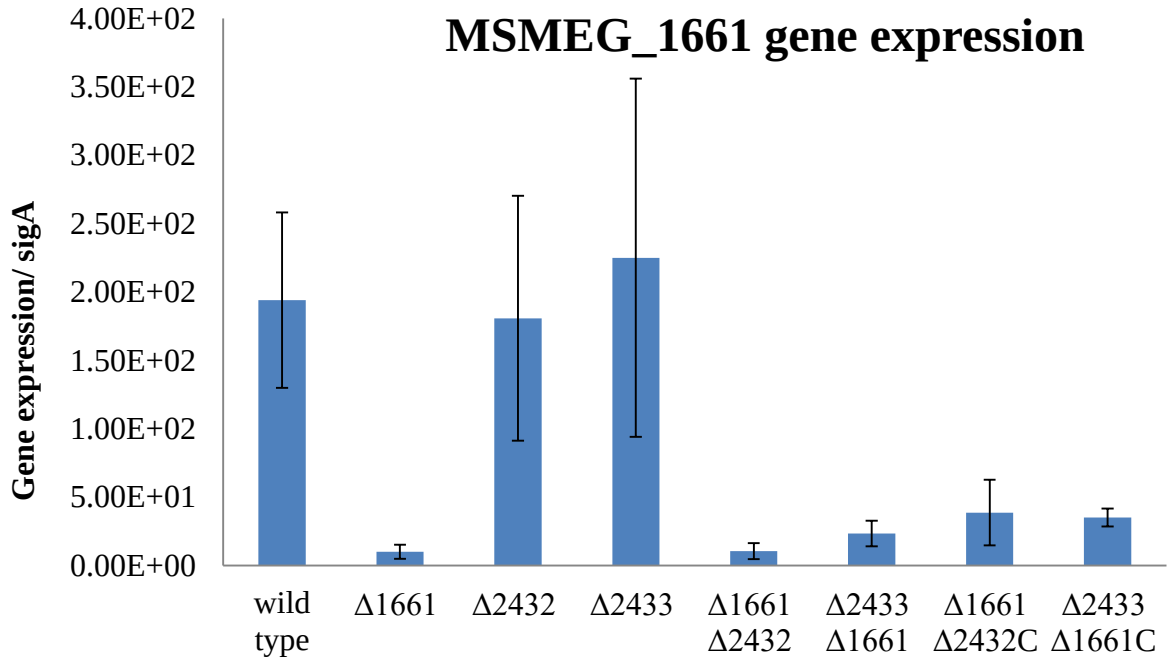

Figure 3.16. Expression analysis of cellular mRNA for MSMEG_1661 relative to *sig*A standard. Analysis was done on three different sets of RNA with the data indicating an average of these three experiments. Error bars indicate standard error.

due to a non-specific product being amplified from the template cDNA as seen by the shift in the melt peaks as well as a change in the melt peak temperature when compared to genomic standards for MSMEG_1661. Similar levels of MSMEG_1661 were detected in the wild type and MSMEG_2433 and MSMEG_2432 deletion strains suggesting no compensatory changes in gene expression. Lower levels of MSMEG_1661 mRNA was detected in the complemented strains when compared to the wild type strain indicating that full restoration of MSMEG_1661 was not achieved, however, melt peak temperature of the complemented derivatives were specific for MSMEG_1661. This data confirms the absence of MSMEG_1661 from the mutant strains – ΔMSMEG_1661, ΔMSMEG_1661 ΔMSMEG_2432 and ΔMSMEG_2433 ΔMSMEG_1661.

3.4 The role of DD-CPases in cell growth

3.4.1 Regulation of *M. smegmatis* growth kinetics

Growth analysis was performed on the wild type, double knockout mutants and their complemented derivatives to determine if DD-CPases have an impact on regulating growth kinetics. This was achieved by carrying out three independent experiments using different batches of 7H9 broth and different freezer stocks. Growth analysis was also carried out in Sauton's minimal media at pH 7.3 and pH 5.5. Growth experiments were set up as described in section 2.12.1. The data collected at every time point was represented using scatter plots, Figure 3.17A- 3.17C.

The data revealed that when grown in standard 7H9 broth, there were no significant differences in growth kinetics between the strains in the first 18 hr of growth. A slight, but non-significant, difference could be seen in the stationary phase of growth, with the wild type reaching a higher OD_{600nm} reading than the other strains. These data suggest that DD-CPases

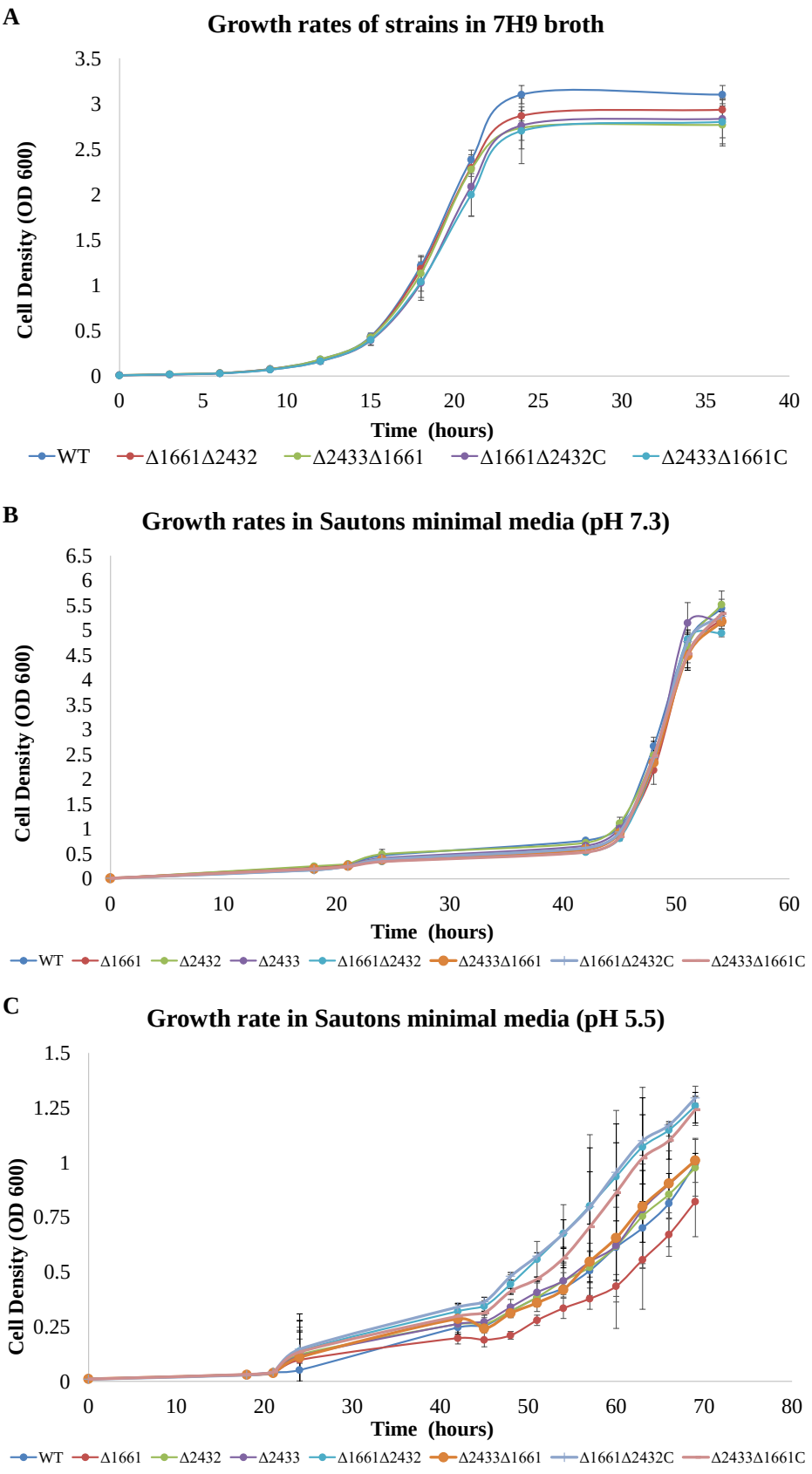

Figure 3.17. Growth kinetics of strains lacking DD-CPases. (A) Graph depicting growth in standard 7H9 broth. (B) Graph depicting growth in Sauton's minimal media pH 7.3. (C) Graph depicting growth in Sauton's

minimal media pH 5.5. Each graph demonstrates an average of three independent experiments with error bars representing standard error.

do not play a significant role in regulating *M. smegmatis* growth kinetics under standard conditions.

Growth in Sauton's minimal media at pH 7.3 also revealed no significant differences in growth kinetics between wild type and any of the mutant strains at any stage of growth, again suggesting that DD-CPases do not play a significant role in regulating growth kinetics of *M. smegmatis* under nutrient depravation as demonstrated in Figure 3.17B.

Growth at pH 5.5 in Sauton's minimal media revealed changes in growth for all strains after 24 hours, Figure 3.17C. The single knockout mutant ΔMSMEG_1661 grew at a much slower rate than all the other strains including wild type. The remaining single knockout mutants – ΔMSMEG_2432 and ΔMSMEG_2433 – as well as the double knockout mutant ΔMSMEG_2433 ΔMSMEG_1661 grew at similar rates to that of the wild type. The complemented strains and the ΔMSMEG_1661 ΔMSMEG_2432 double knockout mutant appeared to grow at a faster rate than the wild type strain during the log phase of growth with these differences being statistically different ($p < 0.05$). This data, in addition to the Sauton's pH 7.3 data, suggest that acid stress affects growth kinetics of *M. smegmatis* in the absence of one or two DD-CPases.

3.4.2 Maintenance of *M. smegmatis* colony morphology

In Mtb, overexpression of DacB2 resulted in defective smooth colonies suggestive of a role in colony formation (Bourai et al., 2011). However, the loss of DacB did not alter colony morphology possibly due to the remaining DD-CPases in the organism (Bourai et al., 2011). Hence, to determine if *M. smegmatis* DD-CPases play a role in colony morphology, all strains were spotted onto 7H10 agar as described in section 2.12.3.

The data indicated that in the absence of one or two DD-CPase genes, colony morphology of *M. smegmatis* was not compromised as shown in Figure 3.18. All strains produced colonies of the same size, colour and cording as expected of *M. smegmatis*. This suggests that DD-CPases do not play a role in colony formation in mycobacteria.

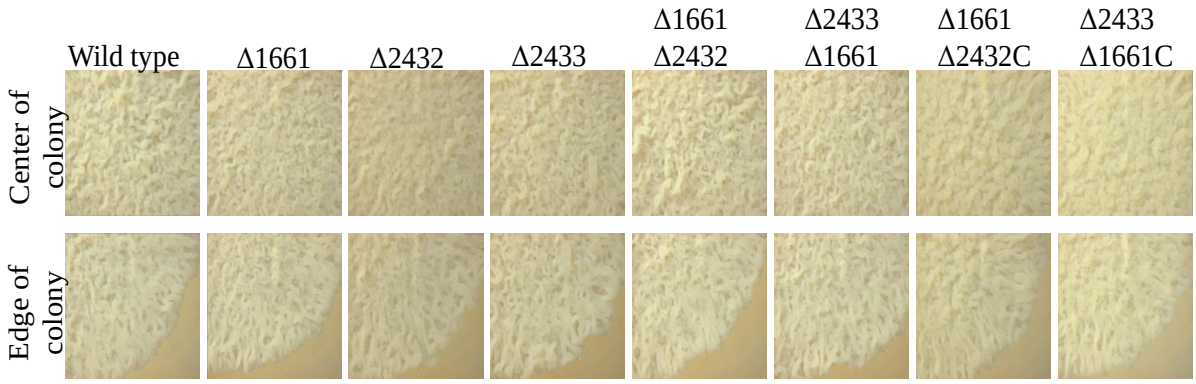

Figure 3.18. The effect of DD-CPase deletions on colony morphology. Image shows one dilution for each strain. Top depicts center of colony and bottom depicts the edge of the same colony. Picture is representative of three experiments.

3.4.3 Maintenance of *M. smegmatis* biofilm formation

E. coli mutants lacking PBP5, PBP6 and PBP7 in different combinations have impaired biofilm forming ability (Gallant et al., 2005). Therefore, we investigated if *M. smegmatis* DD-CPases play a role in biofilm formation. The formation of biofilms at the liquid air interface of stationary phase cultures were observed as described in section 2.12.4. Both *M. smegmatis* and Mtb have been shown to form biofilms, which contribute to drug resistance and the ability of the bacteria to persist in the host (Ojha et al., 2005, Ojha et al., 2008). Mycolic acid biosynthesis in *M. smegmatis* has been linked to biofilm formation with a disruption in this pathway leading to defective biofilm formation (Ojha et al., 2005). Mtb biofilms have been shown to harbor persister cells, with the extracellular matrix structure containing an abundance of free mycolic acids (Ojha et al., 2008).

Biofilm formation for the wild type, mutant and complemented strains, shown in Figure 3.19, was measured by the formation of a pellicle on the surface of the liquid cultures. The image

represents serial dilutions ranging from 10^0 – 10^5 for each strain. All strains grew at a similar rate with biofilm formation observed in all dilutions. No significant differences can be

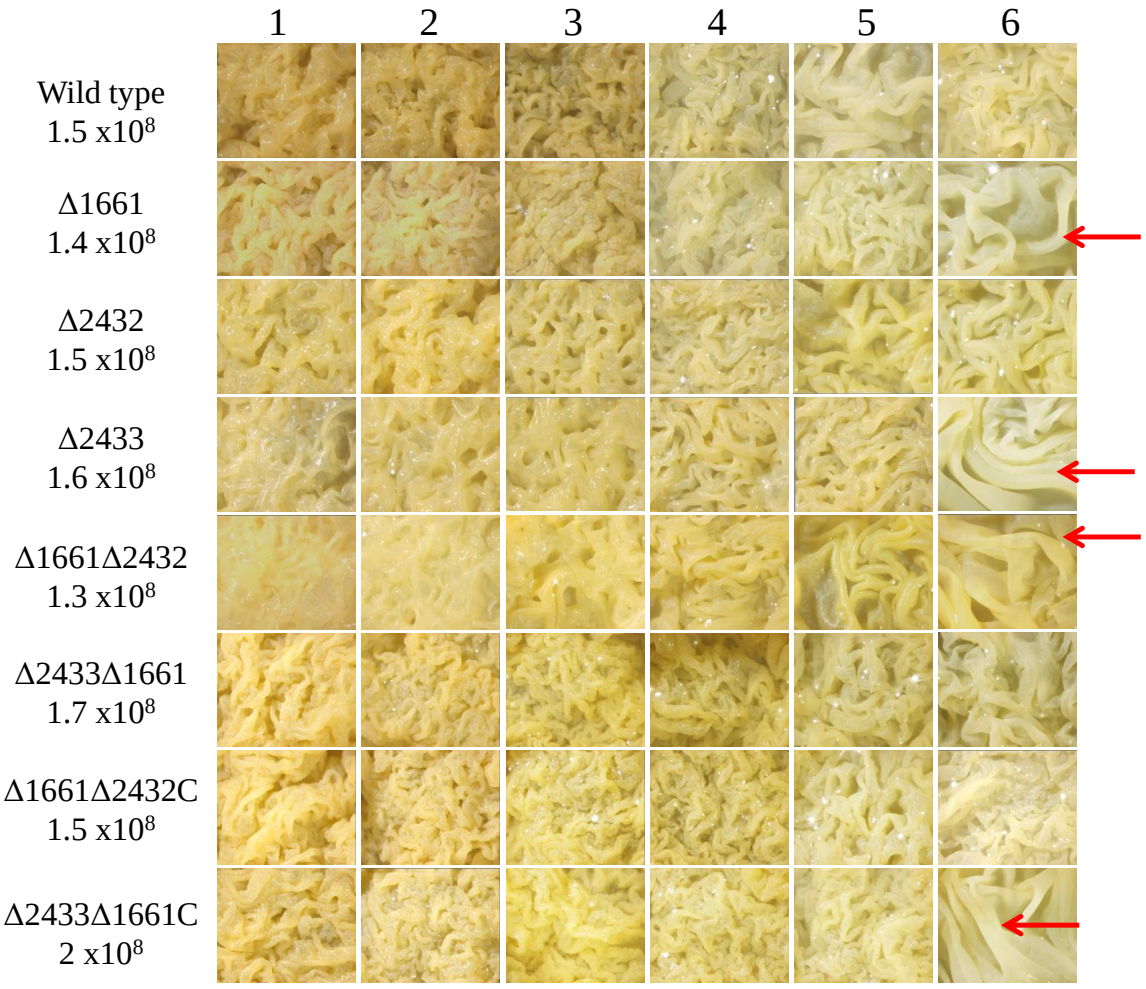

Figure 3.19. Biofilm formation in strains lacking DD-CPases. Images are representative of three experiments. 1 to 6 indicates a serial dilution of the initial inoculum from 10^0 to 10^5. [1] 10^0, [2] 10^1, [3] 10^2, [4] 10^3, [5] 10^4, [6] 10^5. Initial CFUs for stating inoculums of biofilms are indicated under strain names. Red arrow indicates long ruffles. Picture is representative of three experiments.

detected in the 10^0 – 10^4 dilutions. However, slight differences were observed in the highest dilution (10^5) of some strains. The single knockout mutants ΔMSMEG_1661 and ΔMSMEG_2433 as well as ΔMSMEG_1661 ΔMSMEG_2432 and ΔMSMEG_2433 ΔMSMEG_1661::MSMEG_1661 produced ruffles that appear to be longer than those of wild type, indicated by the red arrows. These long ruffles were not seen in the double knockout ΔMSMEG_2433 ΔMSMEG_1661 mutant or any of the strains deficient for MSMEG_2432 (ΔMSMEG_2432, and ΔMSMEG_1661 ΔMSMEG_2432::MSMEG_1661). These data

suggest that MSMEG_1661 and/or MSMEG_2433 could play a role in biofilm formation. However, the phenotype is marginal and requires further confirmation.

3.4.4. Maintenance of *M. smegmatis* sliding motility

Mycobacteria have the ability to translocate on semi-solid media by a sliding mechanism where bacteria spread as a monolayer of cells away from the point of inoculation (Martinez et al., 1999). This sliding ability is due to the presence of certain lipids and macromolecules on the outer surface of cells (Martinez et al., 1999). Since the deletion DD-CPases could affect the structure of the cell wall and possibly affect sliding capacity, we tested the sliding motility of our mutants as described in section 2.12.5. There were no significant differences in mycobacterial sliding between the wild type and any of the mutant or complemented strains tested, as witnessed in Figure 3.20. All strains displayed typical mycobacterial sliding with the initial growth found on the surface of the agar at the point of inoculation after which growth spread outward. These data suggest that DD-CPases do not play a significant role in sliding motility of *M. smegmatis*.

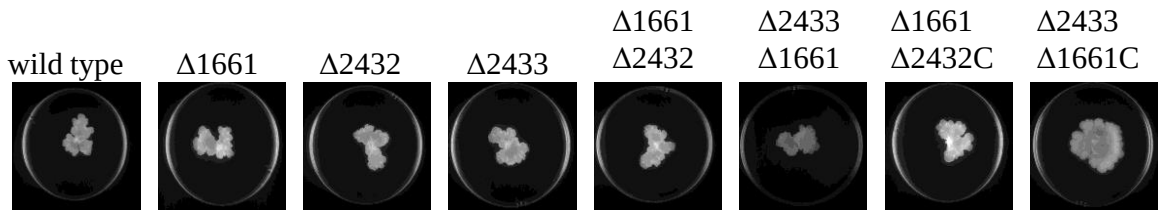

Figure 3.20. Sliding motility of the wild type and DD-CPase knockout strains. Growth was found on the surface of the agar for all strains. Picture is representative of four experiments.

3.5 DD-CPases play a role in antibiotic sensitivity

Deletion of multiple LMW PBPs in *E. coli* render the organism more susceptible to treatment with β- lactam antibiotics (Denome et al., 1999). In Mtb treatment with carbapenems results in pentapeptide accumulation, indicating that a DD-CPase may be the target of the antibiotic (Kumar et al., 2012). We have previously demonstrated that loss of a single DD-CPase does

not alter mycobacterial susceptibility to antibiotics (Ealand et al., unpublished). Hence we tested the antibiotic sensitivity of mutants lacking two DD-CPases by MICs as described in section 2.12.6. Since deletion of DD-CPases could alter cell wall integrity, a range of antibiotics able to damage the cell wall was used, as well as general drugs used to treat TB. MICs were determined in 7H9 broth and the results are shown in Table 3.1. The antibiotics that target the cell wall – Ampicillin, Vancomycin, Imipenem and the Cephalosporins – yielded differential susceptibility for one or both of the double knockout mutants. In some cases, mutants were up to 2-fold more susceptible to antibiotics – Cefamandole, Ceftriaxone

Table 3.1. MIC concentrations (µg/ml) of wild type, double knockout mutants and complemented strains.

ANTIBIOTIC	Wild type	ΔMSMEG_1661 ΔMSMEG_2432	ΔMSMEG_2433 ΔMSMEG_1661	ΔMSMEG_1661 ΔMSMEG_2432C	ΔMSMEG_2433 ΔMSMEG_1661C
Ampicillin	37.5 - 75	18.7	37.5	37.5	37.5 - 75
Vancomycin	0.391 – 0.781	0.195	0.195 – 0.391	0.391 – 0.781	0.195 - 0.391
Imipenem	6.25 – 12.5	1.563 – 3.125	3.125 – 6.25	3.125	6.25 – 12.5
Cefamandole	125	62.5 - 125	125	125 - 250	125 - 250
Cefoxitin	20	10	10 - 20	20	20
Cefotaxime	93.75 - 187.5	46.875 - 93.75	46.875	93.75	93.75
Cefatriaxone	125 - 250	62.5 - 125	125	125 - 250	125 - 250
Cefapirin	50 - 100	12.5 - 25	25 – 50	50	50 - 100
Rifampicin	0.625	0.625	0.625	0.625	0.625
Erythromycin	0.039	0.0195	0.0195 - 0.039	0.039	0.078
D- cycloserine	26.25 – 52.5	26.25 – 52.5	26.25 – 52.5	52.5	52.5

Purple boxes indicate a decrease in the MIC when compared to the wild type strain whereas green boxes indicate an increase in the MIC when compared to the wild type strain. This data is representative of three experiments.

and Cefapirin. In general, the ΔMSMEG_1661 ΔMSMEG_2432 double knockout mutant appeared to be more susceptible than the ΔMSMEG_2433 ΔMSMEG_1661 mutant. Genetic complementation partially restored antibiotic susceptibility.

As differences were marginal, antibiotic susceptibility was also tested on agar plates that contained antibiotics at the concentrations of the MIC determined above. A control plate with no antibiotic was included. Dilutions of cells ranging from 10^0 – 10^5 were spotted onto agar plates containing antibiotic and susceptibility was determined by visualising growth. CFUs were included to ensure there was no bias in initial inoculum between strains. The ΔMSMEG_1661 ΔMSMEG_2432 mutant strain appeared to be more susceptible to Ampicillin, Cefamandole, Cefapirin, Cefoxitin, Ceftriaxone and Vancomycin when compared to the wild type and its complemented derivative as demonstrated in Figure 3.21. The ΔMSMEG_2433 ΔMSMEG_1661 mutant appeared to be more susceptible to Cefamandole, Cefapirin, Cefoxitin and Cefatriaxone as witnessed by the reduced growth of this strain in Figure 3.21. The ΔMSMEG_2433 ΔMSMEG_1661 mutant also appeared to have increased sensitivity to vancomycin. Both complement strains, equivalent to single knockout mutants, display no sensitivity to antibiotics and behave similarly to the wild type, as expected. These data suggest that sensitivity to cell wall antibiotics is increased only in the absence of two DD-CPases.

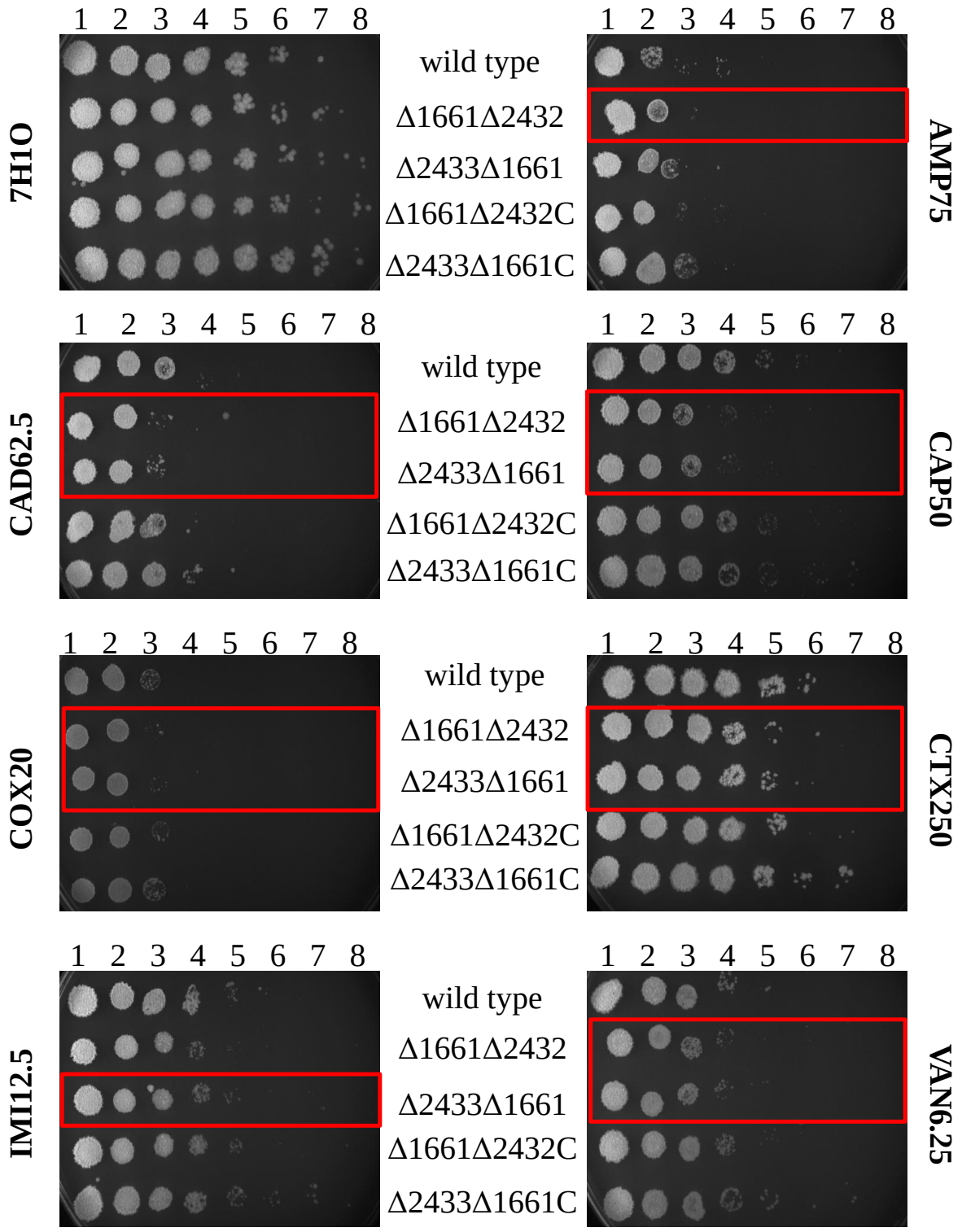

Figure 3.21. Drug susceptibility of wild type and double DD-CPase knockout mutants. 1 to 8 indicates a serial dilution of the initial inoculum from 10^0 to 10^7. [1] 10^0, [2] 10^1, [3] 10^2, [4] 10^3, [5] 10^4, [6] 10^5, [7] 10^6, [8] 10^7. CFU counts for plates (cfu/ml): wild type = 1.6 x10^8, ΔMSMEG_1661 ΔMSMEG_2432 = 1.5 x10^8, ΔMSMEG_2433 ΔMSMEG_1661 = 1.4 x10^8, ΔMSMEG_1661 ΔMSMEG_2432::MSMEG_1661 = 1.6 x10^8, ΔMSMEG_2433 ΔMSMEG_1661::MSMEG_1661 = 1.4 x10^8. AMP75 = ampicillin at 75 µg/ml, CAD62.5 = cefamandole at 62.5 µg/ml, CAP50 = cefapirin at 50 µg/ml, COX20 = cefoxitin at 20 µg/ml, CTX250 = ceftriaxone at 250 µg/ml, IMI12.5 = imipenem at 12.5 µg/ml and VAN6.25 = vancomycin at 6.25 µg/ml. Picture is representative of three experiments.

3.6 Effect of SDS on DD-CPase knockout mutants

In order to determine if enhanced antibiotic susceptibility was due to changes in permeability of double knockout mutants, SDS susceptibility was tested as described in section 2.12.7. In liquid media, all strains did not form colonies after 3 hours treatment with SDS, Figure 3.22A. The double knockout mutants behave similarly to wild type on agar plates supplemented with SDS, Figure 3.22B. Together, these data suggest that the inherent susceptibility to the detergent was not affected by the deletion of DD-CPases. Alternatively, the presence of the remaining DD-CPases may provide sufficient protection against SDS.

3.7 DD-CPases play a role in cell shape and size

3.7.1 Role of DD-CPases on maintaining cell shape

To observe if deletion of DD-CPases affected the cell surface of the bacteria, SEM was performed as described in section 2.12.9.1. An *E. coli* mutant lacking multiple LMW PBPs, in addition PBP5, displayed unusual kinks, bends and branches (Typas et al., 2011). A number of robust phenotypes were observed in our mutants: abnormal septa, V-form, division scars, budding, chaining, kinks, binary fission, fattening of cells and polar bulging as demonstrated in Figure 3.23. These phenotypes were quantified and displayed as a histogram in Figure 3.24, which depicts the four phenotypes that were robustly different between wild type and the double knockout mutants ($p < 0.01$ or $p < 0.05$). These four phenotypes include abnormal septa, division scars, kinks at one end of the cell and chaining formation of cells. Abnormal septa demonstrated by the dark blue arrow in Figure 3.23 were identified as double septa or ringlets and occurred more frequently in the two double knockout mutant strains. Division scars indicated by the pink arrows and kinks indicated by the light blue arrows in Figure 3.23 also occurred more frequently in both double knockout mutant strains as seen in Figure 3.24. Chaining formation of cells indicated by the light green arrows in Figure 3.23

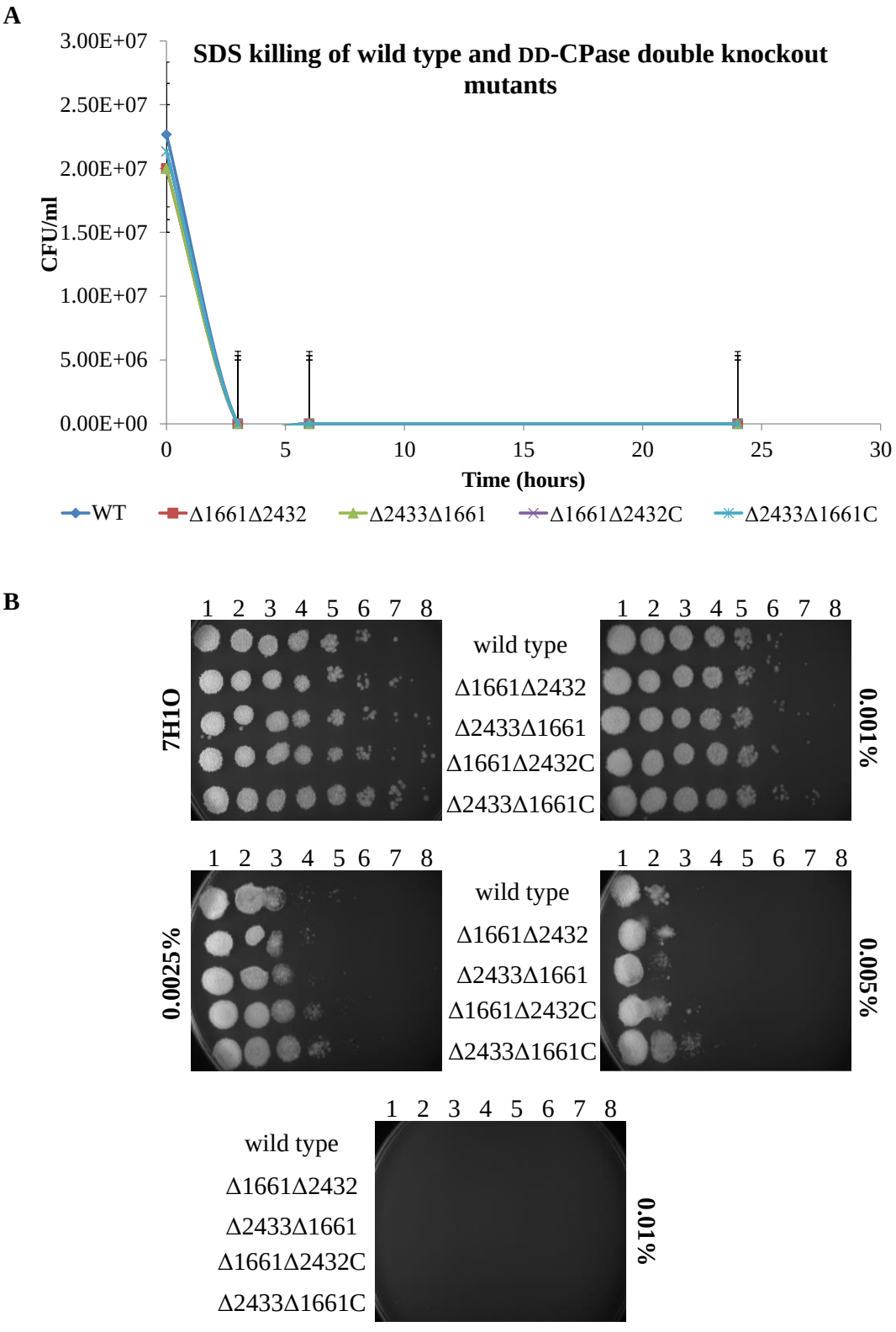

Figure 3.22. SDS killing of wild type and double DD-CPase knockout mutants. (A) Scatter plot depicting killing with 0.2% (w/v) SDS. Graph is representative of three experiments with error bars indicating standard deviation. (B) Photographs depicting killing with different concentrations of SDS on agar plates. 1 to 8 indicates a serial dilution of the initial inoculum from 10^0 to 10^7. [1] 10^0, [2] 10^1, [3] 10^2, [4] 10^3, [5] 10^4, [6] 10^5, [7] 10^6, [8] 10^7. Picture is representative of three experiments. 7H10 agar plate and CFU counts for initial inoculum is the same as Figure 3.21.

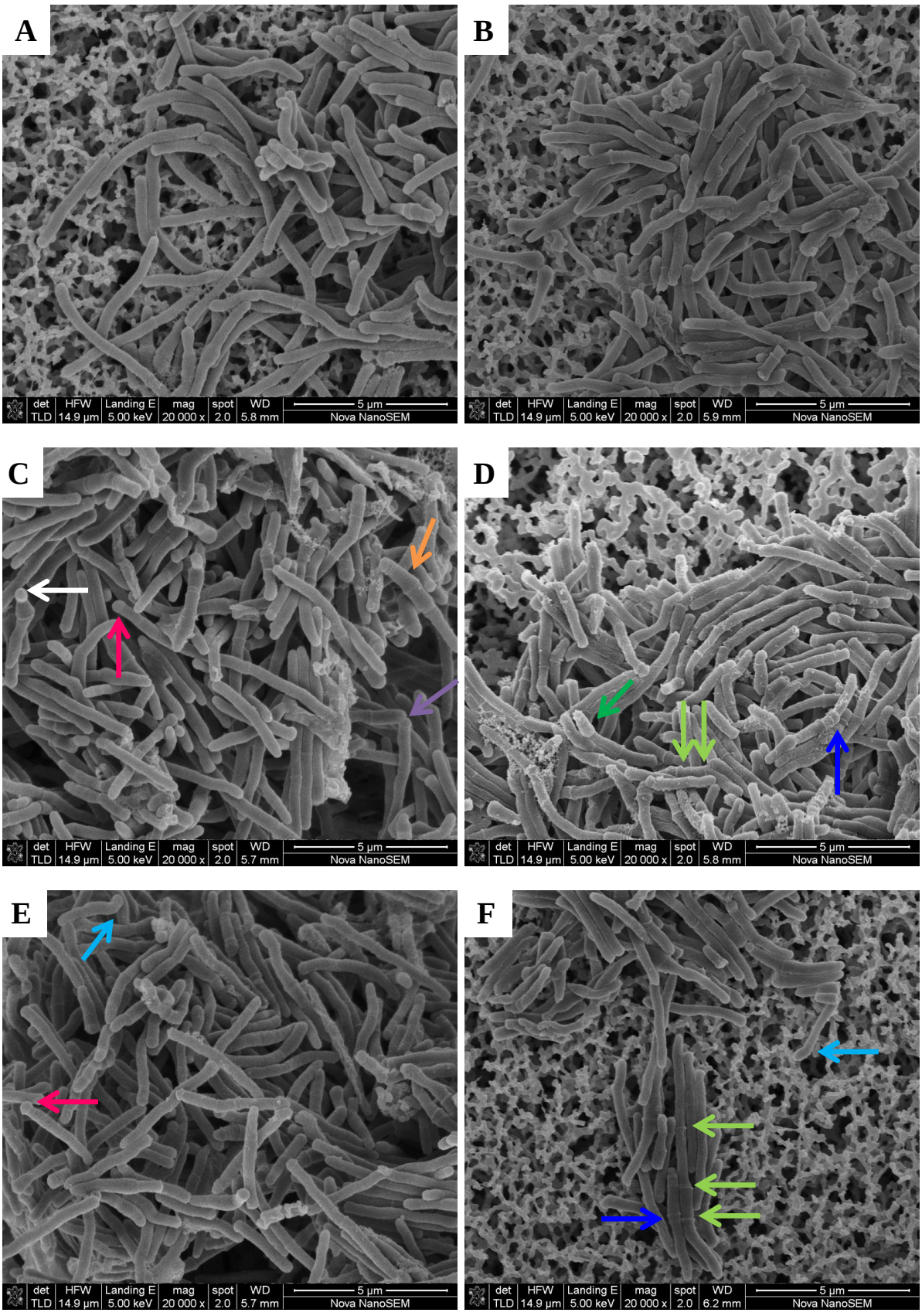

Figure legend on next page.

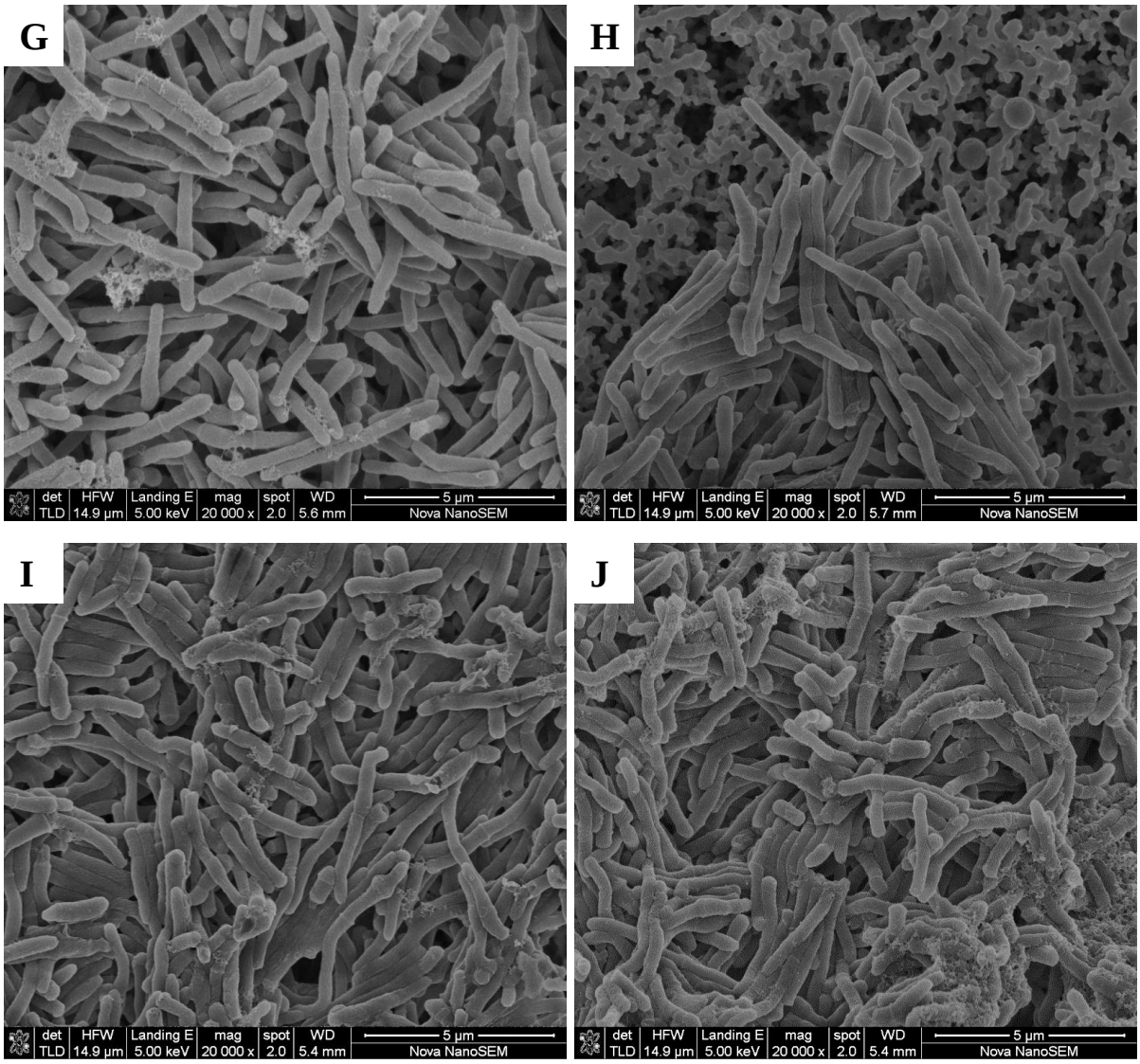

Figure 3.23. SEM images of phenotypes found in wild type and double knockout DD-CPase mutants. (A-B) wild type, (C-D) ΔMSMEG_1661 ΔMSMEG_2432, (E-F) ΔMSMEG_2433 ΔMSMEG_1661, (G-H) ΔMSMEG_1661 ΔMSMEG_2432::MSMEG_1661, (I-J) ΔMSMEG_2433 ΔMSMEG_1661::MSMEG_1661. Arrows indicated the following phenotypes: dark blue = abnormal septa, purple = v-form, pink = division scars, white = budding, light green = chaining, light blue = kinks, orange = fattening of cells and dark green = polar bulging. Picture is representative of three experiments.

occurred more frequently in the ΔMSMEG_1661 ΔMSMEG_2432 strain. This phenotype was also found in the ΔMSMEG_2433 ΔMSMEG_1661 strain but at a lower frequency. The large error bars for this phenotype seen in the ΔMSMEG_2433 ΔMSMEG_1661 mutant could possibly be due to that fact that often cells in this mutant spanned the entire image grid. This resulted in cells that could not be captured from one end to the other, which were then excluded from analysis, causing variation between experiments.

The remaining phenotypes – polar bulging, fattening of cells, v-form and budding demonstrated by the dark green, orange, purple and white arrows respectively - did not differ significantly between the wild type and mutant strains as demonstrated in Figure D9 (page 132).

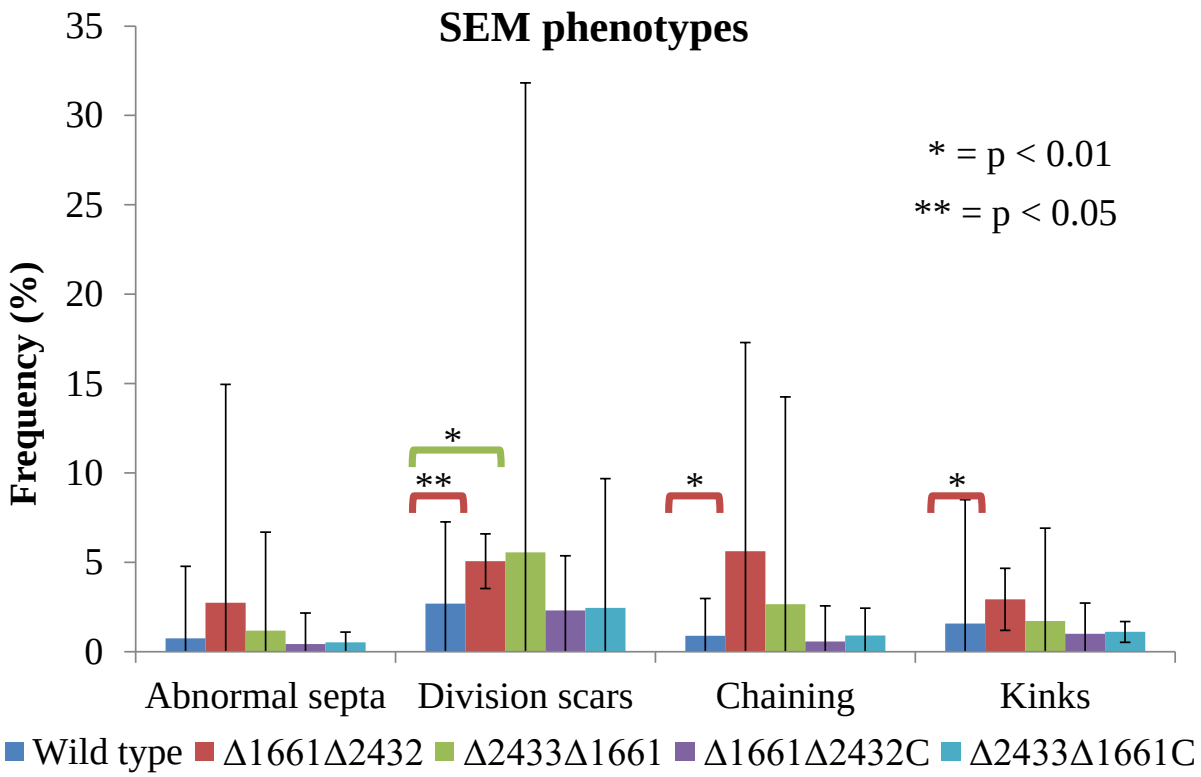

Figure 3.24. Quantification of SEM phenotypes found in wild type and double knockout DD-CPase strains. A significant increase was observed in the ΔMSMEG_1661 ΔMSMEG_2432 mutant in most phenotypes with the ΔMSMEG_2433 ΔMSMEG_1661 mutant showing variation. Graph is representative of three experiments and p values were calculated using the *t*-test.

3.7.2 The role of DD-CPases on maintaining cell size

Using the SEM images, cell lengths were obtained and grouped according to the following sizes: 0-2 µM, 2.1-4 µM, 4.1-6 µM, 6.1-8 µM and 8.1-10 µM as shown in Figure 3.25. As expected, wild type cells were predominantly found in the range of 2.1 – 6 µM, which corresponds to the usual size of *M. smegmatis*. A higher frequency of cells between the ranges of 6.1 - 10 µM was found in the double knockout mutant strains. Both complemented strains behave similarly to the wild type strain, confirming that deletion of two DD-CPases

affects cell length. These observations, combined with the presence of cells with multiple septa, are suggestive of the inability to coordinate cell division in the absence of two DD-CPases.

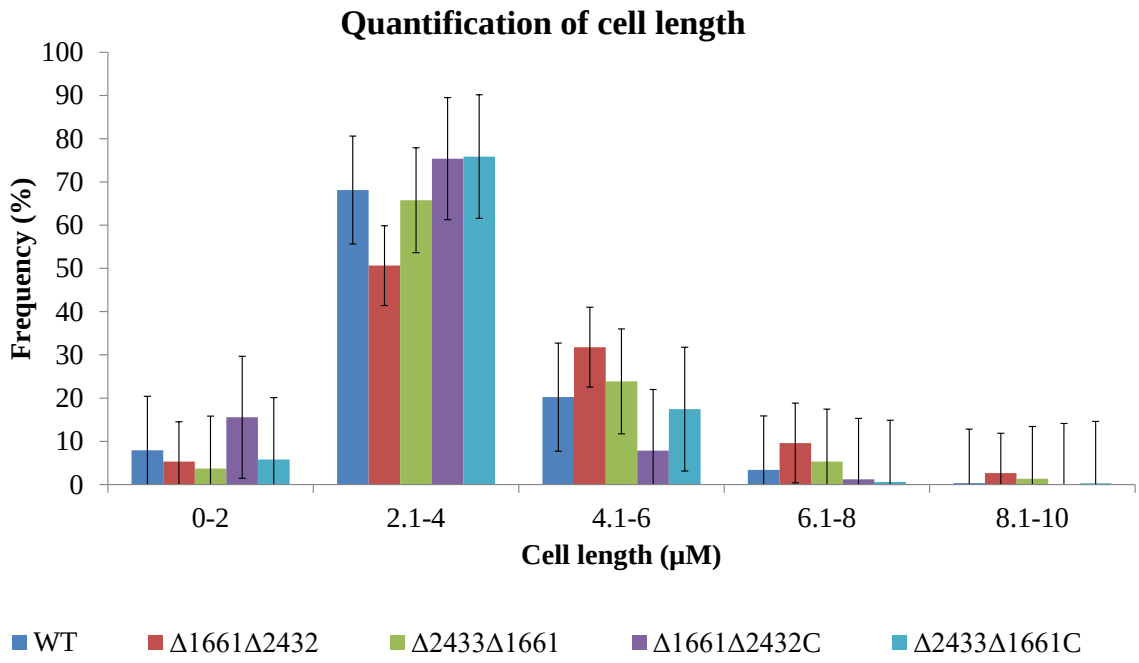

Figure 3.25. Quantification of SEM cell length. The histogram portrays a change in the distribution of cell length found in the mutants when compared to the wild type. The frequency was calculated as the total population observed in three experiments with error bars indicating standard error.

3.8 DD-CPases play a role in cell division

3.8.1 Role of DD-CPases in septal formation/degradation

The presence of multiple septa in our mutants were suggestive of division defects. To further assess if septa were completely formed or were found in multiplicity due to the fact that they were not degraded at the appropriate time, TEM was conducted as described in section 2.12.8.2, to observe cross-sectioned images of cells and septa. All strains harboured the presence of fully formed septa, shown by the orange arrows in Figure 3.26. This data suggests that deletion of DD-CPases do not affect septal formation in *M. smegmatis* but rather timely degradation at the late stages of cell division.

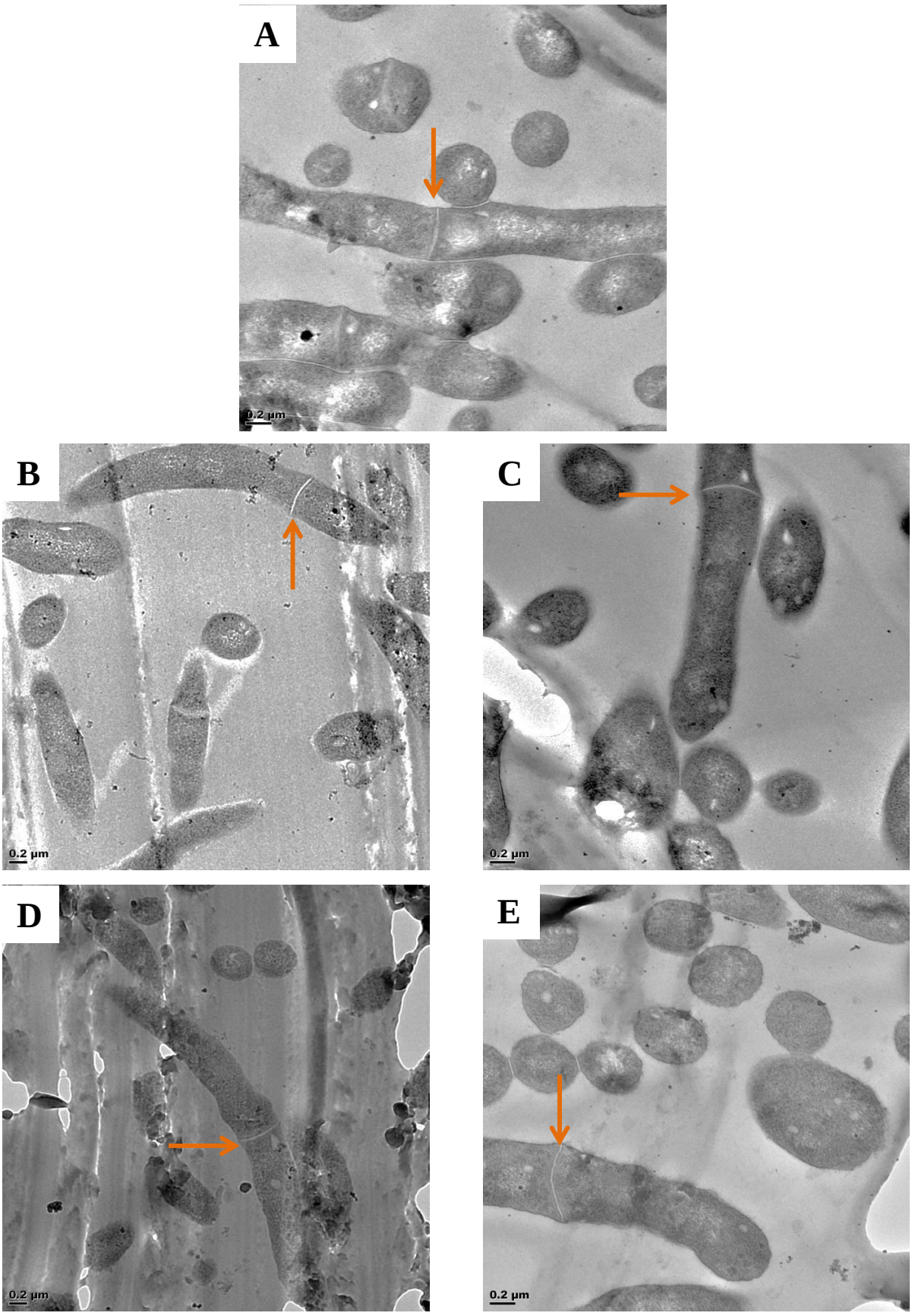

Figure 3.26. Septum formation in wild type and double knockout mutant strains. (A) Wild type, (B) ΔMSMEG_1661 ΔMSMEG_2432, (C) ΔMSMEG_1661 ΔMSMEG_2432::MSMEG_1661, (D) ΔMSMEG_2433 ΔMSMEG_1661, (E) ΔMSMEG_2433 ΔMSMEG_1661::MSMEG_1661. TEM analysis

revealed that all strains had the ability to form proper septa, demonstrated by the orange arrow, indicated that septal formation of degradation processes are not affected in the absence of two DD-CPases. Picture is representative of three experiments.

3.8.2 Role of DD-CPases in cell division

Cell division and remodeling in mycobacteria is performed by a number of enzymes including DD-CPases (Hett and Rubin, 2008, Vollmer and Bertsche, 2008). In order to determine if deletion of the DD-CPases affects the spatial localization of new PG units, cells were stained with BODIPY fluorescent vancomycin as described in section 2.12.9.3. This stain allows for visualization of newly synthesized and incorporated PG. Mycobacterial growth occurs by incorporation of newly synthesized PG at the septum and poles (Brown et al., 2011) described in detail in section 1.5. We saw numerous patterns of fluorescence localization as seen in Figure 3.27, listed as follows: (i) Cells that displayed distinct staining at both poles or at one pole - termed bipolar and monopolar respectively, (ii) Cells that displayed distinct fluorescence at the ends and the middle of a cell - termed polar and septa and (iii) Cells that fluoresce in the middle - termed septal only. In the mutants, two additional groups were observed termed punctate and cells with multiple septa. Punctate cells were identified as cells that displayed distinct fluorescence spots throughout the cell, whereas cells with multiple septa were identified as cells that displayed distinct fluorescence septa throughout the cell. Cells with diffuse staining are defined as cells that were stained with the same intensity across the entire cell. These phenotypes were quantified and a bar graph was generated, Figure 3.27B.

The data indicated that bipolar and monopolar staining was decreased in the mutant strains. Cells carrying stain at the poles and septum were found at a similar frequency in all strains. A higher frequency of cells stained at the septa only was found in the ΔMSMEG_1661

ΔMSMEG_2432 strain – further confirming the observation of cells that were arrested at the late stages of cell division. No cells with punctate staining or multiple septa were observed in

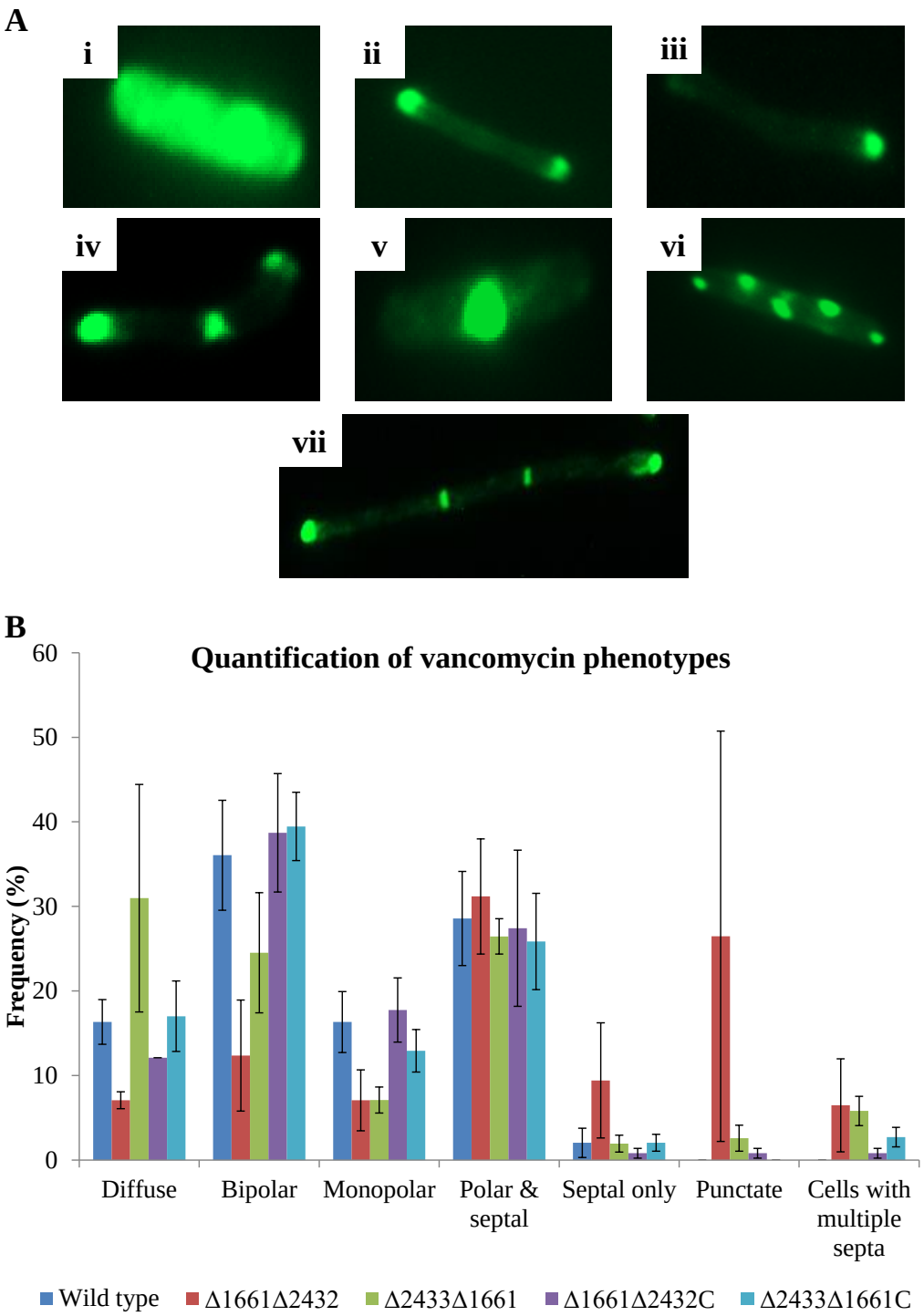

Figure 3.27. Vancomycin staining of wild type and double knockout mutants strains. (A) Observed phenotypes. [i] diffuse, [ii] bipolar, [iii] monopolar, [iv] polar and septal, [v] septal only, [vi] punctate, [vii] multiple septa. . (B) Quantification of observed phenotypes. Graph was generated using data from three independent experiments with error bars indicating the standard error margin.

the wild type strain. In contrast, a high percentage (~30%) of punctate stained cells was found in the ΔMSMEG_1661 ΔMSMEG_2432 strain and this phenotype was reverted to wild type when complemented with only one DD-CPase. A lower percentage (<5%) of punctate stained cells was found in the ΔMSMEG_2433 ΔMSMEG_1661 strain. Cells with multiple septa were found in both mutants.

3.9 Recombinant expression of DD-CPases

3.9.1 Preparation of gene insert fragments for cloning

Genes of interest, MSMEG_6113, MSMEG_1661, MSMEG_2432 and MSMEG_2433, were amplified using Phusion DNA polymerase. The PCR reactions were electrophoresed on low melting (LM) agarose gels as shown in Figure D10 (page 132), and the appropriate band which corresponded to the correct size was gel extracted and purified as described in section 2.6.2. The purified DNA fragments were then digested using *Nde*I and *Hin*DIII. Digested fragments were electrophoresed on LM agarose gels as shown in Figure D12 (page 133), followed by gel extraction and purification.

3.9.2 Preparation of protein expression vector pET29a

A lab freezer stock of pET29a was used and in order to confirm that it was the correct vector, extensive restriction mapping was performed. Plasmid DNA was extracted as described in section 2.3.1.2 and a restriction profile of pET29a was generated using five restriction enzymes as shown in Figure D11 (page 133). All enzymes yielded the expected banding pattern.

Following restriction confirmation, pET29a was digested, dephosphorylated and electrophoresed on a LM agarose gel shown in Figure D12 (page 134). This was followed by ligation of the vector with each gene and transformants were selected for on LA plates containing Kan. The vector pET29a carries a Kan coding resistance cassette therefore

successful transformants will be able to grow in the presence of the antibiotic. After an initial screen (data not shown), one clone of each gene was then chosen and analyzed by restriction mapping to confirm genetic integrity, as shown in Figures 3.28 – 3.31. These confirmed clones were then further analyzed by sequencing (data not shown). All clones displayed expected banding patterns, Figures 3.28 – 3.31, and sequencing results indicated that there no mutations occurred during cloning (data not shown).

A

Restriction enzyme/s	Fragment sizes (bp)
*Hin*DIII	6546
*Hin*DIII + NdeI	5371, 1290
*Not*I	5385, 752, 274, 135
*Pvu*I	4948, 1166, 432
*Nsp*I	2896, 1971, 1020, 367, 292
*Pvu*II	2748, 2320, 999, 386, 93

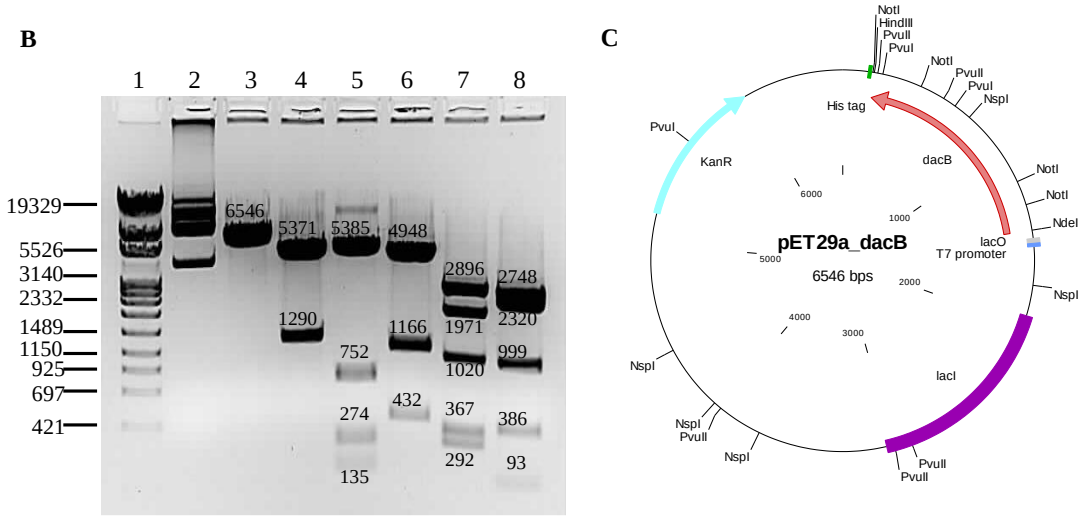

Figure 3.28. Restriction mapping of pET29a_DacB. (A) Expected fragment sizes for restriction digestions. (B) Restriction digestions of pET29a_DacB with several enzymes. Lane 1: Marker IV, Lane 2: uncut DNA, Lane 3: *Hin*DIII, Lane 4: *Hin*DIII + *Nde*I, Lane 5: *Not*I, Lane 6: *Pvu*I, Lane 7: *Nsp*I, Lane 8: *Pvu*II. All bands corresponded to the expected fragment sizes. (C) Vector map of pET29a_DacB.

A

Restriction enzyme/s	Fragment sizes (bp)
*Hin*DIII	6363
*Hin*DIII + NdeI	5371, 1110
*Not*I	5773, 590
*Pvu*I	4246, 1532, 585
*Nsp*I	3733, 1971, 367, 292
*Pvu*II	5271, 999, 93

B

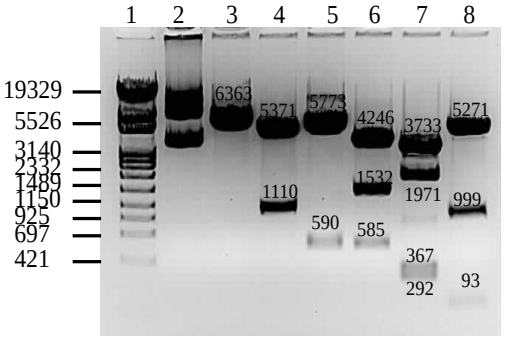

C

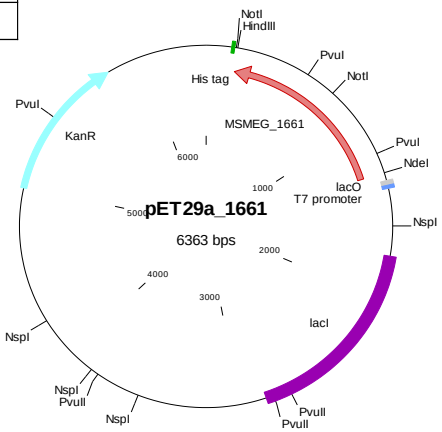

Figure 3.29. Restriction mapping of pET29a_1661. (A) Expected fragment sizes for restriction digestions. (B) Restriction digestions of pET29a_1661 with several enzymes. Lane 1: Marker IV, Lane 2: uncut DNA, Lane 3: *Hin*DIII, Lane 4: *Hin*DIII + *Nde*I, Lane 5: *Not*I, Lane 6: *Pvu*I, Lane 7: *Nsp*I, Lane 8: *Pvu*II. All bands corresponded to the expected fragment sizes. (C) Vector map of pET29a_1661.

A

Restriction enzyme/s	Fragment sizes (bp)
*Hin*DIII	5997
*Hin*DIII + NdeI	5371, 744
*Not*I	4964, 1033
*Pvu*I	4905, 999, 93
*Nsp*I	2737, 1971, 618, 367, 292, 12
*Pvu*II	3423, 1699, 875

B

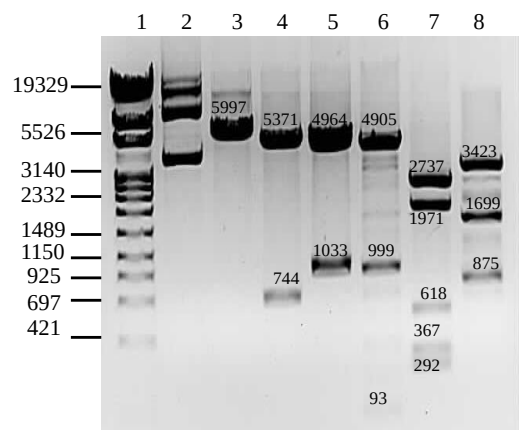

C

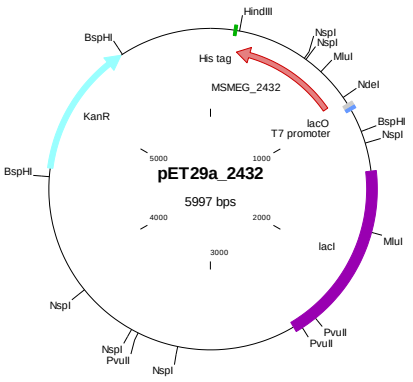

Figure 3.30. Restriction mapping of pET29a_2432. (A) Expected fragment sizes for restriction digestions. (B) Restriction digestions of pET29a_2432 with several enzymes. Lane 1: Marker IV, Lane 2: uncut DNA, Lane 3:

*Hin*DIII, Lane 4: *Hin*DIII + *Nde*I, Lane 5: *Mlu*I, Lane 6: *Pvu*II, Lane 7: *Nsp*I, Lane 8: *Bsp*HI. All bands corresponded to the expected fragment sizes. (C) Vector map of pET29a_2432.

A

Restriction enzyme/s	Fragment sizes (bp)
*Hin*DIII	6051
*Hin*DIII + *Nde*I	5371, 798
*Not*I	5898, 153
*Pvu*I	4959, 999, 93
*Nsp*I	2683, 1971, 630, 367, 292, 108
*Pvu*II	3423, 1753, 875

B

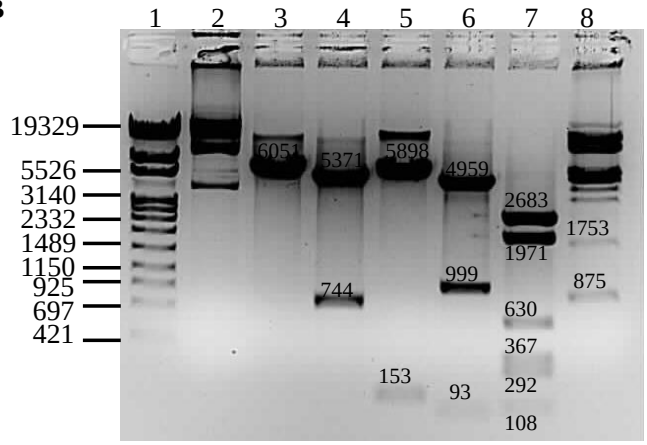

C

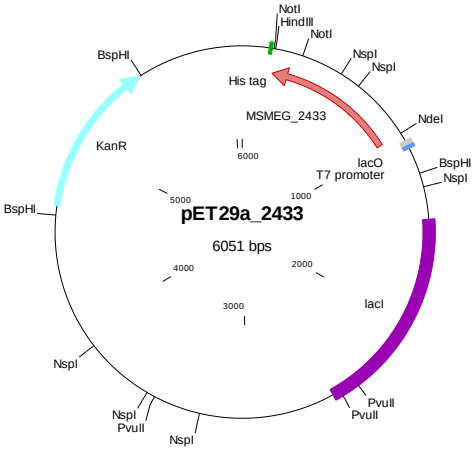

Figure 3.31. Restriction mapping of pET29a_2433. (A) Expected fragment sizes for restriction digestions. (B) Restriction digestions of pET29a_2433 with several enzymes. Lane 1: Marker IV, Lane 2: uncut DNA, Lane 3: *Hin*DIII, Lane 4: *Hin*DIII + *Nde*I, Lane 5: *Not*I, Lane 6: *Pvu*II, Lane 7: *Nsp*I, Lane 8: *Bsp*HI. All bands corresponded to the expected fragment sizes. (C) Vector map of pET29a_2433.

3.10 Transformation into expression host cell line

Once clones were confirmed by restriction profiling and sequencing, they were transformed into the expression host cell line (*E. coli* BL21 (DE3) pLysS) and selected for on LA plates containing Kan and Camp. Two clones of each gene were selected and DNA was extracted. Clones were confirmed by PCR using the DH5α positive clones as a reference. BL21 transformants of all four genes displayed the correct PCR band as demonstrated in Figures 3.32 and 3.33.

3.11 Protein induction of DD-CPases

Using one of the positive BL21 transformants each, IPTG induction of the MSMEG_1661, MSMEG_2432 and MSMEG_2433 DD-CPase proteins was carried out as described in section 2.13.2. Using the B-PER solution, cells were separated into soluble and insoluble fractions followed by visualization of SDS-PAGE gels stained with coomassie blue.

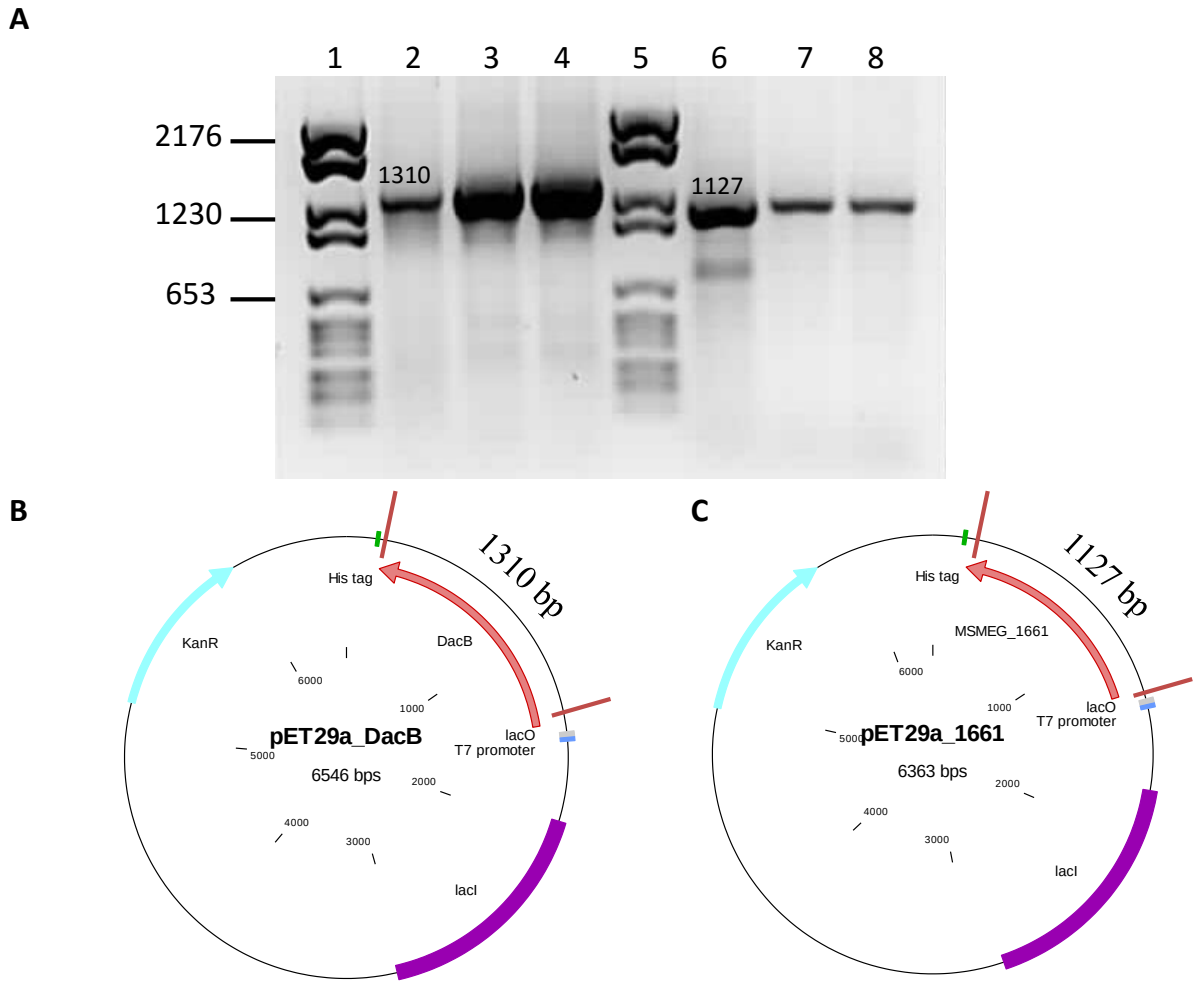

Figure 3.32. PCR confirmation of DacB and MSMEG_1661 *E. coli* BL21 (DE3) pLysS transformants. (A) Agarose gel of possible clones. Lane 1 and 5: Marker VI, Lane 2 and 6: Positive DH5α clones, Lane 3-4 and 7-8: possible transformants. (B) Vector map of pET29a_DacB with amplified region shown by red shaded arrow. (C) Vector map of pET29a_1661 with amplified region shown by red shaded arrow.

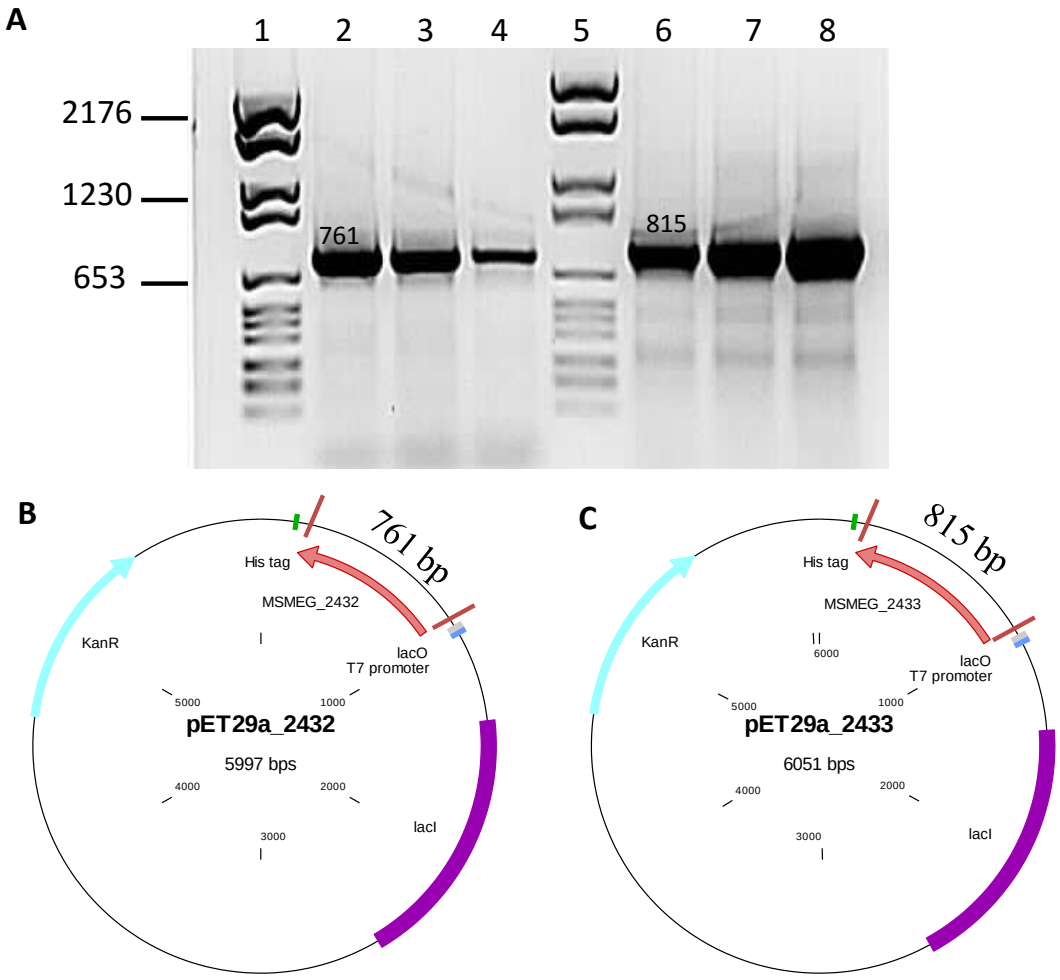

Figure 3.33. PCR confirmation of MSMEG_2432 and MSMEG_2433 *E. coli* BL21 (DE3) pLysS transformants. (A) Agarose gel of possible clones. Lane 1 and 5: Marker VI, Lane 2 and 6: Positive DH5α clones, Lane 3-4 and 7-8: possible transformants. (B) Vector map of pET29a_2432 with amplified region shown by red shaded arrow. (C) Vector map of pET29a_2433 with amplified region shown by red shaded arrow.

Induction with 0.3 mM or 1 mM IPTG did not result in induction of the MSMEG_1661, MSMEG_2432 or MSMEG_2433 proteins (data not shown). No further attempts at induction of these proteins were made.

However, following a similar approach, induction at 37 °C with 0.3 mM and 1 mM IPTG resulted in expression of the DacB protein. This can be seen by the distinct 49 kDa band present in the 2 hour and 3 hour fractions, indicated by the red arrow in Figure 3.34, with

most of the protein found in the insoluble fraction. It was determined that an induction period of 3 hours would be used for purification of the protein.

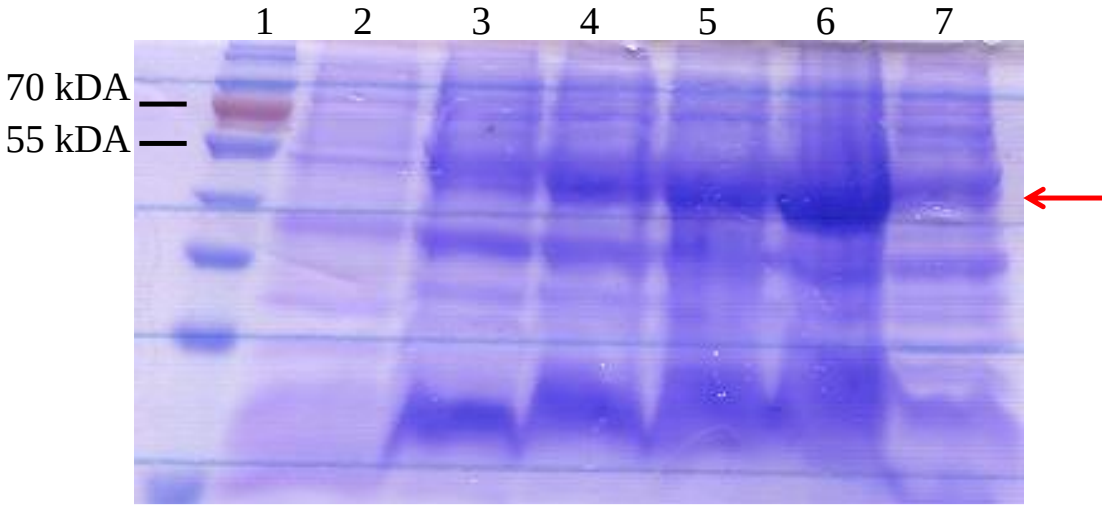

Figure 3.34. IPTG induction of DacB-His. Lane 1: Prestained protein ladder, Lane 2: uninduced, Lane 3: 1 hr induction, Lane 4: 2 hr induction, Lane 5: 3 hr induction, Lane 6: 3 hr induction insoluble fraction, Lane 7: 3 hr induction soluble fraction. Red arrow indicates expected protein.

In an approach to get soluble protein, induction was performed at 30 °C with 0.3 mM and 1 mM IPTG. This strategy was unsuccessful as protein was still being expressed in the insoluble fraction, demonstrated in Figure 3.35.

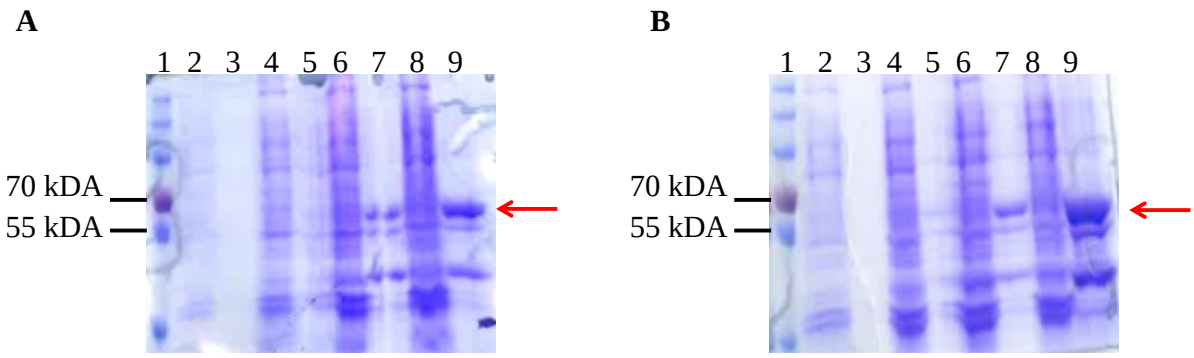

Figure 3.35. IPTG induction of DacB-His at 30 °C. (A) Induction with 0.3 mM IPTG. (B) Induction with 1 mM IPTG. Lane 1: Prestained protein ladder, Lane 2: uninduced soluble fraction, Lane 3: uninduced insoluble fraction, Lane 4: 1 hr induced soluble fraction, Lane 5: 1 hr induced insoluble fraction, Lane 6: 2 hr induced soluble fraction, Lane 7: 2 hr induced insoluble fraction, Lane 8: 3 hr induced soluble fraction, Lane 9: 3 hr induced insoluble fraction. Red arrow shows induced putative DacB-His protein. Red arrow indicates expected protein.

3.12 Protein purification of DacB-His

The DacB-His protein was induced at 37 °C using 0.3 mM and 1 mM IPTG for 3 hours, followed by separation into soluble and insoluble fractions. This was followed by protein purification of the soluble fraction as described in section 2.13.4. The following samples were collected – soluble, insoluble, washes, resin-bound protein and elution. Thereafter, the samples were electrophoresed on two SDS-PAGE gels. One of the gels were stained using coomassie blue and the other was used for Western blotting as described in section 2.13.5. Both IPTG concentrations resulted in the protein being present in the insoluble fraction. Since pET29a carries a His-tag, the monoclonal Anti-poly Histidine antibody was used to identify the protein. Both Westerns blots indicated the presence of a ~70 kDa protein in the insoluble and wash fractions which did not correspond to the expected 49 kDa. The results for 1 mM IPTG induction is shown in Figure 3.36. The band that was over-expressed, did not bind the His-antibody, indicating that it was non-specific, or that the tag was being removed. The latter hypothesis was confirmed by the observation that no protein was detection on the SDS-PAGE gel or western from the eluate off the HIS-bind resin.

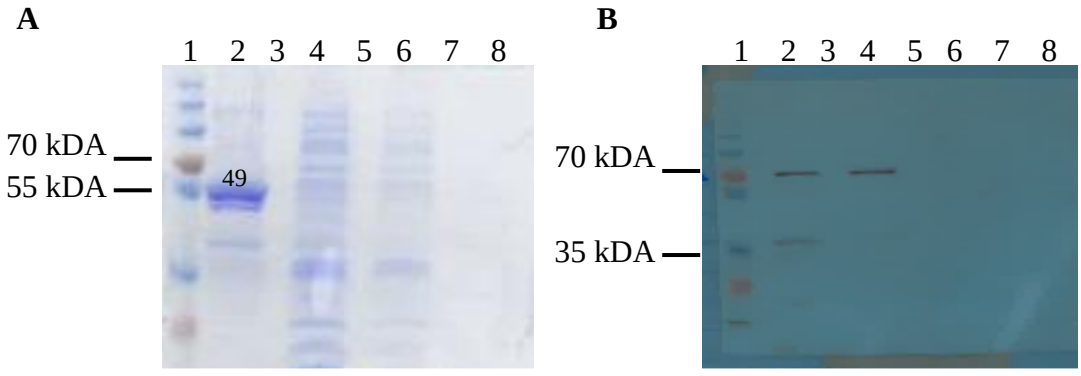

Figure 3.36. Purification of DacB-His at 37 °C. (A) SDS-PAGE gel showing induction of DacB-His. (B) Western blot of DacB-His. Lane 1: Prestained protein ladder, Lane 2: insoluble fraction, Lane 3: soluble fraction, Lane 4: Washes, Lane 5: resin-bound protein, Lane 6: Elution.

3.13 Cloning of DacB domain variants

Since the full length DacB protein could not be expressed as a soluble protein, an alternative approach using three variants of DacB was investigated. These three variants included the DacB domain, the DacB domain lacking 50 amino acids and the DacB domain plus a flanking sequence, referred to as DacB domain, DacB minus and DacB flank respectively. These regions of interest were amplified using Phusion DNA polymerase and electrophoresed on LM agarose gels as indicated in Figure D13 (page 134). The fragments were extracted and purified prior to digestion with *Nde*I and *Hin*DIII. The pET29a vector was digested with the same enzymes and dephosphorylated followed by visualization of all the digested products on LM agarose gels as shown in Figure D14 (page 134). All products were extracted and purified and ligation reactions with the vector were set up for each variant. Ligation reactions were transformed into the cloning host cell line *E.coli* DH5α and selected for on LA plates containing Kan. An initial screen was performed to identify possible transformants (data not shown). One clone of each variant was chosen and analyzed by restriction mapping to confirm genetic integrity, as well as sequencing. All transformants displayed the expected banding patterns, Figures 3.37 – 3.39. Sequencing results indicated no base changes in any of the variants confirming that no mutations had occurred (data not shown).

A

Restriction enzyme	Fragment size
*Hin*DIII	5949
*Bsp*HI	3432, 1651, 875
*Nsp*I	2869, 1971, 450, 367, 292
*Pvu*I	4378, 1139, 432
*Pvu*II	3107, 1750, 999

B

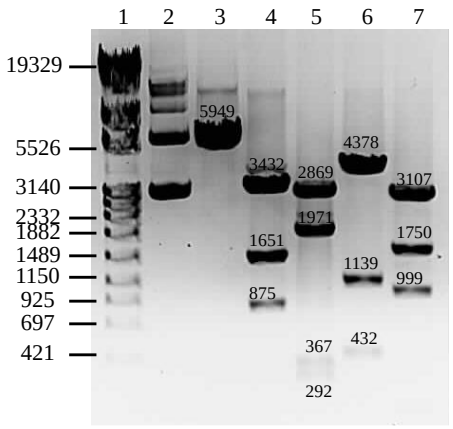

C

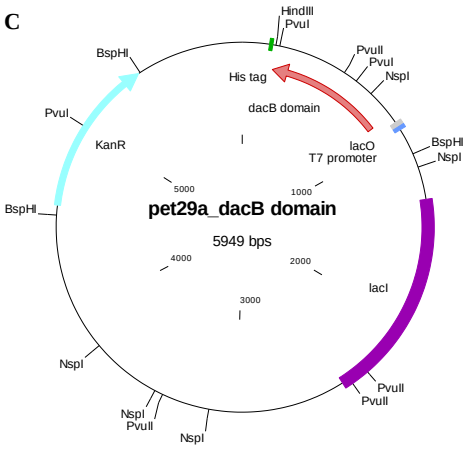

Figure 3.37. Restriction mapping of pET29a_DacB domain. (A) Expected fragment sizes for restriction digestions. (B) Restriction digestions of pET29a_DacB domain with several enzymes. Lane 1: Marker IV, Lane 2: uncut DNA, Lane 3: *Hin*DIII, Lane 4: *Bsp*HI, Lane 5: *Nsp*I, Lane 6: *Pvu*I, Lane 7: *Pvu*II. All bands corresponded to the expected fragment sizes. (C) Vector map of pET29a_DacB domain.

A

Restriction enzyme	Fragment sizes (bp)
*Hin*DIII	5799
*Bsp*HI	3423, 1501, 875
*Nsp*I	3169, 1971, 367, 292
*Pvu*I	4228, 1139, 432
*Pvu*II	3107, 1600, 999, 93

B

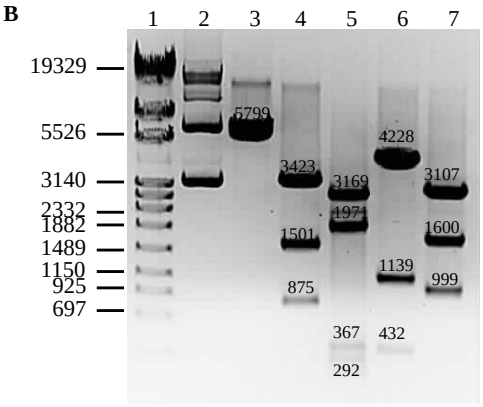

C

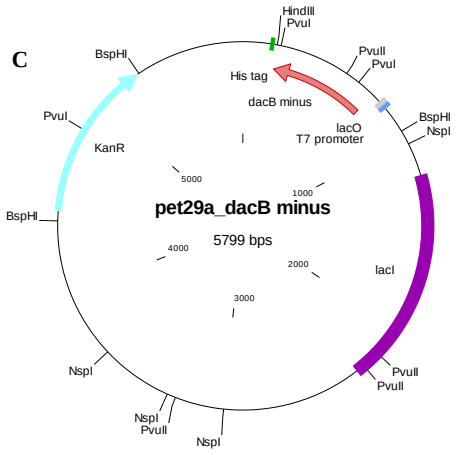

Figure 3.38. Restriction mapping of pET29a_DacB minus. (A) Expected fragment sizes for restriction digestions. (B) Restriction digestions of pET29a_DacB minus with several enzymes. Lane 1: Marker IV, Lane

2: uncut DNA, Lane 3: *Hin*DIII, Lane 4: *Bsp*HI, Lane 5: *Nsp*I, Lane 6: *Pvu*I, Lane 7: *Pvu*II. All bands corresponded to the expected fragment sizes. (C) Vector map of pET29a_DacB minus.

A

Restriction enzyme	Fragment sizes (bp)
*Pvu*II	2748, 1897, 999, 386, 93
*Pvu*I	4525, 1166, 432
*Nsp*I	2896, 1971, 597, 367, 292
*Bsp*HI	3423, 1825, 875
*Hin*DIII	6123

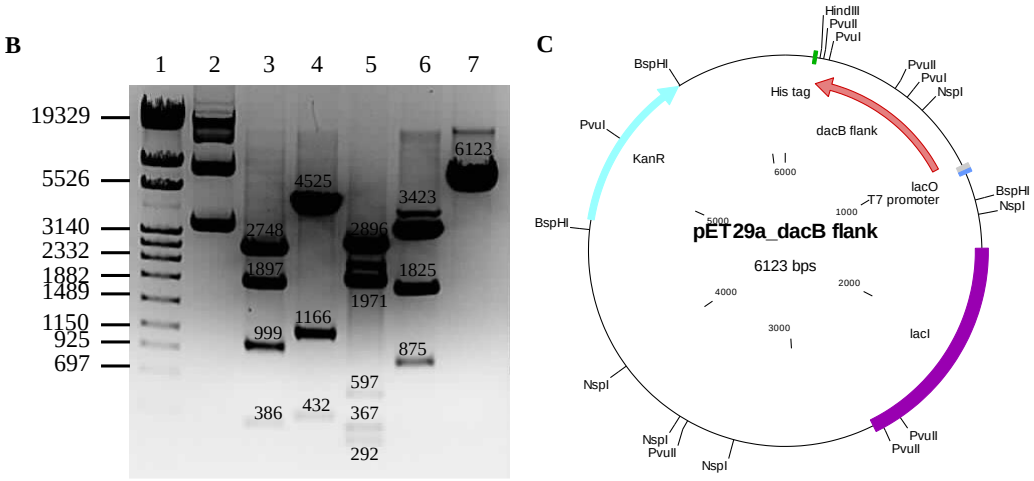

Figure 3.39. Restriction mapping of pET29a_DacB flank. (A) Expected fragment sizes for restriction digestions. (B) Restriction digestions of pET29a_DacB flank with several enzymes. Lane 1: Marker IV, Lane 2: uncut DNA, Lane 3: *Pvu*II, Lane 4: *Pvu*I, Lane 5: *Nsp*I, Lane 6: *Bsp*HI, Lane 7: *Hin*DIII. All bands corresponded to the expected fragment sizes. (C) Vector map of pET29a_DacB flank.

Once clones were confirmed by restriction profiling and sequencing, they were transformed into the expression host cell line *E. coli* BL21 (DE3) pLysS and selected for on LA plates containing Kan and Camp. Two clones of each variant were selected and confirmed by PCR using the DH5α clone as a reference. All of the BL21 transformants matched their respective DH5α reference clones as shown in Figure 3.40 and was taken forward for induction.

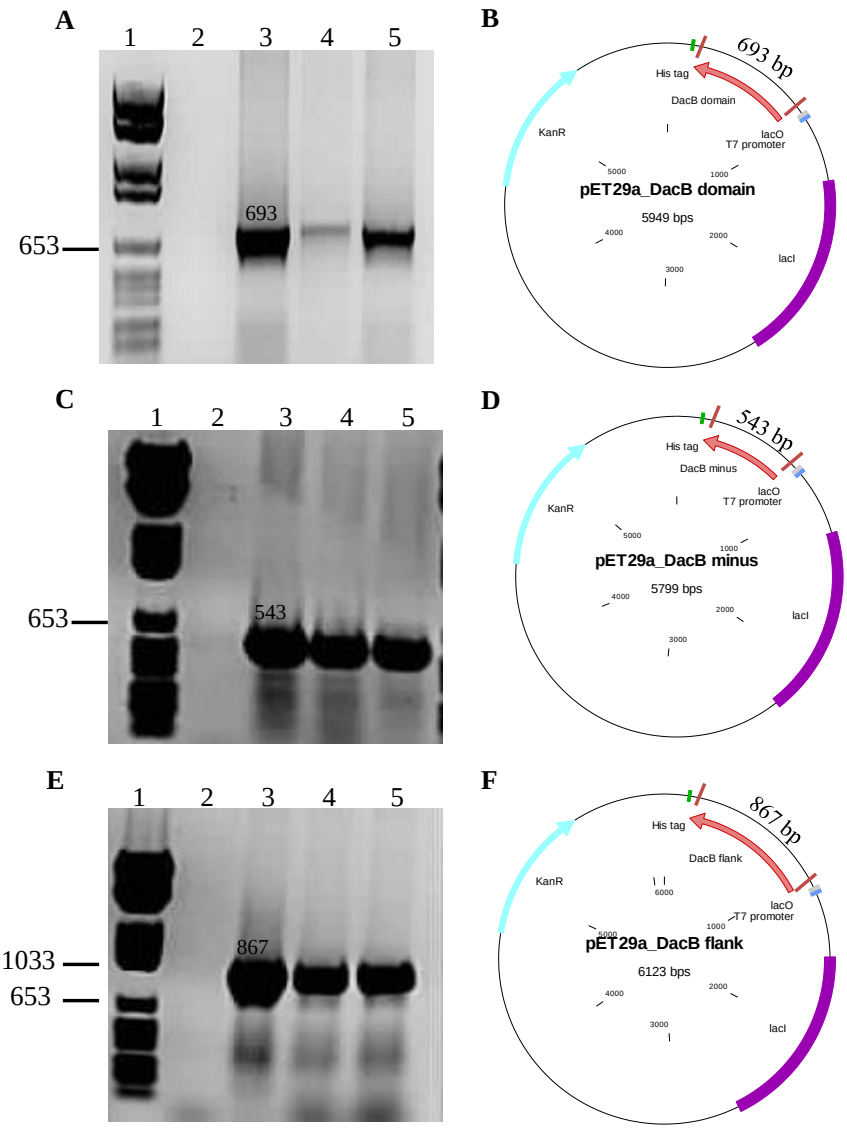

Figure 3.40. PCR confirmation of *E. coli* BL21 (DE3) pLysS DacB variants. (A) DacB domain transformants. (B) Vector map of pET29a_DacB domain with amplified region shown by red shaded arrow. (C) DacB minus transformants. (D) Vector map of pET29a_DacB minus with amplified region shown by red shaded arrow. (E) DacB flank transformants. (F) Vector map of pET29a_DacB flank with amplified region shown by red shaded arrow. Lane 1: Marker VI, Lane 2: no DNA, Lane 3: positive DH5α clone, Lane 4-5: possible transformants.

3.14 Induction of DacB variants

One clone of each variant was induced using 1 mM IPTG at 37 °C for 2 hours. Samples were separated into soluble and insoluble fractions before visualized on coomassie stained SDS-PAGE gels as shown in Figure 3.40. Induction of DacB domain and DacB minus variants resulted in no visible increase of protein expression, Figure 3.41. The DacB flank variant

showed induced expression after only one hour of induction as witnessed by the distinct 32.1 kDa band in Figure 3.40. However, once again the recombinant protein was found in the insoluble fraction. Due to time constraints, no further attempts were made to obtain soluble preparations of DD-CPases from mycobacteria.

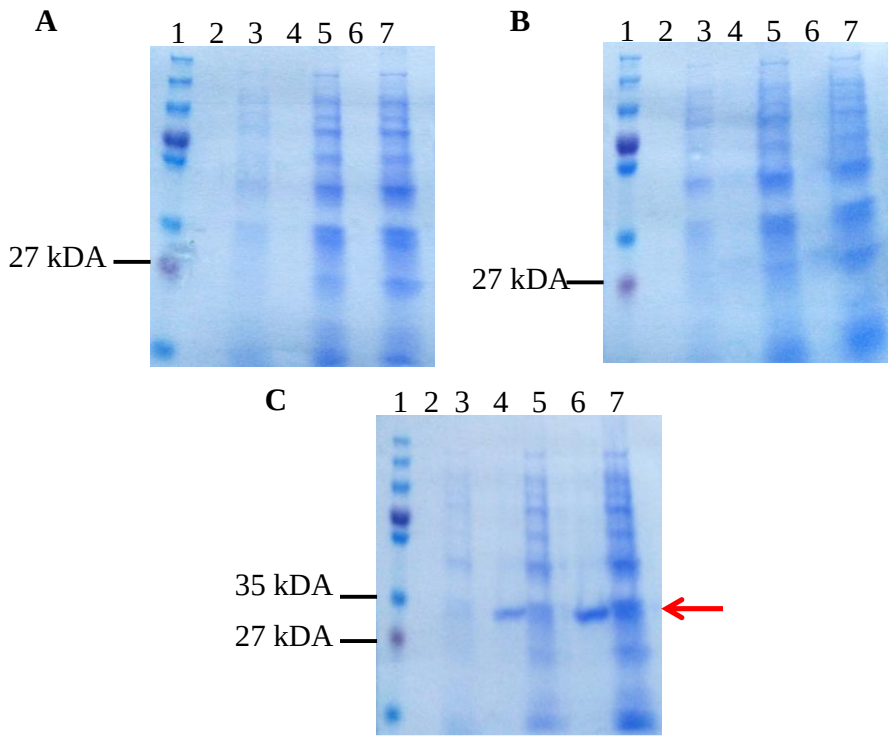

Figure 3.41. IPTG induction of DacB variant proteins. (A) DacB domain. (B) DacB minus. (C) DacB flank. Lane 1: Prestained protein ladder, Lane 2: uninduced insoluble fraction, Lane 3: uninduced soluble fraction, Lane 4: 1 hr induced insoluble fraction, Lane 5: 1 hr induced soluble fraction, Lane 6: 2 hr induced insoluble fraction, Lane 7: 2 hr induced soluble fraction.

4. Discussion

The TB epidemic remains of global health concern due to the high numbers of associated deaths annually (WHO, 2015). The emergence of drug resistant strains is of particular concern considering that these cases account for the majority of deaths (CDC, 2015, WHO, 2015). The inefficiency of the current TB regimen to treat these forms of drug resistant TB has exacerbated the global TB epidemic and appending morbidity. Additionally, LTBI poses a massive threat, as the majority of infected people are predicted to have this form of infection and pose a notable public health challenge as they continuously feed the pool of diseased individuals. It has been predicted that LTBI is characterized by the presence of dormant, metabolically quiescent organisms (Shleeva et al., 2002), which would be refractive to treatment, as most of the current TB antibiotics require active metabolism to achieve vulnerability in the drug target (WHO, 2015). However the fact that INH is efficacious at treating LTBI suggest that LTBI is most likely underpinned by a diversity of organisms that are in different states of growth/metabolic activity (Ferebee and Mount, 1962, Veening, 1968, Barry et al., 2009b, Mulyukin et al., 2009). This lack of clarity regarding bacterial physiology in LTBI, combined with the rapid emergence of drug resistance as created a dire need for new drugs to eradicate TB (WHO, 2015). In order to understand how to effectively combat the TB epidemic a better understanding of the mycobacterial processes that contribute to growth and survival needs to be developed.

In this MSc, we focused on the mycobacterial cell wall with the aim of identifying new drug targets that can be exploited for further development. In addition to the PG, the mycobacterial cell wall is made up of additional layers such as the MAs and the AG, making the overall structure more complex than gram negative or gram positive cell walls (Hett and Rubin, 2008). Disruption of the PG homeostasis affects permeability of the cell wall (Hett and

Rubin, 2008), which could possibly aid in entry of drugs that target components in the cytoplasm, as well as cell death. The targeting of enzymes that remodel PG in the periplasmic compartment of the cell is also advantageous as small molecules do not have to transverse an additional layer before reaching their targets (Crick et al., 2001, Hett and Rubin, 2008).

This MSc study focuses on DD-CPases which are class C LMW PBPs responsible for regulating the amount of cross-linking found in the PG by removing the terminal D-Ala preventing formation of the 3→4 cross-linkages (Ghosh et al., 2008, Sauvage et al., 2008, Vollmer et al., 2008b). These are functionally redundant enzymes with a previous study conducted in our lab indicating that single deletion of the DD-CPase homologues had no observable effects on growth kinetics, biofilm formation, microscopy, exposure to cell wall stresses such as SDS and antibiotic susceptibility (Ealand et al., unpublished). As mentioned previously, deletion of multiple PBPs in *E. coli* were required before any phenotypic differences could be observed (Denome et al., 1999). These observations formed the basis of this study which involved the generation of double deletion mutants lacking different combinations of the *M. smegmatis* DD-CPases in an attempt to dissect the function of these proteins in mycobacteria and to validate them as possible future drug targets.

A study conducted at the CBTBR revealed that the DD-CPases in *M. smegmatis* were expressed at different transcript abundances, an effect that was similar during all phases (early-log, mid-log and stationary) of broth culture. In this case, MSMEG_2433 always displaying the highest expression, followed by MSMEG_1661, DacB and finally MSMEG_2432, which was expressed at the lowest level (Ealand et al., unpublished). Our expression analysis profiling for the single deletion mutants was consistent with these results thus confirming a differential requirement for the various DD-CPases during growth. However, we also found that the expression of MSMEG_2433 was upregulated in the ΔMSMEG2432 strain, suggestive of compensatory gene expression effects that point to some

level of redundancy in function. In *M. smegmatis*, MSMEG_2432 and MSMEG_2433 have been shown to be duplications of the Mtb DacB protein which could further explain the compensatory effect and perhaps also suggest some form of coordinated gene regulation (Machowski et al., 2014).

Bourai and colleagues (2011) constructed an Mtb mutant lacking DacB2 (Δ*dacB2*) and evaluated its growth in various liquid media. Growth of the Δ*dacB2* strain was found to be similar to the wild type H37Rv strain when grown in 7H9 and Sauton's minimal media (pH 7) (Bourai et al., 2011). However, growth of the mutant in Sauton's minimal media (pH 5.5) was severely impaired, with this phenotype more pronounced in stationary versus shaking cultures indicating that this protein is required under stress conditions, especially when oxygen is limited in stationary culture (Bourai et al., 2011). In addition, loss of DacB2 in this strain could have altered the PG structure/composition thus enhancing susceptibility to acid stress. Previous experiments conducted in our lab indicated that lack of any single DD-CPase in *M. smegmatis* did not alter growth kinetics in 7H9 broth. (Ealand et al., unpublished). Our study revealed that the loss of two DD-CPases, in two combinations, did not alter growth in 7H9 broth or Sauton's minimal media (pH 7.3). However, in Sauton's minimal media (pH 5.5), a single deletion lacking MSMEG_1661 resulted in impaired growth. The remaining single mutants (ΔMSMEG_2432 and ΔMSMEG_2433) as well as the double mutant lacking both MSMEG_2433 and MSMEG_1661 grew at similar rates to the wild type. The complemented strains and the ΔMSMEG_2432 ΔMSMEG_1661 double knockout strain showed better growth than the wild type in the late-log and stationary phases of growth. These results suggest a few possible theories: (i) MSMEG_1661 could possible play required under acid stress conditions, (ii) Deletion of another DD-CPase in the absence of MSMEG_1661 results in variable upregulation of another protein that may play a role under acid stress conditions and (iii) expression of MSMEG_1661 at a different locus provides

additional protection against acid stress. These findings could also point to MSMEG_1661 functioning as part of a regulon which controls the growth and survival of *M. smegmatis* under stressful conditions.

Changes in colony morphology, biofilm formation and sliding motility are often associated in many mycobacterial mutant strains (Martinez et al., 1999, Recht et al., 2000, Recht and Kolter, 2001, Ojha et al., 2002). Morphology changes in a colony can be caused by disruption of surface components of the cell that affect the cell wall structure and or hydrophobicity (Bourai et al., 2011). The overexpression of DacB2 resulted in smooth mucoid Mtb colonies indicating that the LMW PBPs may play a role in maintaining colony morphology (Bourai et al., 2011). *E. coli* single, double and triple mutants lacking PBP4, PBP5 and PBP7 were shown to have reduced biofilm formation while growth in planktonic culture was unaffected (Gallant et al., 2005), confirming that LMW PBPS either a play direct role in biofilm formation or interact with proteins required for biofilm formation or maturation. The high lipid content of mycobacterial species allows for the formation of biofilms on the surface of liquid media with these bacterial communities contributing to antibiotic tolerance (Etienne et al., 2002, Branda et al., 2005, Ghosh et al., 2013). Mycobacteria are non-motile organisms that lack flagella and have been shown to be able to move across solid surfaces by a sliding mechanism which requires the presence of glycopeptidolipids (Martinez et al., 1999). Deletion of one or two DD-CPases did not alter colony morphology or sliding ability of the bacteria suggesting that the presence of the remaining DD-CPases may be compensating for the loss. Biofilm formation was slightly affected in mutants lacking MSMEG_1661 and MSMEG_2433 displaying longer ruffles, demonstrating that these two proteins could either directly affect cell wall biosynthesis or interact with other proteins that are responsible for biofilm formation. Given that this observation is only qualitative, our explanation in this regard is largely speculative and requires further substantiation.

Lavollay and colleagues (2008) demonstrated that mycobacterial PG displays a difference in the amount of 3→4 and 3→3 cross-links found during the different stages of growth. *E. coli* predominantly contains 3→4 cross-links except in the stationary phase of growth, where the organism contains an increased ratio of 3→3 cross-links (Lavollay et al., 2008). This was initially described for mycobacteria as well, with 80% of the crosslinks in the stationary phase being 3→3 crosslinks (Lavollay et al., 2008). However, a recent study demonstrated that these crosslinks predominate at a 3:2 (3→3: 4→3) ratio with no significant differences observed during the different growth phases (Kumar et al., 2012). As mentioned previously, the 3→3 cross-links are formed by Ldts whereas the 3→4 cross-links are formed by DD-transpeptidases which are generally HMW PBPs (Mainardi et al., 2002, Sauvage et al., 2008). The heavily 3→3 cross-linked mycobacterial PG is necessary for maintenance of infection and plays a role in antibiotic stress (Kieser and Rubin, 2014) as evidenced by an Mtb mutant lacking Ldt_{Mt2}. This Ldt_{Mt2} mutant was unable to persist during the chronic stage of infection in a mouse model and displayed increased sensitivity to β-lactams (Gupta et al., 2010). In Mtb, tetrapeptides are exclusively produced by DD-CPases and these tetrapeptides are the specific donor substrates used for the formation of the 3→3 cross-links by Ldts (Cordillot et al., 2013). Remodeling of the PG by cell wall associated proteins such as the DD-CPase DacB1 has been shown to be required for survival in hosts such as primates with mutation in these genes resulting in 38.58% attenuation (Dutta et al., 2010). Furthermore, these unique 3→3 cross-links are important for survival in the host, maintenance of colony morphology, growth of Mtb in mouse models as well as viability and virulence of the organism (Gupta et al., 2010, Kumar et al., 2012). Mtb is intrinsically resistant to β-lactams due to the production of class A β-lactamases (BlaC), consequently these drugs are not used to treat the TB disease (Dubee et al., 2012). More recently carbapenems, a class of β-lactams, have been shown to inactivate Ldts and can target the DD-CPases as well (Mainardi et al., 2007,

Lavollay et al., 2008, Dubee et al., 2012). Consistent with this, treatment of Mtb with meropenem, which belongs to the carbapenem family, resulted in the accumulation of pentapeptides which suggested that a DD-CPase was being targeted (Kumar et al., 2012). It is likely that both 3→3 and 4→3 cross-links need to be targeted in order to effectively kill Mtb.

A relationship between the LMW PPBs and antibiotic resistance has been established with the DacB enzyme of *E. coli*, which displays high levels of inherent resistance to ampicillin and presumably confers similar resistance properties to the organism (Gondre et al., 1973). As a result, the deletion of *dacB* with other PBPs has resulted in increased susceptibility of *E. coli* to antibiotics, specifically β- lactam antibiotics (Denome et al., 1999). Resistance to penicillin binding drugs has been shown to be exceptionally high during the stationary phase of growth and the shift in PG cross-linking is predicted to be responsible for this (Boshoff and Barry, 2006). During the stationary phase of growth, *pbp3* of *E. coli* is down regulated while *pbp6* is up regulated, coupled with an increase in the amount of 3→3 cross-links (Dougherty and Pucci, 1994, Boshoff and Barry, 2006). The Mtb DacB2 enzyme can bind penicillin but its catalytic activity is not affected by the antibiotic whereas meropenem has been shown to inhibit DacB (Bourai et al., 2011). A previous study conducted at the CBTBR demonstrated that deletion of individual DD-CPases from *M. smegmatis* did not sensitize mutants to antibiotics (Ealand et al., unpublished). Our results indicate that the absence of two DD-CPases results in increased sensitivity of the organism to various antibiotics, depending on the combination of DD-CPases that were deleted. In liquid media, both mutants showed increased sensitivity to vancomycin, cefoxitin, cefotaxime, and cefatriaxone with different MIC concentrations between strains. The strain lacking MSMEG_1661 and MSMEG 2432 displayed increased sensitivity to cefamandole whereas the strain lacking MSMEG_2433 and MSMEG_1661 showed increased sensitivity to imipenem. Both cefamandole and imipenem are β-lactam antibiotics with the latter been shown to be highly

resistant to β- lactamases. These data suggest some form of functional overlap between these enzymes. Our double deletion mutants were unaffected by rifampicin, erythromycin and vancomycin which inhibit RNA transcription, protein synthesis and PG cross-linking respectively. Additionally, sensitivity of both double deletion mutants to the β-lactams were increased on solid media as well. A possible explanation of why the mutants show variable sensitivity to imipenem could be due to the overexpression of a β-lactamase in the ΔMSMEG_1661 ΔMSMEG_2432 mutant. There is a precedent for this in *E. coli* where *bolA* regulates PBP5 and PBP6 expression thereby controlling normal morphology of the cell and the amount of precursors available for crosslinking by the transpeptidase PBP2 (Santos et al., 2002). In addition, *bolA* regulates AmpC which is a β-lactamase thus linking the expression of DD-CPases to β-lactamase induction (Santos et al., 2002). Additional resistance mechanisms to β-lactams includes the compensatory expression of PBPs which have low binding affinity to antibiotics (Nikolaidis et al., 2013). Consequently, the lack of DD-CPases in our double mutants could reduce the bioavailability of PBPs in the cell and thereby allow enhanced binding of antibiotics to HMW PBPs, which have been shown to play an important role in PG assembly. This would ultimately result in increased sensitivity of the mutants to antibiotics due to disruption of the PG layer. Additionally, lack of the DD-CPases could result in a decrease of the 3→3 cross-links, which could also play a role in antibiotic susceptibility, Figure 4.1.

The commonly used detergent, SDS, has a strong anionic dodecyl and is used for the degradation of lipids and proteins as well as lysis of cells. Since deletion of DD-CPases may result in altered of permeability of the PG, we hypothesized that our mutants would display enhanced susceptibility to SDS. Failure of SDS to differentially affect the mutants and the wild type indicates that lipid degradation or remodeling processes are not affected in the absence of DD-CPases, suggesting that (i) these enzymes do not play a role in controlling

these processes nor do they interact with proteins involved in lipid degradation/remodeling or (ii) the remaining DD-CPases are sufficient to maintain the cell wall and provide protection against SDS stress.

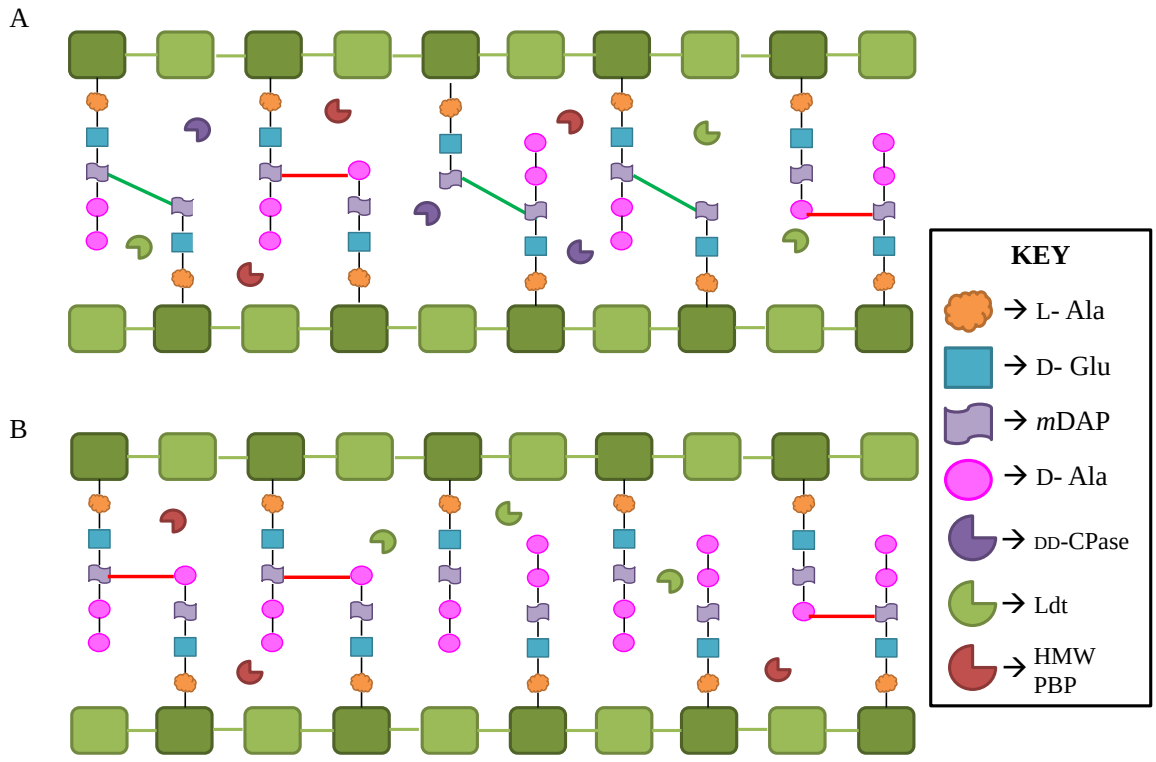

Figure 4.1.Effect of DD-carboxypeptidase deletions on peptidoglycan cross-linking. (A) Peptidoglycan layer containing a 3:2 ratio of 3→3: 3→4 cross-links when LD-transpeptidases, high molecular weight penicillin binding proteins and DD-carboxypeptidases are present. (B) Loss of DD-carboxypeptidases results in a decrease of the 3→3 cross-links as the tetrapeptide substrate required by the LD-transpeptidases is not generated. This could result in the accumulation of pentapeptides as well as an increase in 3→4 cross-links generated by the high molecular weight penicillin binding proteins.

Following elongation of mycobacterial cells, a multiprotein complex known as the divisome is responsible for the division at approximately midcell resulting in two daughter cells (Kieser and Rubin, 2014). The divisome coordinates the synthesis and subsequent cleavage of the septum (Kieser and Rubin, 2014) with polymerization of FtsZ initiating the division process (Mukherjee and Lutkenhaus, 1998). In *E. coli*, PBP1b and PBP3 are responsible for synthesis of the septa and the amidases AmiA, AmiB or AmiC are responsible for separation of the two daughter cells through degradation of septal PG (Typas et al., 2011). In

mycobacteria, FtsZ has been shown to interact with FtsW and PBP2 (homologous to *E. coli* PBP3), forming a complex and stabilizing the Z-ring at the future division site (Datta et al., 2002, Datta et al., 2006, Typas et al., 2011). The cell division protein CrgA interacts with this complex, stabilizing it with loss of CrgA resulting in elongated cells and the inability of the cell to recruit PBP2 to the divisome (Plocinski et al., 2011). PBP2 is required for septum synthesis and has been shown to interact with Wag31 which localizes to the division site after the septum is formed (Mukherjee et al., 2009, Zhang et al., 2012, Santi et al., 2013). Another protein involved in the septum synthesis/degradation is the essential PG hydrolase RipA, with depletion resulting in chaining of cells that fail to grow (Hett et al., 2008). RipA has been shown to interact with RpfB (Hett et al., 2007) and then cleave PG (Hett et al., 2008) with the interaction of RipA and PBP1 counteracting the RipA-RpfB interaction, thus ensuring that septal synthesis is achieved before cleavage (Kieser and Rubin, 2014). Our TEM results reveal that the septal synthesis pathway is not affected in the *M. smegmatis* double deletion mutants. There are two possible reasons which explain this: (i) there is no interaction between the DD-CPases and the divisome complex or (ii) there is no disruption of HMW PBPs such as PBP2 which is recruited to the future division site during the early stages of cell division.

In Mtb V-forms are proposed to be temporal structures as they only form part of a small subset of the population (Dahl, 2004). These structures form due to the inner PG layer expanding with the outer layer remaining intact during septum synthesis (Dahl, 2004). Once the septum is complete, the inner layer continues to grow exerting pressure on the outer layer which eventually ruptures on one side of the cell. This results in the bending of the two daughter cells, still attached at one side, yielding a V-form, Figure 4.2 (Dahl, 2004). Consistent with this, <3% of the cells in all our strains were found in this form.

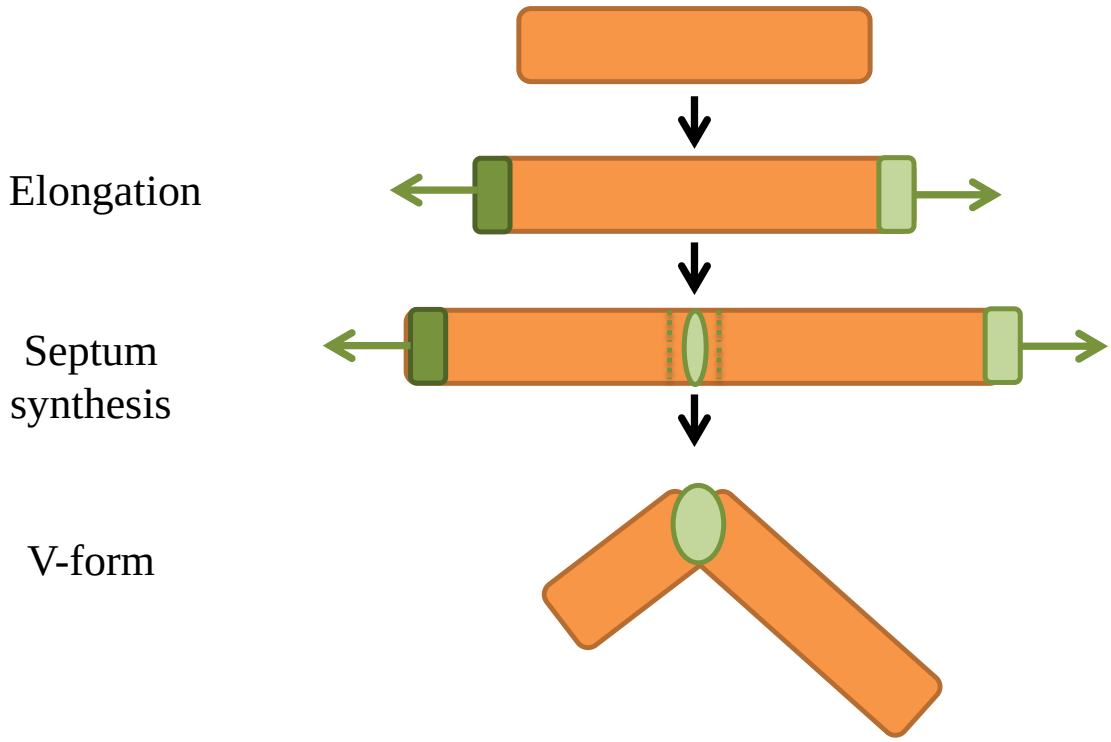

Figure 4.2.V-snapping division of mycobacteria. Newly synthesized peptidoglycan is inserted at the poles as shown by light green and dark green colour which represents the old and new pole respectively. The peptidoglycan layer continues to expand while the outer layer remains intact during septum formation. Once septum synthesis is complete the peptidoglycan layer continues to exert pressure on the outer layer which eventually ruptures on one side resulting in the bending of the two daughter cells which are still attached to one another thus resulting in a V-form. (Dahl, 2004, Santi et al, 2013)

Division scars have previously been described in Mtb as ridges that remain after cell division indicating where the cells have separated, with the newly synthesized PG appearing as a terminal bud (Dahl, 2004). A significant increase in the frequency of division scars was observed in the DD-CPase double deletion mutants, possibly indicating that once division is complete, PG processes such as remodeling, are still not functioning efficiently. As mentioned previously, the continuous remodeling of the mycobacterial cell wall is required for expansion. It is possible that loss of the DD-CPases affects remodeling of the PG which is required in the next division event for expansion of the cell. *E. coli* lacking PBP5 displayed slight morphological defects with the removal of additional PBPs resulting in cells with kinks, bends and branches (Typas et al., 2011). In our mutants the frequency of kinks increased, pointing to defects in polar PG synthesis. We consequently hypothesize that

deletion of the DD-CPases results in a decrease of 3→3 cross-links and thus a decrease in the rigidity of the cell wall. This misregulation of cross-links could result in kinking due to an imbalance of PG synthesis occurring at one end of the cell. This hypothesis needs further confirmation.

BODIPY vancomycin is a form of fluorescently labelled vancomycin which binds D-Ala-D-Ala motif that is specifically found in newly synthesized PG (Hett and Rubin, 2008). It allows visualization of newly incorporated PG, which is usually found at the septum and poles in mycobacterial cells (Hett and Rubin, 2008). The deletion of two DD-CPases resulted in two interesting phenotypes (i) Cells with multiple septa, which was observed in SEM as well, indicating that cell division is hampered in these mutant strains and from the TEM data, this is most likely due to poor degradation of the septum (ii) Punctate localization of new PG, pointing to newly synthesized PG at the septum, poles and throughout the cell. Mycobacteria lack the negative regulatory systems required for placement of the Z-ring in *E. coli* and *B. subtilis* as discussed in section 1.5. FtsZ, an essential protein, localizes at the division site to form the Z- ring which serves as a scaffold for recruitment of other cell division proteins such as FtsW and PBP2 and guides septal synthesis (Datta et al., 2002, Dziadek et al., 2003, Datta et al., 2006). Mycobacterial polar PG synthesis is controlled by Wag31 which is the homologue of the gram positive early cell division protein DivIVA (Cole et al., 1998). In mycobacteria, Wag31 is essential and localizes to the pole with depletion of the protein resulting in one end of the cell becoming rounded (Kang et al., 2008). Thus, Wag31 has been implicated in regulating cell shape, growth and cell wall synthesis by localizing PG synthesis to the poles and maintaining the rod shape of the bacteria (Kang et al., 2008). Wag31 has also been shown to localize to the septum during the later stages of cell division coinciding with cytokinesis (Santi et al., 2013). Together FtsZ and Wag31 guide PG synthesis to the septum and poles respectively ensuring that this process is controlled and the shape of the organism

is maintained (Kang et al., 2008, Typas et al., 2011). Since DD-CPase mutants displayed punctate localization of new PG precursors, it is possible that the functioning of FtsZ and Wag31 is disrupted in the absence of these enzymes, indicating a possible interaction between the LMW PBPs and the cell division proteins.

Future studies

Future work could entail dissecting the role of the remaining DD-CPases of *M. smegmatis* as well as investigating these enzymes in Mtb. The behavior of the essential DacB (Rv3627c) enzyme could be explored in the absence of the dispensable DD-CPases. This would involve the localization of DacB and the other DD-CPases in both *M. smegmatis* and Mtb mutants lacking different combinations of the DD-CPases. Additionally, a panel of mutants lacking both Ldts and DD-CPases can be created to explore the spatial localization of PG. The specific change in PG in DD-CPase mutants should be investigated in future work.

Concluding remarks

Collectively, this study identified the DD-CPases as important enzymes for regulated mycobacterial growth and division. This is evidenced by the dysregulated spatial distribution of new PG synthesis and lack of coordinated cell division observed in the mutants lacking two DD-CPases. Our results confirm an important role of the DD-CPases in maintaining antibiotic resistance, as witnessed by the increased sensitivity of mutants to a range of β-lactam antibiotics. Together this and future studies may identify possible drug targets in the PG of mycobacteria that can be exploited to effectively treat TB.

5. Appendices

Appendix A – Media and solutions

Table A1. Culture media and supplements

Media/ Supplement	Components
Luria- Bertani Agar (LA)	5 g yeast extract, 10 g tryptone, 10 g NaCl and 1.5 g agar dissolved in 1 L sdH_20.
Luria- Bertani Broth (LB)	5 g yeast extract, 10 g tryptone and 10 g NaCl a dissolved in 1 L sdH_20.
2xTY	10 g yeast extract, 16 g tryptone and 10 g NaCl dissolved in 1 L sdH_20.
Middlebrook 7H9	4.7 g Difco Middlebrook 7H9 powder and 2 ml glycerol dissolved in 986 ml sdH_20. Autoclave. 10 ml 100 X glucose salts and 2 ml Tween80.
Middlebrook 7H10	19 g Difco Middlebrook 7H10 powder and 5 ml glycerol dissolve in 985 ml sdH_20. Autoclave. 10 ml 100 X glucose salts.
Sauton's minimal media	0.5 g magnesium phosphate, 0.5 g potassium dihydrogenorthophosphate, 2 g citric acid, 4 g L-asparagine, 1 ml 5% ferric ammonium acid, 100 µl 1% $ZnSO_4$ and 60 ml glycerol. Adjusted pH with ammonium hydroxide. Autoclave.
Glucose salts (100X)	20 g glucose and 8.5 g NaCl dissolved in 100 ml sdH_20.
Tween80 (25%)	10 ml Tween80 dissolved in 40 ml sdH_20
Sucrose (75%)	75 g sucrose dissolved in 100 ml sdH_20
X-gal (2%)	1 g X-gal dissolved in 50 ml deionized DMF

Table A2. Solutions used for plasmid extractions from *E. coli*

Solution	Composition
Solution I	50 mM glucose, 25 mM Tris-HCl (pH 8) and 10 mM EDTA dissolved in sdH_20. Autoclave.
Solution II	1% SDS and 0.2 M NaOH dissolved in sdH_20.
Solution III	3 M Potassium acetate and 11.5% acetic acid dissolved in sdH_20.

Table A3. Solutions used for DNA extraction from *M. smegmatis*

Solution	Composition
TE buffer	10 mM Tris-HCl (pH 8) and 10 mM EDTA dissolved in sdH_20. Autoclave.
CTAB/ NaCl	4.1% NaCl and 10% N- cetyl- N, N, N - trimethyl ammonium bromide dissolved in sdH_20. Filter sterilize.

Table A4. Solutions used for precipitation of DNA

Solution	Composition
Chloroform: Isoamyl alcohol	24 ml chloroform and 1 ml isoamyl alcohol.

Sodium Acetate	3 M sodium acetate dissolved in sdH_20 (pH5.2). Autoclave.

Table A5. Solutions used for electrophoresis of DNA

Solution	Composition
TAE	50 X stock solution: 242 g Tris base, 57.1 ml glacial acetic acid and 100 ml EDTA (pH 8) made up to 1 L with sdH_20.
Ethidium bromide	10 mg/ml dissolved in sdH_20.

Table A6. Agarose gel recipes

Gel percentage	Amount of agarose in 50 ml TAE (g)
0.8	0.4
1	0.5
2	1

Table A7. Solutions used for E. coli competent cells preparation

Solution	Composition
TfbI	30 mM potassium acetate, 100 mM rubidium chloride, 10 mM calcium chloride, 50 mM manganese chloride and 15% v/v glycerol made up in sdH_20. Adjusted to pH 5.8 with acetic acid.
TfbII	10 mM rubidium chloride, 75 mM calcium chloride, 10 mM MOPS and 15% v/v glycerol made up in sdH_20. Adjusted to pH 6.5 with diluted NaOH.

Table A8. Solutions used for Southern blotting

Solution	Composition
Denaturation solution	1.5 M NaCl and 0.5 M NaOH dissolved in sdH_20.
Depurination solution	0.25 M HCl dissolved in sdH_20.
TBE (1X)	100 ml 10 X Tris-Borate-EDTA (Sigma) dissolved in 900 ml sdH_20.
SSC (20X)	0.3 M sodium citrate and 3 M NaCl dissolved in sdH_20.
SDS (10%)	10g SDS powder dissolved in 100ml sdH_20.
Solution I	0.1% SDS and 2 X SSC dissolved in sdH_20.
Solution II	0.1% SDS and 0.5 X SSC dissolved in sdH_20.
Maleic Acid Buffer	1.5 M NaCl and 1 M Maleic acid dissolved in sdH_20. Adjusted to pH 7.5 with NaOH pellets.
Wash buffer	0.1 M Maleic Acid Buffer and 0.3% Tween20.
Blocking solution (Roche)	1 X blocking solution dissolved in Maleic Acid Buffer.
Detection buffer	0.1 M NaCl and 0.1M Tris-HCl dissolved in sdH_20 (pH 9.5)
Antibody solution (Roche)	Dilute 1: 10000 in blocking solution.
CSPD (Roche)	Disodium 3-(4-methoxyspiro {1,2-dioxetane-3,2′-(5′-

	chloro)tricyclo [3.3.1.1^{3,7}]decan}-4-yl)phenyl phosphate
Stripping solution	0.2 M NaOH and 0.1% SDS dissolved in sd$H_2$0.

Table A9. Solutions used for protein extractions

Solution	Composition
B-PER Reagent	Cell lysis reagent
Protease inhibitor cocktail	1 protease inhibitor cOmplete ultra tablet (Roche) dissolved in 10 ml B-PER solution.

Table A10. Solutions used for electrophoresis of proteins

Solution	Composition
bis-acrylamide	40% working solution.
Tris-HCl	0.5 M (pH 6.8) and 1.5 M (pH 8.8) made up in sd$H_2$0. Autoclave.
SDS (10%)	10 g SDS dissolved in 100 ml sd$H_2$0. Autoclave.
APS (10%)	0.1 g ammonium persulphate dissolved in 1 ml sd$H_2$0. Store at 4°C.
TEMED	N, N, N, N- tetramethyl- ethylenediamine.
Loading buffer (5X)	3.8 ml sd$H_2$0, 1.6ml 10% SDS, 1ml 0.5 M Tris-HCl (pH 6.8), 0.8 ml glycerol, 0.4 ml bromophenol blue and 0.4 ml β- mercaptoethanol.
Running buffer	303 g Tris, 144 g glycine and 10 g SDS made up to 1 L in sd$H_2$0.
Coomassie blue	40% ethanol, 10% acetic acid and 0.1% coomassie dissolved in sd$H_2$0.
Destain	40% ethanol and 10% acetic acid dissolved in sd$H_2$0.

Table A11. SDS-PAGE gel recipes

Ingredient	Gel Percentage	
	10%	**15%**
bis-acrylamide	2.5 ml	3.75 ml
Tris-HCl	3.75 ml	5.625 ml
d$H_2$0	3.6 ml	400 µl
SDS (10%)	100 µl	150 µl
APS (10%)	50 µl	75 µl
TEMED	5 µl	7.5 µl

Table A12. Solutions used for purification of His-tagged proteins

Solution	Composition
Ni-NTA resin	Nickel-charged resin
Buffer A	50 mM Tris, 500 mM NaCl, 20% glycerol and 10 mM imidazole dissolved in sd$H_2$0. Store at 4°C.
Buffer B	50 mM Tris, 500 mM NaCl, 20% glycerol and 250 mM imidazole dissolved in sdH20. Store at 4°C.

Table A13. Solutions used for Western blotting

Solution	Composition
Transfer buffer	28.8 g glycine, 6 g Tris, 2 g SDS and 400 ml methanol dissolved in 2 L sdH_20.
TBS (10X)	80 g NaCl and 24.2 g Tris dissolved in 1 L sdH_20 (pH 7.6).
TBST	1X TBS and 0.1% Tween20 made up in sdH_20.
Blocking solution	5% nonfat dry milk (Cell signal) dissolved in TBST.
CPS Reagent (Sigma)	Chemiluminescent Peroxidase Substrate

Appendix B – Primers

Table B1. Primers used for PCR confirmation of knockout mutants

Gene	Primer name	Sequence	Amplicon	
			Wild type	Mutant
MSMEG_1661	Δ1661_F	AATCACAAGATTCACACG	1394 bp	236 bp
	Δ1661_R1	TGGCGGCCAGCGTGTTGA		
	Δ1661_R2	GTGCGTCGCGCACACGAC	701 bp	
MSMEG_2432	Δ2432_F	GGACCGTTCGGCGAGCAT	1028 bp	236 bp
	Δ2432_R1	GCATGTTGGCCGCGTCGT		
	Δ2432_R2	CGGCGACTGGATCGACCG	500 bp	
MSMEG_2433	Δ2433_F	GCAGTCGAATAGTCCACC	1091 bp	236 bp
	Δ2433_R1	CCGCGTCGTTGCCCGACG		
	Δ2433_R2	GTTGTCGGGGCGCAGATG	500 bp	

Table B2. Primers used for generation of Southern blot probes

Gene	Primer name	Sequence (5' - 3')
MSMEG_1661	1661_USF	CGCGAAGCTTGCGAGGCCGTCGAGAGCG
	1661_USR	CGCGCATATGCACCGCGCGTCGCGTCAT
	1661_DSF	CGCGCATATGCAGCGCCCGCAGCACTGA
	1661_DSR	CGCGGGTACCGTAGCCGACCGTGAGAGCGA
MSMEG_2432	2432_USF	CGCGAAGCTTCCGGGAACGCAGGCAGC
	2432_USR	CGCGCATATGCGCCGCGAACAGTCTTCGCAC
	2432_DSF	CGCGCATATGGACTACGGCTTCAGCCAGTAG
	2432_DSR	CGCGGGTACCGGCCGACTTCGACCTGTCG
MSMEG_2433	2433_USF	CGCGAAGCTTACGATCCCGCGGACCAGG
	2433_USR	CGCGCATATGCCCGAAGGCGTACCTCCACAT
	2433_DSF	CGCGCATATGGCGAGCATCGGGGCGCTCTGA
	2433_DSR	CGCGGGTACCATCGGCCACGGCCGCATC

Table B3. Primers used to confirm site specific integration of complementing vector

Primer name	Sequence (5' - 3')	Amplicon
*att*BS2	ACAGGATTTGAACCTGCGGC	320 bp
*att*L4	AATTCTTGCAGACCCCTGGA	
*att*BS1	ACGTGGCGGTCCCTACCG	282 bp
*att*L1	CTTGGATCCTCCCGCTGCGC	

Table B4. Primers used for gene expression analysis by qPCR

Gene	Primer name	Sequence (5' - 3')	Amplicon
MSMEG_1661	1661_qF	GAGCATCATCAAGGTCCTCA	148 bp
	1661_qR	CAGCAGATCGTTGATCGTGT	
MSMEG_2432	2432_qF	GCTGAACTATCCGGTGATCG	202 bp
	2432_qR	GTACATCTGCACCACCACCA	
MSMEG_2433	2433_qF	GCTGGTCAACCAGAACGAGT	153 bp
	2433_qR	TCTTTCACCAGGCCGTACAT	

Table B5. Primers used for amplification of genes for protein expression

Gene	Primer name	Sequence (5' - 3')	Amplicon
MSMEG_DacB	DacB_pF	CATATGCTGTTCACCGGCAAACAC	1293 bp
	DacB_pR	CAAGCTTTGCGCCGCATCCGCAGCT	
	DacB_domF	CATATGGAATCGGTGATGCTCGAC	693 bp
	DacB_domR	AAGCTTCGCGGCCAGAGCGTCGAT	
	DacB_minusF	CATATGGGCGGCACCACAATCGCC	543 bp
	DacB_minusR	AAGCTTCGCGGCCAGAGCGTCGAT	
	DacB_flankF	CATATGGCCCGCATCAGCGACCTC	867 bp
	DacB_flankR	AAGCTTTGCGCCGCATCCGCAGCT	
MSMEG_1661	1661_pF	CATATGCCCGGCTGGACTGCCCA	1110 bp
	1661_pR	AAGCTTGTGCTGCGGGCGCTGATT	
MSMEG_2432	2432_pF	CATATGCCGGCCGCCGCACCGGCG	744 bp
	2432_pR	AAGCTTCTGGCTGAAGCCGTAGTC	
MSMEG_2433	2433_pF	CATATGGCCGACATCCAGCAGGTC	798 bp
	2433_pR	AAGCTTGAGCGCCCCGATGCTCGC	

Table B6. Primers used for sequencing of pET29a vectors

Construct	Primer name	Sequence (5' - 3')
pET29a_dacB	dacB_sF1	CCGACACCTGGTACAAGG
	dacB_sF2	CCGTGAGGTCGCCGAGGC
pET29a_1661	1661_sF1	TCAACGATCTGCTGCACG
	1661_sF2	CGCGGTGTTGCTCAAGGG
pET29a_2432	2432_sF1	CCGCATCGCCGTCGGGTC

pET29a_2433	2433_sF1	TGGTCACCCCCTCGGGAC

Appendix C – Molecular Weight Markers

DNA molecular weight Marker IV

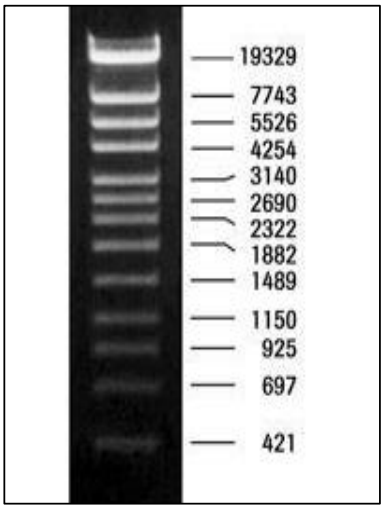

DNA molecular weight Marker VI

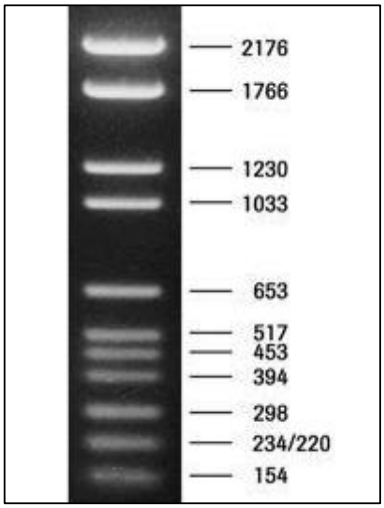

Page Ruler^{TM} Plus Prestained Protein Ladder

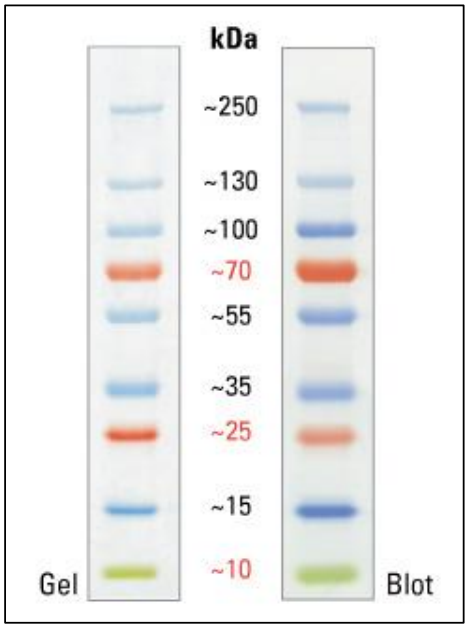

Appendix D – Figures

A

Restriction enzyme	Fragment sizes (bp)
NotI	6010, 5978, 1580, 906, 333, 16
PvuII	10940, 2557, 819, 363, 144
MluI	6060, 4187, 3371, 780, 425
EcoRI	5850, 4539, 1863, 1655, 766, 150
PvuI	5523, 2678, 2384, 1318, 726, 657, 604, 480, 453
BamHI	11751, 3072

B

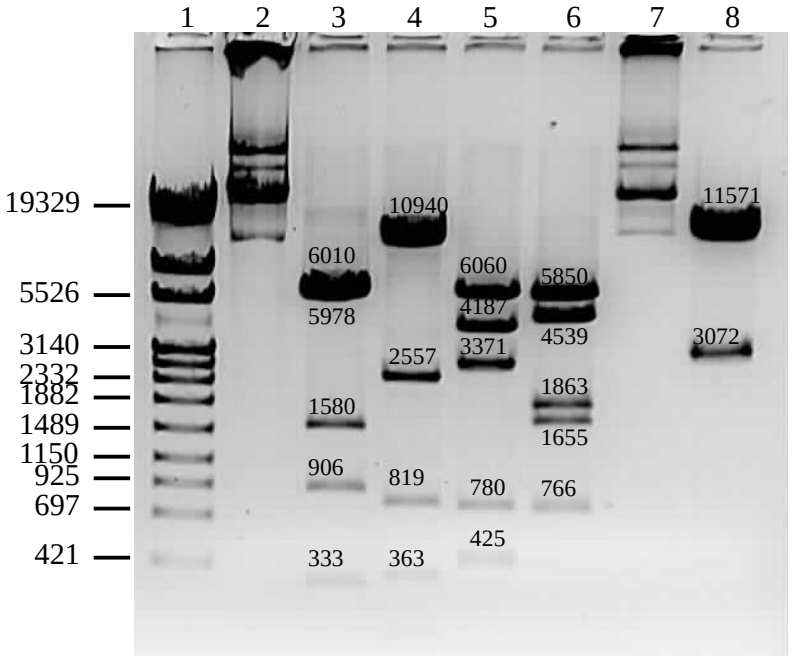

C

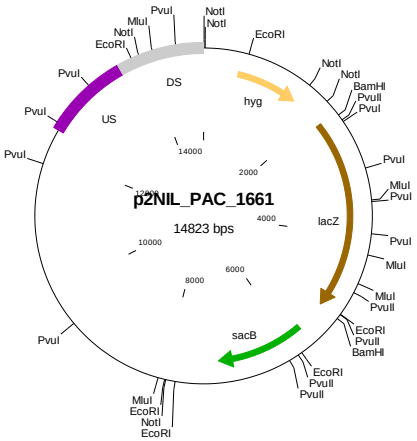

Figure D1. Restriction mapping of p2NIL_PAC_1661. (A) Expected fragment sizes for restriction digestions. (B) Restriction digestions of p2NIL_PAC_1661 with several enzymes. Lane 1: Marker IV, Lane 2: uncut DNA, Lane 3: *Not*I, Lane 4: *Pvu*II, Lane 5: *Mlu*I, Lane 6: *Eco*RI, Lane 7: *Pvu*I, Lane 8: *Bam*HI. All bands correspond to expected sizes. (C) Vector map of p2NIL_PAC_1661.

A

Restriction enzyme	Fragment sizes (bp)
NotI	6010, 5417, 1580, 779, 357, 333, 262, 75, 16
PvuII	10946, 2557, 819, 363, 144
MluI	10253, 3371, 780, 425
EcoRI	7511, 4539, 1863, 766, 150
PstI	5696, 3933, 3169, 2031
BamHI	7425, 3245, 3072, 1087

B

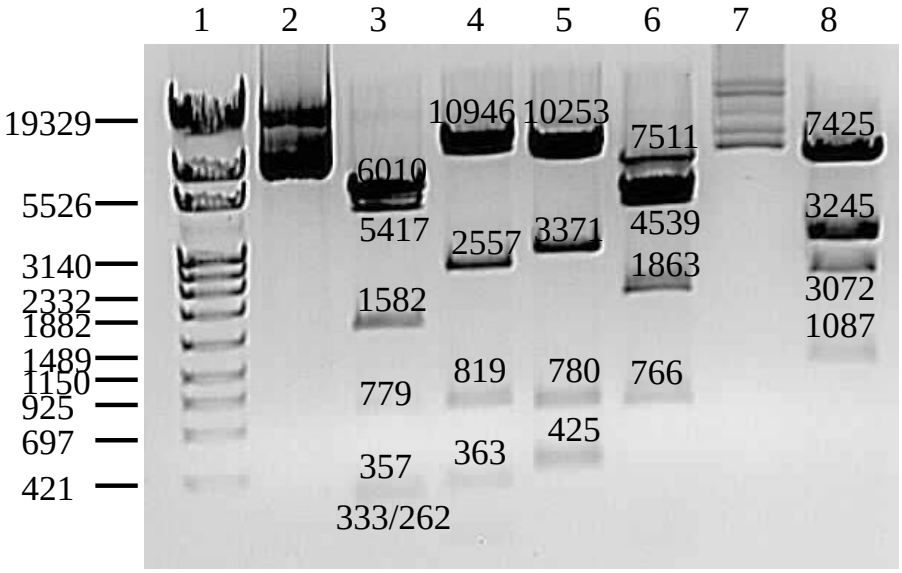

C

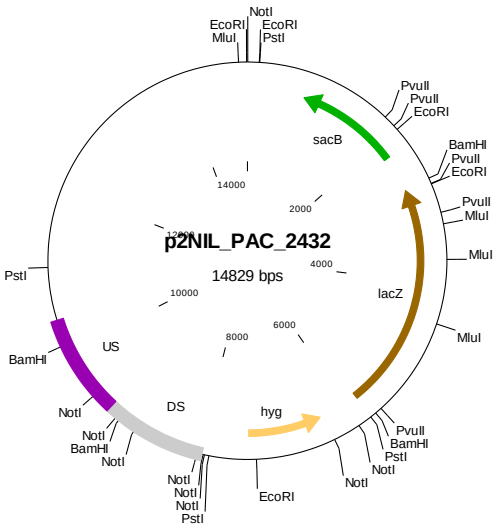

Figure D2. Restriction mapping of p2NIL_PAC_2432. (A) Expected fragment sizes for restriction digestions. (B) Restriction digestions of p2NIL_PAC_2432 with several enzymes. Lane 1: Marker IV, Lane 2: uncut DNA, Lane 3: *Not*I, Lane 4: *Pvu*II, Lane 5: *Mlu*I, Lane 6: *Eco*RI, Lane 7: *Pst*I, Lane 8: *Bam*HI. All bands correspond to expected sizes. (C) Vector map of p2NIL_PAC_2432.

A

Restriction enzyme	Fragment sizes (bp)
NotI	6010, 4603, 1580, 1147, 900, 333, 219, 16
PvuII	10925, 2557, 819, 363, 144
MluI	5094, 4331, 3371, 807, 780, 425
EcoRI	7490, 4539, 1863, 766, 150
AccI	3689, 3650, 2897, 2537, 2035
BamHI	9388, 3072, 2348

B

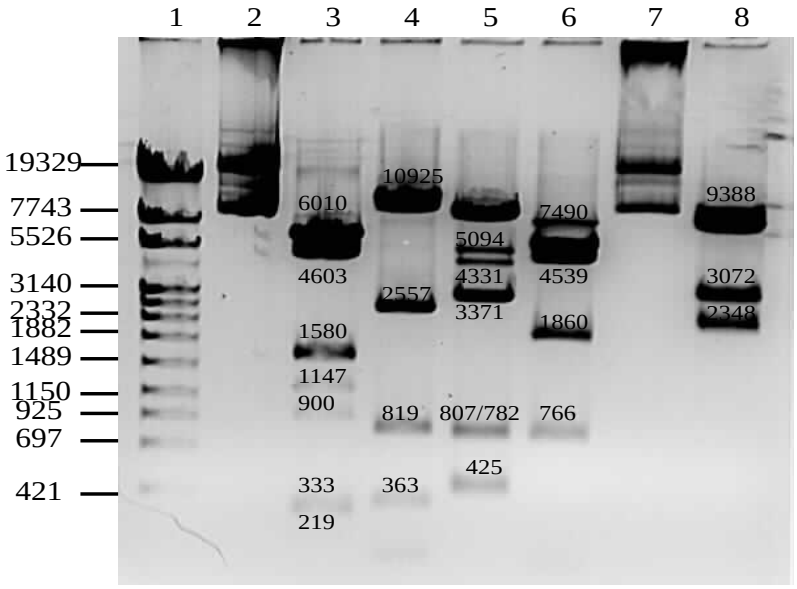

C

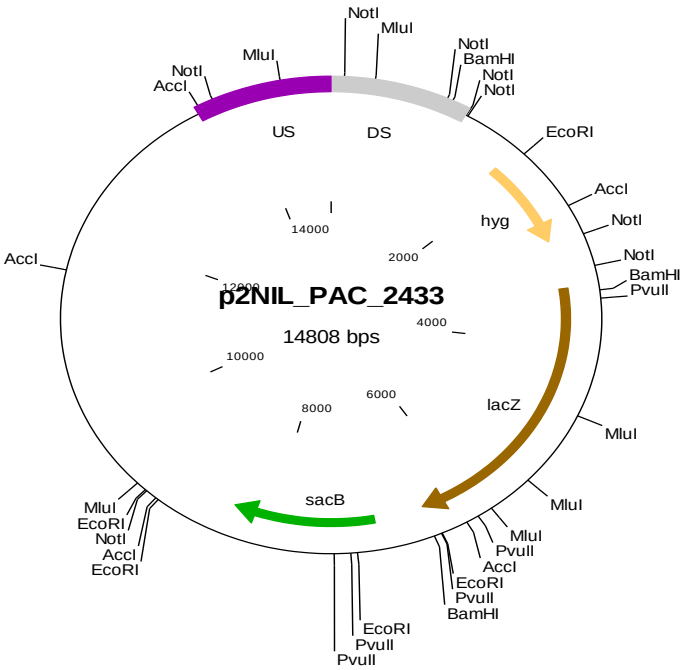

Figure D3. Restriction mapping of p2NIL_PAC_2433. (A) Expected fragment sizes for restriction digestions. (B) Restriction digestions of p2NIL_PAC_2433 with several enzymes. Lane 1: Marker IV, Lane 2: uncut DNA, Lane 3: *Not*I, Lane 4: *Pvu*II, Lane 5: *Mlu*I, Lane 6: *Eco*RI, Lane 7: *Acc*I, Lane 8: *Bam*HI. All bands correspond to expected sizes. (C) Vector map of p2NIL_PAC_2433.

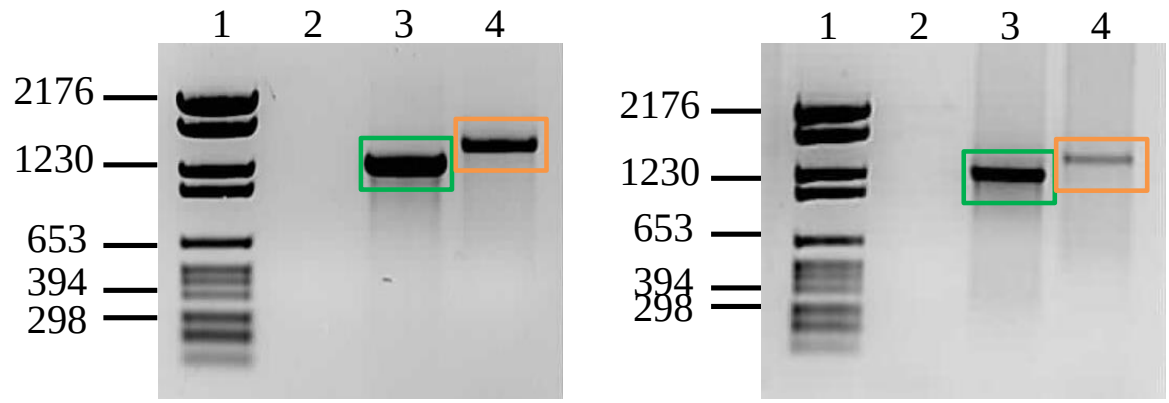

Figure D4. Generation of MSMEG_1661 probes for Southern blots. (A) upstream, (B) downstream. Lane 1: Marker VI, Lane 2: No DNA, Lane 3: unlabeled fragment, Lane 4: DIG labeled fragment. Green box indicates unlabeled probes and orange box indicates DIG labeled probes.

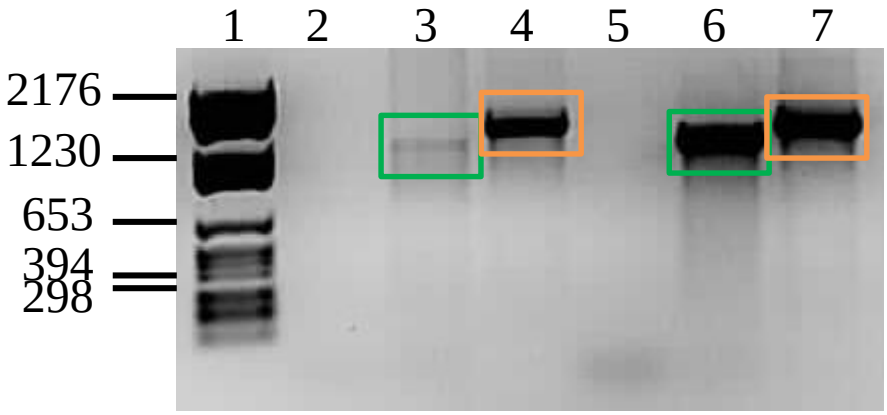

Figure D5. Generation of MSMEG_2432 probes for Southern blots. Lane 1: Marker VI, Lane 2 and 5: No DNA, Lane 3: unlabeled upstream fragment, Lane 4: DIG labeled upstream fragment, Lane 6: unlabeled downstream fragment, Lane 7: DIG labeled downstream fragment. Green box indicates unlabeled probes and orange box indicates DIG labeled probes.

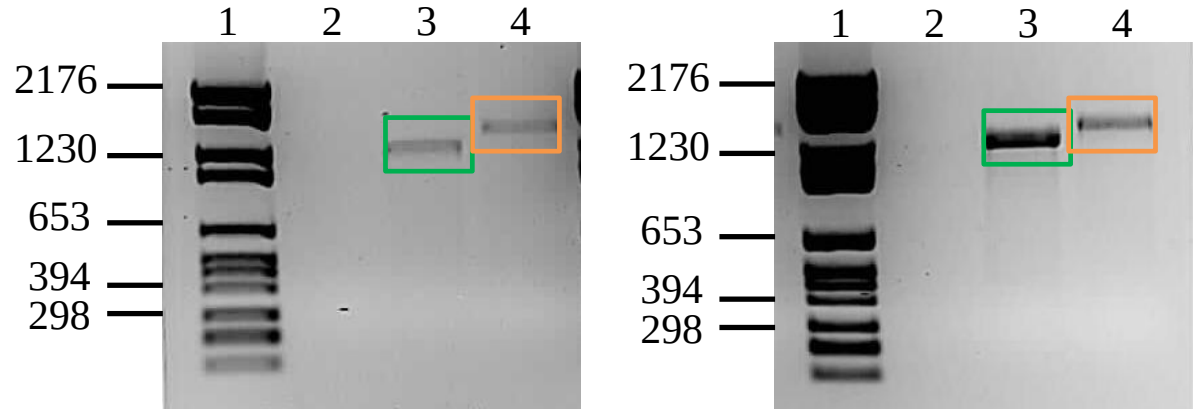

Figure D6. Generation of MSMEG_2433 probes for Southern blots. (A) upstream probe, (B) downstream probe. Lane 1: Marker VI, Lane 2: No DNA, Lane 3: unlabeled fragment, Lane 4: DIG labeled fragment Green box indicates unlabeled probes and orange box indicates DIG labeled probes.

A

Restriction enzyme/s	Fragment sizes (bp)
MluI + PstI	3462, 753, 725, 625, 56
MluI + PvuI	4170, 585, 419, 346, 101
NotI	4850, 771
AatII	2904, 2672, 45

B

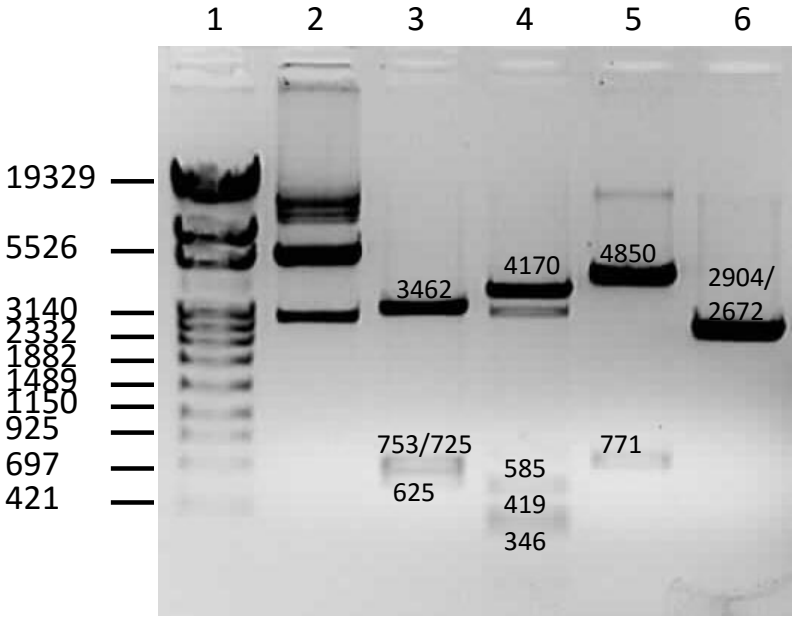

C

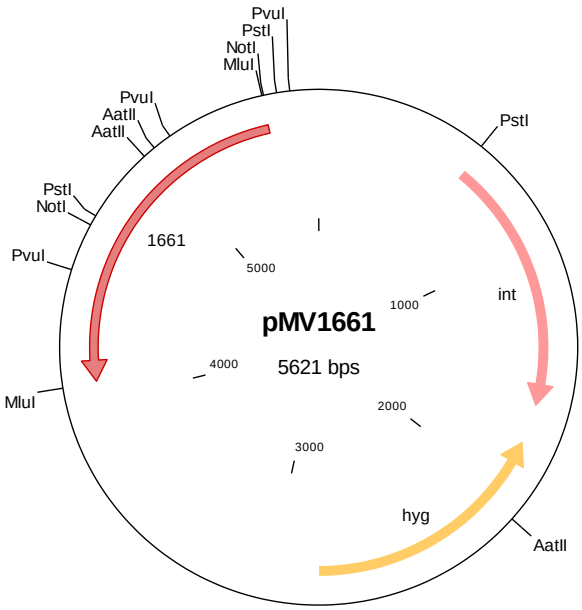

Figure D7. Restriction mapping of pMV1661. (A) Expected fragment sizes for restriction digestions. (B) Restriction digestions of pMV1661 with several enzymes. Lane 1: Marker IV, Lane 2: uncut DNA, Lane 3: *Mlu*I + *Pst*I, Lane 4: *Mlu*I + *Pvu*I, Lane 5: *Not*I, Lane 6: *Aat*II. All bands correspond to expected sizes. A partial digest was seen in Lane 4 as witnessed by the band that corresponds to the uncut sample. (C) Vector map of pMV1661.

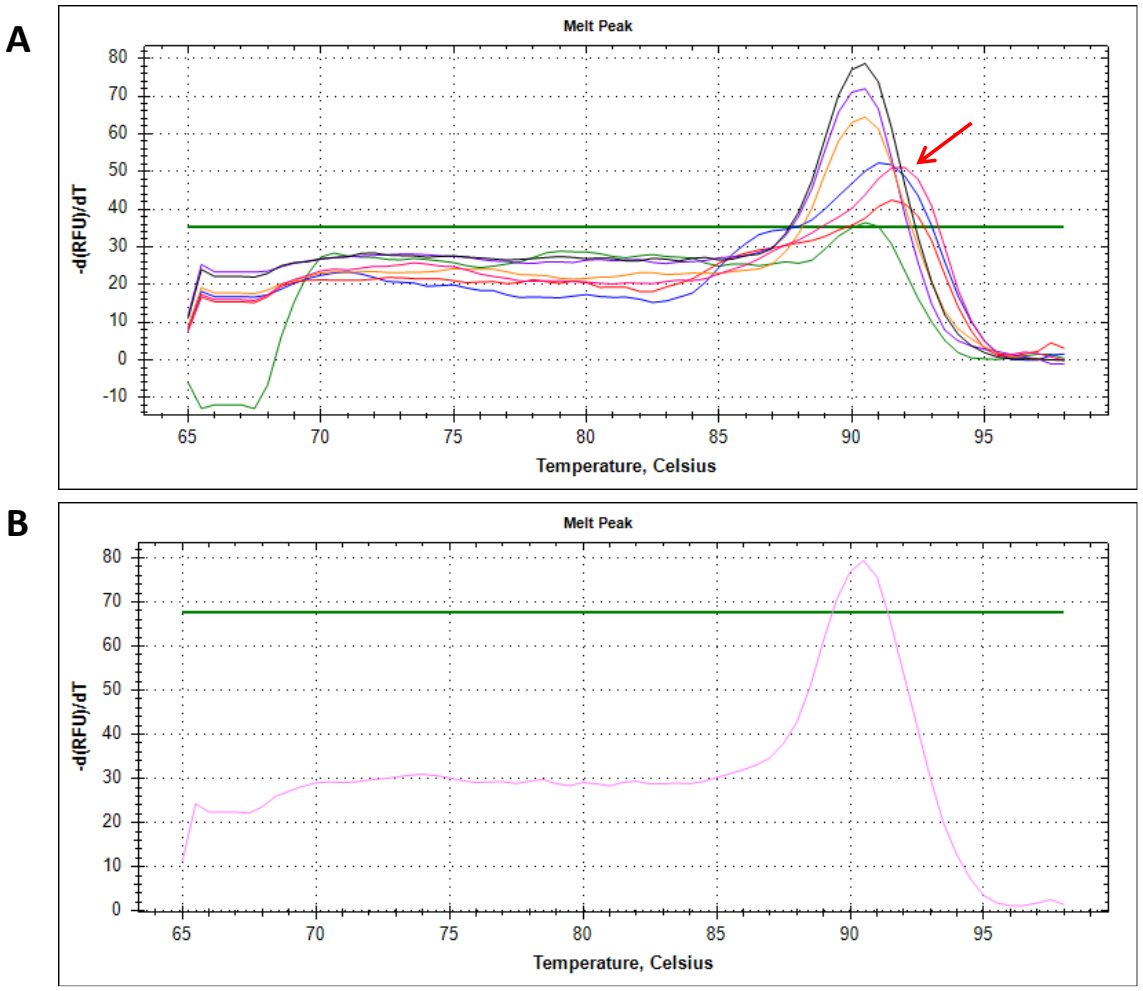

Figure D8. Melt curves of amplicons from qPCR for MSMEG_1661. (A) Curve showing wild type - black, Δ\MSMEG_1661 - pink, ΔMSMEG_2432 - orange, ΔMSMEG_2433 - purple, ΔMSMEG_1661ΔMSMEG_2432 - red, ΔMSMEG_2433 ΔMSMEG_1661 - blue and ΔMSMEG_1661 ΔMSMEG_2432::MSMEG_1661 - green. (B) Curve showing ΔMSMEG_2433 ΔMSMEG_1661::MSMEG_1661 - light pink. Red arrow indicates example of non-specific peak which appeared in all mutant strains lacking MSMEG_1661.

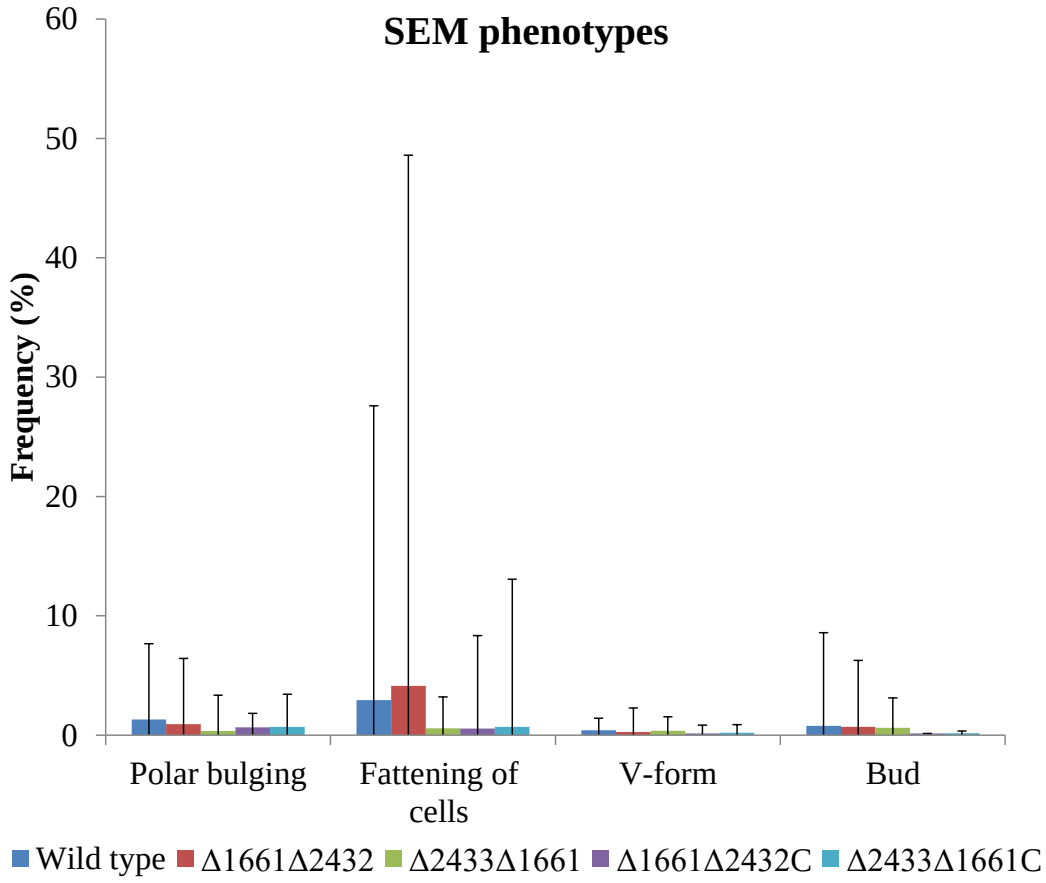

Figure D9. SEM phenotypes observed in wild type, double knockout mutants and complemented strains. All strains produced p values higher than what was considered statistically significant. Graph represents the average of three experiments with error bars showing standard error.

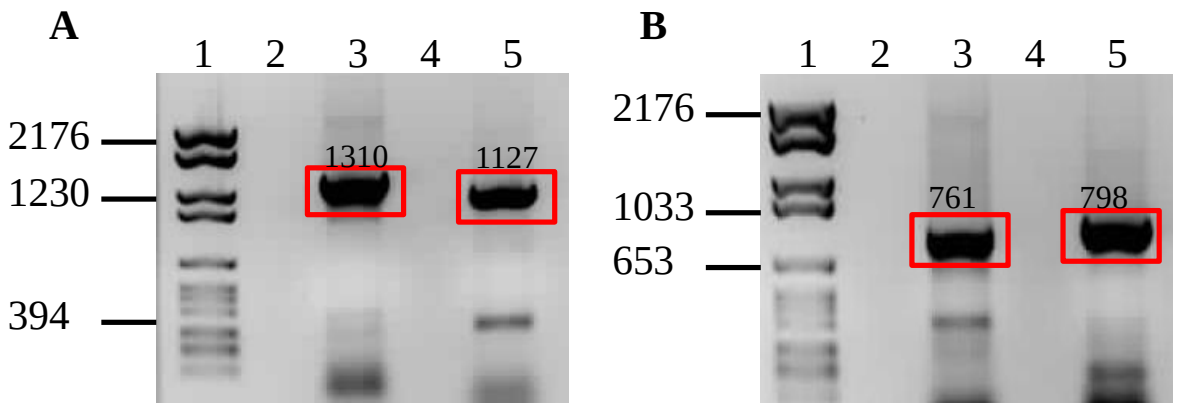

Figure D10. Phusion PCR of gene fragments to be cloned into pET29a. (A) PCR fragments of DacB and MSMEG_1661. Lane 1: Marker VI, Lane 2: no DNA, Lane 3: DacB, Lane 4: no DNA, Lane 5: MSMEG_1661. (B) PCR fragments of MSMEG_2432 and MSMEG_2433. Lane 1: Marker VI, Lane 2: no DNA, Lane 3: MSMEG_2432, Lane 4: no DNA, Lane 5: MSMEG_2433. Red boxes indicate fragments that were excised and purified.

A

Restriction enzyme	Fragment sizes (bp)
BamHI	5371
BspHI	3421, 1073, 875
NspI	2741, 1971, 367, 292
PvuII	4279, 999, 93
AccI	2816, 2555

B

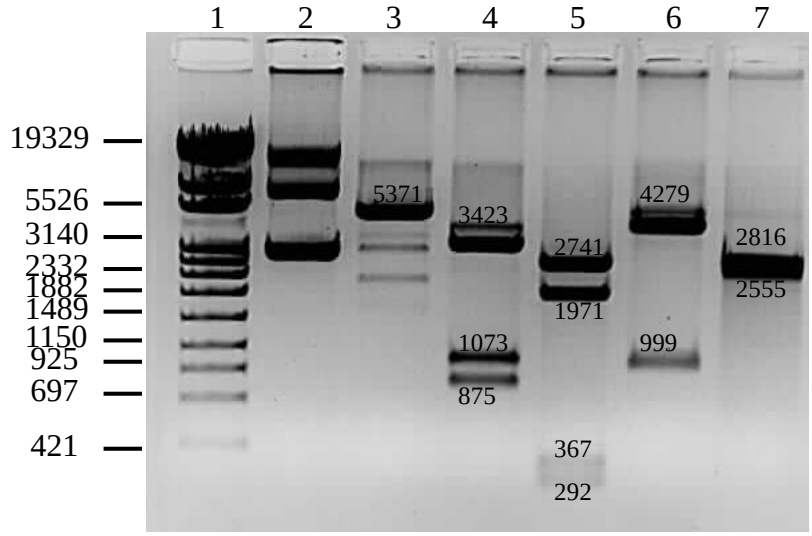

C

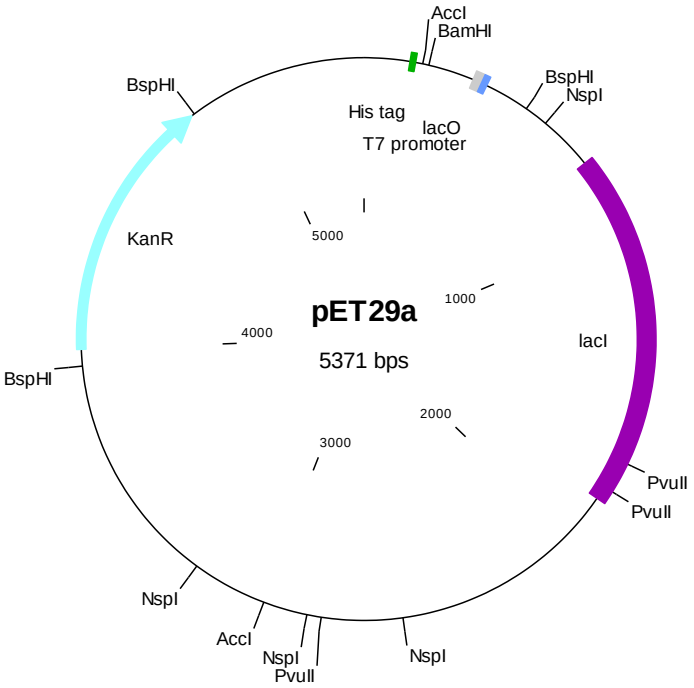

Figure D11. Restriction analysis of pET29a expression vector. (A) Expected fragment sizes for restriction digests. (B) Restriction digests of pET29a with several enzymes. Lane 1: Marker VI, Lane 2: Uncut DNA, Lane 3: *Bam*HI, Lane 4: *Bsp*HI, Lane 5: *Nsp*I, Lane 6: *Pvu*II, Lane 7: *Acc*I. All bands corresponded to the expected sizes. (C) pET29a vector map.

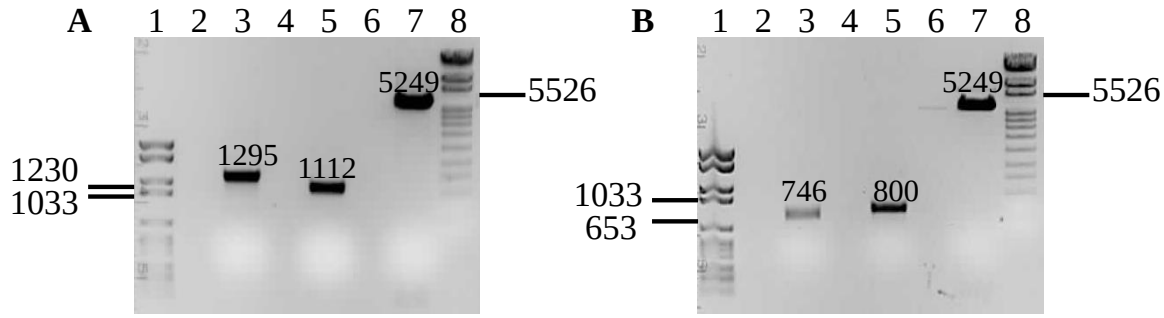

Figure D12. Digested fragments for cloning. (A) DacB, MSMEG_1661 and pET29a digested with *Hin*DIII and *Nde*I. Lane 1: Marker VI, Lane 2, 4, and 6: no sample, Lane 3: DacB, Lane 5: MSMEG_1661, Lane 7: pET29a, Lane 8: Marker IV. (B) MSMEG_2432, MSMEG_2433 and pET29a digested with *Hin*DIII and *Nde*I. Lane 1: Marker VI, Lane 2, 4, and 6: no sample, Lane 3: MSMEG_2432, Lane 5: MSMEG_2433, Lane 7: pET29a, Lane 8: Marker IV.

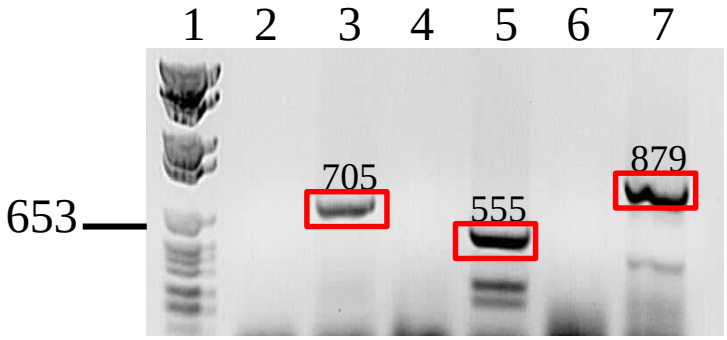

Figure D13. Phusion PCR of DacB variants to be cloned into pET29a. Lane 1: Marker VI, Lane 2, 4 and 6: no DNA, Lane 3: DacB domain, Lane 5: DacB minus, Lane 7: DacB flank. Red boxes indicate fragments that were excised and purified.

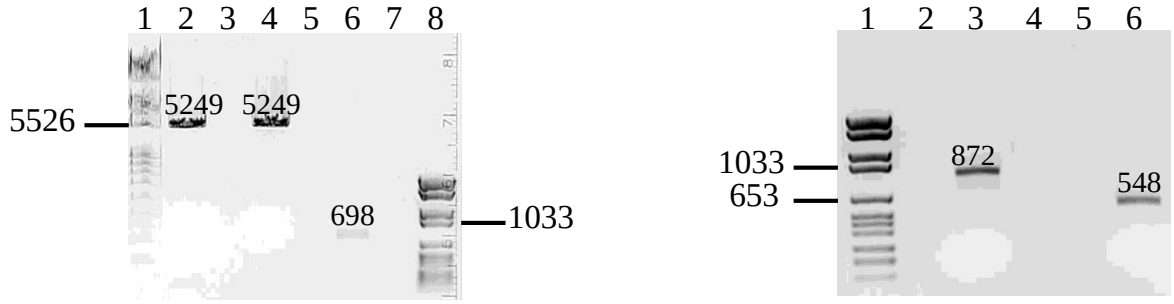

Figure D14. Digested DacB variant fragments for cloning. (A) pET29a and DacB domain digested with *Hin*DIII and *Nde*I. Lane 1: Marker IV, Lane 2 and 4: digested pET29a, Lane 3, 5, and 7: no sample, Lane 6: digested DacB domain, Lane 8: Marker VI. (B) DacB flank and DacB minus digested with *Hin*DIII and *Nde*I. Lane 1: Marker VI, Lane 2, 4, and 5: no sample, Lane 3: digested DacB flank, Lane 6: digested DacB minus.

6. References

ADAMS, D. W. & ERRINGTON, J. (2009) Bacterial cell division: assembly, maintenance and disassembly of the Z-ring. *Nat Rev Microbiol,* 7**,** 642-53.

ALDRIDGE, B. B., FERNANDEZ-SUAREZ, M., HELLER, D., AMBRAVANESWARAN, V., IRIMIA, D., TONER, M. & FORTUNE, S. M. (2012) Asymmetry and aging of mycobacterial cells lead to variable growth and antibiotic susceptibility. *Science,* 335**,** 100-4.

ALSTEENS, D., VERBELEN, C., DAGUE, E., RAZE, D., BAULARD, A. R. & DUFRENE, Y. F. (2008) Organization of the mycobacterial cell wall: a nanoscale view. *Pflugers Arch,* 456**,** 117-25.

ANDRIES, K., VERHASSELT, P., GUILLEMONT, J., GOHLMANN, H. W., NEEFS, J. M., WINKLER, H., VAN GESTEL, J., TIMMERMAN, P., ZHU, M., LEE, E., WILLIAMS, P., DE CHAFFOY, D., HUITRIC, E., HOFFNER, S., CAMBAU, E., TRUFFOT-PERNOT, C., LOUNIS, N. & JARLIER, V. (2005) A diarylquinoline drug active on the ATP synthase of *Mycobacterium tuberculosis*. *Science,* 307**,** 223-7.

ANUCHIN, A. M., MULYUKIN, A. L., SUZINA, N. E., DUDA, V. I., EL-REGISTAN, G. I. & KAPRELYANTS, A. S. (2009) Dormant forms of *Mycobacterium smegmatis* with distinct morphology. *Microbiology,* 155**,** 1071-9.

ATRIH, A., BACHER, G., ALLMAIER, G., WILLIAMSON, M. P. & FOSTER, S. J. (1999) Analysis of peptidoglycan structure from vegetative cells of *Bacillus subtilis* 168 and role of PBP 5 in peptidoglycan maturation. *J Bacteriol,* 181**,** 3956-66.

BANERJEE, A., DUBNAU, E., QUEMARD, A., BALASUBRAMANIAN, V., UM, K. S., WILSON, T., COLLINS, D., DE LISLE, G. & JACOBS, W. R., JR. (1994) *inhA*, a gene encoding a target for isoniazid and ethionamide in *Mycobacterium tuberculosis*. *Science,* 263**,** 227-30.

BANSAL-MUTALIK, R. & NIKAIDO, H. (2014) Mycobacterial outer membrane is a lipid bilayer and the inner membrane is unusually rich in diacyl phosphatidylinositol dimannosides. *Proc Natl Acad Sci U S A,* 111**,** 4958-63.

BAQUERO, M. R., BOUZON, M., QUINTELA, J. C., AYALA, J. A. & MORENO, F. (1996) *dacD*, an *Escherichia coli* gene encoding a novel penicillin-binding protein (PBP6b) with DD-carboxypeptidase activity. *J Bacteriol,* 178**,** 7106-11.

BARNA, J. C. & WILLIAMS, D. H. (1984) The structure and mode of action of glycopeptide antibiotics of the vancomycin group. *Annu Rev Microbiol,* 38**,** 339-57.

BARRETEAU, H., KOVAC, A., BONIFACE, A., SOVA, M., GOBEC, S. & BLANOT, D. (2008) Cytoplasmic steps of peptidoglycan biosynthesis. *FEMS Microbiol Rev,* 32**,** 168-207.

BARRY, C. E., 3RD, BOSHOFF, H. I., DARTOIS, V., DICK, T., EHRT, S., FLYNN, J., SCHNAPPINGER, D., WILKINSON, R. J. & YOUNG, D. (2009a) The spectrum of latent tuberculosis: rethinking the biology and intervention strategies. *Nat Rev Microbiol,* 7**,** 845-55.

BARRY, C. E., BOSHOFF, H., DARTOIS, V., DICK, T., EHRT, S., FLYNN, J., SCHNAPPINGER, D., WILKINSON, R. J. & YOUNG, D. (2009b) The spectrum of latent tuberculosis: rethinking the goals of prophylaxis. *Nat Rev Microbiol,* 7**,** 845-855.

BARRY, C. E., CRICK, D. C. & MCNEIL, M. R. (2007) Targeting the formation of the cell wall core of *M. tuberculosis*. *Infect Disord Drug Targets,* 7**,** 182-202.

BESRA, G. S. & BRENNAN, P. J. (1997) The mycobacterial cell wall: biosynthesis of arabinogalactan and lipoarabinomannan. *Biochem Soc Trans,* 25**,** 845-50.

BHATT, K. & SALGAME, P. (2007) Host innate immune response to *Mycobacterium tuberculosis*. *J Clin Immunol,* 27**,** 347-62.

BI, E. F. & LUTKENHAUS, J. (1991) FtsZ ring structure associated with division in *Escherichia coli*. *Nature,* 354**,** 161-4.

BOSHOFF, H. I. & BARRY, C. E. (2006) Is the mycobacterial cell wall a hopeless drug target for latent tuberculosis? *J Infect Dis,* 3**,** 237-245.

BOURAI, N., JACOBS, W. R., JR. & NARAYANAN, S. (2011) Deletion and overexpression studies on DacB2, a putative low molecular mass penicillin binding protein from *Mycobacterium tuberculosis* H(37)Rv. *Microb Pathog,* 52**,** 109-16.

BRANDA, S. S., VIK, S., FRIEDMAN, L. & KOLTER, R. (2005) Biofilms: the matrix revisited. *Trends Microbiol,* 13**,** 20-6.

BRENNAN, P. J. (2003) Structure, function, and biogenesis of the cell wall of *Mycobacterium tuberculosis*. *Tuberculosis (Edinb),* 83**,** 91-7.

BROOME-SMITH, J. K., IOANNIDIS, I., EDELMAN, A. & SPRATT, B. G. (1988) Nucleotide sequences of the penicillin-binding protein 5 and 6 genes of *Escherichia coli*. *Nucleic Acids Res,* 16**,** 1617.

BROWN, P. J., KYSELA, D. T. & BRUN, Y. V. (2011) Polarity and the diversity of growth mechanisms in bacteria. *Semin Cell Dev Biol,* 22**,** 790-8.

BUGG, T. D., WRIGHT, G. D., DUTKA-MALEN, S., ARTHUR, M., COURVALIN, P. & WALSH, C. T. (1991) Molecular basis for vancomycin resistance in *Enterococcus faecium* BM4147: biosynthesis of a depsipeptide peptidoglycan precursor by vancomycin resistance proteins VanH and VanA. *Biochemistry,* 30**,** 10408-15.

CABEEN, M. T. & JACOBS-WAGNER, C. (2005) Bacterial cell shape. *Nat Rev Microbiol,* 3**,** 601-10.

CACERES, N. E., HARRIS, N. B., WELLEHAN, J. F., FENG, Z., KAPUR, V. & BARLETTA, R. G. (1997) Overexpression of the D-alanine racemase gene confers resistance to D-cycloserine in *Mycobacterium smegmatis*. *J Bacteriol,* 179**,** 5046-55.

CAMINERO, J. A., SOTGIU, G., ZUMLA, A. & MIGLIORI, G. B. (2010) Best drug treatment for multidrug-resistant and extensively drug-resistant tuberculosis. *Lancet Infect Dis,* 10**,** 621-9.

CAVA, F., KURU, E., BRUN, Y. V. & DE PEDRO, M. A. (2013) Modes of cell wall growth differentiation in rod-shaped bacteria. *Curr Opin Microbiol,* 16**,** 731-7.

CDC (2015) A global perspective on TB.

CHAO, M. C. & RUBIN, E. J. (2010) Letting sleeping dos lie: does dormancy play a role in tuberculosis? *Annu Rev Microbiol,* 64**,** 293-311.

COHEN, J. (2013) Infectious disease. Approval of novel TB drug celebrated--with restraint. *Science,* 339**,** 130.

COLE, S. T., BROSCH, R., PARKHILL, J., GARNIER, T., CHURCHER, C., HARRIS, D., GORDON, S. V., EIGLMEIER, K., GAS, S., BARRY, C. E., 3RD, TEKAIA, F., BADCOCK, K., BASHAM, D., BROWN, D., CHILLINGWORTH, T., CONNOR, R., DAVIES, R., DEVLIN, K., FELTWELL, T., GENTLES, S., HAMLIN, N., HOLROYD, S., HORNSBY, T., JAGELS, K., KROGH, A., MCLEAN, J., MOULE, S., MURPHY, L., OLIVER, K., OSBORNE, J., QUAIL, M. A., RAJANDREAM, M. A., ROGERS, J., RUTTER, S., SEEGER, K., SKELTON, J., SQUARES, R., SQUARES, S., SULSTON, J. E., TAYLOR, K., WHITEHEAD, S. & BARRELL, B. G. (1998) Deciphering the biology of *Mycobacterium tuberculosis* from the complete genome sequence. *Nature,* 393**,** 537-44.

CORDILLOT, M., DUBEE, V., TRIBOULET, S., DUBOST, L., MARIE, A., HUGONNET, J. E., ARTHUR, M. & MAINARDI, J. L. (2013) In vitro cross-linking of *Mycobacterium tuberculosis* peptidoglycan by LD-transpeptidases and inactivation of these enzymes by carbapenems. *Antimicrob Agents Chemother,* 57**,** 5940-5.

CRICK, D. C., MAHAPATRA, S. & BRENNAN, P. J. (2001) Biosynthesis of the arabinogalactan-peptidoglycan complex of *Mycobacterium tuberculosis*. *Glycobiology,* 11**,** 107R-118R.

DAFFE, M., BRENNAN, P. J. & MCNEIL, M. (1990) Predominant structural features of the cell wall arabinogalactan of *Mycobacterium tuberculosis* as revealed through characterization of oligoglycosyl alditol fragments by gas chromatography/mass spectrometry and by 1H and 13C NMR analyses. *J Biol Chem,* 265**,** 6734-43.

DAFFE, M. & ETIENNE, G. (1999) The capsule of *Mycobacterium tuberculosis* and its implications for pathogenicity. *Tuber Lung Dis,* 79**,** 153-69.

DAHL, J. L. (2004) Electron microscopy analysis of *Mycobacterium tuberculosis* cell division. *FEMS Microbiol Lett,* 240**,** 15-20.

DANIEL, R. A., HARRY, E. J. & ERRINGTON, J. (2000) Role of penicillin-binding protein PBP 2B in assembly and functioning of the division machinery of *Bacillus subtilis*. *Mol Microbiol,* 35**,** 299-311.

DATTA, P., DASGUPTA, A., BHAKTA, S. & BASU, J. (2002) Interaction between FtsZ and FtsW of *Mycobacterium tuberculosis*. *J Biol Chem,* 277**,** 24983-7.

DATTA, P., DASGUPTA, A., SINGH, A. K., MUKHERJEE, P., KUNDU, M. & BASU, J. (2006) Interaction between FtsW and penicillin-binding protein 3 (PBP3) directs PBP3 to mid-cell, controls cell septation and mediates the formation of a trimeric complex involving FtsZ, FtsW and PBP3 in mycobacteria. *Mol Microbiol,* 62**,** 1655-73.

DE BACKER, A. I., MORTELE, K. J., DE KEULENAER, B. L. & PARIZEL, P. M. (2006) Tuberculosis: epidemiology, manifestations, and the value of medical imaging in diagnosis. *JBR-BTR,* 89**,** 243-50.

DENOME, S. A., ELF, P. K., HENDERSON, T. A., NELSON, D. E. & YOUNG, K. D. (1999) *Escherichia coli* mutants lacking all possible combinations of eight penicillin binding proteins: viability, characteristics, and implications for peptidoglycan synthesis. *J Bacteriol,* 181**,** 3981-93.

DEPARDIEU, F., PODGLAJEN, I., LECLERCQ, R., COLLATZ, E. & COURVALIN, P. (2007) Modes and modulations of antibiotic resistance gene expression. *Clin Microbiol Rev,* 20**,** 79-114.

DEROUAUX, A., SAUVAGE, E. & TERRAK, M. (2013) Peptidoglycan glycosyltransferase substrate mimics as templates for the design of new antibacterial drugs. *Front Immunol,* 4**,** 78.

DHOPLE, A. M. (1983) Effect of lysozyme on *Mycobacterium leprae*. *Lepr India,* 55**,** 455-64.

DIACON, A. H., DAWSON, R., VON GROOTE-BIDLINGMAIER, F., SYMONS, G., VENTER, A., DONALD, P. R., VAN NIEKERK, C., EVERITT, D., WINTER, H., BECKER, P., MENDEL, C. M. & SPIGELMAN, M. K. (2012) 14-day bactericidal activity of PA-824, bedaquiline, pyrazinamide, and moxifloxacin combinations: a randomised trial. *Lancet,* 380**,** 986-93.

DOMENECH, P., REED, M. B. & BARRY, C. E., 3RD (2005) Contribution of the *Mycobacterium tuberculosis* MmpL protein family to virulence and drug resistance. *Infect Immun,* 73**,** 3492-501.

DOUGHERTY, T. J. & PUCCI, M. J. (1994) Penicillin-binding proteins are regulated by *rpoS* during transitions in growth states of *Escherichia coli*. *Antimicrob Agents Chemother,* 38**,** 205-10.

DOWNING, K. J., MISCHENKO, V. V., SHLEEVA, M. O., YOUNG, D. I., YOUNG, M., KAPRELYANTS, A. S., APT, A. S. & MIZRAHI, V. (2005) Mutants of *Mycobacterium tuberculosis* lacking three of the five rpf-like genes are defective for growth in vivo and for resuscitation in vitro. *Infect Immun,* 73**,** 3038-43.

DUBEE, V., TRIBOULET, S., MAINARDI, J. L., ETHEVE-QUELQUEJEU, M., GUTMANN, L., MARIE, A., DUBOST, L., HUGONNET, J. E. & ARTHUR, M. (2012) Inactivation of *Mycobacterium tuberculosis* LD-transpeptidase LdtMt(1) by carbapenems and cephalosporins. *Antimicrob Agents Chemother,* 56**,** 4189-95.

DUCATI, R. G., RUFFINO-NETTO, A., BASSO, L. A. & SANTOS, D. S. (2006) The resumption of consumption - a review on tuberculosis. *Mem Inst Oswaldo Cruz,* 101**,** 697-714.

DUTTA, N. K., MEHRA, S., DIDIER, P. J., ROY, C. J., DOYLE, L. A., ALVAREZ, X., RATTERREE, M., BE, N. A., LAMICHHANE, G., JAIN, S. K., LACEY, M. R., LACKNER, A. A. & KAUSHAL, D. (2010) Genetic requirements for the survival of tubercle bacilli in primates. *J Infect Dis,* 201**,** 1743-52.

DZIADEK, J., RUTHERFORD, S. A., MADIRAJU, M. V., ATKINSON, M. A. & RAJAGOPALAN, M. (2003) Conditional expression of *Mycobacterium smegmatis ftsZ*, an essential cell division gene. *Microbiology,* 149**,** 1593-603.

ETIENNE, G., VILLENEUVE, C., BILLMAN-JACOBE, H., ASTARIE-DEQUEKER, C., DUPONT, M. A. & DAFFE, M. (2002) The impact of the absence of glycopeptidolipids on the ultrastructure, cell surface and cell wall properties, and phagocytosis of *Mycobacterium smegmatis*. *Microbiology,* 148**,** 3089-100.

FEREBEE, S. H. & MOUNT, F. W. (1962) Tuberculosis morbidity in a controlled trial of the prophylactic use of isoniazid among household contacts. *Am Rev Respir Dis,* 85**,** 490-510.

FEUCHT, A., EVANS, L. & ERRINGTON, J. (2003) Identification of sporulation genes by genome-wide analysis of the sigmaE regulon of *Bacillus subtilis*. *Microbiology,* 149**,** 3023-34.

FRIRDICH, E. & GAYNOR, E. C. (2013) Peptidoglycan hydrolases, bacterial shape, and pathogenesis. *Curr Opin Microbiol,* 16**,** 767-78.

GALLANT, C. V., DANIELS, C., LEUNG, J. M., GHOSH, A. S., YOUNG, K. D., KOTRA, L. P. & BURROWS, L. L. (2005) Common beta-lactamases inhibit bacterial biofilm formation. *Mol Microbiol,* 58**,** 1012-24.

GANDHI, N. R., MOLL, A., STURM, A. W., PAWINSKI, R., GOVENDER, T., LALLOO, U., ZELLER, K., ANDREWS, J. & FRIEDLAND, G. (2006) Extensively drug-resistant tuberculosis as a cause of death in patients co-infected with tuberculosis and HIV in a rural area of South Africa. *Lancet,* 368**,** 1575-80.

GHOSH, A. S., CHOWDHURY, C. & NELSON, D. E. (2008) Physiological functions of D-alanine carboxypeptidases in *Escherichia coli*. *Trends Microbiol,* 16**,** 309-17.

GHOSH, A. S. & YOUNG, K. D. (2003) Sequences near the active site in chimeric penicillin binding proteins 5 and 6 affect uniform morphology of *Escherichia coli*. *J Bacteriol,* 185**,** 2178-86.

GHOSH, S., INDI, S. S. & NAGARAJA, V. (2013) Regulation of lipid biosynthesis, sliding motility, and biofilm formation by a membrane-anchored nucleoid-associated protein of *Mycobacterium tuberculosis*. *J Bacteriol,* 195**,** 1769-78.

GHUYSEN, J. M. (1991) Serine beta-lactamases and penicillin-binding proteins. *Annu Rev Microbiol,* 45**,** 37-67.

GITAI, Z., DYE, N. A., REISENAUER, A., WACHI, M. & SHAPIRO, L. (2005) MreB actin-mediated segregation of a specific region of a bacterial chromosome. *Cell,* 120**,** 329-41.

GOLA, S., MUNDER, T., CASONATO, S., MANGANELLI, R. & VICENTE, M. (2015) The essential role of SepF in mycobacterial division. *Mol Microbiol,* 97**,** 560-76.

GOMEZ, J. E. & MCKINNEY, J. D. (2004) *M. tuberculosis* persistence, latency, and drug tolerance. *Tuberculosis (Edinb),* 84**,** 29-44.

GONDRE, B., FLOURET, B. & VAN HEIJENOORT, J. (1973) Release of D-alanyl-D-alanine from the precursor of the cell wall peptidoglycan by a peptidase of *Escherichia coli* K 12. *Biochimie,* 55**,** 685-91.

GORDHAN, B. G. & PARISH, T. (2001) Gene Replacement using Pretreated DNA. *Methods Mol Med,* 54**,** 77-92.

GUINANE, C. M., COTTER, P. D., ROSS, R. P. & HILL, C. (2006) Contribution of penicillin-binding protein homologs to antibiotic resistance, cell morphology, and virulence of *Listeria monocytogenes* EGD. *Antimicrob Agents Chemother,* 50**,** 2824-8.

GUPTA, R., LAVOLLAY, M., MAINARDI, J. L., ARTHUR, M., BISHAI, W. R. & LAMICHHANE, G. (2010) The *Mycobacterium tuberculosis* protein LdtMt2 is a nonclassical transpeptidase required for virulence and resistance to amoxicillin. *Nat Med,* 16**,** 466-9.

GUPTA, S., BANERJEE, S. K., CHATTERJEE, A., SHARMA, A. K., KUNDU, M. & BASU, J. (2015) Essential protein SepF of mycobacteria interacts with FtsZ and MurG to regulate cell growth and division. *Microbiology,* 161**,** 1627-38.

HAMMES, W. P. & SEIDEL, H. (1978) The activities in vitro of DD-carboxypeptidase and LD-carboxypeptidase of *Gaffkya homari* during biosynthesis of peptidoglycan. *Eur J Biochem,* 84**,** 141-7.

HEIDRICH, C., TEMPLIN, M. F., URSINUS, A., MERDANOVIC, M., BERGER, J., SCHWARZ, H., DE PEDRO, M. A. & HOLTJE, J. V. (2001) Involvement of *N*-acetylmuramyl-L-alanine amidases in cell separation and antibiotic-induced autolysis of *Escherichia coli*. *Mol Microbiol,* 41**,** 167-78.

HETT, E. C., CHAO, M. C., DENG, L. L. & RUBIN, E. J. (2008) A mycobacterial enzyme essential for cell division synergizes with resuscitation-promoting factor. *PLoS Pathog,* 4**,** e1000001.

HETT, E. C., CHAO, M. C., STEYN, A. J., FORTUNE, S. M., DENG, L. L. & RUBIN, E. J. (2007) A partner for the resuscitation-promoting factors of *Mycobacterium tuberculosis*. *Mol Microbiol,* 66**,** 658-68.

HETT, E. C. & RUBIN, E. J. (2008) Bacterial growth and cell division: a mycobacterial perspective. *Microbiol Mol Biol Rev,* 72**,** 126-56, table of contents.

HIGGINS, D. & DWORKIN, J. (2011) Recent progress in *Bacillus subtilis* sporulation. *FEMS Microbiol Rev,* 36**,** 131-48.

HIRST, R. A., GOSAI, B., RUTMAN, A., GUERIN, C. J., NICOTERA, P., ANDREW, P. W. & O'CALLAGHAN, C. (2008) *Streptococcus pneumoniae* deficient in pneumolysin or autolysin has reduced virulence in meningitis. *J Infect Dis,* 197**,** 744-51.

JACOBS, C., HUANG, L. J., BARTOWSKY, E., NORMARK, S. & PARK, J. T. (1994) Bacterial cell wall recycling provides cytosolic muropeptides as effectors for beta-lactamase induction. *EMBO J,* 13**,** 4684-94.

JONES, L. J., CARBALLIDO-LOPEZ, R. & ERRINGTON, J. (2001) Control of cell shape in bacteria: helical, actin-like filaments in *Bacillus subtilis*. *Cell,* 104**,** 913-22.

JOYCE, G., WILLIAMS, K. J., ROBB, M., NOENS, E., TIZZANO, B., SHAHREZAEI, V. & ROBERTSON, B. D. (2012) Cell division site placement and asymmetric growth in mycobacteria. *PLoS One,* 7**,** e44582.

KANA, B. D., GORDHAN, B. G., DOWNING, K. J., SUNG, N., VOSTROKTUNOVA, G., MACHOWSKI, E. E., TSENOVA, L., YOUNG, M., KAPRELYANTS, A., KAPLAN, G. & MIZRAHI, V. (2008) The resuscitation-promoting factors of *Mycobacterium tuberculosis* are required for virulence and resuscitation from dormancy but are collectively dispensable for growth in vitro. *Mol Microbiol,* 67**,** 672-84.

KANG, C. M., NYAYAPATHY, S., LEE, J. Y., SUH, J. W. & HUSSON, R. N. (2008) Wag31, a homologue of the cell division protein DivIVA, regulates growth, morphology and polar cell wall synthesis in mycobacteria. *Microbiology,* 154**,** 725-35.

KARCZMAREK, A., MARTINEZ-ARTEAGA, R., ALEXEEVA, S., HANSEN, F. G., VICENTE, M., NANNINGA, N. & DEN BLAAUWEN, T. (2007) DNA and origin region segregation are not affected by the transition from rod to sphere after inhibition of *Escherichia coli* MreB by A22. *Mol Microbiol,* 65**,** 51-63.

KAUR, D., GUERIN, M. E., SKOVIEROVA, H., BRENNAN, P. J. & JACKSON, M. (2009) Chapter 2: Biogenesis of the cell wall and other glycoconjugates of *Mycobacterium tuberculosis*. *Adv Appl Microbiol,* 69**,** 23-78.

KELL, C. M., SHARMA, U. K., DOWSON, C. G., TOWN, C., BALGANESH, T. S. & SPRATT, B. G. (1993) Deletion analysis of the essentiality of penicillin-binding proteins 1A, 2B and 2X of *Streptococcus pneumoniae*. *FEMS Microbiol Lett,* 106**,** 171-5.

KESAVAN, A. K., BROOKS, M., TUFARIELLO, J., CHAN, J. & MANABE, Y. C. (2009) Tuberculosis genes expressed during persistence and reactivation in the resistant rabbit model. *Tuberculosis (Edinb),* 89**,** 17-21.

KIESER, K. J. & RUBIN, E. J. (2014) How sisters grow apart: mycobacterial growth and division. *Nat Rev Microbiol,* 12**,** 550-62.

KORAT, B., MOTTL, H. & KECK, W. (1991) Penicillin-binding protein 4 of *Escherichia coli*: molecular cloning of the *dacB* gene, controlled overexpression, and alterations in murein composition. *Mol Microbiol,* 5**,** 675-84.

KORSAK, D., LIEBSCHER, S. & VOLLMER, W. (2005a) Susceptibility to antibiotics and beta-lactamase induction in murein hydrolase mutants of *Escherichia coli*. *Antimicrob Agents Chemother,* 49**,** 1404-9.

KORSAK, D., VOLLMER, W. & MARKIEWICZ, Z. (2005b) *Listeria monocytogenes* EGD lacking penicillin-binding protein 5 (PBP5) produces a thicker cell wall. *FEMS Microbiol Lett,* 251**,** 281-8.

KUMAR, A., KUMAR, S., KUMAR, D., MISHRA, A., DEWANGAN, R. P., SHRIVASTAVA, P., RAMACHANDRAN, S. & TANEJA, B. (2013) The structure of Rv3717 reveals a novel amidase from *Mycobacterium tuberculosis*. *Acta Crystallogr D Biol Crystallogr,* 69**,** 2543-54.

KUMAR, P., ARORA, K., LLOYD, J. R., LEE, I. Y., NAIR, V., FISCHER, E., BOSHOFF, H. I. & BARRY, C. E., 3RD (2012) Meropenem inhibits DD-carboxypeptidase activity in *Mycobacterium tuberculosis*. *Mol Microbiol,* 86**,** 367-81.

LAVOLLAY, M., ARTHUR, M., FOURGEAUD, M., DUBOST, L., MARIE, A., VEZIRIS, N., BLANOT, D., GUTMANN, L. & MAINARDI, J. L. (2008) The peptidoglycan of stationary-phase *Mycobacterium tuberculosis* predominantly contains cross-links generated by LD-transpeptidation. *J Bacteriol,* 190**,** 4360-6.

LECHARTIER, B. & COLE, S. T. (2015) Mode of Action of Clofazimine and Combination Therapy with Benzothiazinones against *Mycobacterium tuberculosis*. *Antimicrob Agents Chemother,* 59**,** 4457-63.

LEE, W. B., KANG, J. S., YAN, J. J., LEE, M. S., JEON, B. Y., CHO, S. N. & KIM, Y. J. (2012) Neutrophils Promote Mycobacterial Trehalose Dimycolate-Induced Lung Inflammation via the Mincle Pathway. *PLoS Pathog,* 8**,** e1002614.

LEWIS, K. (2010) Persister cells. *Annu Rev Microbiol,* 64**,** 357-72.

MACHOWSKI, E. E., SENZANI, S., EALAND, C. & KANA, B. D. (2014) Comparative genomics for mycobacterial peptidoglycan remodelling enzymes reveals extensive genetic multiplicity. *BMC Microbiol,* 14**,** 75.

MAHAPATRA, S., YAGI, T., BELISLE, J. T., ESPINOSA, B. J., HILL, P. J., MCNEIL, M. R., BRENNAN, P. J. & CRICK, D. C. (2005) Mycobacterial lipid II is composed of a complex mixture of modified muramyl and peptide moieties linked to decaprenyl phosphate. *J Bacteriol,* 187**,** 2747-57.

MAINARDI, J. L., HUGONNET, J. E., RUSCONI, F., FOURGEAUD, M., DUBOST, L., MOUMI, A. N., DELFOSSE, V., MAYER, C., GUTMANN, L., RICE, L. B. & ARTHUR, M. (2007) Unexpected inhibition of peptidoglycan LD-transpeptidase from *Enterococcus faecium* by the beta-lactam imipenem. *J Biol Chem,* 282**,** 30414-22.

MAINARDI, J. L., MOREL, V., FOURGEAUD, M., CREMNITER, J., BLANOT, D., LEGRAND, R., FREHEL, C., ARTHUR, M., VAN HEIJENOORT, J. & GUTMANN, L. (2002) Balance between two transpeptidation mechanisms determines the expression of beta-lactam resistance in *Enterococcus faecium*. *J Biol Chem,* 277**,** 35801-7.

MALMROS, H. (1948) The efficacy of BCG. vaccination. *Br Med J,* 1**,** 1129-32.

MARTINEZ, A., TORELLO, S. & KOLTER, R. (1999) Sliding motility in mycobacteria. *J Bacteriol,* 181**,** 7331-8.

MC DERMOTT, W. (1958) Microbial persistence. *Yale J Biol Med,* 30**,** 257-91.

MCCALL, K. A., HUANG, C. & FIERKE, C. A. (2000) Function and mechanism of zinc metalloenzymes. *J Nutr,* 130**,** 1437S-46S.

MCNEIL, M., DAFFE, M. & BRENNAN, P. J. (1990) Evidence for the nature of the link between the arabinogalactan and peptidoglycan of mycobacterial cell walls. *J Biol Chem,* 265**,** 18200-6.

MEBERG, B. M., PAULSON, A. L., PRIYADARSHINI, R. & YOUNG, K. D. (2004) Endopeptidase penicillin-binding proteins 4 and 7 play auxiliary roles in determining uniform morphology of *Escherichia coli*. *J Bacteriol,* 186**,** 8326-36.

MELLROTH, P., SANDALOVA, T., KIKHNEY, A., VILAPLANA, F., HESEK, D., LEE, M., MOBASHERY, S., NORMARK, S., SVERGUN, D., HENRIQUES-NORMARK, B. & ACHOUR, A. (2013) Structural and functional insights into peptidoglycan access for the lytic amidase LytA of *Streptococcus pneumoniae*. *MBio,* 5**,** e01120-13.

MENDELSON, N. H. (1976) Helical growth of *Bacillus subtilis*: a new model of cell growth. *Proc Natl Acad Sci U S A,* 73**,** 1740-4.

MENICHE, X., OTTEN, R., SIEGRIST, M. S., BAER, C. E., MURPHY, K. C., BERTOZZI, C. R. & SASSETTI, C. M. (2014) Subpolar addition of new cell wall is directed by DivIVA in mycobacteria. *Proc Natl Acad Sci U S A,* 111**,** E3243-51.

MIGLIORI, G. B., DE IACO, G., BESOZZI, G., CENTIS, R. & CIRILLO, D. M. (2007) First tuberculosis cases in Italy resistant to all tested drugs. *Euro Surveill,* 12**,** E070517 1.

MIKUSOVA, K., MIKUS, M., BESRA, G. S., HANCOCK, I. & BRENNAN, P. J. (1996) Biosynthesis of the linkage region of the mycobacterial cell wall. *J Biol Chem,* 271**,** 7820-8.

MILLER, C., THOMSEN, L. E., GAGGERO, C., MOSSERI, R., INGMER, H. & COHEN, S. N. (2004) SOS response induction by beta-lactams and bacterial defense against antibiotic lethality. *Science,* 305**,** 1629-31.

MOLL, A., DORR, T., ALVAREZ, L., DAVIS, B. M., CAVA, F. & WALDOR, M. K. (2015) A DD-carboxypeptidase is required for *Vibrio cholerae* halotolerance. *Environ Microbiol,* 17**,** 527-40.

MORLOT, C., NOIRCLERC-SAVOYE, M., ZAPUN, A., DIDEBERG, O. & VERNET, T. (2004) The DD-carboxypeptidase PBP3 organizes the division process of *Streptococcus pneumoniae*. *Mol Microbiol,* 51**,** 1641-8.

MORLOT, C., PERNOT, L., LE GOUELLEC, A., DI GUILMI, A. M., VERNET, T., DIDEBERG, O. & DESSEN, A. (2005) Crystal structure of a peptidoglycan synthesis regulatory factor (PBP3) from *Streptococcus pneumoniae*. *J Biol Chem,* 280**,** 15984-91.

MUKAMOLOVA, G. V., TURAPOV, O. A., KAZARIAN, K., TELKOV, M., KAPRELYANTS, A. S., KELL, D. B. & YOUNG, M. (2002) The rpf gene of *Micrococcus luteus* encodes an essential secreted growth factor. *Mol Microbiol,* 46**,** 611-21.

MUKAMOLOVA, G. V., YANOPOLSKAYA, N. D., KELL, D. B. & KAPRELYANTS, A. S. (1998) On resuscitation from the dormant state of *Micrococcus luteus*. *Antonie Van Leeuwenhoek,* 73**,** 237-43.

MUKHERJEE, A. & LUTKENHAUS, J. (1998) Dynamic assembly of FtsZ regulated by GTP hydrolysis. *EMBO J,* 17**,** 462-9.

MUKHERJEE, P., SUREKA, K., DATTA, P., HOSSAIN, T., BARIK, S., DAS, K. P., KUNDU, M. & BASU, J. (2009) Novel role of Wag31 in protection of mycobacteria under oxidative stress. *Mol Microbiol,* 73**,** 103-19.

MULYUKIN, A. L., KUDYKINA, Y. K., SHLEEVA, M. O., ANUCHIN, A. M., SUZINA, N. E., DANILEVICH, V. N., DUDA, V. I., KAPRELYANTS, A. S. & EL'-REGISTAN, G. I. (2009) Intraspecies Diversity of Dormant Forms of *Mycobacterium smegmatis*. *Mikrobiologiia,* 79**,** 461-471ss.

NIKITUSHKIN, V. D., DEMINA, G. R., SHLEEVA, M. O., GURYANOVA, S. V., RUGGIERO, A., BERISIO, R. & KAPRELYANTS, A. S. (2015) A product of RpfB and RipA joint enzymatic action promotes the resuscitation of dormant mycobacteria. *FEBS J,* 282**,** 2500-11.

NIKOLAIDIS, I., FAVINI-STABILE, S. & DESSEN, A. (2013) Resistance to antibiotics targeted to the bacterial cell wall. *Protein Sci,* 23**,** 243-59.

OJHA, A., ANAND, M., BHATT, A., KREMER, L., JACOBS, W. R., JR. & HATFULL, G. F. (2005) GroEL1: a dedicated chaperone involved in mycolic acid biosynthesis during biofilm formation in mycobacteria. *Cell,* 123**,** 861-73.

OJHA, A. K., BAUGHN, A. D., SAMBANDAN, D., HSU, T., TRIVELLI, X., GUERARDEL, Y., ALAHARI, A., KREMER, L., JACOBS, W. R., JR. & HATFULL, G. F. (2008) Growth of *Mycobacterium tuberculosis* biofilms containing free mycolic acids and harbouring drug-tolerant bacteria. *Mol Microbiol,* 69**,** 164-74.

OJHA, A. K., VARMA, S. & CHATTERJI, D. (2002) Synthesis of an unusual polar glycopeptidolipid in glucose-limited culture of *Mycobacterium smegmatis*. *Microbiology,* 148**,** 3039-48.

PAIK, J., KERN, I., LURZ, R. & HAKENBECK, R. (1999) Mutational analysis of the *Streptococcus pneumoniae* bimodular class A penicillin-binding proteins. *J Bacteriol,* 181**,** 3852-6.

PARISH, T. & STOKER, N. G. (2000) Use of a flexible cassette method to generate a double unmarked *Mycobacterium tuberculosis* tlyA plcABC mutant by gene replacement. *Microbiology,* 146 (Pt 8)**,** 1969-75.

PETERS, N. T., DINH, T. & BERNHARDT, T. G. (2011) A fail-safe mechanism in the septal ring assembly pathway generated by the sequential recruitment of cell separation amidases and their activators. *J Bacteriol,* 193**,** 4973-83.

PLOCINSKI, P., ARORA, N., SARVA, K., BLASZCZYK, E., QIN, H., DAS, N., PLOCINSKA, R., ZIOLKIEWICZ, M., DZIADEK, J., KIRAN, M., GORLA, P., CROSS, T. A., MADIRAJU, M. & RAJAGOPALAN, M. (2011) *Mycobacterium tuberculosis* CwsA interacts with CrgA and Wag31, and the CrgA-CwsA complex is involved in peptidoglycan synthesis and cell shape determination. *J Bacteriol,* 194**,** 6398-409.

POPHAM, D. L., GILMORE, M. E. & SETLOW, P. (1999) Roles of low-molecular-weight penicillin-binding proteins in *Bacillus subtilis* spore peptidoglycan synthesis and spore properties. *J Bacteriol,* 181**,** 126-32.

POPHAM, D. L., ILLADES-AGUIAR, B. & SETLOW, P. (1995) The *Bacillus subtilis dacB* gene, encoding penicillin-binding protein 5*, is part of a three-gene operon required for proper spore cortex synthesis and spore core dehydration. *J Bacteriol,* 177**,** 4721-9.

PRIGOZHIN, D. M., MAVRICI, D., HUIZAR, J. P., VANSELL, H. J. & ALBER, T. (2013) Structural and biochemical analyses of *Mycobacterium tuberculosis N*-acetylmuramyl-L-alanine amidase Rv3717 point to a role in peptidoglycan fragment recycling. *J Biol Chem,* 288**,** 31549-55.

PRIYADARSHINI, R., POPHAM, D. L. & YOUNG, K. D. (2006) Daughter cell separation by penicillin-binding proteins and peptidoglycan amidases in *Escherichia coli*. *J Bacteriol,* 188**,** 5345-55.

PROSSER, G. A. & DE CARVALHO, L. P. (2013) Metabolomics Reveal D-Alanine:D-Alanine Ligase As the Target of D-Cycloserine in. *ACS Med Chem Lett,* 4**,** 1233-1237.

RAMASWAMY, S. V., REICH, R., DOU, S. J., JASPERSE, L., PAN, X., WANGER, A., QUITUGUA, T. & GRAVISS, E. A. (2003) Single nucleotide polymorphisms in genes associated with isoniazid resistance in *Mycobacterium tuberculosis*. *Antimicrob Agents Chemother,* 47**,** 1241-50.

RECHT, J. & KOLTER, R. (2001) Glycopeptidolipid acetylation affects sliding motility and biofilm formation in *Mycobacterium smegmatis*. *J Bacteriol,* 183**,** 5718-24.

RECHT, J., MARTINEZ, A., TORELLO, S. & KOLTER, R. (2000) Genetic analysis of sliding motility in *Mycobacterium smegmatis*. *J Bacteriol,* 182**,** 4348-51.

RUSSELL-GOLDMAN, E., XU, J., WANG, X., CHAN, J. & TUFARIELLO, J. M. (2008) A *Mycobacterium tuberculosis* Rpf double-knockout strain exhibits profound defects in reactivation from chronic tuberculosis and innate immunity phenotypes. *Infect Immun,* 76**,** 4269-81.

SANDERS, A. N., WRIGHT, L. F. & PAVELKA, M. S., JR. (2014) Genetic characterization of mycobacterial LD-transpeptidases. *Microbiology,* 160**,** 1795-806.

SANI, M., HOUBEN, E. N., GEURTSEN, J., PIERSON, J., DE PUNDER, K., VAN ZON, M., WEVER, B., PIERSMA, S. R., JIMENEZ, C. R., DAFFE, M., APPELMELK, B. J., BITTER, W., VAN DER WEL, N. & PETERS, P. J. (2010) Direct visualization by cryo-EM of the mycobacterial capsular layer: a labile structure containing ESX-1-secreted proteins. *PLoS Pathog,* 6**,** e1000794.

SANTI, I., DHAR, N., BOUSBAINE, D., WAKAMOTO, Y. & MCKINNEY, J. D. (2013) Single-cell dynamics of the chromosome replication and cell division cycles in mycobacteria. *Nat Commun,* 4**,** 2470.

SANTOS, J. M., LOBO, M., MATOS, A. P., DE PEDRO, M. A. & ARRAIANO, C. M. (2002) The gene *bolA* regulates *dacA* (PBP5), *dacC* (PBP6) and *ampC* (AmpC), promoting normal morphology in *Escherichia coli*. *Mol Microbiol,* 45**,** 1729-40.

SAUVAGE, E., KERFF, F., TERRAK, M., AYALA, J. A. & CHARLIER, P. (2008) The penicillin-binding proteins: structure and role in peptidoglycan biosynthesis. *FEMS Microbiol Rev,* 32**,** 234-58.

SCANGA, C. A. & FLYNN, J. L. (2010) Mycobacterial infections and the inflammatory seesaw. *Cell Host Microbe,* 7**,** 177-9.

SCANGA, C. A., MOHAN, V. P., JOSEPH, H., YU, K., CHAN, J. & FLYNN, J. L. (1999) Reactivation of latent tuberculosis: variations on the Cornell murine model. *Infect Immun,* 67**,** 4531-8.

SCHEFFERS, D. J. & ERRINGTON, J. (2004) PBP1 is a component of the *Bacillus subtilis* cell division machinery. *J Bacteriol,* 186**,** 5153-6.

SCHOONMAKER, M. K., BISHAI, W. R. & LAMICHHANE, G. (2014) Nonclassical transpeptidases of *Mycobacterium tuberculosis* alter cell size, morphology, the cytosolic matrix, protein localization, virulence, and resistance to beta-lactams. *J Bacteriol,* 196**,** 1394-402.

SHAM, L. T., TSUI, H. C., LAND, A. D., BARENDT, S. M. & WINKLER, M. E. (2012) Recent advances in pneumococcal peptidoglycan biosynthesis suggest new vaccine and antimicrobial targets. *Curr Opin Microbiol,* 15**,** 194-203.

SHARMA, S. S. G., KISHORE, V. & RAGHUNAND, T. R. (2015) Identification and fuctional annotation of mycobacterial septum formation genes using cell division mutants of *Escherichia coli*. *Res Microbiol***,** 1-7.

SHLEEVA, M. O., BAGRAMYAN, K., TELKOV, M. V., MUKAMOLOVA, G. V., YOUNG, M., KELL, D. B. & KAPRELYANTS, A. S. (2002) Formation and resuscitation of "non-culturable" cells of *Rhodococcus rhodochrous* and *Mycobacterium tuberculosis* in prolonged stationary phase. *Microbiology,* 148**,** 1581-91.

SHLEEVA, M. O., KUDYKINA, Y. K., VOSTROKNUTOVA, G. N., SUZINA, N. E., MULYUKIN, A. L. & KAPRELYANTS, A. S. (2010) Dormant ovoid cells of *Mycobacterium tuberculosis* are formed in response to gradual external acidification. *Tuberculosis (Edinb),* 91**,** 146-54.

SINGH, B., GHOSH, J., ISLAM, N. M., DASGUPTA, S. & KIRSEBOM, L. A. (2010) Growth, cell division and sporulation in mycobacteria. *Antonie Van Leeuwenhoek,* 98**,** 165-77.

SINGH, B., NITHARWAL, R. G., RAMESH, M., PETTERSSON, B. M., KIRSEBOM, L. A. & DASGUPTA, S. (2013) Asymmetric growth and division in Mycobacterium spp.: compensatory mechanisms for non-medial septa. *Mol Microbiol,* 88**,** 64-76.

SNAPPER, S. B., MELTON, R. E., MUSTAFA, S., KIESER, T. & JACOBS, W. R., JR. (1990) Isolation and characterization of efficient plasmid transformation mutants of *Mycobacterium smegmatis*. *Mol Microbiol,* 4**,** 1911-9.

TAKAYAMA, K., WANG, C. & BESRA, G. S. (2005) Pathway to synthesis and processing of mycolic acids in *Mycobacterium tuberculosis*. *Clin Microbiol Rev,* 18**,** 81-101.

TELENTI, A. (1997) Genetics of drug resistance in tuberculosis. *Clin Chest Med,* 18**,** 55-64.

TELENTI, A., IMBODEN, P., MARCHESI, F., LOWRIE, D., COLE, S., COLSTON, M. J., MATTER, L., SCHOPFER, K. & BODMER, T. (1993) Detection of rifampicin-resistance mutations in *Mycobacterium tuberculosis*. *Lancet,* 341**,** 647-50.

TIPPER, D. J. & STROMINGER, J. L. (1965) Mechanism of action of penicillins: a proposal based on their structural similarity to acyl-D-alanyl-D-alanine. *Proc Natl Acad Sci U S A,* 54**,** 1133-41.

TRUEBA, F. J. (1982) On the precision and accuracy achieved by *Escherichia coli* cells at fission about their middle. *Arch Microbiol,* 131**,** 55-9.

TUFARIELLO, J. M., JACOBS, W. R., JR. & CHAN, J. (2004) Individual *Mycobacterium tuberculosis* resuscitation-promoting factor homologues are dispensable for growth in vitro and in vivo. *Infect Immun,* 72**,** 515-26.

TUFARIELLO, J. M., MI, K., XU, J., MANABE, Y. C., KESAVAN, A. K., DRUMM, J., TANAKA, K., JACOBS, W. R., JR. & CHAN, J. (2006) Deletion of the *Mycobacterium tuberculosis* resuscitation-promoting factor Rv1009 gene results in delayed reactivation from chronic tuberculosis. *Infect Immun,* 74**,** 2985-95.

TYPAS, A., BANZHAF, M., GROSS, C. A. & VOLLMER, W. (2011) From the regulation of peptidoglycan synthesis to bacterial growth and morphology. *Nat Rev Microbiol,* 10**,** 123-36.

UEHARA, T., DINH, T. & BERNHARDT, T. G. (2009) LytM-domain factors are required for daughter cell separation and rapid ampicillin-induced lysis in *Escherichia coli*. *J Bacteriol,* 191**,** 5094-107.

UEHARA, T. & PARK, J. T. (2007) An anhydro-*N*-acetylmuramyl-L-alanine amidase with broad specificity tethered to the outer membrane of *Escherichia coli*. *J Bacteriol,* 189**,** 5634-41.

UEHARA, T., PARZYCH, K. R., DINH, T. & BERNHARDT, T. G. (2010) Daughter cell separation is controlled by cytokinetic ring-activated cell wall hydrolysis. *EMBO J,* 29**,** 1412-22.

VAN DEUN, A., MAUG, A. K., SALIM, M. A., DAS, P. K., SARKER, M. R., DARU, P. & RIEDER, H. L. (2010) Short, highly effective, and inexpensive standardized treatment of multidrug-resistant tuberculosis. *Am J Respir Crit Care Med,* 182**,** 684-92.

VEENING, G. J. (1968) Long term isoniazid prophylaxis. Controlled trial on INH prophylaxis after recent tuberculin conversion in young adults. *Bull Int Union Tuberc,* 41**,** 169-71.

VELAYATI, A. A., MASJEDI, M. R., FARNIA, P., TABARSI, P., GHANAVI, J., ZIAZARIFI, A. H. & HOFFNER, S. E. (2009) Emergence of new forms of totally drug-resistant tuberculosis bacilli: super extensively drug-resistant tuberculosis or totally drug-resistant strains in Iran. *Chest,* 136**,** 420-5.

VERSCHOOR, J. A., BAIRD, M. S. & GROOTEN, J. (2012) Towards understanding the functional diversity of cell wall mycolic acids of *Mycobacterium tuberculosis*. *Prog Lipid Res,* 51**,** 325-39.

VOLLMER, W. & BERTSCHE, U. (2008) Murein (peptidoglycan) structure, architecture and biosynthesis in *Escherichia coli*. *Biochim Biophys Acta,* 1778**,** 1714-34.

VOLLMER, W., BLANOT, D. & DE PEDRO, M. A. (2008a) Peptidoglycan structure and architecture. *FEMS Microbiol Rev,* 32**,** 149-67.

VOLLMER, W., JORIS, B., CHARLIER, P. & FOSTER, S. (2008b) Bacterial peptidoglycan (murein) hydrolases. *FEMS Microbiol Rev,* 32**,** 259-86.

WANG, S., FURCHTGOTT, L., HUANG, K. C. & SHAEVITZ, J. W. (2012) Helical insertion of peptidoglycan produces chiral ordering of the bacterial cell wall. *Proc Natl Acad Sci U S A,* 109**,** E595-604.

WANG, X. & WOOD, T. K. (2011) Toxin-antitoxin systems influence biofilm and persister cell formation and the general stress response. *Appl Environ Microbiol,* 77**,** 5577-83.

WAXMAN, D. J. & STROMINGER, J. L. (1983) Penicillin-binding proteins and the mechanism of action of beta-lactam antibiotics. *Annu Rev Biochem,* 52**,** 825-69.

WEIGEL, L. M., CLEWELL, D. B., GILL, S. R., CLARK, N. C., MCDOUGAL, L. K., FLANNAGAN, S. E., KOLONAY, J. F., SHETTY, J., KILLGORE, G. E. & TENOVER, F. C. (2003) Genetic analysis of a high-level vancomycin-resistant isolate of *Staphylococcus aureus*. *Science,* 302**,** 1569-71.

WHO (2015) Global tuberculosis report 2015.

WIETZERBIN, J., DAS, B. C., PETIT, J. F., LEDERER, E., LEYH-BOUILLE, M. & GHUYSEN, J. M. (1974) Occurrence of D-alanyl-(D)-meso-diaminopimelic acid and meso-diaminopimelyl-meso-diaminopimelic acid interpeptide linkages in the peptidoglycan of Mycobacteria. *Biochemistry,* 13**,** 3471-6.

WYKE, A. W., WARD, J. B., HAYES, M. V. & CURTIS, N. A. (1981) A role in vivo for penicillin-binding protein-4 of *Staphylococcus aureus*. *Eur J Biochem,* 119**,** 389-93.

YANG, D. C., TAN, K., JOACHIMIAK, A. & BERNHARDT, T. G. (2012) A conformational switch controls cell wall-remodelling enzymes required for bacterial cell division. *Mol Microbiol,* 85**,** 768-81.

YANO, T., KASSOVSKA-BRATINOVA, S., TEH, J. S., WINKLER, J., SULLIVAN, K., ISAACS, A., SCHECHTER, N. M. & RUBIN, H. (2011) Reduction of clofazamine by mycobacterial type 2 NADH:quinone oxireductase: a pathway for the generation of bactericidal levels of reactive oxygen species. *J Biol Chem,* 286**,** 10276-10287.

YOUNG, K. D. (2010) Bacterial shape: two-dimensional questions and possibilities. *Annu Rev Microbiol,* 64**,** 223-40.

ZHANG, Y. (2005) The magic bullets and tuberculosis drug targets. *Annu Rev Pharmacol Toxicol,* 45**,** 529-64.

ZHANG, Y. J., IOERGER, T. R., HUTTENHOWER, C., LONG, J. E., SASSETTI, C. M., SACCHETTINI, J. C. & RUBIN, E. J. (2012) Global assessment of genomic regions required for growth in *Mycobacterium tuberculosis*. *PLoS Pathog,* 8**,** e1002946.